



Politecnico di Torino

Master's Degree in Architecture Construction City
A.Y. 2020/2021
Graduation period July 2021

Use Of Physical Models In The Structural Analysis Of Spatial Structures:

An Application To Masonry Arches And Vaults

Supervisors:

Prof. Fiammetta Venuti
Prof. Filiberto Chiabrandi
Prof. Amedeo Domenico Bernardo Manuello Bertetto

Candidate:

Francesco Roselli

Abstract

The use of unreinforced masonry spatial structures, in particular arches and vaults, represents a typical solution in historical buildings. The Italian architectural heritage is heavily characterized by the use of this kind of structures, which are particularly sensitive to the seismic action. In recent years, the use of in-scale models to investigate the structural behaviour of vaults has largely increased in scientific research. Actually, physical models allow to examine the complex three-dimensional failure mechanism derived by pseudo-static response of the structures due to large displacement of the supports, simulating seismic behaviour of the building components.

The experimental campaign carried out in this thesis is based on the investigation on 1:5 in-scale models of round arches and barrel vaults with mortar joints, to investigate their different structural behaviour under settlement of the abutments derived from two different brick patterns: radial arrangement, with bed joints orthogonal to the head arch plane, and vertical arrangement, with bed joints parallel to the head arch plane.

The first phase of the research is devoted to investigating and test the materials adopted to build the models, concerning different mortar mixes, different in-scale bricks and their production methodology. Preliminary tests are carried out on in-scale models of a circular arch with two different masonry apparatus, subjected to opening displacement until collapse, i.e., simulating movement of one abutment in the direction of the arch thrust. These tests aim at acquiring basic knowledge about the construction process and the behaviour of the structure, in terms of ultimate displacement and failure mechanism, as well as to develop a suitable acquisition strategy consistent with the destructive nature of the tests.

With these premises, the second phase of the experimental campaign is carried out in the ModLab of Politecnico di Torino, where a new experimental set-up for the vault models is designed and built. Two tests for each brick arrangement are carried out on the barrel vault models, for a total of four trials. The vault models are tested with shear settlement, involving the movement of one of the abutments normally to the head arches plane. The acquisition process involves image and high-resolution video recorded during the tests, while a constant monitoring of a portion of the structures is conducted with Digital Image Correlation (DIC) cameras. Close-range photogrammetry and structured light technology are used to

acquire point clouds of the models in specific steps of the tests. The data acquired with geomatic techniques are processed and related together obtaining metric three-dimensional dense clouds of each recorded step of the tests. Combining the information from each source the macroscopic behaviour of the vault during the abutment settlement has been reconstructed and, in part, related with the microscopic behaviour of a significative portion of the structure, analysed through DIC, in one test. For each test, crack patterns, rotations, ultimate displacements and failure mechanisms are recorded. Comparison of the obtained results has highlighted quite different behaviour between the vaults built with the two brick arrangements, in terms of different typical crack phenomena leading to different, local or global, failures of the vault. The results of the research could be used, in future work, in the validation of numerical models and tools for brick vaults analysis.

Index

1. Introduction	1
2. Masonry vaults and arches in architecture	5
2.1 Arches and vaults evolution	
2.2 The brick arrangement	12
3. Physical - Architectural models	17
3.1 Use of models in architecture	
3.2 Historic structural models	22
3.3 Contemporary use of structural models	26
4. Description of the case studies	33
4.1 Identification of case studies	
4.2 Arch model	35
4.3 Vault model	38
5. Construction of the models	43
5.1 Materials of the models	
5.1.1 Premise	
5.1.2 Mortar	
5.1.3 Blocks	45
5.1.3.1 Timber blocks	
5.1.3.2 Cement-based blocks	
5.2 Experimental Set-up	51
5.2.1 Arch model – description	
5.2.2 Vault model	54
5.2.2.1 Requirement	
5.2.2.2 Design and construction	
5.3 Arch Models	62
5.3.1 Models construction	
5.3.1.1 Radial arrangement	
5.3.1.2 Vertical arrangement	64
5.4 Vault Models	66
5.4.1 Models construction	
5.4.1.1 Radial arrangement	
5.4.1.2 Vertical arrangement	68

6. Data Acquisition for in-scale model testing	71
6.1 Requirements	
6.2 Geomatic techniques	72
6.2.1 Range-based acquisition: structured light scanner	74
6.2.2 Image-based acquisition: close-range photogrammetry	79
6.3 Digital Image Correlation	84
7. Experimental tests	89
7.1 Test description	
7.1.1 Arch – Opening tests	
7.1.2 Vault -Shear tests	92
7.2 Acquisition and postprocessing	95
7.2.1 Image and video acquisition and processing	
7.2.2 Geomatics' Techniques	100
7.2.2.1 Range-based acquisition: Stonex F6 SR	
7.2.2.1.1 Data Acquisitions	103
7.2.2.1.2 Data Processing	
7.2.2.1.3 Coordinate system setting	106
7.2.2.2 Image-based acquisition: close-range photogrammetry	108
7.2.2.2.1 Data Acquisitions	
7.2.2.2.2 Data Processing	111
7.2.3 Digital Image Correlation	114
7.2.3.1 Data Acquisitions	
8. Results	117
8.1 Arch models	
8.2 Vault models	121
8.2.1 Crack patterns, rotations, and collapse mechanisms	
8.2.2 Point clouds comparison	131
8.2.2.1 Absolute displacements	132
8.2.2.2 Relative displacements	134
8.2.2.3 Sample point distances	136
8.2.3 DIC monitoring	138
9. Conclusions	143
10. Appendix	149
11. Bibliography	165

1. Introduction

For centuries, masonry represented the most employed construction technique in building, characterizing a great part of the western cultural heritage. The arches first and later the vaults represent the first overcome to the ancient trilithic system. They represent two of the most used masonry structure typologies in common and monumental buildings. Before the introduction, at the beginning of the XIX century, of the new construction techniques (such as iron and concrete) the masonry work has been largely used in different geographical areas, evolving along with the populations and the traditions and characterizing the images of the building and the cities: starting from the first Mesopotamian and Greek structures built in dry stone assemblage, passing thought the great development of the matter by the Romans, with great usage of masonry bricks and mortar joints arched and vaulted structures, along with the medieval builders of the great cathedral and the baroque complex solution, till the last experiences of the Catalan modern architects with catenary shapes. This great variety in terms of shapes, materials, and construction techniques leads to the presence of rich and heterogenous constructed heritage. In virtue of their mass uses, arched and vault structures represent one of the principal issues in masonry building preservation. The recent seismic activity in Italy is proof of the delicate role of these structures inside the system-building and leads to reflect about the importance of the interaction between the different building components in the evaluation of the structural response of these masonry spatial constructions. On one hand, these catastrophic events highlight the fragility of our constructed heritage and the necessity of intervention, on the other hand, they show how arches and vaults can accommodate their shape to an even large displacement of their supports, despite the common sense involving the extreme fragility of these structures. These accommodations are performed through the development of plastic hinges with obtaining new static determined states different from the undeformed ones. In the last year, along with the investigation related to the seismic activities, the interest about the topic, from the scientific community, is strictly related to the evaluation of other typologies of displacement, different from the sudden post-earthquake deformations: the field of research has been extended also to the effect of slow soil movement, subsidence, landslide and second-order effects because of the hydrogeological risks that menace the constructed heritage. The design and construction phases of

arched and vault structures in masonry, for centuries, followed geometrical and empirical rules, perfectioned by the builders over the time: the multitude of masonry construction still in use and built before Galileo's theory about the material resistance confirms the importance of geometry and shapes into the masonry matter. For this reason, still today, the principal investigations about the topic use methods suitable to evaluate the stability of the structures and the boundary condition rather than the resistance of the involved materials. In particular, in recent years, is developing the use of computational and experimental tools in the masonry simulation, in which results are related together. The in-scale physical modelling in the structural evaluation of the masonry is spreading into the scientific community because it represents a good and suitable alternative in destructive tests to the complex and expensive ones performed on full-scale structures. Moreover, the use of physical modelling tools is increasing in the validation of the computational tools utilized in the analyses of masonry arched and vaulted structures. Nevertheless, it is demonstrated how the performances of only analytical and computation procedures, without the respective experimental tests, can lead to overestimations of the desired parameters (Ferrero et al, 2021, Van Mele et al, 2012) if the tools are not calibrated as a consequence (Dell'Endice et al, 2020). The construction techniques and procedures represent an important step in understanding the behaviour of these structures, in virtue of their great variety and complexity. Nowadays, the literature presents a good number of contributes in the field of physical modelling the structural evaluation, but deeper investigations are still needed, especially comparing the knowledge about masonry with the other construction techniques. In particular, the theme of the brick arrangement, one of the focus of the present research, is scarcely discussed, usually reported in construction manuals but not investigated deeply in the field of structural analysis. In light of these premises, the present work aims to individuate a functional and robust methodology in the use of physical models in the structural analysis of spatial structures, involving the individuation of case studies, the geometrical design of the models, the materials and their assemblage, the construction techniques, the experimental set-up, and the data acquisition and post-processing phase. Through the physical modelling the research aims to understand the difference in the behaviour of arched and vaulted structures under great displacement of the supports when are involved different typologies of brick arrangement bounded with mortar joints. Nevertheless, a part of the research focuses

on developing a methodology in the three-dimensional data managing, through the use of point clouds, to perform the deformation analyses of the in-scale models under ongoing imposed displacement and to relate the visible phenomena collected during the tests with the cloud comparison information.

2. Masonry vaults and arches in architecture

2.1 Arches and vaults evolution

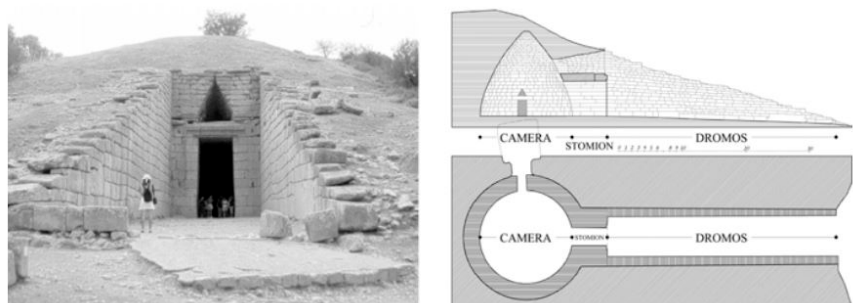
Western architecture is historically heavily characterized by the use of masonry, from ancient times to the very beginning of the XX century, until the introduction of new modern structural materials, such as steel and concrete. The basic principle that rules masonry is the assemblage of units or blocks (cut stone, bricks, rubble, etc.), eventually bonded with mortar to help the laying process in order to form a solid and continuous structure. Arched and vaulted structures use the natural equilibrium obtained through the contrast between the building components and the horizontal thrust that derives. Their use in the building does not correspond perfectly, involving different load conditions: the arches are usually placed inside the vertical elements of a building, supporting the walls, while the vaults are used to stand the floors and their thrust is absorbed by the vertical loads of the lateral wall system (Cangi, 2012). Differently from the ancient wooden construction with flat surfaces, the masonry arches and vaults are used in history to realize the floors in the building by designing curved shapes able to work properly with pure compressive loads. Nevertheless, focusing on the behaviour of the structures under their dead loads, it is commonly accepted to evaluate the two different structure typologies (arches and vaults) by similar parameters involving geometry, thrust, and stability, despite the different bi-dimensional and three-dimensional global behaviour of each of them. One of the best suggestions in understanding the simple masonry spatial structures conception is given by Leon Battista Alberti, in its third book of the "De Re Aedificatoria", where he describes vaults as curved walls ruled in the construction by the same techniques employed for the masonry walls. The metaphor suggested by the Italian architect let us understand how these structural elements can be very relevant into the construction process, in particular in view of their construction process and relation to the other building components. It is clear that this conception cannot be extended to the more complex vaulted shapes developed in history, such as rib and fan vaults, but it is worth noticing the strong impact that this image can lead in the field of arches and vaults. There is no doubt about the strong relationship between these two structural typologies, especially if we consider the barrel vault as a sequence of several arches. The use of arched and vaulted structures in architecture has a long tradition in history. Still today, the origin of these curved masonry structures remains uncertain: the first documented

examples go back to ancient Egypt, Greek, and Mesopotamian cultures starting from the third millennium B.C. and involve principally primitive typologies of vaults made in mud bricks. Among them, we can refer to two different typologies: corbelled or false vaults and pitched vaults. The first typology is characterized by a different structural behaviour due to the assemblage of several parallel rows of masonry, typically in stones, laying one on the top of the other with a progressive corbelling. This technique was largely employed in the Mycenaean tholos tombs construction (Como, 2008), such as the Treasury of Atreus (Fig. 2.1).

Fig. 2.1

Treasury of Atreus: view of the entrance, with the corbelled discharge arch above the lintel, plan and section

From: Como, 2007.

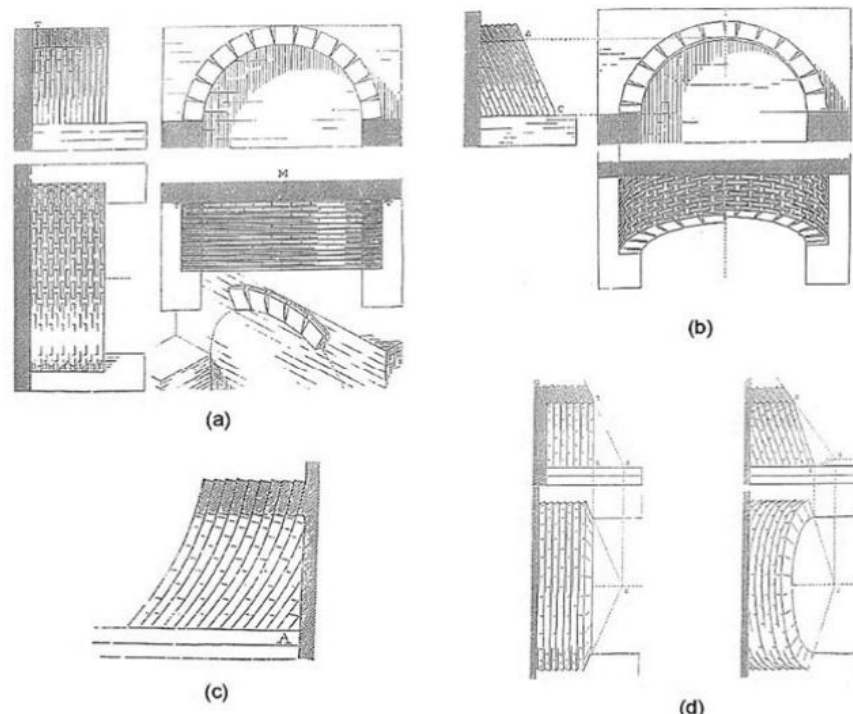


The pitched vaults (Fig. 2.2) are constructed by the systematic inclination of the bricks to avoid the use of temporary scaffolding (Choisy, 1883). The bricks are assembled so as to form inclined self-supporting arches, contrasted by a boundary wall (Huerta, 2009; Karydis, 2012), while the lime mortar is used to prevent the sliding between the elements.

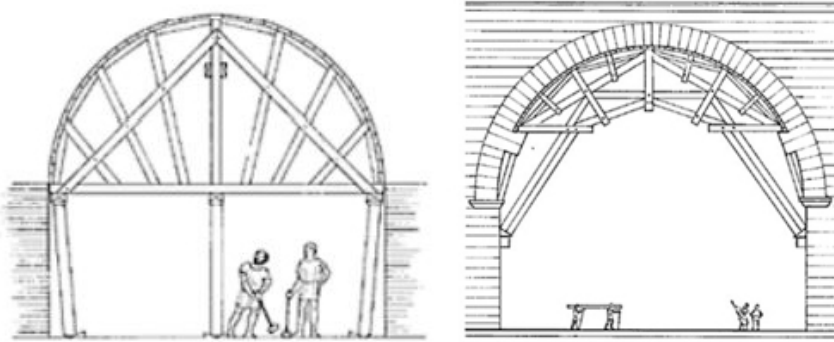
Fig. 2.2

Pitched vaults with different brick arrangements.

From: Huerta, 2009.



After these first examples, vaults are fully developed by the Romans, with the addition of the simple arched structures previously employed by the Etruscan and Greeks in some ancient examples, in the process that Adam (1989) defines as "the conquest of space". One of the most notable examples is represented by the Porta Rosa (Fig. 2.3) in the Greek colony of Velia, built in 340 B.C., where a civic entrance is realized by an arched opening into the city walls, made with cut stone. It is worth noticing the use of a second arch bonded into the masonry, straight above the entrance arch, to help the load discharge from the main arch. The Romans developed new construction techniques that brought the usage of the arched and vaulted structures to a new level: besides the great number of usages in minor buildings, one of the most impressive and systematic uses of arches can be found into the great roman aqueducts. These gigantic infrastructures, that connected the water sources to the main cities of the empire, are a constructed compendium in the usage of the arched structures. Despite the lack of any direct representation, by the Roman, of the use of centering, it is accepted by the scientific community their importance in the development of this device (Adam, 1989). Putlogs and corbelled pieces are found in many of the aqueducts, still visible today, meaning the use of temporary hanged supporting (Fig. 2.4) employed in the arches and construction, as visible in the Pont du Gard (Fig. 2.5), built in 15 A.D. After this, it is also reasonable to assume the use of full centering, with a large span, and a complete structure, supported on the ground (Fig. 2.4), also in vaults construction.



The other great improvement in the arches and vault technology is resembled by the systematic use of modular elements made by the Romans: along with the development of stereotomy ashlar construction, Roman architecture is heavily characterized by the use of bricks, known as *opus testaceum*. During the imperial period, the material has undergone a mass-production with the progressive abandonment of



Fig. 2.3

Porta Rosa in the ancient city of Velia, 340 B.C.

Fig. 2.4

Drawings of two different centering typologies:

Left - full frame centering supported on the ground;

Right - suspendend centering.

From: Adam, 1989.



Fig. 2.5

Pont du Gard, France, 15 A.D.



Fig. 2.6

Giotto, Cappella degli Scrovegni, Padova, 1300 - 1305.

the stone extraction, and it is not surprising to read, in ancient and modern writings on Rome, about scholars who were impressed by the amount of brick masonry found in the skeletal remains. This technical development, of course, is reflected also in arches and vaults construction, with the birth, and the successive evolution through history, of different construction techniques linked to the use of brick masonry. Despite the great use of arched structures, both in the prementioned aqueducts or in the civil and monumental buildings (e.g. the Colosseum and the various Triumph Arches), the Romans do not make intensive use of the barrel vault in brick masonry, in virtue of the punctual structural system employed most of the time, that privileges the use of composite solutions, such as the cross vaults.

The spread of the barrel-vaulted solutions comes in church designs, starting from the Byzantine period up to the first gothic experience, and later in some Renaissance and Baroque buildings. The architectural typology of the church is developed along with one of his main components: the ceiling and roof structures, composed of a brick or stone masonry vault and a timber roof. This ensemble has the double aim of protecting the wooden roof from fire, very common in ancient churches, and preventing water infiltration in the masonry. This solution is visible in well-known buildings from different periods, such as the Scrovegni Chapel (Fig. 2.6), by Giotto, built between 1300 and 1305, the entrance and the central nave in the Sant' Andrea Basilica in Mantova, by Leon Battista Alberti, designed in 1472, and in the Gallery of Palazzo Spada, realized in 1632 by Francesco Borromini. In general, despite the use of arches and vaults in different contexts and solutions and the good number of experiments they have undergone, the principles of masonry have remained nearly the same in history.

This brief list of barrel vaults and arches examples aims to demonstrate the great use of these structures in different periods and to reflect the evolution in time. Along with the typologies evolution, the medieval builders start to speculate about the geometry of the masonry structures: as already known by Romans, the arched and vaulted structures are strictly dependent on their shape and their dimension, and builders and designers used empirical rules in the realization of new structures, based on the direct experience on ancient building. Rules of proportion and the imitation of the existing building have been the main element in masonry design for centuries. Since it is not possible to prove what kind of eva-

luation the Romans made in the arches and vaults design, it is reasonable to assume that their use of empirical methods was not so different from the one utilized during the Renaissance (Adam, 1989). This method involves the evaluation of the abutment thickness by a graphical calculation based on the span and the cross-section geometry (Fig. 2.7)

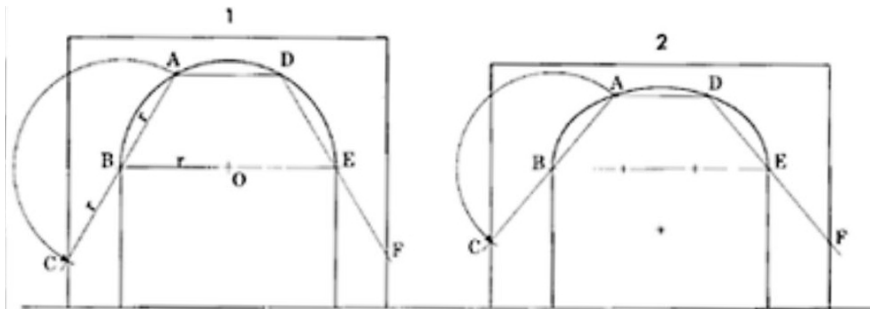


Fig. 2.7

Reinassance grapich method to estimate the abutment thickness.

From: Adam, 1985.

The geometry remains for centuries as the main guideline in masonry construction, considered as the base of the stability and interpreted as the *Firmitas*, one of the three main needs in the building elaborated Vitruvius in the "De architectura" (I century B.C.). The geometrical approach reaches surprising developments in terms of mathematical evaluation in the work of mathematicians and designers, such as Guarino Guarini in the XVII century. It is reasonable to assume that Guarini never knew the theories of Galileo Galilei concerning the resistance of materials (Sakarovitch, 2003) exposed in the "Discourses and Mathematical Demonstrations Relating to Two New Sciences" (1638) and considered as the base to the modern structural mechanics, but it is possible to claim his deep knowledge in masonry work that led to some of the most complex and daring arched and vaulted structures like the Holy Shourd Chapel (Napoli, 2008) (Fig. 2.8t), built after 1668, and San Lorenzo Church Dome, built between 1634 and 1680, both in Turin. Guarini's work is totally based upon the geometrical conception of the spatial structures, and this is demonstrated by his speculation, started from the work of Palladio, and exposed in the "Euclides adauctus" (1671) about the geometrical primitives and their intersection as the base of the design and the realization of the vaults. Moreover, Guarini in his treatise "Civil Architecture" (1671) exposes his disappointment regarding the scarce consideration of the construction issues in building arched and vaulted structures by the practitioners of his time (Spallone, 2012), despite the design and construction difficulties constantly noticed during in the building construction.

The XVIII century represents the golden age of the structu-



Fig. 2.8

Guarino Guarini, arch system in the Holy Shroud Chapel, Torino. about 1668.

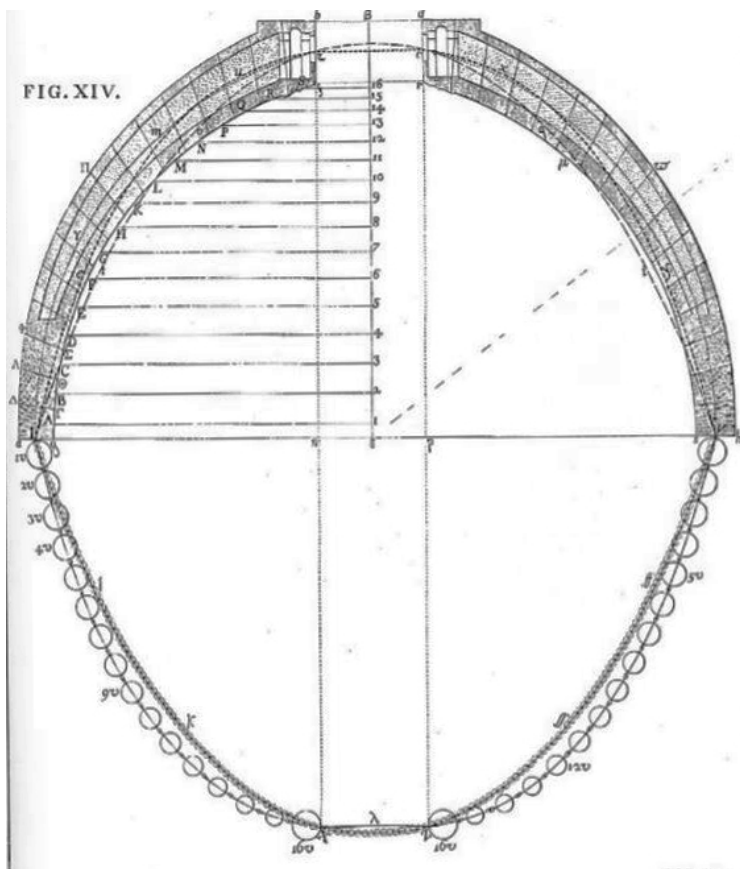
From: Napoli, 2009.

ral discussion in the arched and vaulted structures field, with many treatises involving geometry and material properties. Probably the most remarkable evaluation about the theme is coming from the Italian mathematician and engineer Giovanni Poleni. During his career he worked on the structural evaluation of the St. Peter's Cathedral Dome and in 1748, referring to the Robert Hooks research about the hanging chain (as the best configuration for an uniformly loaded arch) conducted a century earlier, he is probably the first in history to give a scientific evaluation of the stability of a dome. The hanging chain of Michelangelo's dome in Poleni's famous drawing (Fig. 2.9) resembles for the first time the distribution and the flow of the thrust inside the mass of the structure.

Fig. 2.9

Giovanni Poleni, static evaluation of the St. Peter's Basilica Dome.

From: Poleni, 1748.



The past pure geometrical and imitating approaches leave the place to new methodologies based on the analytic evaluation of different elements. Nevertheless, the masonry construction field preserved an empirical approach in the structure dimensioning: for example still during the Victorian age, the scientific literature about the arch and vault dimensioning has experienced a great spread, with many contributors, involving the geometry of the arch represented by the span, the rise, and the global shape. These elements are used to derive the thickness of the structure. In Fig. 2.10 are reported some of the empirical formulas theorized during this period:

$h = \sqrt{36650 S}$	(Rankine)
$h = 220\sqrt{f}$	(Hurst)
$h = 82 + 182\sqrt{\frac{S}{2} + f}$	(Troutwine)
$h = \sqrt{40000 S}$	(Deput - Semi-circular)
$h = \sqrt{20000 S}$	(Deput - Segmental)
$h = 150(1 + \sqrt{S})$	(Sejourne- Semi-circular)

Where:

- **h** = thickness of the arch
- **f** = rise (typically assumed as 1/2 or 1/3 of the span)
- **S** = the span

Nowadays, one of the most accepted and used theories about the structural behaviour of masonry is the one introduced by Jaques Heyman (1966,1995). According to this theory, the masonry behaviour can be evaluated through three simple assumptions:

- masonry has no tensile strength;
- masonry has infinity compressive strength;
- absence of sliding failure between the elements.

Under these assumptions, masonry can be imagined as composed of totally rigid blocks with no-tension interfaces at the joints, and the failure can only occur by the opening of hinges in these joints, due to the impossibility of sliding phenomena. If the voussoir arched structure is stable under self-weight, failure can occur only by the movement of the abutments that lead to new accommodation in the general shape of the arch or by the imposing of external forces (both vertical or seismic): according to the three assumptions about the material, the blocks (or bricks) cannot deform or slide, but just rotate around contact points, interpreted as hinges, and creating cracks. It is clear, under these assumptions, that cracks can only occur along the joints, typically composed of weak mortar, and not along the rigid elements (Fig. 2.11). These assumptions are also used in the performing of Limit analysis (Heyman, 1966): the thrust line represents the geometry of the ideal arch to support a certain load (as an inverted chain), and it must lie inside the boundaries of the masonry structure. With this premise, it is clear that a simple arch can contain inside its boundaries (between extrados and intrados) poten-

Fig. 2.10

Empirical formulas used for dimensioning during Victorian Age.

From: Reda Taha, 2005.

tially an infinite number of inverted chains. For this reason, the master safe theorem (Heyman, 1995) states the need to find a single thrust line, not even the "actual" one, to assess the safety of the structure. The representing of the thrust line with graphical methods can also help to understand the behaviour of the structures (arches or vaults, assumed as a series of parallel arches) when subjected to changes in the loading or geometric conditions. These variations lead to the opening of hinges at the joints, as previously described, in correspondence of the thrust line contact to the intrados or the extrados of the structures. It is demonstrated that the stable structure becomes a collapse mechanism in correspondence of the appearance of specific hinges, depending on the structure geometry and the nature of the loads. In arches and barrel vault under opening spreads of the supports, as an example, the mechanisms is triggered by the presence of a fourth hinge (Fig. 2.11) (or fifth in the ideal structure).

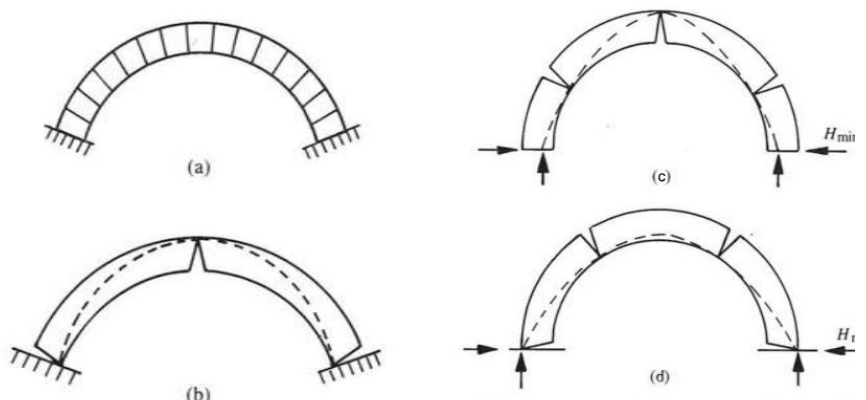
Fig. 2.11

Structural behaviour of a voussoirs arch:

Left - stable state of a cracked voussoir arch;

Right - minimum and maximum thrust undr its own weight.

From: Heyman, 1995.



2.2 The brick arrangement.

Since the first examples of arched and vaulted structures, partially described in the previous section, the arrangement of the elements has been an important aspect in the construction process. As seen in the examples cited by Choisy, and reported by Huerta, the ancient pitched vaults had different typologies of arrangement with variation in the vertical tilting of the mud bricks, involving different behaviours of the elements during the construction. The great built heritage left us by the Romans also shows variations in the arrangements of the bricks, now used and produced in a systematic way: this variety includes the use of single or multiple rows of bricks both in the construction of arches and vaults, leading to many different solutions, often present in the same building (such as in the Aqua Alexandrina aqueduct, Fig. 4.9). The sim-

plete solutions involve the use of multiple rows of bricks laid with mortar bed joint orthogonal or parallel to the abutments: these solutions, continuously re-used in the centuries, in virtue of their simple realization, also taken into account by Heyman (Fig. 2.12) are the two arrangements selected to be tested in the experimental investigation of the present research and are exposed in detail in Ch.4.

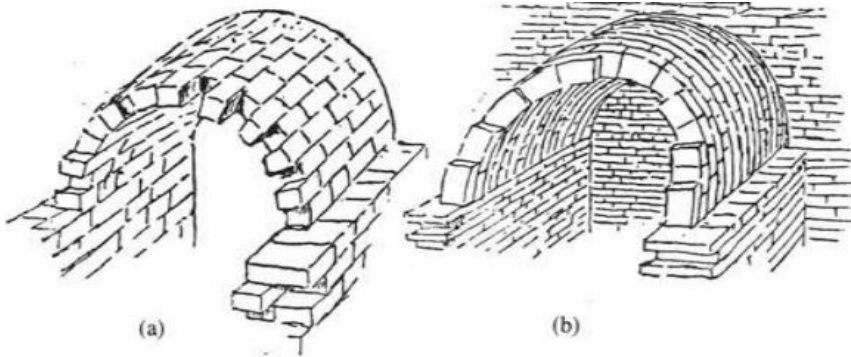


Fig. 2.12

Radial and vertical arrangement of the bricks in a barrel vault.

From: Heyman, 1995.

These two simple solutions represent two opposite and clear construction techniques, with many variations, in history, including mixes of the two arrangements together and use with other bricks dispositions. The employment of these techniques appears to be strongly related to the local cultures and tradition, along with the formal solution employed in the arches and vault geometry: Choisy (1883) continues his description of the ancient techniques by reporting examples of mixes between radial courses of bricks and pitched ones, to ease the construction without centering (Fig. 2.13) while Alberto Grimoldi (Brumana et al, 2017) describes the strange situation discovered in the pavilion vaults of two adjacent rooms on the first floor of Palazzo Magio Grasselli, in Piacenza, built over the XVII century, on a late medieval building. In particular, Grimoldi notices, after thermographic acquisitions of the vaults, plastered on the intrados, that the two structures, with similar dimension and built in the same period, have two different arrangements of the bricks, probably depending on the presence of two different building teams in the construction site, at the same time.

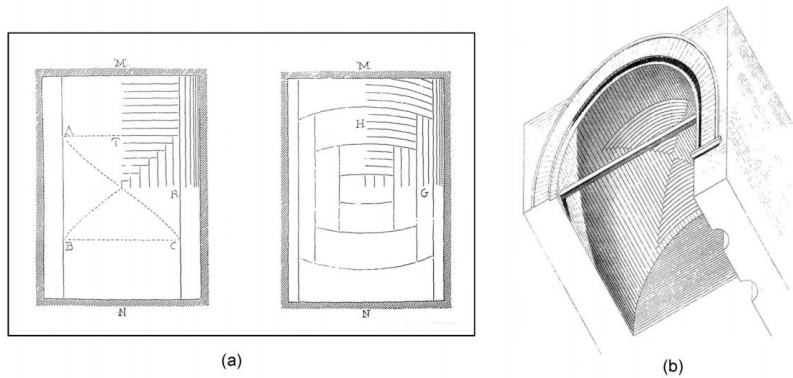


Fig. 2.13

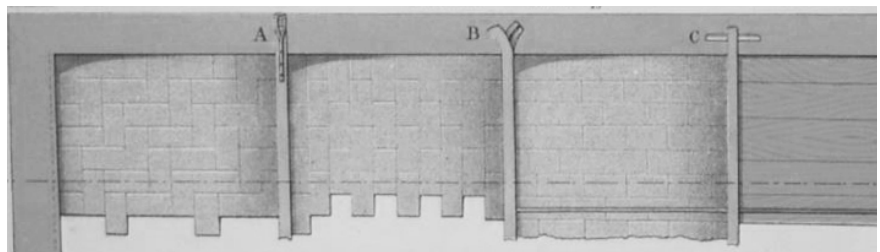
Mixed brick arrangement of a barrel vault.

From: Huerta, 2009.

Fig. 2.14

Three different brick arrangement in little flooring vault.

From. Musso and Copperi, 1887.



The use of these techniques and their variation has spread over time, and still, at the end of the XIX century, they are largely used in the masonry construction: the building manuals of the time, such as "Particolari di cotruzioni murali e finimenti di fabbricati" (Musso and Copperi), published in 1887, report drawings and instruction to arrange the bricks in different vault typologies (Fig. 2.14) to help the designers and the masons during the construction.

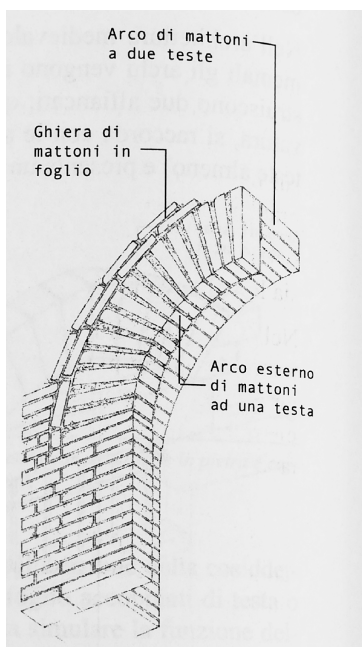


Fig. 2.15

Typical brick arrangement in a Tuscan Renaissance arch.

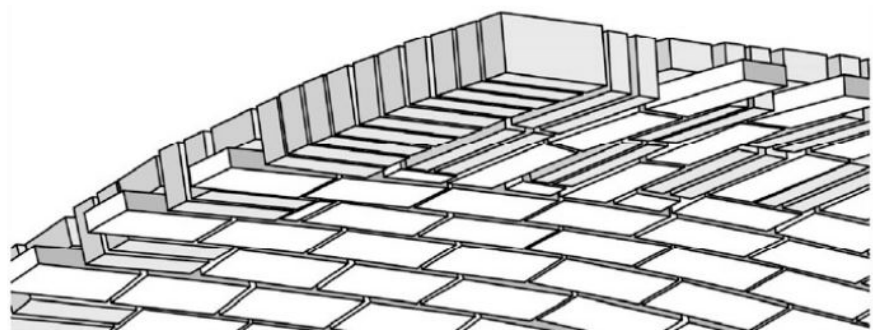
From. Cangi, 2012.

But despite the classifications on the base of the bricks or joints direction, made by scholars and designers, in reality, the common practice often leads to more complex solutions, in which even the definition of a principal arrangement direction is challenging, both in arches and vault construction. This is the case of the typical arches used in Tuscan Renaissance (Cangi, 2012) with multiple layers of radial and vertical oriented bricks, arranged in several arches and reinforced with masonry ferrules (Fig. 2.15) or the complex arrangement of the pavilion vault, mentioned before, in Palazzo Magio Grasselli in Cremona, where the *in-folio* arrangement of the bricks in most parts of the structure is alternated, along the intersections with stiffening arches on the extrados, with random-appearance oriented bricks (Fig. 2.16). The same issues are noticed by Piccoli (1999) in the analyses of the construction methodologies involved in the planterian vault, typical complex-shaped vaulted structures of the Piedmont region's architecture, where the high presence of stiffening elements and geometrical intersections leads to the use of huge mortar quantities to bond the bricks, sometimes individually manually shaped, in free directions.

Fig. 2.16

Complex brick arrangement in the stiffening of a pavilion vault in Palazzo Magio Grasselli, Piacenza, XVIth century.

From: Brumana, 2017.



In conclusion, the arrangement of the bricks still represents an open field of research, with many discordant interpretations about their contributes to the structural behaviour of the arched and vaulted structures: the theme is briefly treated by Heyman (1995) who states the substantially similar global behaviour between the two different arranged structures in the collapse mechanism, with slight variations into the deformed states and crack patterns. On the contrary, Cangi (2012) interprets the arrangement of the bricks as one of the most important elements in the evaluation of the resistant mechanisms developed by the vaults, in virtue of the different crack pattern possibilities related to different structural issues in the building. Nowadays, the scientific literature about the topic still does not present a reasonable number of sources involving the evaluation of the structural behaviour of masonry spatial structures in relation to their different brick arrangement.

3. Architectural models

3.1 Use of models in architecture

The use of physical models in architecture is systematically documented since the great spread of the drawing and construction treatises during the Renaissance. Nevertheless, it is possible to find wide evidence in the use of objects to resemble the three-dimensional representation of a building.

One of the more ancient examples is represented by the use of little earthenware models of buildings (White et al, 2016) (Fig. 3.1), in China, dating back to the Han dynasty (II and II centuries BC): these objects reproduce towers, castles, and simple houses and are usually part of funerary equipment. They can be interpreted like the well-known Egyptian and Greek-Roman ones, with a high symbolic value: these models, typically decorated with bird figures, are offered to the deceased as a new house in the afterlife. This kind of model has a strong historical value because of the representation of popular Chinese architecture from the Han dynasty period, even if already idealistic.

Other pieces of evidence in the use of symbolic models are found, in Western culture, in the traditional Christian iconography of the ex-voto: typically employed in ecclesiastic architectures, these are mosaics or frescos representing the important personality of the Church donating a model of the architecture itself to the Mother Mary or the Saints. The wide diffusion of this practice is proven by the presence of two ex-voto in as many different and far buildings. The first in a Pieve in Galliano (Tosco, 2016) in Cantù (CO), in Italy. It is a fresco, dated back to 1007 A.D., representing Milan's Archbishop Ariberto da Intimiano in the act of donating the model of the little church to an angel (Fig. 3.2). The second is a mosaic commissioned by the Byzantine emperor Basil II, after the defeat of the Bulgarians, in a lunette on the western entrance of Hagia Sophia in Istanbul: it represents the emperor Justinian I while donating the model of the basilica to the Mother Mary with the Child, along with Constantine who gives her a model of his own city, Constantinople (Fig. 3.2). The highly symbolic value of the ex-voto has a double meaning: on one hand, it represents the will of the building clients, e.g., the Lombard ecclesiastic class or the Byzantine rulers, to celebrate themselves and their deeds; on the other hand, their use involves the high consideration of the Roman people to the value of the three-dimensional in-scale representation of an important building. Nevertheless, no one of the models represented has



Fig. 3.1

Earthenware model of traditional house, Han Dynasty, University of Pennsylvania Museum, Object Number: C365.



Fig. 3.2

Top - Ariberto da Intimiano donate the model of the Pieve di Galliano, 1007, Cantù (CO).

Bottom - Costantin and Justinian who give model of the city and the church to the Mother Mary, uncertain dating between 989 and 1019, Hagia Sophia, Istanbul.

arrived at our days, probably due to the exclusive use of the figurative representation without the respective physical model.

As mentioned before, the great development of the architectural model practice takes place in the Renaissance as a representation and design tool. The use of the models can be classified into two different categories, as reported in the studies of Sebastianelli and Muscarelli (2016): the work and study model and the exhibition ones. The first is realized to study the building or a part of it, using poor materials, little in-scale reduction, and no decoration. These models are also made to ease the design conception to the customers and the workers on the building site. Study models are usually composed of various number of different pieces, representing joints and constructive tips. A very poor number of this kind of model has survived, from the period to nowadays, because of the operative function and their presence in the building sites. Some of them have been reproduced differently from the originals, typically described in the letters between the architects and the customers or in the payment orders. The second typology includes the model used in exhibitions and ceremonies: they are designed to expose the whole project to the customers to be approved before the construction phase. This kind of model is usually preserved in a better way than the previous ones, conserved in archives and museums.

In the treatise "De re Aedificatoria" (about 1450), Leon Battista Alberti deals with the topic, by describing the operative nature of the model in the architectural practice: he describes the model not as refined, shiny, or perfect but as essential and simple to expose the design conception, not the technical execution. In the treatise, the modelling is directly linked to the architectural drawing, which occupies a great part of Alberti's theory. The three-dimensional representation, for him, is a tool to prove the physical capacity of the object to exist after the geometrical conception. It is known the existence of at least one in-scale model made by Alberti (Vasari, 1550; Burns, 1998) for the Sant'Andrea church in Mantova. The models, lost, are used to expose the project to the customer Ludovico Gonzaga and manage the construction by Luca Fancelli, Alberti's collaborator, after the death of the master in 1472.

A decade later, Antonio di Pietro Averlino, known as Filarete, describes the use of the physical model in his treatise, while describing his ideal city Sforzinda to the duke of Milan, Fran-

cesco Sforza. Filarete refers to *disegno rilevato* as a three-dimensional wooden model employed as the last step in the design process. For the first time (Spallone, 2012) the models are systematically used as a representation technique along with the drawing. As a consequence, in the treatise, Filarete uses pseudo-perspective elevation drawings to simulate the three-dimensional features of the models.

These treatises highlight a new and common use of the physical model in the architectural process, probably reflecting the professional practice of the XVst century. Vasari refers to the design habits of Filippo Brunelleschi, who typically fabricated wooden models of the architecture that are left on the building site, as a guide for the masters. This habit is also confirmed by the payment orders from the Opera di Santa Maria del Fiore from which we know that, in 1418, Brunelleschi, along with Nanni di Banco e Donatello, is paid for a brick-and-mortar model of the cathedral's dome, destroyed in 1432. This model is integrated, later, with the other two wooden models of the balcony and the lantern. The presence in the order of two sculptors tells us the aim of the model to exhibit the final form of the building with aesthetic value, besides guiding the bricklayer during the construction. Once the dome is completed, in 1436, a new architectural competition was opened for the realization of the lantern above the structure. The competitors were invited to present a physical model of the projects (Fig. 3.3). This particular request shows the importance of the modelling in the renewed architectural practice of the bigger commissions. Brunelleschi won the competition with a "tricky" model, as described by Vasari (it is designed to hide some of the features of the project). This model has been used after the death of Brunelleschi as a guide for the lantern construction, as expressed in his own last wills. Today a slightly different replica is exposed in the Museo dell'Opera di Santa Maria del Fiore in Florence.

As mentioned previously, a great part of these models has not survived during the years, replaced by replicas or lost. Vasari, while telling the personal history of his contemporary colleagues, refers to a great number of models of well-known buildings: the one realized by Francesco di Giorgio Martini for the Palazzo Ducale di Urbino after he succeeded to Luciano Laurana and also the model of the Belvedere stairs realized by Bramante for the St. Peter's complex. Vasari tells the story of Giuliano da Sangallo who gives a model of a royal palace as a present to the emperor Charles VIII of France while visi-



Fig. 3.3

Wooden model of the lantern, about 1430-46, Museo dell'Opera di Santa Maria del Fiore, Florence.

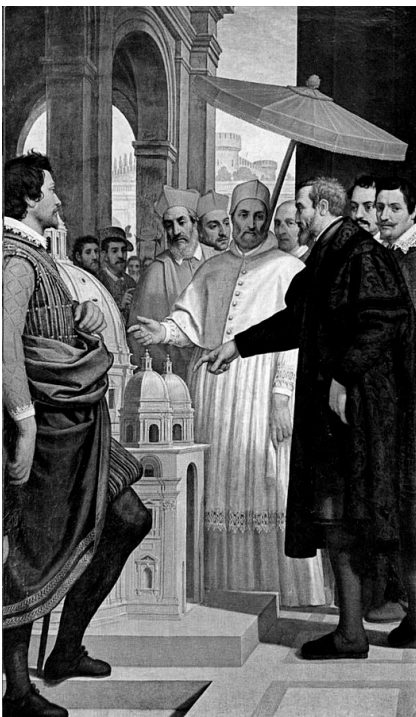


Fig. 3.4

Passignano, Michelangelo presents the model of St Peter to Pope Paul IV, XVIith century, Casa Buonarroti, Florence.^t

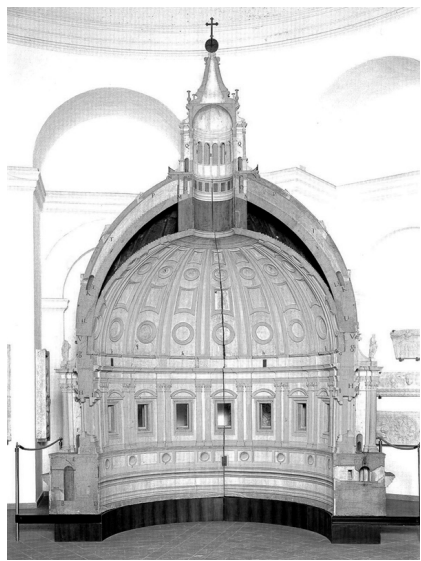


Fig. 3.5

Michelangelo and Battista da Carrara, Model of the St. Peter's dome, view of the cross-section, 1558-1561, Museo Petriano, Rome.

ting him with the cardinal Giuliano della Rovere, in 1496. This episode has a significative meaning in the comprehension of the new importance of the modelling in architecture, with this practice assuming a role not so different from the ancient ex-voto. A similar event is reported in a fresco by Antonio Crespi, known as Passignano, in Casa Buonarroti, Michelangelo's native house. In the fresco, the architect is showing the model of his project for St. Peter's Basilica to Pope Paul IV during a public ceremony (Fig. 3.4). The Basilica is linked to two of the most known architectural models in the history of the subject. The first is the model representing the Michelangelo dome, realized between 1558 and 1561, together with the carpenter Battista da Carrara, is exposed in the Museo Petriano in the Basilica: it is a 1:5 in-scale reproduction of the dome, constructed in basswood, that offers the possibility to be opened and show the section profile of the structure along with the interior (Fig. 3.5).

The second model is the well-known representation of the Antonio da Sangallo's project for the Basilica. It is the focus of extensive research and documentaries because of its features and history. The model of Sangallo (Fig. 3.6) is a one-of-a-kind artwork realized in wood and stucco: it occupies an area of 45 m² and it is more than 4 m high, composed of thousands of pieces in the layout of several components assembled together. This object has the unique feature of being visitable also in the interior, with a great number of details. Realized in 1:30 scale, it is fabricated by a team of carpenters, led by Antonio Lobacco, taking a period of seven years for the construction and costing around 4.800 scudi (the amount of money needed for the construction of a real little church, at the time). Sangallo's project will be never realized, but the model is still exposed in the Basilica, after a long and expensive restoration performed during the last years of the XX century: this is a clear example of the importance of the physical model, at the time and still nowadays, as a project tool for the designers and for preserving the historical memory of the construction that represents.

The collaboration of a team of carpenters in the construction of St. Peter's model, once again reported by Vasari and the daily payment orders by the Fabbrica di San Pietro, is meaningful to understand the professional practice of the time. A global overview about an exposition model realization procedure is proposed by Roger Pratt, an English architect, who visited Italy and the big construction sites during 1643

and 1649. He describes the process as the result of the work of a team: after the design phase, the architect chooses the scale of representation and works together with the carpenter to select the better wooden support for the scale chosen. Then he draws the prices directly on the wooden panels, the carpenter provides to cut and later assemble the components. The more the architect is present in the design phase of the model, the less he is involved directly in the construction of the object.

During the XVIII century the use of physical models assumes an important place in the professional activity of the architects, with many pieces of evidence still visible, as the well decorated and baroque models used for teaching in the Accademia di San Luca or the collection of the models linked to the various projects of the St. Peter's basilica, by Francesco Fontana. The role of the models increases with the spectacularization of the architecture in the period, concerning the construction of the great public buildings and the interest of the scholars involved in the Grand Tour. A proof of the use in the practice is reported by Filippo Juvarra who, in his letters with the customers, expresses the helpful role of modelling in visualizing the final result of the design with fewer misunderstandings than the classical drawing (Curcio, 2000). The suggestion of Juvarra is reflected in his work by many models, such as the big one realized, along with the carpenter Carlo Maria Ugliengo, for the Rivoli's Castle, between 1717 and 1718 and nowadays exposed at Museo Civico d'Arte Antica in Turin (Fig. 3.7). It is realized in wood and represents the volume of the castle and the detail of the facades. In the past it was completed by adding a second model representing the terraces at the base of the building, today lost. The realization of the model is remarkable for features like the possibility to be opened revealing the architectural section passing through the stairs, the presence of the interior decoration, and the presence of the complex vault systems realized with multiple thin layers of engraved wood. In the same period, in Rome, the models are largely used in the design of great buildings: the payment orders registered for the carpenters show the evolution in the needs of the designers, and it is possible to compare the 650 scudi paid for the model of the Sagrestia Vaticana, in 1715, to the 230 scudi paid for the model of the Fontana di Trevi in 1735 (Di Marco, 2017). This gap in the expenses needed for the model realization can be interpreted as the development of a structured tradition in the use of wood carpentry along with the architectural design. This theory is confirmed by



Fig. 3.6

Antonio da Sangallo and Antonio Labacco, Model of St. Peter's basilica, view of the cross-section, 1539-1546, Museo Petriano, Roma.

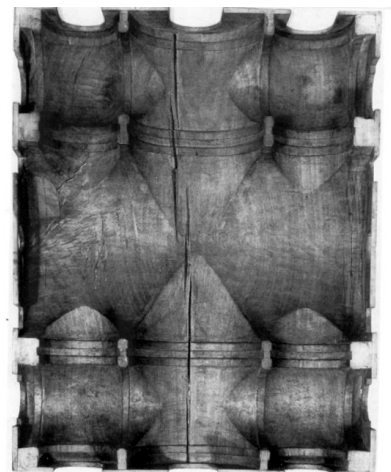


Fig. 3.7

Top - Carlo Maria Ugliengo, Model of the Rivoli Castle, particolare delle volte, 1717-1718, Museo Civico d'Arte Antica, Turin.

Bottom - detail of the vault representation.

the numerous citations of the carpenter Carlo Camporese in the document linked to the Fontana di Trevi construction. Moreover, the figure of Camporese is described, at the period, as a well-known professional figure highly requested in the works of the Roman aristocracy.

In the XIX century, it is worth noticing the approach of some scholars to the use of the physical model as teaching support in the architectural faculties. Giovanni Curioni, professor at Politecnico di Torino, realizes a collection of models representing structures, construction machines, and building solutions, with a high degree of detail and mechanisms of action. In 1872 the collection is composed of 104 models, some of them today gone lost (AA. VV., 1989). These models were exposed to the public in the halls of the Valentino Castle, in Torino, and were used as examples to the students, along with a new laboratory to test the materials. It appears clear that the birth of the new construction science has influenced the use of these supports also in the academic field. Among the lost models, as emerging from the inventory of the collection, there were two models of stereotomy stone bridges, where the voussoirs are cut individually and then assembled to show the students the building procedures.

It is probably in the XX century that the use of models, in the architectural professional practice and teaching, has largely spread in the design and exposition phases: the renewed professional activity, the intellectual speculation during the post-war period, and the great architectural contests are the main characters in the architecture of the century, and all of them bring new usage and rules in the physical modelling. This is proven by the request of models as a compulsory condition to participate in the contests and the big spread of conceptual modelling, in which the pure form is expressed as the main feature of the object.

This brief excursus shows the evolution of the use of the physical models in the architectural practice until nowadays, with the great development in the use of virtual three-dimensional models still in course. The examples reported are selected because of their relevance as the most notable and meaningful uses of the physical modelling tool in architecture to illustrate the great potential of the modelling.

3.2 Historic structural models

Quite all the models illustrated in the previous section have the main purpose of representing the design conception of the architect to the customers, the committee, and the workers. They belong to the exhibition model typology (realized for the committee and customers), with the main intrinsic characteristics of representing the building. It is worth noticing that it is documented, in history, at least one other different usage of the physical models in the architectural and engineering practice: this kind of modelling involves the evaluation, through physical and experimental observations, of the object spatial and structural behaviour. The experiences of Alberti and Juvarra, in the previous pages, demonstrate the use of this kind of model as study tools in the past centuries. In particular, we can refer to a precise typology of models as structural models, the subject of the present thesis work. These models have the main aim of investigating experimentally the structural behaviour of a building component, using an in-scale representation. These investigations typically involve the evaluation of the geometry and the stability of the elements, especially in the masonry fields. Another usage of the models regarding the material resistance will be not treated here, despite their large use, also documented in the scientific literature.

There are few reliable sources about the topic, probably depending on the operative nature of these tools and the professional activities: as reconstructed by Ricci (2008), Filippo Brunelleschi was used to constructing study models to evaluate the geometry of the buildings, but he was very careful not to allow anyone to watch them, as for a wooden and rope model constructed on the Arno's bay to evaluate the geometry of the Santa Maria del Fiore dome. This episode, along with many others confirmed by Vasari, can clearly represent the tendency of the designers in professional practice to preserve some of the practical tools developed by the designer. Naturally, this can be only one of the many causes of the lack of information about the topic. Still nowadays, organic and complete research about the use of physical models in structural analysis is lacking. Similarly to the exhibition models, unfortunately, also most of the structural models documented in history are lost or destroyed, especially due to their usage as study tools during the design phase.

There is no particular evidence of the use of physical models by the ancient Greeks and Romans in the construction field, while some references can be found, still scarce, about their

use during the medieval age: Jaque Heyman, a great scholar in ancient construction techniques, speculates about the use of models also in the big gothic cathedral construction, with the aim of demonstrating the geometrical principles used to design complex masonry structures. This thesis seems to fit well with the design principles used in the cathedral construction based on pure geometrical and empirical relations. Heyman also reports the existence of a physical model of the San Petronio cathedral in Bologna (1995), today gone lost. This is a 18 meters long model made of bricks and plaster, dating to about 1390, the period in which Antonio di Vincenzo was the chief architect of the construction. The San Petronio model aims to evaluate the stability of the building in relation to its single parts, with the same geometrical approach previously described.

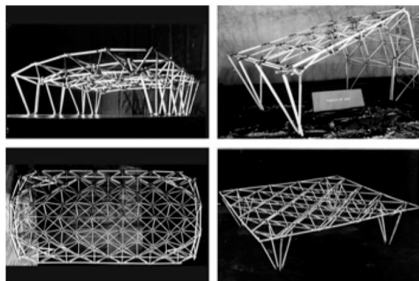


Fig. 3.8

Robert Le Ricolais, Structural models of hangars, 1940 - 1950.

From Vrontissi, 2016.

Charles Perrault in his memories (1909) reports the episodes involving Gian Lorenzo Bernini with the construction of full-scale masonry models: during his brief time in Paris, at the court on Louis XIV in 1665, the Italian architect commissions two vault models, with the boundary walls, testing the different construction practice of both Italy and France and different load conditions. Roberto Gabetti (1989) reports the experience of Soufflot and Rondellet, employed in the Pantheon construction in Paris. According to the author, the two designers, famous for the calculation and design of the armoured stone, performed the test of geometrical stability of vault and supports along with the material resistance testing. With a conception close to the great gothic builders, Soufflot believes in the high value of the empirical and experimental evidence, along with the mathematical observation. For this reason, he built some wooden models to evaluate the stability of the structure. Gabetti also reports the use by Alessandro Antonelli of a 1:20 in-scale model of the San Gaudenzio Basilica's dome, highlighting the tendencies in Antonelli's design process to privilege experimental solution and direct observation in the great masonry structures construction.



Fig. 3.9

Ludwig Mies van der Rohe, structural model of the Chicago el Convention Hall, 1953.t

From Cabanillas Cuesta, 2018.

A wider spread of physical structural models started at the end of the XIX century, involving the design of spatial structures, in which the in-scale modelling of the shapes can help to evaluate the global behaviour of the structure. The use of this strategy is common to designers as Richard Buckminster Fuller, Eduardo Torroja, Felix Candela, Robert Le Ricolais (Sardo, 2004), and Ludwig Mies Van der Rohe (Cabanillas Cuesta, 2019); in particular, Le Ricolais and Mies used physical models

to evaluate the behaviour and the geometry of space frames, e.g. in the Le Ricolas hangars (1940 – 1950) (Fig. 3.8) and the Mies's Chicago Convention Hall (1953) (Fig. 3.9). The research about compression-only structures involves the studies of Antoni Gaudí for his arched and vaulted structures. The Catalan architect was used to evaluate the global shape of the catenary arches and vaults by fabricating models of hanging chains, loaded with little led weights, obtaining a tensile-only structure configuration, then reversed: this solution allows the designer to obtain the best and optimized solution by the principle involving the catenary as the better thrust distribution in an arched structure. Every adjustment of the led weights upon the chains leads to an automatically physical re-computation of the optimal shape of the structures, allowing the designer to invert the model, with the use of simple mirrors, to design the arches and vault. Gaudí used this solution in many of his projects, e.g. the Sagrada Família in Barcellona and the incomplete Church in Colonia Guell (Fig. 3.10). Another notable example is resembled by Frei Otto, well-known for his use of the physical models in the design phase of his structures, converged in the book "Thinking by modelling", published two years after his death, as an exposition of the models built during his professional activity. Among this great model production, it is worth noticing the use of a hanging chain model in the structural design of the gridshell roofs in the Mannheim Multihalle (Liddell, 2015) (Fig. 3.11) during the '70s. The 1:100 in-scale model is composed of small hanging piers in wooden material that holds the boundary lines of the inverted structure: the linking lines connected through little metal rings and composing the inverted webs representing the gridshell elements are connected to the boundary line through the use of metal springs, in order to register the forces inside the web and control the curvature in both directions. Other typical models used by Frei Otto in spatial structures design are composed of little metallic frames hanging a net of wool threads drenched in a liquid soap and water solution: in this way, it is possible to visualize the minimal surfaces between the net, formed by the water and soap solution (Fig. 3.12). A similar approach can be found in the work of the Italian engineer Sergio Musmeci (Nicoletti, 1999), who is particularly aware about the conception of special structural form through modelling: if the shape of a structure is determined by the way the forces pass through the matter in the space, then the physical visualization through the model is the best way to analyse the spatial distribution of the static actions involved by the shape itself. The theory of Musmeci is reflected upon the design of his well-known Basen-



Fig. 3.10

Antoni Gaudí, Tensile-only model of the Church in Colonia Guell. 1898 - 1917.

From dataphys.org.

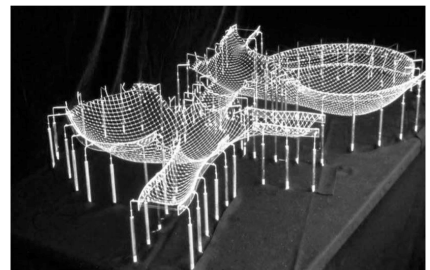


Fig. 3.11t

Frei Otto, gridshell roofs in the Mannheim Multihalle model, about 1970.

From Liddell, 2015.



Fig. 3.12

Frei Otto, Modeling With Soap Films.

From Domus, 2015.

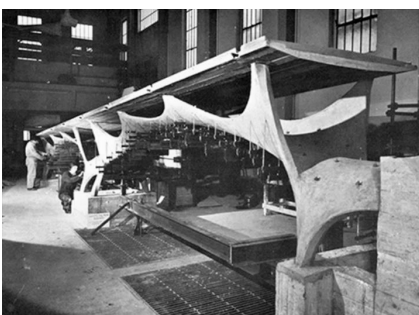


Fig. 3.13

Sergio Musmeci, Basento Bridge 1:10 in scale model, about 1967.

From Lapenna, 2020.

to Bridge, in which the structural minimum surface is performed with a 1:10 in-scale model (Fig. 3.13), made of micro-concrete. The model is tested with hydraulic jacks to understand the distribution of the forces under different load configurations in order to optimize the shape of the thin concrete membrane designed to support the bridge deck.

3.3 Contemporary use of structural models

In the last decade, the research about the structural behaviour of masonry arches and vaults has largely made use of in-scale physical models: based on Heyman's assumption, these researches are based on principles involving the geometry and the stability of the structure more than the material resistances. This approach is also supported by the fact that the big spread in the use of arched and vaulted structures, along with the construction of many of the most complex and innovative ones, is anterior to the research of Galileo Galilei about the resistance of the material, in the XVI century. For these reasons, it is commonly accepted, in the modern scientific community, the use of in-scale models to test masonry spatial structure considering only geometric and stability features and neglecting the scale effect, typically considered in tests involving forces and resistances. Moreover, a series of new solutions in the field of data acquisition and managing is nowadays available, making it possible to perform more effective tests on the in-scale models, involving parameters not possible to be measured in a traditional way with the simple observation of the phenomena. In the following, a brief report about the state of the art in the field of the structural test on the in-scale models is reported, highlighting the procedures and the aims of the researches.

The research by Ochsendorf (2006) and Romano and Ochsendorf (2010) can be considered as parts of the first modern experimental campaign about the masonry arches behaviour under large displacements of the supports. This research involves respectively segmental round (Fig 3.14) and pointed arch models made of cast concrete dry joint voussoirs, that are tested under opening of the abutments, to simulate the response of the structures to the movement of the supports. As for many other experimental campaigns involving arch models, the data acquisition is based upon image capturing of the main vertical plane of the arch: this is due to the simple bidimensional behaviour of an arched structure under in-plane displacement of the abutments. In particular, this resear-

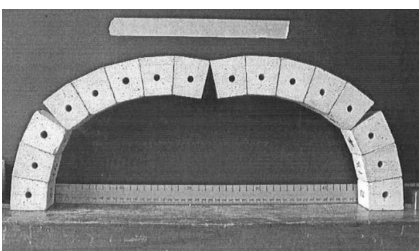


Fig. 3.14

Segmental round arch model, from Ochsendorf, 2006.

ch aims to evaluate the arch behaviour in terms of ultimate displacement, hinge opening, hinge configuration, and their relation with the line of thrust. With these aims, the authors develop a MATLAB algorithm to perform iterative comparisons between the images (2006) to perform the limit analysis on different configurations of the arch. In the 2010 publication they expose a new procedure that integrates the previous one, where the line of thrust is also found by the use of the graphical method. In 2007 the results collected by Verstrynge et al. during a student workshop are published. The students build a model of a parabolic arch (probably the only one experimentally investigated in the last decades) in masonry blocks bonded by lime mortar (Fig. 3.15). The arch is tested under a centric load and opening displacements of the abutment. A custom software interface is designed to obtain in CAD environment the description of the line of thrust derived by the direct observation and image capturing of the arch behaviour. The experiences here described have been the basis of the procedures of many other research projects on the theme, sometimes focusing on a specific feature in the investigation (geometry, displacement, model discretization, interfaces, etc.) where the basic limit analyses method is replaced by modern and more sophisticated computational tools. In this category falls the work by Galassi et al. (2020), which aims to evaluate the behaviour of a pointed arch model (Fig. 3.16) under large displacement of the abutment with a focus about the element discretization and some of its constructive features. In particular, the results show a different response of the arch in the presence or absence of a keystone in terms of both collapse mechanism and ultimate displacement. The experimental results are used to validate an innovative tool based on the modelling of interfaces (joints) with a precise stiffness to evaluate, in an iterative way, the ultimate displacement, the hinge position, and the collapse mechanism of arches under the tested displacement. In the same year, the results of the experimental test on a 1:5 in-scale segmental round arch model by Alfonso et al. are published. In this case the model is made by an assemblage of wooden blocks bonded with low cohesion lime mortar and tested under opening displacement (Fig. 3.17). The ultimate displacement is acquired by a digital measuring tool, while the data concerning the evolution in the stability of the arch model and the hinge opening are collected by the use of a high-resolution camera, acquiring at fixed steps of the imposed displacement. The results, in terms of collapse mechanism, hinge position, and ultimate displacement are compared with a new proposal of

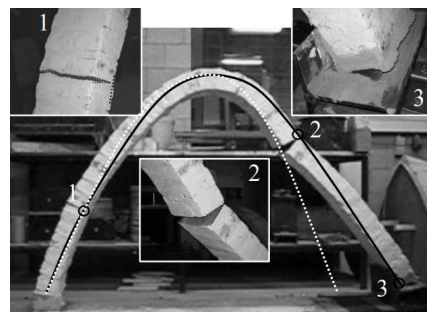


Fig. 3.15

Parabolic arch model collapse under opening displacement,
from Verstrynge et al. 2007.



Fig. 3.16

Pointed arch model collapse under opening displacement,
from Galassi et al. 2020.

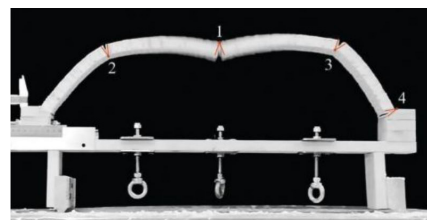


Fig. 3.17

Segmental round arch model collapse under opening displacement,
from Alfonso et al. 2020.

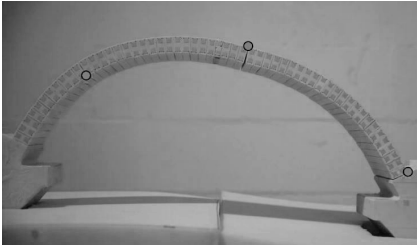


Fig. 3.18

Segmental round arch model, hinges opening under inclined in-plane displacement,

from Ferrero et al, 2021.

a computational tool for the micro-modelling of the masonry structure, obtaining a good matching between experimental and numerical results. More recently, a new research campaign (Ferrero et al, 2021) has involved a series of experimental tests of a dry joint segmental arch model (Fig. 3.18), realized in bicomponent casting material. In this case, the focus of the research is on the behaviour of the structures under in-plane large displacements of the supports with different directions, from purely vertical and purely horizontal to different degrees of variation. The experimental results, also in this case, are used to validate two different computational tools which are used later to assess the difference in the arch behaviour in terms of hinge position, collapse mechanisms, and ultimate displacement in relation to the direction of the in-plane imposed displacement and the number of voussoirs in which the model is discretised.

One of the first experiences involving the use of an in-scale vault model is reported by Van Mele (2012). Here, the research aims to investigate the complex three-dimensional collapse mechanism of a double-curvature cross vault, by using physical and computational models. The main focus is the computational evaluation of the ultimate displacement that leads to the collapse of the structure and the capacity of the numerical tool to predict the experimental results obtained in the tests. The experimental campaign is performed on a vault formed by the geometrical intersection of two barrel vaults with 150 mm of internal radius and 24.4 mm of thickness. The in-scale structure is modelled in Rhinoceros and constructed by the assemblage of dry joints individually shaped voussoirs, obtained by 3D printing with plastic material. The vault is placed upon four separate abutments and the movement of one of them, in horizontal, vertical, and inclined direction imposes the displacement that leads to the collapse of the structure (Fig. 3.19). The data acquisition is performed through the use of optical devices and the experimental results are compared with the computational ones.

In the same year, Shapiro publishes the results obtained during her Master's Degree Thesis at the Massachusetts Institute of Technology. The experimental campaign is performed with different typologies of dry joint in-scale vault models under different conditions of load and displacement. In particular, she tests two different barrel vaults (Fig. 3.20) and a cross vault by opening spreads of the supports, vertical point load, point load on initially deformed configurations, and constant

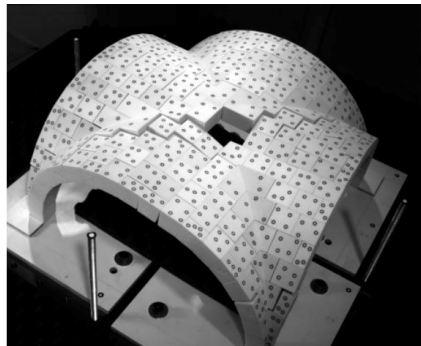


Fig. 3.19

Cross vault model, hinges opening under in-plane displacement,

from Van Mele et al, 2012.

horizontal acceleration of the structures obtained by tilting the reference plane of the models with different angles of inclination. The in-scale models are designed with Rhinoceros software and the dry joint individually shaped voussoirs are obtained by the application of multiple layers of powder material to adhesive layers. The models are designed with similar geometrical features, with a mean radius of 350 mm. It is worth noticing the use of an uncommon solution in the realization of the centering: in spite of the classical convex shape, used in the masonry common practice, the model is assembled on concave support adhering on the extrados of the in-scale vaults, subsequently tilted on the supports. The data acquisition is performed with the usage of high-frequency cameras to catch the frames of the collapse mechanisms.

Rossi et al (2015) report the results of an experimental campaign performed on a 1:5 in-scale model of a cross vault (Fig. 3.21) and compare to the results obtained with a custom numerical tool, in order to validate it. The research aims to simulate the in-plane displacement capacity of a masonry vault, through the use of a model corresponding to a real masonry cross vault of 3,1 m of span, under seismic actions. The model is designed and discretized with trapezoidal-shaped voussoirs and special pieces to realize the ribs of the vault. All the components are obtained by 3D printing with plastic material and weighed down with the insertion of little metal plates inside specifically designed pockets in the voussoirs to prevent accidental failures of the model during the experimental activities. Four centerings mounted on rails are used to assemble the voussoirs and the four abutments are rigidly fixed on as many metal plates connected by metal rods to activate the displacement mechanism and measure the force. With this set-up configuration, both simple and pure shear tests and opening tests are performed. The data concerning the forces are acquired by the use of load cells near the mechanism actuator and strain gauges applied to the activation bar, while the geometrical data are captured with high-frequency and high-resolution cameras.

A 1:10 model of a pavilion vault is analysed in Rossi et al, 2016 (Fig. 3.22), by performing opening tests to evaluate the crack pattern, the ultimate displacements, and the collapse mechanism, and by comparing experimental results with observations of real structures in historical masonry buildings by the evaluation of the line of thrust. The model is realized fabricated with dry joint trapezoidal cross-section voussoirs, de-

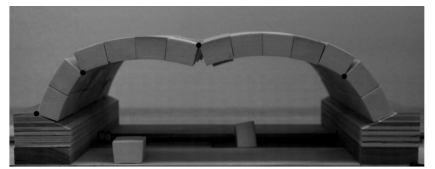


Fig. 3.20

Barrel vault model, hinges opening under opening displacement,
from Shapiro, 2012.

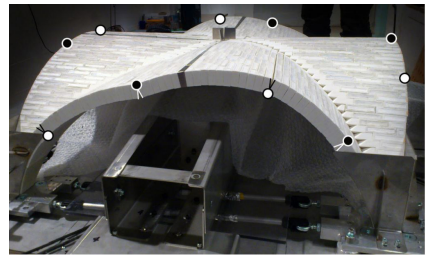


Fig. 3.21

Cross vault model, hinges opening under in-plane displacement,
from Rossi et al, 2015.

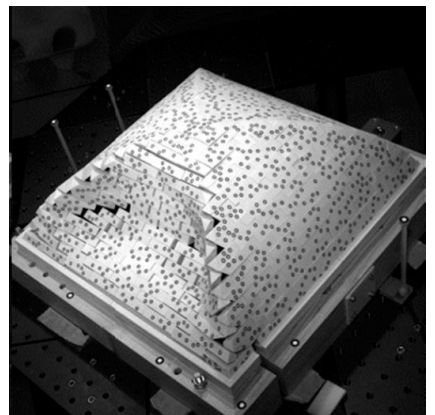


Fig. 3.22

Pavilion vault model collapse under opening displacement,
from Rossi et al, 2016.



Fig. 3.23

Cross vault model, hinge opening under shear displacement,

from Carfagini et al, 2018.

signed as an ensemble of multiple bricks and mortar joints in the same position as in a real structure. This solution allows the easing of the work by reducing the number of voussoirs and limiting the use of extremely tiny pieces. Due to the closed shape of the pavilion vault, the centering is simply lowered down under the structure without a complete removing, to not interfere with the experimental set-up composed of multiple moveable plates. In this way it is possible to test different conditions of displacement by changing the quantity of the abutments involved in the movement. The data acquisition is performed by the four optical sensors mounted on fixed tripods, one for each side of the vault. The sensors are able to evaluate the displacements of the single voussoirs by tracking the univocal four-dotted patterns printed on each piece.

In 2018, the research published by Carfagini et al. aims to assess the behaviour of a cross vault and its arches in the field of large displacement of the supports. The model reproduces the geometry of a real quadripartite cross vault in the lateral nave of the Holyrood gothic cathedral in Edinburgh. The 1:4 in-scale model Fig. 3.23), of about 1 x 1 meters of base and 0,76 m of rising, is realized of wooden blocks bonded with lime mortar. The construction of the model follows the real practice in this building typology, with the assemblage of the main arches and of the vault on light partial scaffoldings. The vault model is realized upon four concrete blocks as abutments and a rigid wood panel is attached to one of the arches to simulate the rigid response of the external walls of the cathedral. A simple shear test is performed by sliding of two abutments on rails, to avoid buckling phenomena, and the geometrical data are collected with the usage of a total station by monitoring selected points of the extrados (main arch, ribs, a portion of the shell, etc.). The experimental results, in terms of displacements and crack pattern, are compared with the one obtained with linear and non-linear analysis tools. Another research, performed with the same methodology exposed in the previous one, is reported by D'Altri et al, 2019. In particular, the research is focused on the use of a 1:12 model of a pointed barrel vault reproducing the typical structures used in Scottish architecture of the XVth century (Fig. 3.24). The model is made of macro wooden blocks, approximating the measure of a group of blocks in the real construction. These blocks are bonded with lime mortar. The model is tested under the linear displacement of one of the abutments by pulling down one of the corners of the vault. The geometrical data are acquired with a total station, while the cracks are hi-



Fig. 3.24

Pointed barrel vault model, hinge opening under linear vertical displacement,

from D'Altri et al, 2019.

ghlighted in the image acquisitions by the application of dye material inside the hinges. The experimental results are used to validate the numerical tool developed for this kind of vault and then other displacement conditions are tested on the same geometry by computational simulations.

4. Description of the case studies

4.1 Identification of case studies

The models tested in the present research are based, directly or indirectly, upon the in-scale models tested in Rossi, 2015 and Alfonso et al, 2020, both previously exposed in the section about the state of the art in the use of physical models in structural analysis.

In the first study, a 1:5 in-scale model of a cross vault is built and tested, until collapse, under different loading conditions. The model is produced as a replica of a typical square base cross vault, in masonry with 3,5 m of span, and made of typical brick blocks 60 x 120 x 240 mm. The brick arrangement is derived by a review of scientific literature (Cangi, 2005). The use of cross vaults with these dimensions is typical both in religious and civil Italian buildings, with many examples in churches lateral nave or transect and in residential buildings porticos. In particular, in this work, two convergent slices of the ideal cross vault model are evaluated (Fig. 4.1) with a graphical method (Mery, 1840), to estimate the line of trust (Fig. 4.2) in the static limit analysis perspective (Heyman, 1995). This method consists of a graphical schematization of half an arch (in presence of symmetric structures) into separate voussoirs, between a range of 90° and 30° in the angle of embrace. The thrust line is constructed with a funicular polygon made by the voussoirs loads summed into a forces polygon. Due to the indeterminate nature of the problem, the finding of a single thrust line implies the stability of the section. After that, the analysis is performed also on the diagonal ribs.

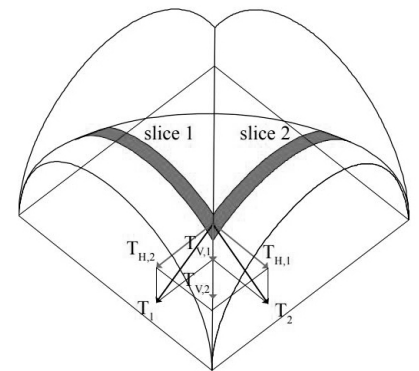


Fig. 4.1

Typical subdivision of a cross vault into slices to perform the graphic static limit analysis.

From Rossi, 2015.

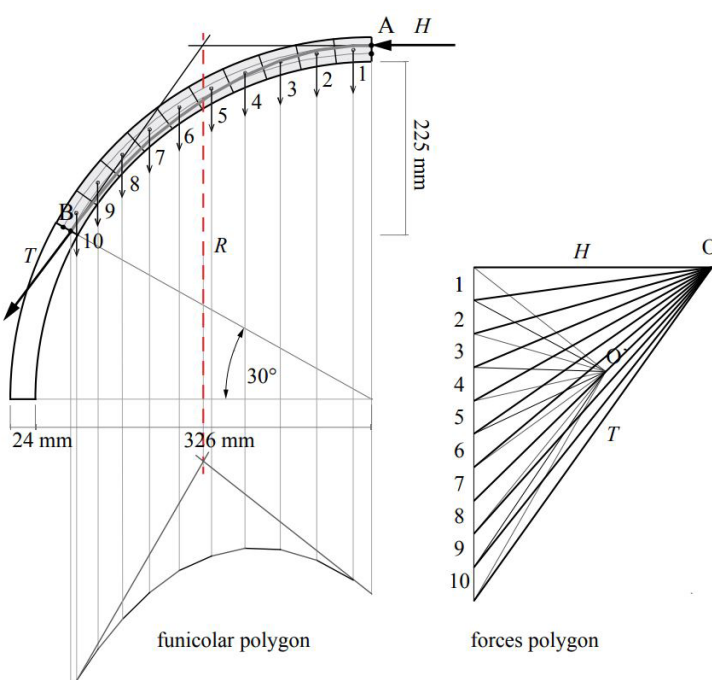


Fig. 4.2

Graphic static limit analysis performed on the slice of a typical cross-vault.

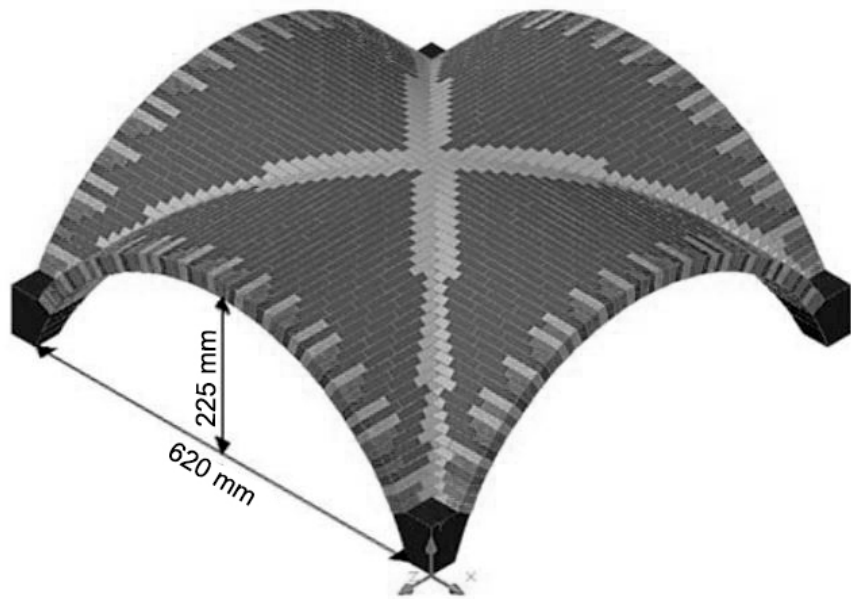
From Rossi, 2015

After the analytic response on the arch stability, the model is designed and constructed starting from head arches with a span of 620 mm and a rise of 225 mm and 1032 custom shaped voussoirs, shaped to follow the several portions of bricks and joints.

Fig. 4.3

In-scale cross-vault model.

From Rossi, 2015.



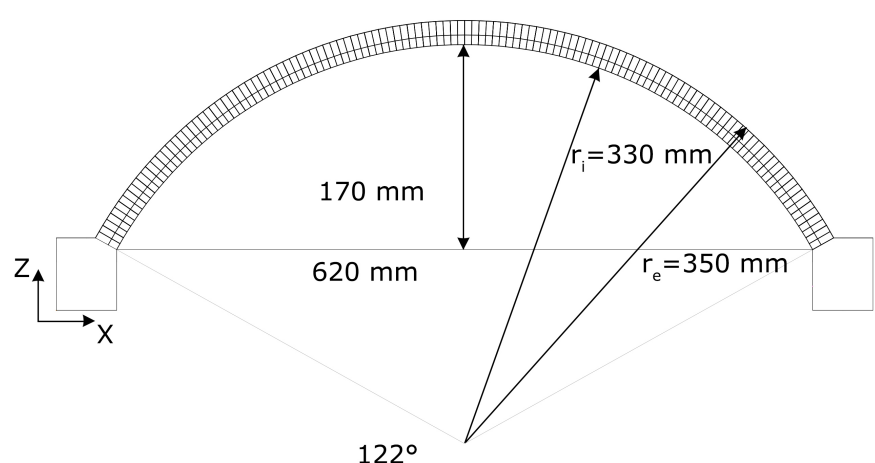
The work presented by Alfonso is directly referred to the one exposed in the Ph.D. thesis of Rossi. In fact, the in-scale arch model tested is the reproduction of one of the head arches of the cross-vault model exposed before. This allows the models' behaviour to be compared by basing new research on geometries tested and well documented in scientific literature. The arch has the same 620 mm of net span and 170 mm of rise, in virtue of the minor angle of embrace considered (122°), with an internal radius (r_i) of 330 mm and an external radius (r_e) of 350 mm (Fig. 4.4).

The experimental campaign of the present thesis, as declared in the introduction, moves from this last experience, with

Fig. 4.4

Segmental round arch: geometric features.

Courtesy of Marco Alfonso.



the aim of investigating the different behaviour of the arches in relation to their brick arrangement. For these reasons, the geometry of the models, exposed in the following sections, derives directly from the one tested by Alfonso et al., in virtue of the usage of the same experimental set-up to impose the displacement, with slight variation in the measures.

4.2 Arch Models

A new centering is realized to perform the tests of the present thesis work, as reported in the previous section. The net span and the rise of the arches are fixed respectively to 600 mm and 182 mm, adapting the other dimensions to the geometry of the existent device. The geometrical and three-dimensional design of the arches is performed with Autodesk AutoCAD: starting from fixed dimensions, such as the radii and the span, various designs are evaluated to optimize the number of bricks and the joint dimension in relation to the overall geometry: the design process, started with the arch model with radial arrangement of the bricks, involves several trials compared with experimental results, before the reaching of the final configuration. As will be reported in detail in the Tab 7.1, at least three voussoirs discretization configuration are tested, respectively with 62, 69, and 65 bricks. The first two are discarded because of the mortar joint dimension: too big in the first case and too small in the second case. After the experience gained with the first arrangement, a new typology of model, with vertical arrangement, is designed by following the same principles. In the final configurations, the 1:5 in-scale arch models correspond to full-scale arches with 3 meters of net span and about one meter of rising, representing the typical dimensions of arches in a historical masonry portico.

As stated in the Introduction, the main aim of the research is to investigate the different behaviour of masonry spatial structures with the same overall geometry but different brick arrangements. Two arrangements are selected to be tested, among the various exposed in the Ch. 2 in virtue of their common use and the ease in the construction:

- **Radial arrangement (AR)** (Fig. 4.5): the arch is composed of a single row of bricks arranged orthogonal to the main vertical plane of the arch. The bricks are laid vertically on their short edge (rowlock orientation) (Fig. 4.6). With the use of these brick arrangement, the arch has a single type of transversal bed joints, wedge-shaped, laid between

Fig. 4.5

Arch with radial arrangement of the bricks: isometric view.

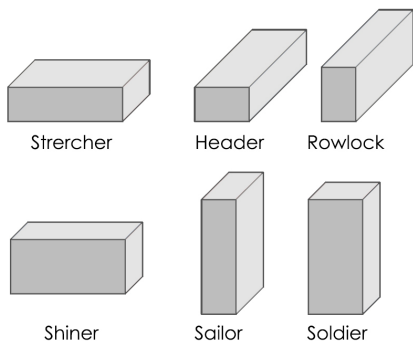
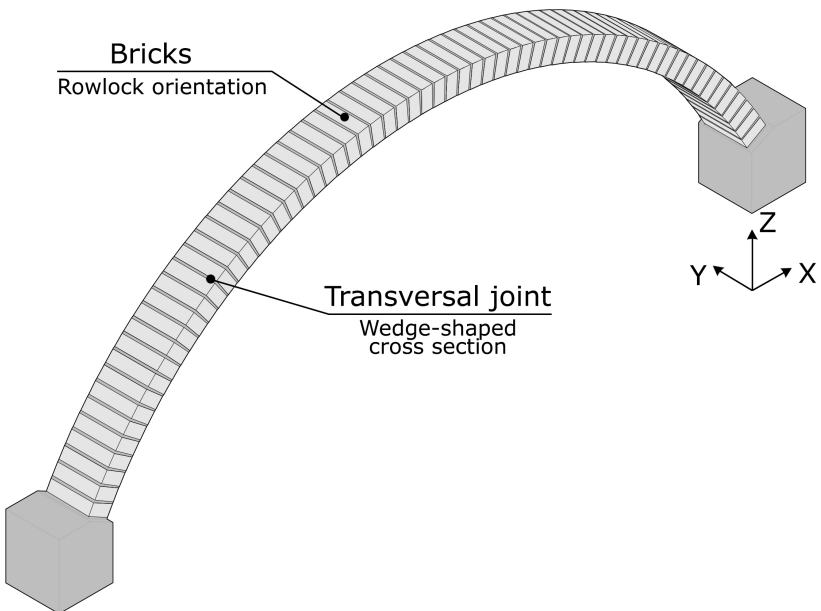


Fig. 4.6

Nomenclature of the typical brick orientations in traditional masonry.

the major faces of the bricks. The final configuration of the arches models with RA involve the presence of 65 cement-based bricks each and wedge-shaped mortar joints with variable thicknesses between 1,3 mm and 1,9 mm.

- **Vertical arrangement (AV)** (Fig. 4.7): the arch model has a similar geometry to the one of the arches with AR arrangement, with the principal variation in the shiner brick orientation. The use of four rows, forming four parallel arches, is preferred to a configuration with three arches (with a depth more similar to the AR) in virtue of major out-of-plane stability and a higher number of joints, involving higher possibilities in evaluating the collapse mechanism. Due to the presence of multiple rows of bricks, the bed joints are divided into two typologies: shorter transversal wedge-shaped joint, between each pair of bricks laying on the same arch, with measures between 28 mm and 1 mm, and longer longitudinal joint with rectangular cross-section, laying between each arch, with a thickness of 5 mm. The configuration of the arches with VA involves the presence of 74 cement-based bricks for each model organized in two couple of arches composed respectively by 18 and 19 bricks.

Both arrangements are typically used in historical masonry (Adam, 1989, Huerta, 2009, Piccoli, 1991) and well documented in the scientific literature (Heyman, 1995). The vertical arrangement in arch construction is quite an atypical solution compared to the most common radial one. Nevertheless, a

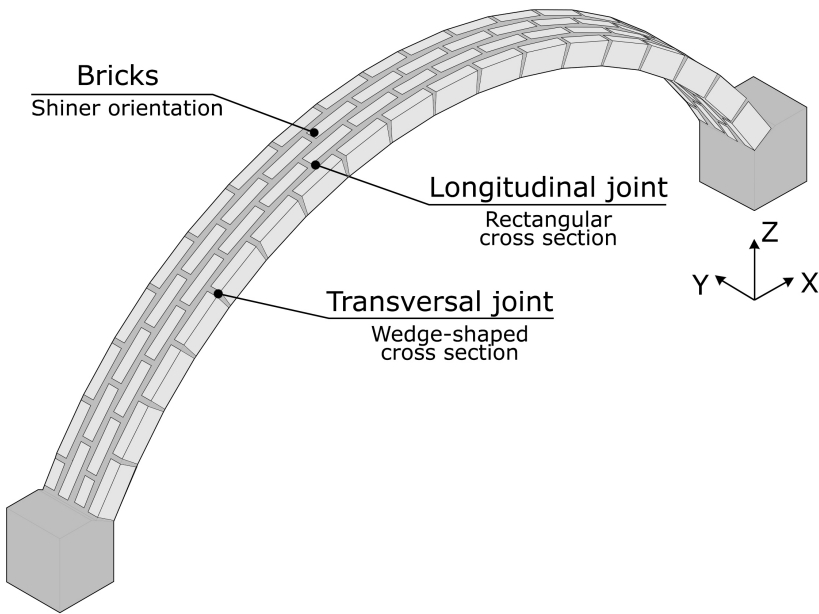


Fig. 4.7

Arch with vertical arrangement of the bricks: isometric view.

sparse number of arches built with this construction pattern can be found in ancient architecture: some examples are present in ancient Roman architecture, such as in an access corridor to the furnaces of the Baths of the Six Columns in Ostia (Fig. 4.8), from the first half of the II century AD, where the bricks are oriented orthogonally to the arch main plane but with a stretcher orientation. On the other hand, the radial arrangement represents probably the most common solution in masonry arch building. Examples of this technique can be found in the majority of simple round arches from all historical periods. It is used commonly in single or multiple concentring rows: the Aqua Alexandrina aqueduct (Fig. 4.9), built in AD 226 and still visible in Rome, presents both the single row radial arrangement of the bricks in the lower arches and the double rows radial arrangements on the upper arches.

As a result of what exposed, the arch models are designed with an external radius (r_e) of 360 mm and an internal radius (r_i) of 342 mm (Fig. 4.10, 4.11).



Fig. 4.8

An access corridor to the furnaces of the Baths of the Six Columns in Ostia, second century AD.

From: Adam, Roman building, 1989.



Fig. 4.9

Portion of the Aqua Alexandrina aqueduct, 226 AD, Rome.

From: romanacqueduct.info.

Fig. 4.10

Arch with Radial arrangement of the bricks: geometric features.

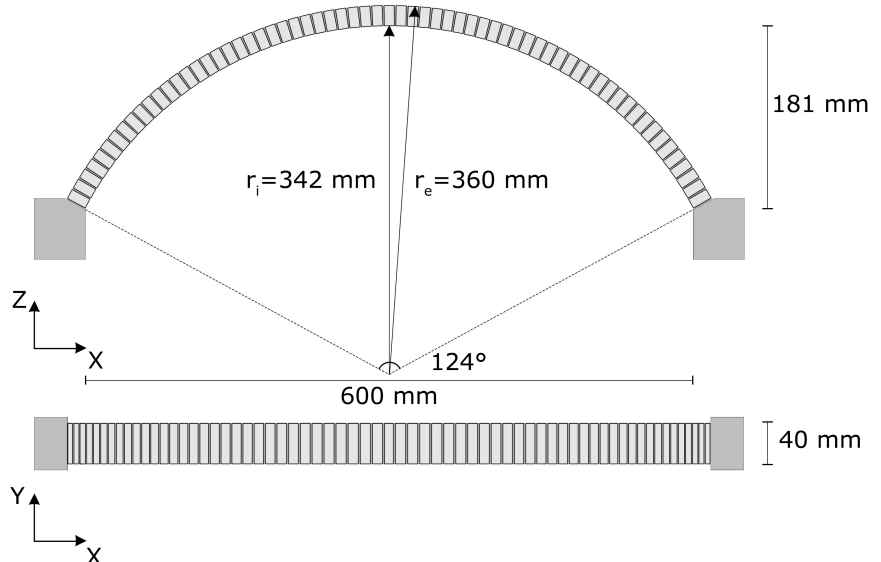
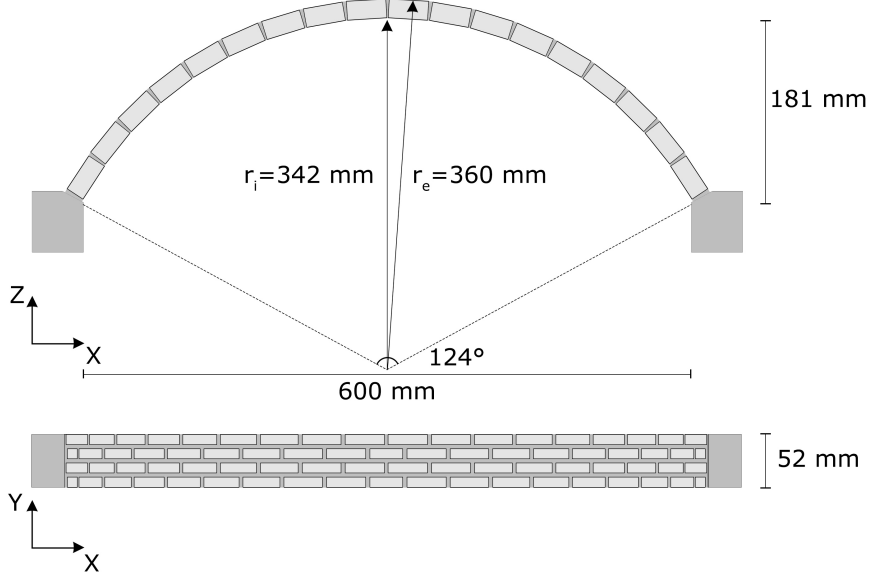


Fig. 4.11

Arch with Vertical arrangement of the bricks: geometric features.



4.3 Vault Models

The in-scale vault models are designed on the base of the arch models previously investigated: the nature of the barrel vault, with the cross-section comparable to an arch, makes it possible to use the experience gained both in the geometry design and manual modelling and construction. The main dimensions of the model are fixed by scaling the measures used in the arch models. On one hand, the overall geometry of the vault model is not completely comparable with the arch models, on the other hand, the use of smaller spans and rises allows the construction of a larger number of models in a reasonable amount of time, estimated on the base of the direct experience in construction during the first phase of the experimental campaign on the arch models. The rise of the vault is fixed to 121 mm, while the net span 400 mm and

matched with the same length, obtaining a segmental barrel vault with a square base. The geometrical and three-dimensional design of the vaults is performed with Autodesk AutoCAD, as during the arch design: besides the evaluation of the various designs, to optimize the number of the bricks and the joints dimension in relation to the overall geometry, the use of a three-dimensional design tools allows to better evaluate the features as for the joints geometry and dimension definition, figuring out also the mortar quantity necessary to the whole model construction. These 1:5 in-scale models correspond to a full-scale vault with 2 meters of net span and about 0,6 meters of rising.

As for the arch models exposed before, two different brick patterns are used to investigate the different behaviour under the same imposed shear displacement. The two tested arrangements are:

- **Radial arrangement (VR)** (Fig. 4.12): the vault model is composed of multiple rows of rowlock oriented bricks, placed orthogonal to the main vertical plane of the vault. This arrangement involves the use of bricks parallel to the abutment direction. It has two different types of bed joints: the main wedge-shaped longitudinal head joints between the major faces of the bricks, with a 4,2 mm base, and the minor rectangular cross-section head joints between the bricks of each longitudinal row, measuring between 2,7 mm and 1,8 mm.

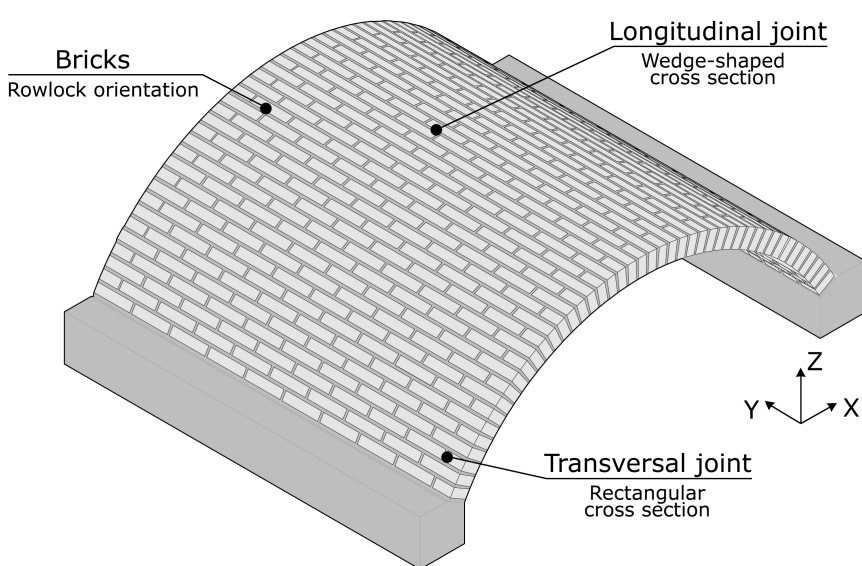


Fig. 4.12

Vault with Radial arrangement of the bricks: isometric view.

- **Vertical arrangement (VV)** (Fig. 4.13): in this vault model the bricks are laid with a shiner orientation in parallel rows

to the main vertical plane of the structure, in the same configuration exposed for the AV models. Multiple brick rows are used in the building of the vault model to obtain an equal mass to the vaults with a VR arrangement. The transversal joints measures 4,2 mm x 0,8 mm while the radial joints have a rectangular cross-section with a base of 1,3 mm.

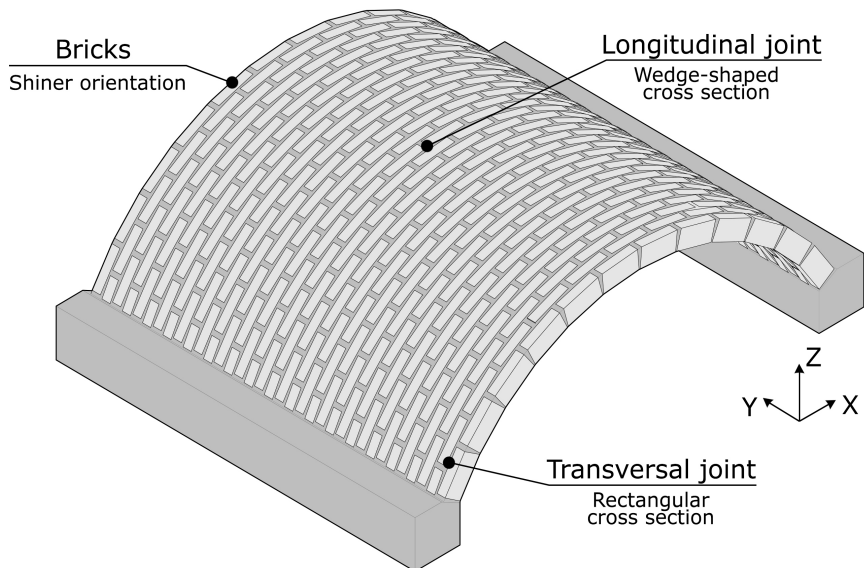


Fig. 4.13

Vault with Vertical arrangement of the bricks: isometric view.

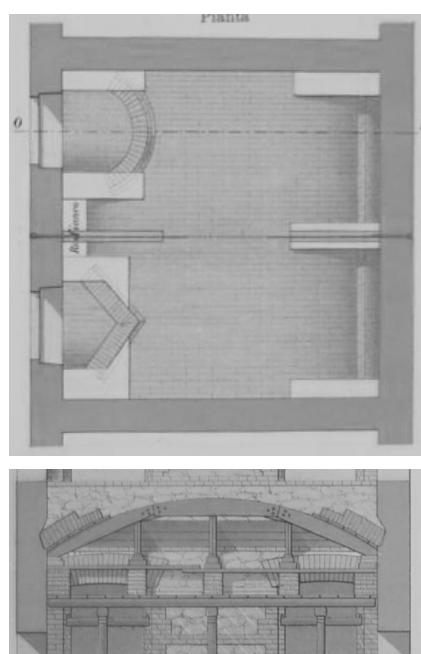


Fig. 4.14

Top: vertical arrangement of the bricks in a composite barrel vault.

Bottom: centering design for a barrel vault with radial arrangement.

From: Musso e Copperi, Particolari di costruzioni murali e finimenti di fabbricati, 1887

Both the tested arrangements are used in traditional masonry and are well documented in the literature. Notably, both solutions are reported in construction manuals (Fig. 4.14) still at the end of the XIX century, meaning they were widely adopted in masonry common practice (Musso e Copperi, 1887). The radial arrangement is probably the most used solution in vault construction: it is worth noticing that in Piedmont, during the XVII and XVIII centuries, considered as the masonry vault golden age in Italian architectural heritage (Spallone, 2012), this arrangement represents the common solution used as a base to the most complex shaped vault arrangement (Piccoli, 1999). In the sources, the vertical arrangement is typically used for minor portion of for vault of smaller dimension. A great tradition in Nubian architecture involve the use of the vertical arrangement of the bricks, where the tilting of the brick courses with a certain angle allows the use of parallel arches to provide the possibility of bricklaying without the use of centering (Wendland, 2006; Huerta, 2009).

As the result, the vault models are designed with an external radius (r_e) of 249 mm and an internal radius (r_i) of 229 mm. Both models present the same span, the same rise and the

same depth (Fig. 4.15, 4.16). All the models are composed of 450 cement-based bricks with a similar global mortar quantity.

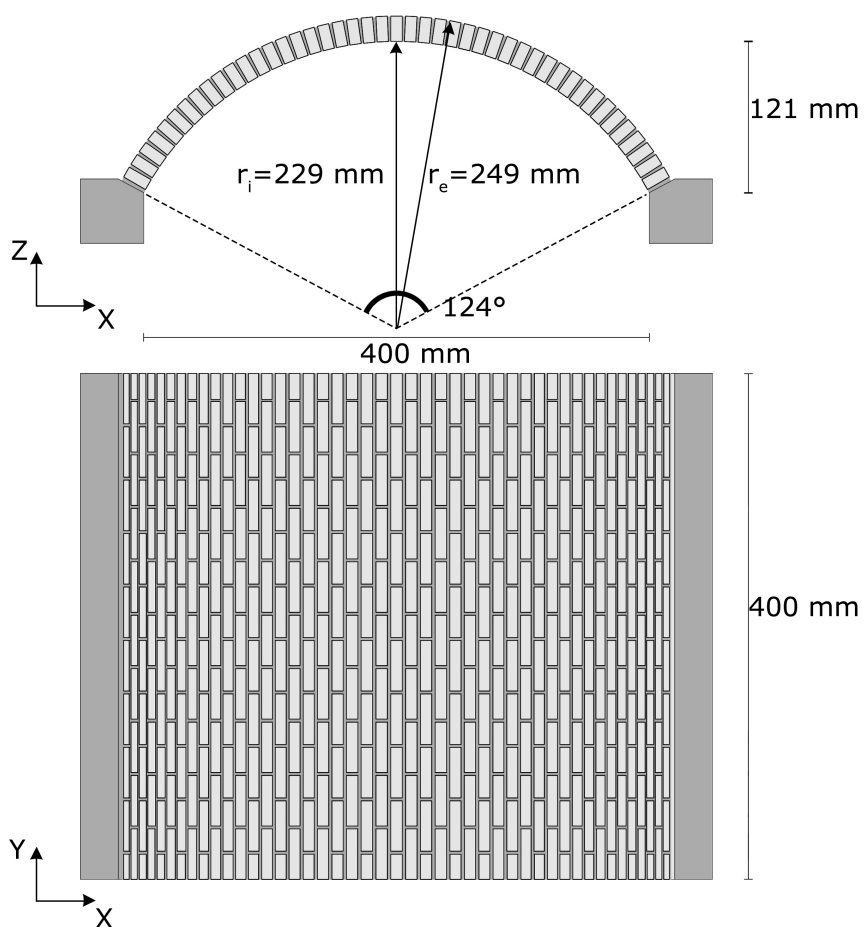


Fig. 4.15

Vault with Radial arrangement of the bricks: geometric features.

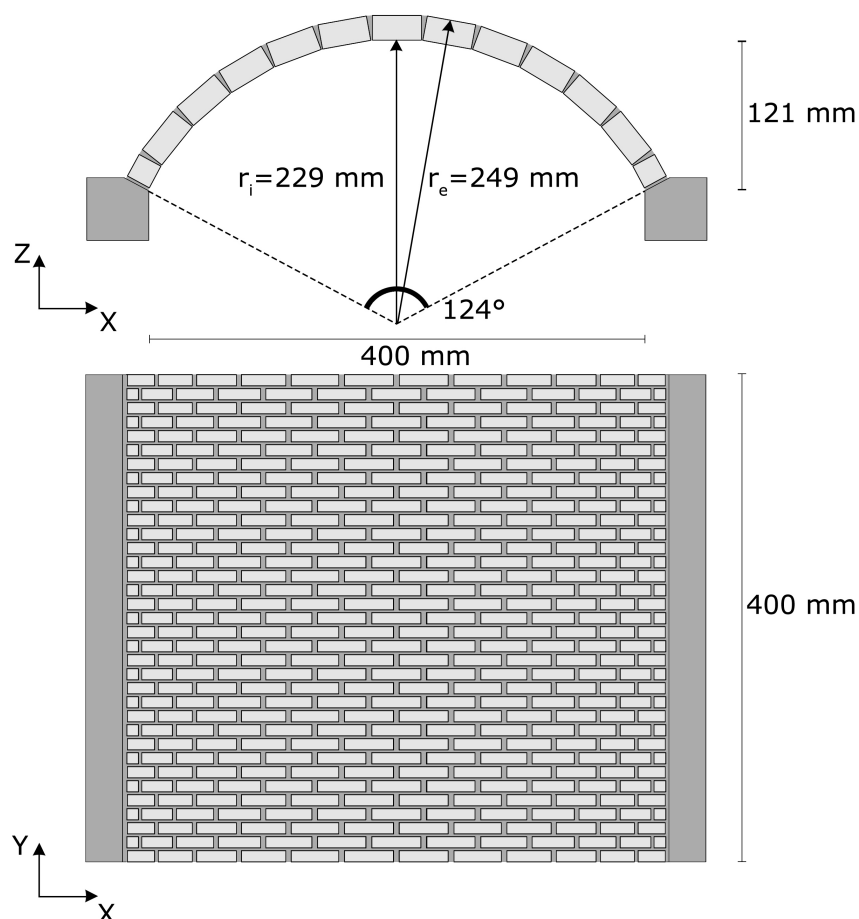


Fig. 4.16

Vault with Vertical arrangement of the bricks: geometric features.

5. Construction of the models

5.1 Materials of the models

5.1.1 Premise

The present work is inspired to the experimentation started by Fiammetta Venuti and Marco Alfonso (Alfonso et al. 2020) concerning the in-scale model of an arch with radial arrangement of the bricks subjected to opening of one of the abutments. The materials adopted in the test and the obtained results were used as basis for the tests carried out in this work and for the optimization of the experimental process. All the considerations exposed in this chapter are referred to the same brick arrangement: the tests on radial arches, more numerous than the others, have been used to compare materials and techniques, to develop a methodology of work and to achieve confidence with the manual brick laying and the modelling of the structures.

The research of suitable materials occupied a great part of the present work: starting from solutions well documented in the literature (reported in ch. 3.3 , “Contemporary use of structural models” paragraph), the tests allowed to optimize the process of modelling and testing, according to the specific needs of the experimental campaign. All the remarks reported in this chapter are based on direct empirical observation linked to the possibility of developing the work according to theoretical knowledges of structural mechanics and structural engineering. All the choices were made on the base of operational considerations including e.g., availability of materials, ease of fabrication, possibility of reducing errors by using professional tools, duration of the processes and economical evaluation. Moreover, the COVID-19 pandemic situation, occurring during the whole period of the experimental campaign, strongly influenced the tests development, especially because of the reduced availability of materials, laboratories and professional tools.

5.1.2 Mortar

Two different types of mortar (tab. 3.1) have been used for the bricklaying of the arches, tested on the same geometrical parameters (radial arrangement with 65 voussoirs), and both are derived from scientific literature about experimental studies of masonry models behaviour.

Tab. 5.1

Mortar mixes tested during the experimental campaign.

MIX	COMPONENTS
MIX 1	3 pt. Silica sand - 1 pt. Lime - 1 pt. Water - PVA glue
MIX 2	3,2 pt. Silica sand - 1 pt. Lime - 0,88 pt. Water

- **Mix 1:** This mix was used for several experimental studies about masonry models (D'Altri et al., 2019). In the cited study, the ratio between water and the other components of the mix was not specified, it was therefore assumed 1 part of water for construction purposes. This mortar has weak bond power that allows the failures to occur along the joints, according to the classical Heyman's theory (negligible tensile strength). The use of a little amount of glue in the mix leads to a better workability of the mortar.
- **Mix 2:** This mix of a quasi-brittle mortar aimed to reproduce Roman's concrete for models with low cohesive masonry and no-negligible tensile stress (Albuerne et al., 2019). The result of this mix is a drier mortar than the one previously tested, with worse workability for the building of the structure.

The quantity of water expressed in the mix descriptions must be intended as the initial amount of liquid with slight variation during the building process to obtain the desired workability of the mortar. The decision of testing two different mixes of mortar derives from the hypothesis of a non-negligible tensile strength developed by the joint on a 1:5 scale model differently from a full-scale structure. Despite this assumption is rejected by classical theory, in many historical structures the mortar joint, still weaker than the bricks, applies a resistance to the separation between the blocks. This behaviour, documented for example in Roman concrete vaulted structures, where the bond agent was casted together with stone's shards or bricks (*opus caementicium*), is still visible in the fragment of the collapsed cross vault of the Basilica of Maxentius in Rome (Albuerne and Williams, 2017).

With similar conditions of use (thickness of the joints, geometry of the arch, number of voussoirs) the two mixes don't show substantial differences in terms of maximum displacement or failure mechanism: discarding outlier results, the maximum displacement of the arches with radial arrangement (within the accepted tests) has a mean absolute deviation of 2,79%, considered acceptable for the manual nature of the construction work, while the failure mechanism hasn't shown

significant variation from the expected results linked to the typology of employed mortar mixes. The results of these observations concern the selection of the mix based on operational factors: mix 1 is easier to use than mix 2 due to a minor ratio between sand-lime and water and to the presence of a little amount of PVA glue that helps the workability of the mixture. The mortar made with mix 1 works better on modelling thin and shaped joints with the usage of jigs.

5.1.3 Blocks

The research about the material for the composition of the bricks occupied a fundamental part of the work. A preliminary investigation on the products available on the market showed that 1:5-scale bricks consistent with the research purposes were not available. So, due to the nature of the work, focused on realize and optimize the processes of the research itself, it was decided to realize the bricks starting from raw materials. Properties of the materials like weight, consistency and strength have been taken to account according to production methodologies (possibility of producing a large number of unities, dimensional uniformity, time of production, ease of fabrication).

5.1.3.1 Timber blocks

The first bricks used, fabricated by Marco Alfonso for the preliminary test, were obtained from a spruce lath with thickness of 9 mm, depth of 20 mm and cut in length of 40 mm (Fig 5.1). These blocks were obtained by manual sawing of the timber, so they presented slight dissimilarity among the unities. After the cutting the blocks were covered with a layer of enamel to reduce the absorption of water from the wood in direct contact with the wet mortar. To reduce the uncertainty linked to the length measure of the blocks, some tests on the timber were carried out using computerized numerical control machines for laser cutting: the aim of the test was to obtain monolithic blocks starting from Medium Density Fibreboard panels (two unities of 9 mm and 10 mm thickness were tested). Unfortunately, the machines used were not able to cut through panels of the desired thickness, severely burning the wood and altering the final geometry of the blocks. Considering this, the use of computerized numerical control machines was discarded. The progress of tests on the arches shown several criticisms related to the use of timber. The hygroscopic



Fig. 5.1

Timber block used during the first phase of the experimental campaign.

behaviour of the spruce heavily altered the tests: despite the enamel treatment, the blocks tended to swell while in contact with the mortar, probably due to the high ratio between the dimension of the bricks and the joints, modifying the whole geometry of the arch after the drying. For this reason, the block at the key was always put in place after at least 4 hours after the construction of the rest of the model. This behaviour led to failure of the structure, especially during summertime with uncontrolled temperature and humidity's conditions, when the lack of pressure between the altered quoins did not allow the arch to resist while lowering the centring. Another criticism came out from a physical property of the timber: due to the low density of the spruce, the arch, while standing, was heavily influenced by the vibrations derived from laboratory's activity carried out in the surrounding environment, with visible out of plane oscillations of the structure.

All the exposed factors led to discard the timber for the proceeding of the research, focusing on casting materials, in order to reduce the global uncertainty related to the construction of the masonry models.

5.1.3.2 Cement-based blocks

In order to resolve the issues noticed during the tests with timber blocks, some attempts with casting materials were carried out. Cement was selected as binder and tested in six different mixes, trying to optimize the production and the results. Three parameters were adopted for the selection of the best configuration: the ratio between the components of the mix, the compaction of the material and the time of framework stripping. This last parameter, negligible for a small number of blocks, e.g., the ones necessary for the arches' tests, was crucial for the vaults' tests due to the high number of required blocks.

The firsts three tested mixes, mix 1, 2 and 3, (fig 5.2- a, b, c) were not suitable for use. Specifically, they allowed to highlight some operative aspects useful to optimize the mixes and the process:

- The lack of compaction of the material casted in the mould compromise the geometrical regularity of the block, with air bubble inside the block and often on the surface, as well as the mechanical resistance (empirically tested by falling of the bricks simulating the collapse of the structure);

- The presence of PVA glue (used in literature with binders as lime to improve the mortar) does not significantly improve the workability of the mix for this type of objects;
- Lubricating the mould helps to obtain a perfect shaped block from the form stripping, with less cracking and imperfections.

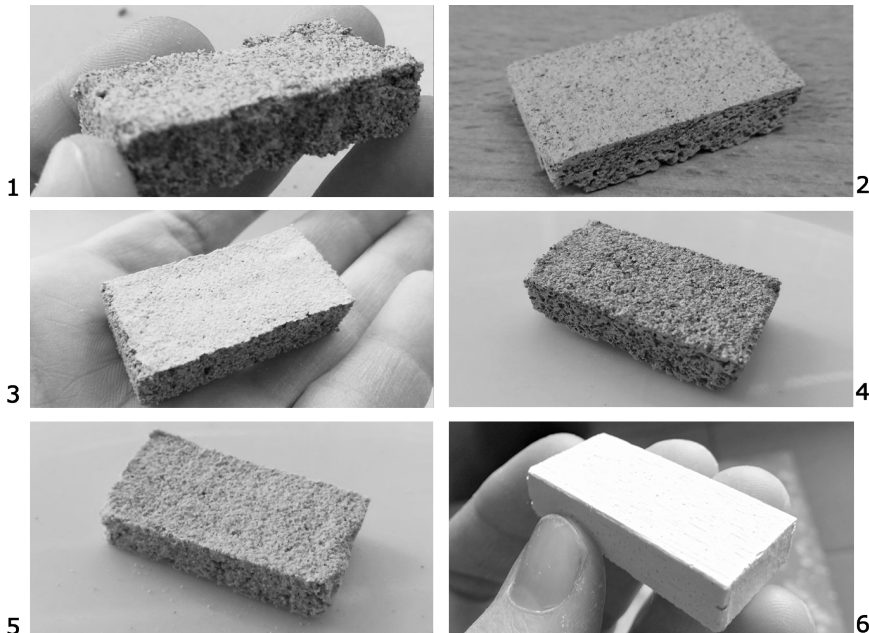


Fig. 5.2

Cement-based brick tested:

Top -Mix 1, Mix 2;
Center - Mix 3, Mix 4;
Bottom - Mix 5, Mix 6.

These observations led to the testing of other three mixes with the same condition of fabrication and drying: reducing the variability only to the presence of sand as aggregate, these last tests gave acceptable results to start using cement-based blocks in the construction of the models. The different nature of the adopted aggregate, quartz sand for mix 4) and silica sand for mix 5, shows negligible differences for the purposes of research but a large gap in the uniformity of the bricks if compared with the mix 6, composed only by cement and water. This mix offers the best solution with the minimum effort and issues: despite a little shrinkage of the material, involving the face exposed to the open air and solved with the usage of sand paper to level the surface, the resultant blocks were much more regular and smooth in comparison to other mixes. The absence of aggregate material, like sand, simplifies the compaction of the casting material with a significant reduction of the air bubble inside and on the surface of the blocks. During the tests, mix 6 was optimized in the time of stripping, from 24 h to 12 h (reported as mix 6.1) (Tab. 5.2), enough for the cement paste to develop the hydration and reach the setting. In order to reduce the abrasion action of the sand-based mortar on the blocks, each unity has been

treated with a ply of concrete impregnating, helping to reuse several times the blocks and preventing the alteration of the shape. The mixes tested are summarized in the following table (Tab 5.2).

Tab. 5.2

Components and features of cement-based brick mixes tested during the first phase of the experimental campaign.

MIX	COMPONENTS	COMPACTION	STRIPPING
Mix 1	4 pt. Quartz sand 1 pt. Cement 2 pt. Water	No	1 h
Mix 2	4 pt. Quartz sand 1 pt. Cement 1 pt. Water	No	1 h
Mix 3	4 pt. Quartz sand 1 pt. Cement 1 pt. Water PVA glue	No	2 h
Mix 4	4 pt. Quartz sand 1 pt. Cement 1 pt. Water	Yes	24 h
Mix 5	4 pt. Silica sand 1 pt. Cement 1 pt. Water	Yes	24 h
Mix 6	2 pt. Cement 1 pt. Water	Yes	24 h
Mix 6.1	2 pt. Cement 1 pt. Water	Yes	12 h

The use of cement-based material allows to solve most part of the issues raised during the tests with timber blocks: higher density, high impact resistance from falling after structure's failure, reusability after coupling with lime and sand-based mortar. In addition, differently from wooden elements, this material allows to shift the focus of the fabrication from the single block's unity to the mould, reducing the effort of precision work to a specific step of the process, simplifying the production of a great number of elements.

In order to optimize the process of blocks fabrication, several moulds have been built searching for the best solution suitable for the work's purpose, with different typologies and materials employed. The first fabricated mould is a 12-unities steel grid (Fig. 5.3), obtained from flat bars (10 mm wide and 1 mm thick) through the use of manual power tools, shaped with half-lap joint to match longitudinal pieces, with steps of 20 mm, and cross pieces, with steps of 40 mm. The result is a grid with both ends opened, used with a stiff panel of Medium Density Fibreboard (MDF) as support for the casting of the material: this panel, supported by simple wooden pieces, which provide a horizontal surface for the bottom faces of the blocks, allows to transmit vibrations induced with the use

of manual power tools for the compaction of the casted mix. This type of mould has shown good results in achieving the desired geometrical shape: the jointed steel elements are stiff enough to be disassembled without deformations that lead to breaks in the edges of the blocks. The use of mineral oil to lubricate the mould helped the extraction of the bricks after the material drying. The limit of the steel-grid mould is in the manual shaping: the accumulation of millimetric errors in the measures due to the use of manual tools represents a criticism in the final uniformity of the blocks.

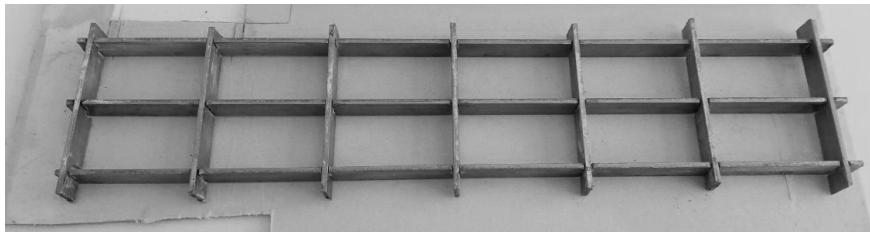


Fig. 5.3

12 unities steel grid mould.

To reduce manual work-based errors, the research has proceeded with the usage of professional power tools and Computerized Numerical Control (CNC) machines available at ModLab Arch of Politecnico di Torino: here, other two moulds have been fabricated, in order to optimize the first 12-unity grid mould used to test the mixes. To increase the precision the work has been carried out with a Trotec Speady 400 laser cutting machine. Due to the inability of cutting steel plates, a 3 mm-thick AVIO plywood panel (plywood with high number of layer, used in static modelling) was chosen by virtue of his high stability compared to other plywood panels of the same thickness. The new mould is a 70 unities wooden grid with open ends (Fig 5.4), having the same spacing, 20 mm x 40 mm, of the previous one. All the pieces were treated with enamel and two plies of wood impregnating agents in order to reduce the swelling, due to the contact of wet casting material with the wood.

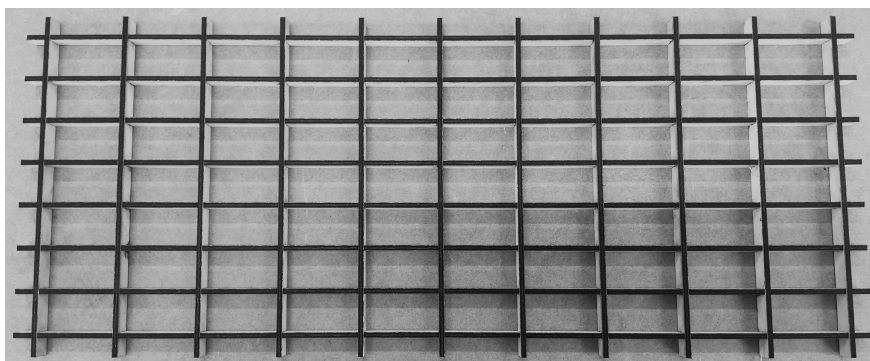


Fig. 5.4

70 unities wooden grid mould, obtained by laser cut.

This treatment failed in the aim of preventing the swelling of the components: despite the application of a mineral oil's

layer, the distortion of the elements after the casting made it difficult to disassemble the mould, increasing the breaks in the edges of the blocks, also due to the lower stiffness of the wood compared to the steel. To overcome this problem, a new version of the same mould was fabricated (Fig. 5.5), by cutting the transversal component of the grid to reduce the whole stiffness of the mould.

Fig. 5.5

70 unities wooden grid mould, second version:

Left - single raw assembled;

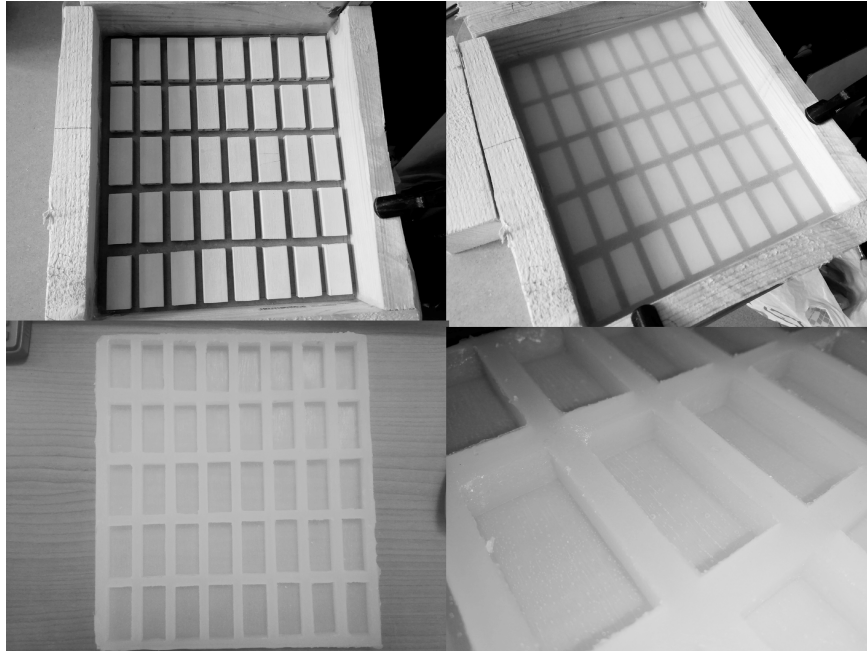
Right- entire mould assembled with stiffen elements.



Each grid component was divided in parts equal to the desired spacing between the longer elements (20 mm), using a T-shape to allow half overlap of the joints. This solution showed better results than the previous version, but still not acceptable from the geometric point of view. Furthermore, the grid required a great amount of time to be assembled and required the addition of stiffen elements (Fig. 5.5) to prevent slipping of the pieces while casting. For these reasons, the grid type mould was discarded.

The best result was obtained with the usage of a bicomponent silicone rubber (Fig. 5.6): this two-parts polymer presents all the advantages related to the needs previously exposed (availability of materials, ease of fabrication, possibility of reducing errors by using professional tools, etc.). With a relatively low cost it offers high properties of durability and ease of casting and stripping out, shifting the focus of the work only on the fabrication of the mould. The negative mould was obtained by casting the polymer inside an open end mould made of spruce lath and MDF panel, in which a series of 40 blocks were fixed to prevent their slipping during casting of the silicone rubber. These blocks were accurately selected among the timber ones previously presented: all the 40 blocks were measured and fixed in the length in order to obtain the best uniformity in the dimensions. The result is a 40-unities negative mould with an open end, used for casting in combination with a rigid MDF panel to transmit the vibrations induced with a power tool into the cement-based materials. The highly elastic nature of the silicone rubber, useful for the stripping out

phase, represents the only limit detected for this kind of work: it visibly dampens the induced vibrations, reducing the efficacy of the compaction, resulting in longer time to obtain acceptable results.



All the operative considerations exposed about the moulds are summarized in the Tab 5.3, where are reported pros and cons of the different typologies tested, in the opinion of the writer.

Fig. 5.6

Silicone rubber mould;

Top - Positive mould, casting of the silicone rubber;

Bottom - negative mould, detail of the mould

Tab. 5.3

Tested moulds comparison.

TYPE	PROS	CONS
STEEL GRID	High stiffness Ease of disassembling High duration Good results in geometry of the blocks Good results in compaction	More difficult realization Impossibility of use CNC machines Longer maintenance phase
WOODEN GRID	Possibility of use CNC machines Ease of realization Short time of realization Good results in compaction	Low stiffness Swelling phenomena Bad results in geometry of the blocks Longer time of assembling Longer maintenance phase
SILICONE RUBBER MOULD	Good results in geometry of the blocks Ease of realization Short time of realization High duration Shorter maintenance phase	Lower quality compaction

5.2 Experimental Set-up

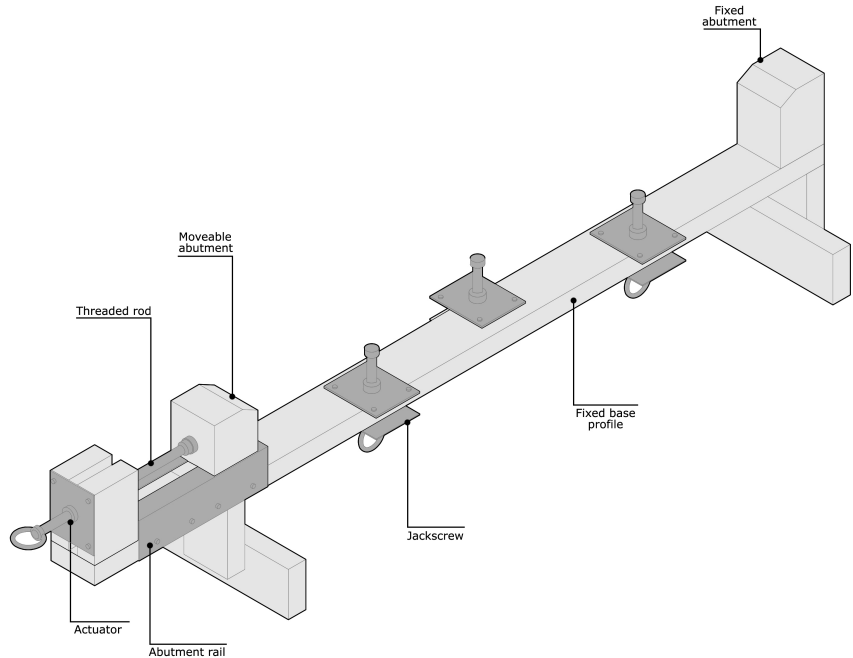
5.2.1 Arch models - Description

The first part of the experimental campaign developed in the present thesis, adopted an existing experimental set-up, tested in Alfonso et al, 2020, mentioned in the previous section.

This set-up is a simple wooden structure with the double aim of allowing the construction of the arch models and imposing a controlled displacement of one of the abutments. The device (Fig. 5.7) is composed of a fixed structure, obtained from spruce lath, with a rigid base profile supported by T-shaped legs, and two wooden abutments, with custom inclined surfaces to contrast arch thrusts.

Fig. 5.7

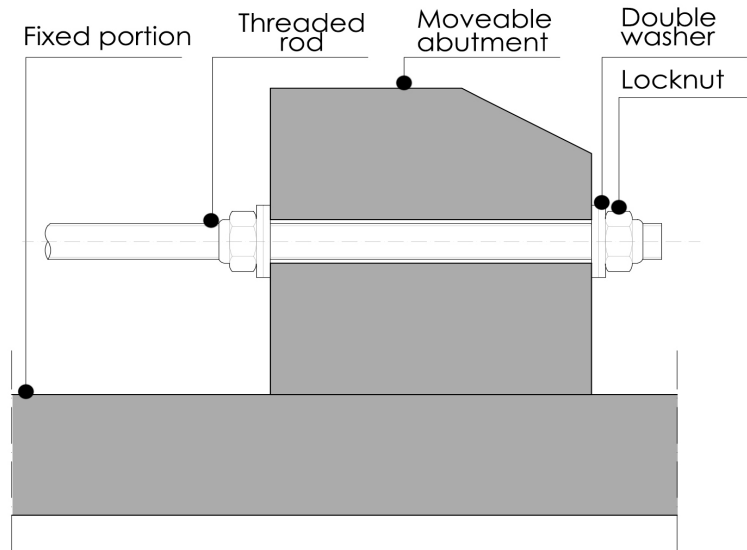
Arch experimental set-up overview.



One of the abutments, free to slide upon the base profile, is linked to a fixed block through a threaded rod inserted in a fixed threaded plate (actuator of the mechanism): the twisting of this rod allows to move the abutment in the direction of the arch thrusts, thus imposing an opening displacement (in the following, this displacement will be intended as the base

Fig. 5.8

Detail of the moveable abutment.



for Opening Tests). The abutment is free to move in virtue of the link solution with the threaded rod, composed of two lock-nuts tightened on the rod with the usage of double washers: this solution (Fig. 5.8) helps to reduce friction between the twisting nuts and the wooden abutment, allowing it to slide on the fixed wooden part.

Two L-shaped aluminium profiles are used as rails for the moveable abutment to avoid buckling phenomena to the rod under the horizontal thrust of the arch model and the vibration induced by the actuation of the mechanism. A second part of the arch's set-up is represented by the centering (Fig. 5.9) that allows the effective construction of the arch models. With a net span of 600 mm and a rise of 182 mm, it has been realized using CNC machines to obtain the best precision in the curved shape. The two sides of the centering are composed of 3 layers of 3 mm Finnboard (panels composed of wood pulp) each, glued together: the exterior layer is 3 mm wider than the interior ones, realizing a rabbet joint for the positioning of a curved laser-cut piece of Finnboard. The structure is stiffened by three internal diaphragms, also supporting the curved surfaces, linked to the side panels with mortice-tenon joints. The centering is now screwed in a spruce lath profile having three blind holes in the lower surface: these holes allow to lift and lower the centering through the use of three jackscrews fixed on the set-up (Fig. 5.7). These jackscrews are composed of two threaded plates fixed on the main device and a threaded rod ending with a locknut: these elements, fitting in the blind holes on the lower portion of the centering, maintain the structure in place during the bricklaying.

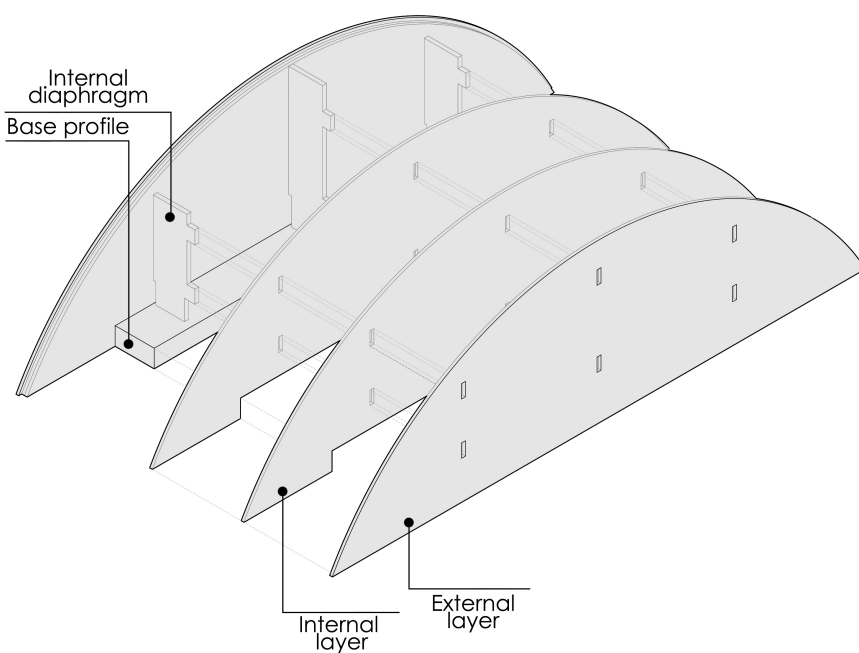


Fig. 5.9

Arch model centering structure.

5.2.1 Vault model

5.2.1.1 Requirements

Starting from the experience gained on the arch models and the research of similar objects in scientific literature, a new experimental set-up is designed to carry on the research also on the vault models. Various possibilities about the set-up fabrication were analysed, considering the aim of the research, acquiring and monitoring techniques, quality control, and availability of professional tools and space for the construction. In the following a list of requirements on which the design (subject of the next section) has focused is reported:

- Possibility to reuse the set-up after the present work for different research purposes: it involves the design of the object with more features than the final ones described in the next Ch.
- Presence of two abutments moveable according to different directions, allowing to perform both opening and shear tests;
- Use of reversible connection to allow changes in the configurations;
- Use of composite elements to allow substitutions for different tests;
- Employment of easy-to-work materials in a way compatible with the available tools;
- Employment of material suitable to CNC machines for the more delicate phases of the work involving the final in-scale model geometry;
- Possibility to fix a calliper to measure the imposed displacement without interferences;
- Building a lightweight but stiff centering to support the dead load of the brickwork;
- Building a support system for the centering to ease the lowering phase;
- Building a system of clamps to ease the construction of models with the vertical arrangement of the bricks.

5.2.1.2 Design and Construction

The construction phase of the experimental set-up is carried on with the help of the ModLabs of Politecnico di Torino: the wood carpentry is realized in the ModLab Design, while

the rest of the construction is performed in the ModLab Arch.

The experimental set-up used for the arch models has been used as a guideline for the design of the vault's set-up: the principle of using threaded rods to manually activate the mechanisms shows good results in the first phase of the research, so it is used as the base for the design of the new testing device. The general idea is to have a base plane where both the abutments can slide on rails, to test the structure constructed above: this panel must be stiff enough not to bend under loads of the centering and the structure and it is dimensioned to host the vault models' abutment on the shortest side, while the length exceeding the net span of the vault hosts the abutments and the excursion for the opening test. The base panel must also include, under the vault model projection, the jackscrews to sustain the centering (Fig. 3.9). A 650x400 mm portion is obtained, with mechanical sawing, from a 19 mm thick MDF panel to realize the base panels of the device.

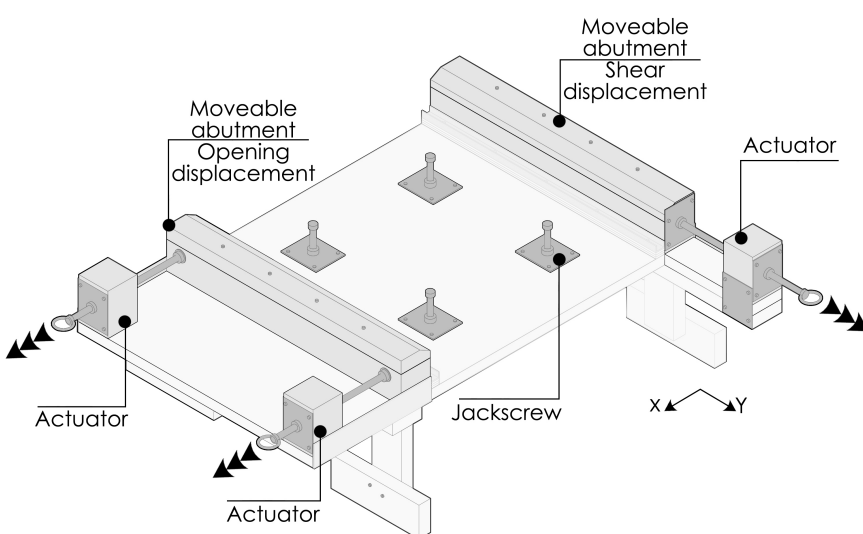


Fig. 5.10

Vault model experimental set-up: main features.

The abutments, simply laying on the base, are designed with two different components: a principal wooden body, mechanically linked to the actuators to impose the displacements, and a second wooden top piece, shaped to contrast the thrust coming from the vault. This solution will allow the testing of different shapes of the vault (in subsequent works) by only changing the geometry of the top portion, without modifying the displacement mechanism. Both the abutments are laterally constrained by metal profiles to void buckling phenomena of the rods, while a third constraint under the vault span delimitates the run of the opening abutment helping to reposition it after each test, without altering the net span of the masonry vault (Fig 5.11). These constraints are also

used as support to disengage the centering during the lowering phase. They are realized by an assemblage of MDF layers with an aluminium U-shaped profile: these pieces are screwed together to the base plane obtaining two 400 mm length support for the centering that also helps to maintain in place the two abutments during their movements.

Fig. 5.11

Schematic description of the centering lowering and disengage from the jackscrews with the composite constraint for the opening abutment.

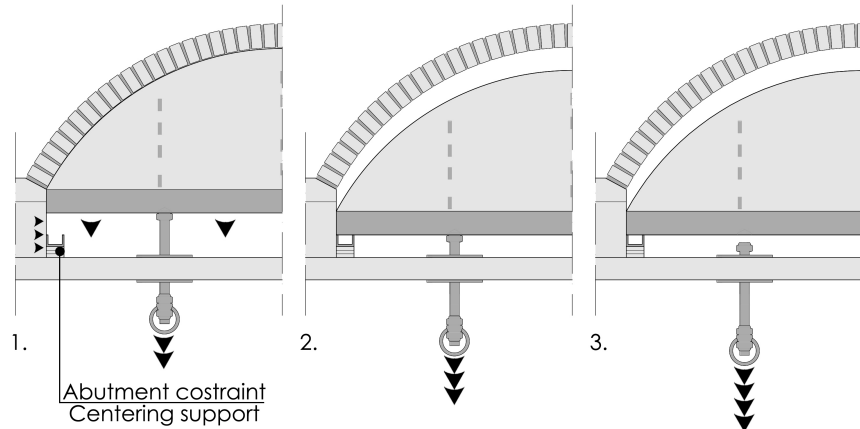


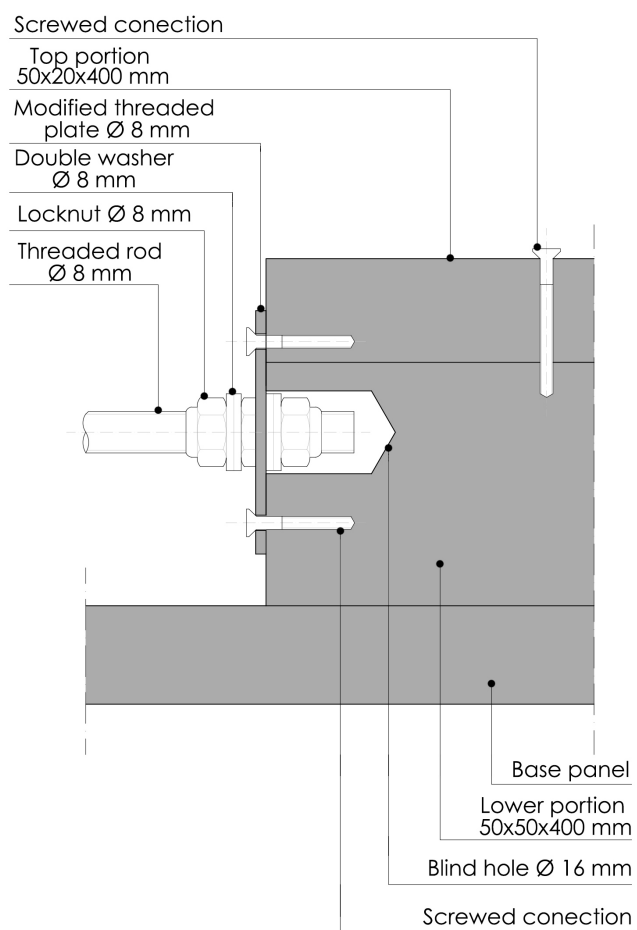
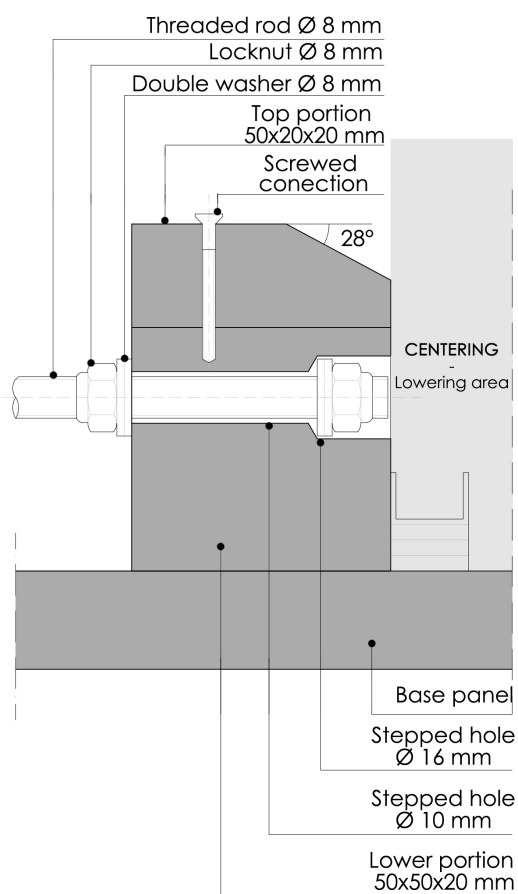
Fig. 5.12

Detail: Opening abutment.

Fig. 5.13

Detail: Shear abutment.

The opening abutment is connected through two threaded rods, inserted on the long side, with two contrast blocks: this solution, on one hand, increases the possibility to apply different movement of the abutment, while on the other hand avoids the possibility of buckling of a hypothetical single central rod and the twisting of the abutment on its plane.



The component, obtained from spruce lath, is pierced on the long side realizing two stepped holes: these holes allow to fix the threaded rod inside the abutment (Fig. 5.12), to avoid interfering with the lowering of the centering. On the top of the main component, for both the abutments, are placed two laths portions with 28° angle cut, to follow the vault models geometry and fit the bricklaying during the construction. The shear abutment has a single rod, on the shorter side, connected with a single contrast block. In this case, a wood profile is added below the main panel to increase the surface on which the shear abutment can slide. The addition of this piece to the principal panel is made possible thanks to the T-shaped legs linked together by a wooden lath to improve the stability of the device. The shear abutment is pierced on the short side where is inserted the threaded rod, connected to the activation block (Fig. 5.13). This solution requires the modification of the plate attached to the abutment to transmit the displacement from the twisting of the actuator to the support. The main device's body (Fig. 5.15) is completed adding four legs to rise the structure, allowing to operate on jackscrews to lowering the centering: these T-shaped legs are composed of a horizontal $150 \times 50 \times 20$ mm component and a vertical $150 \times 50 \times 20$ mm one. They are obtained from spruce lath and screwed together in an orthogonal way. The legs are

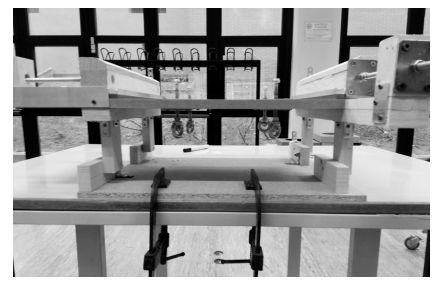
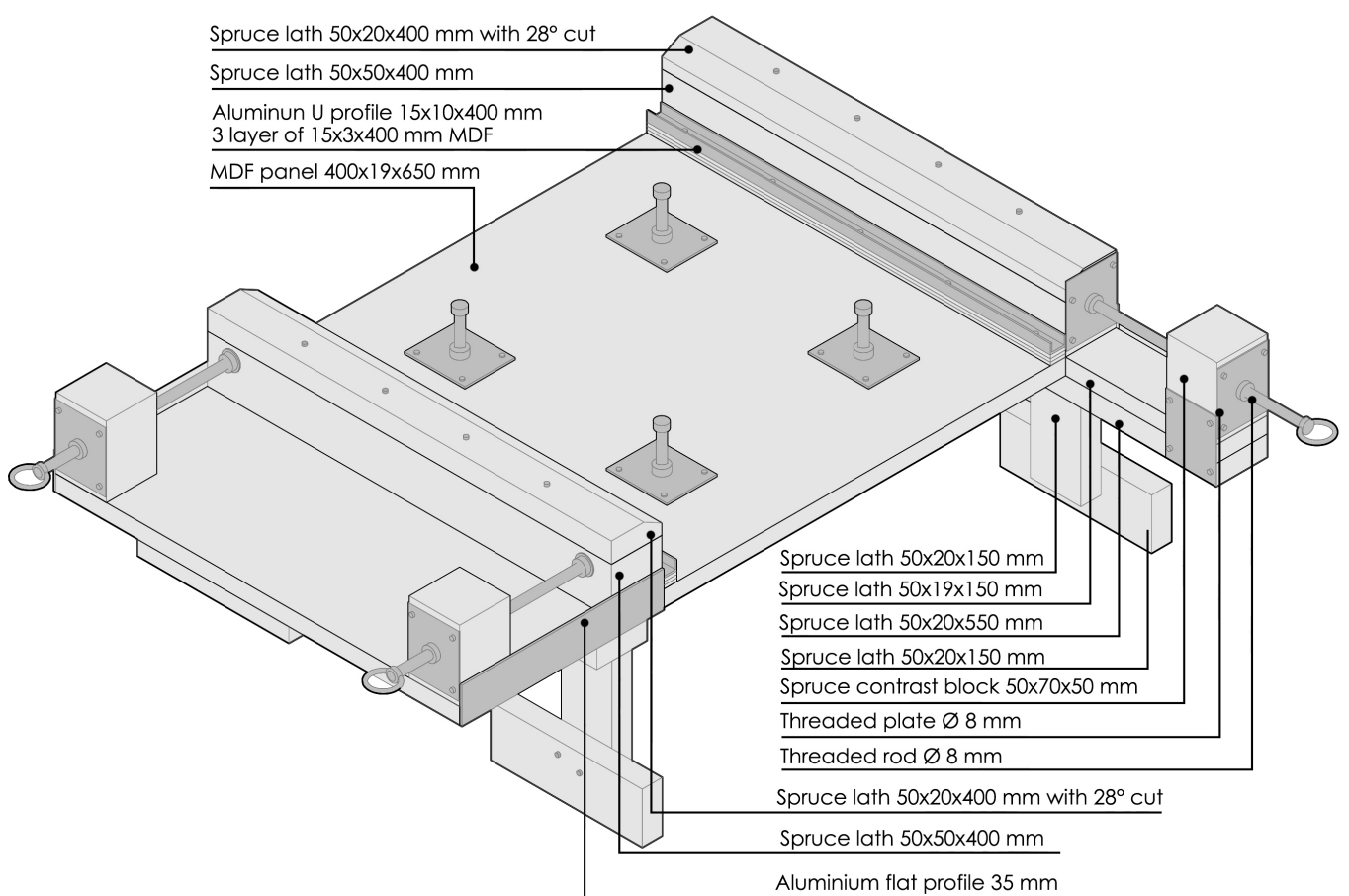


Fig. 5.14

Detail: Overview of the main device with the connection of the device to a fixed plane. In the image are visible the brackets for the connection of the legs from below the sliding plane.

Fig. 5.15

Detail: Experimental set -up main device: description of the components.

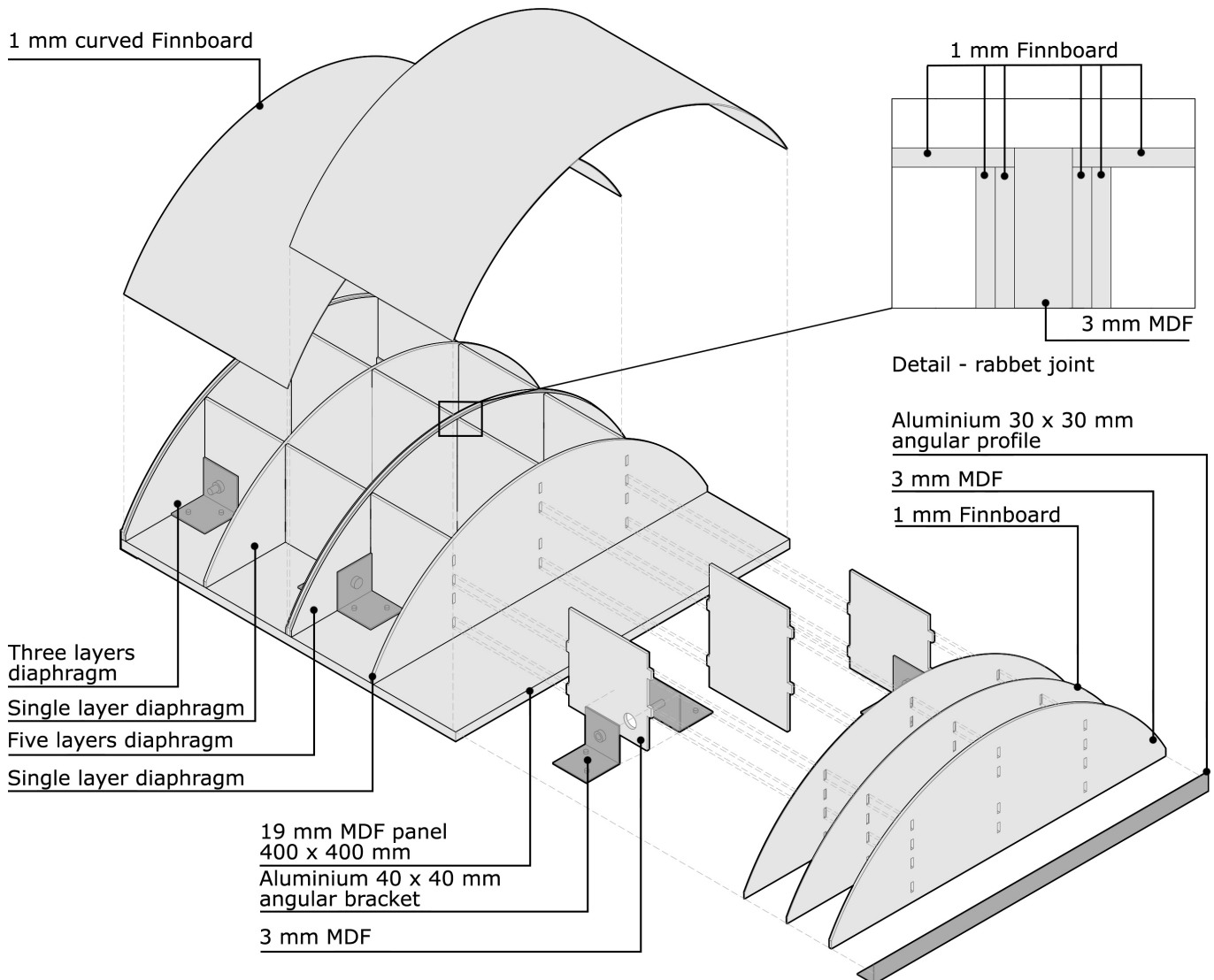


now connected, using screws and metal brackets, with two different wooden profiles forming two frames: these support frames are simply screwed to the base plane from below, to not compromise the abutments' sliding surface. To avoid accidental movement of the structure the main device is now linked to an external wood panel through two metal brackets bolted to the legs and screwed in a wood panel; this panel is then fixed on a table with two woodworking clamps (Fig. 5.14).

The centering is designed with a rigid base panel and a grid structure composed of several orthogonal diaphragms. These pieces are shaped with the laser-cut machine to obtain the best precision and assembled with the same principles tested in the arch centering: external packs of multiple layers are glued together form rabbet joints to insert the curved top plane, while the central pack hosts both the curved panels used for the coverage. The other radial diaphragms are used to give support to these top surfaces. The structure is stiff-

Fig. 5.16

Detail: Vault model centering: description of the components.



ned with the use of orthogonal diaphragms shaped with tenons to fit the mortice joints on the radial ones. The centering (Fig. 5.16) measures a 400 x 400 mm at the base panel. On this base is screwed the orthogonal grid of diaphragms. The main, components are extracted from a 3 mm thick MDF foil while secondary radial diaphragms are obtained from 1mm thick Finnboard foil. The internal orthogonal diaphragms are also obtained from the e 3 mm foil and shaped for fitting tenon-mortice joints with the radial ones. The grid is completed with the positioning of two aluminium angular profile on the heads of the centering to protect the wood during the slide on the metal supports when the centering is disengaged from the jackscrews during the lowering. The centering structure is finished with the addition of curved surfaces for the support of the brick during the vault construction.

The device and the centering are now matched for determining the position of the four lifting mechanisms (Fig. 5.17). The two base panels are pierced together with precision tools to ensure the best correspondence in the assemblage. On the main device panel are realized passing through holes, while on centering panel are realized blind hole to host the lifting mechanism ends. Two threaded plates are used as a base to activate the pulling and lowering mechanism of each jackscrew (Fig. 5.18), composed of simples threaded rods and

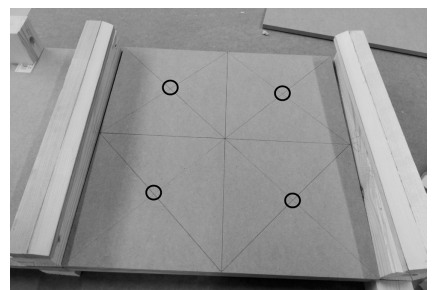
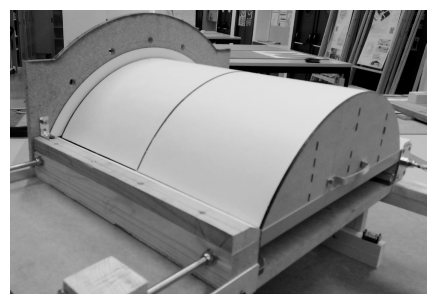


Fig. 5.17

Detail The centering assembled and matched with the main device to determine the position of the jackscrews.

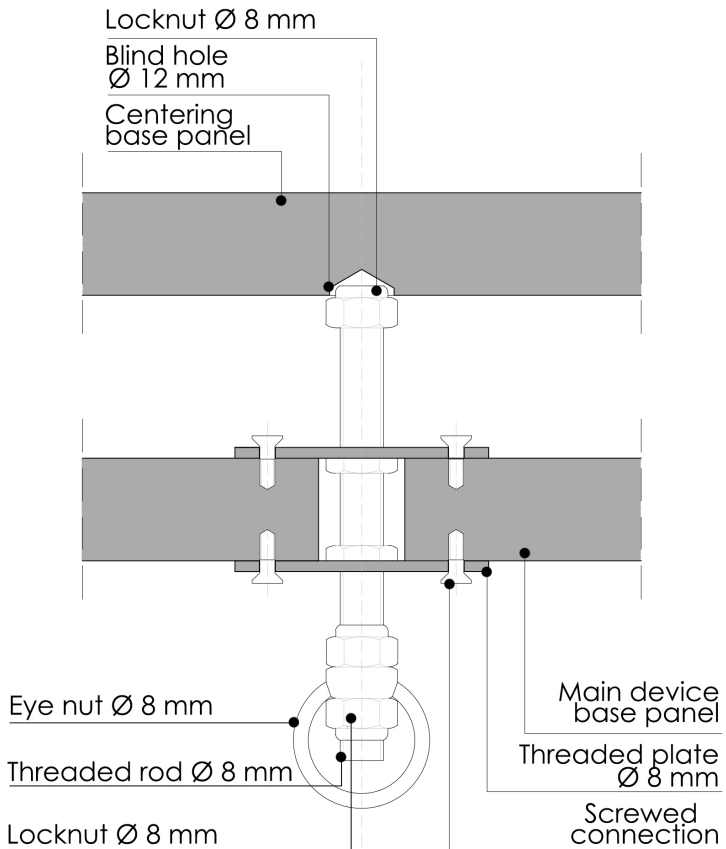


Fig. 5.18

Detail of the jackscrew.

nuts. This configuration allows to completely disengage the centering during the lowering phase once reached the metal support described previously (Fig. 5.11).

As a result of the experience gained during the AV tests, an additional component is designed only for the test on the vertical arrangement of the bricks in the vault (Fig. 5.19): a contrast panel, attached on one side of the set-up, with the presence of moveable clamps, in wood and threaded rods, to give a little amount of precompression during the bricklaying. This allows maintaining in place the bricks while the construction proceeds and helps the cohesion between the arches

Fig. 5.19

Clamp system: main components.

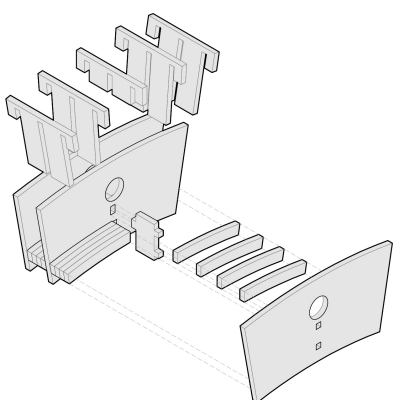
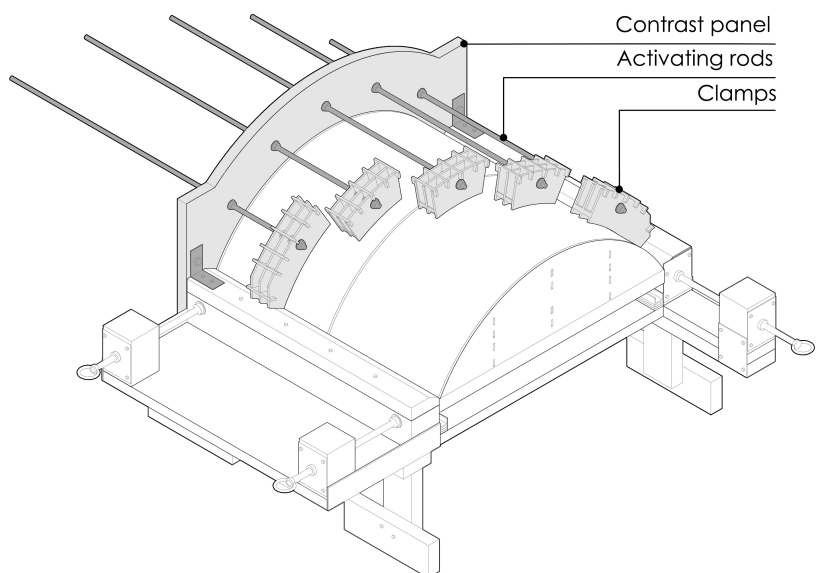


Fig. 5.20

Clamp: components.

This clamp system is realized starting from a 16 mm chipboard cut with a CNC laser machine: beyond the shaping of the element, the use of CNC machine allows to set a guideline for realizing the holes for the clamp. This step is crucial in order to fit the curvature of the centering and the clamps in the best way (they are shaped following the same curvature), and to maintain the rods parallel to the centering extrados, avoiding buckling phenomena in the brick rows while tightening the clamps. The panel is now bolted to the set-up with reversible connections and metal brackets. The clamps are designed to reduce the risk of instability in the vault's portion during the tightening (Fig. 5.21) and are composed of several pieces obtained from a 3 mm thick MDF panel, glued together (Fig. 5.20). The obtained clamps are used during the construction by linking the rods to the contrast panel with the usage of a locknut and a wingnut: in this way it is possible to fine register the trust inside the clamp system for preventing acci-

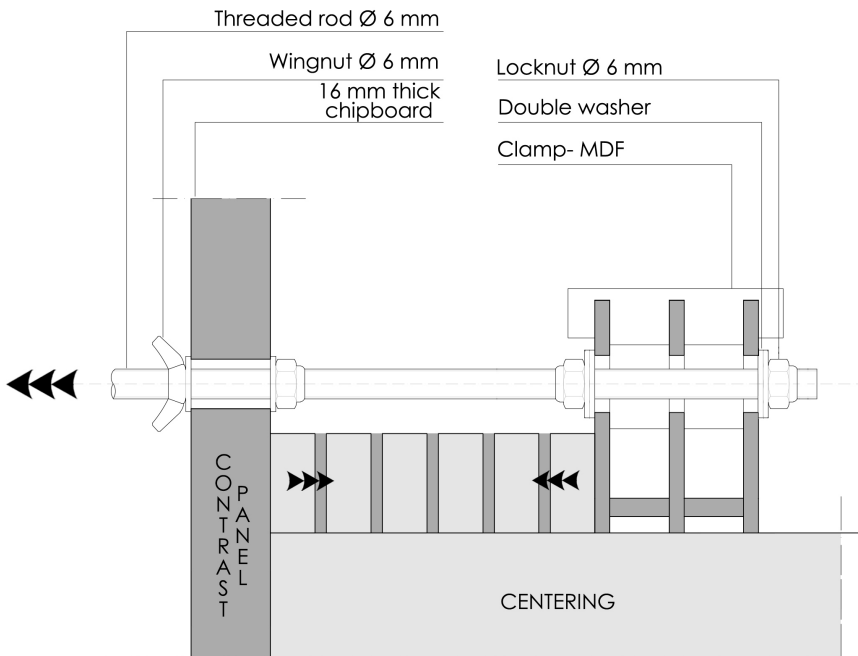


Fig. 5.21

Schematic behaviour of the clamps system.

dental damage to the vault model. During the experimental campaign, the main device is modified to improve the performances in the VV tests. The tests performed on the VR models show that the first caliper configuration, with the use of simple screws to hold the instrument in place, (Fig. 5.22) do not perform properly, with measure issues in the proceeding of the VR_2 tests, due to final visible misalignment of the tool. To prevent the occurring of this phenomenon, a new configuration is realized with a custom plate for tight in place the caliper in a more effective way (Fig. 5.24): a custom two-components clamp, screwed in the shear displacement actuator block, that allows being tightened with a pair of bolts and nuts, while a second clamp is obtained, on the shear abutment, with the screwing-holding mechanism for the moveable part of the measure tool. At the end, this solution has completely fixed the problem noticed in the previous experiences. Also, the actuator block for the shear test is modified to enlarge the net excursion of the abutment: during the proceeding of the campaign, it is noticed that the evaluated range of displacement could be not long enough to lead a complete collapse in the VV model. So, the original contrast block for the shear mechanism activation is replaced with a less thicker wood element, fixed to the device's leg thought an angular metal brackets (Fig. 5.25), gaining 50 mm of excursion for the displacement than the previous configuration.

In the Tab. 5.4 are summarized all the material employed in the construction of the experimental set-up and their division into the components previously described in the Fig. 5.15,

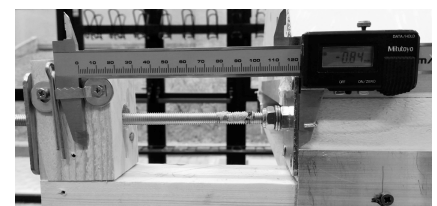


Fig. 5.22

First calliper configuration.



Fig. 5.23

Second calliper configuration with a custom design metal plate.

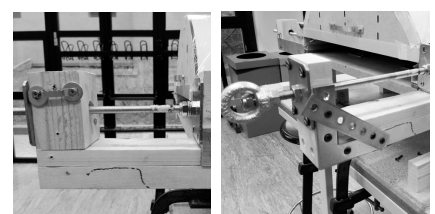


Fig. 5.24

The two shear displacement actuator's configurations:

Left – first configuration;

Right– second configuration.

5.16, 5.18, and 5.19 (the bill report only the material, without the count of joints elements).

WOOD CARPENTRY

Spruce lath 50 x 50 x 2500 mm	x 1
Components	
3 x 70 mm	
2 x 40 mm	
Spruce lath 50 x 20 x 2000 mm	x 2
Components	
2 x 400 mm with 28° cut	
1 x 400 mm	
1x 550 mm	
8 x 150 mm	
1 x 150 mm with 19 mm thickness	
MDF panel 1100 x 400 x 19 mm	
Components	
1 x 650 x 400 mm	
1 x 400 x 400 mm	
MDF foil 1400 x 1400 x 3mm	x 1
MDF foil 1000 x 800 x 1mm	x 5
Chipboard panel x 800 x 16 mm	1000 x 1

HARDWARE

Threaded rod Ø8 mm	x 2
Components	
3 x 300 mm	
4 x 150 mm	
Threaded rod Ø6 mm	x 3
Components	
5 x 500 mm	
Aluminun angle profile x 20 x 20 mm	1000 x 1
Components	
2 x 400 mm	
Aluminun angle profile 1000 x 40 x 40 mm	x 1
Components	
12 x 40 x 40 x 40 mm	
Aluminun flat profile x 35 x 2 mm	1000 x 1
Components	
1 x 400 mm	
2 x 250 mm	
5 x 50 mm	
Aluminun U profile 1000 x 15 x 10 mm	x 1
Components	
2 x 400 mm	

Tab. 5.4

Bill of the material employed in the experimental set-up construction.

5.3 Arch Models

5.3.1 Models construction

5.3.1.1 Radial arrangement

The construction of the arches with the radial arrangement of the bricks represents the simplest way to build a brick masonry arch: each brick is posed, above the centering, with a single layer of mortar forming a wedge-shaped joint t. The first trials in the in-scale model construction are carried out with free-hand shaping of the joints, revealing the importance of precisely dosing the mortar quantity to achieve the desired overall shape of the arches. The 1:5 in-scale nature of the model involves the realization of mortar joints with variable thicknesses between 1,3 mm and 1,9 mm. After several trials, the building process did not show good results in the precision of the shape, due to the difficulty in shaping these little thicknesses without a jig. To overcome this problem, a series of wooden jigs (Fig. 5.26) are realized to ease the work: the principle

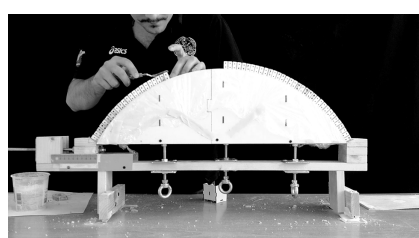


Fig. 5.25

Images of the AR model construction.

is to build a jig shaped to host a single brick and the desired mortar quantity. This way the bed joint is already shaped for the laying after stripping the brick from the jig (Fig. 5.27).

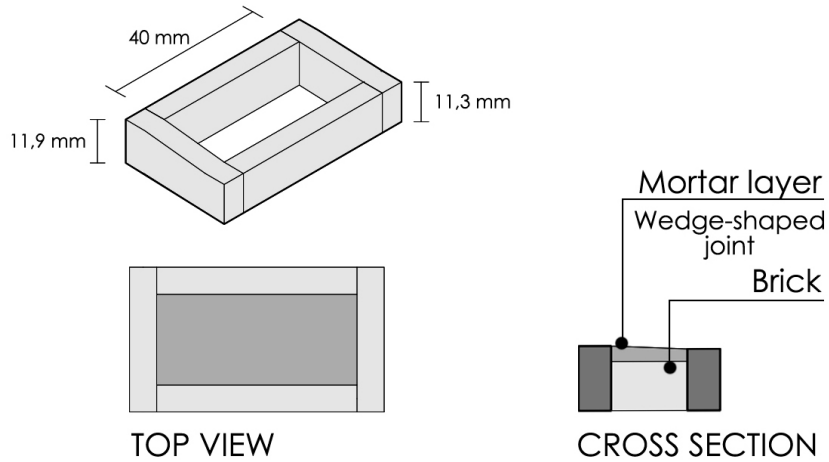


Fig. 5.26

AR jig: measures and description.

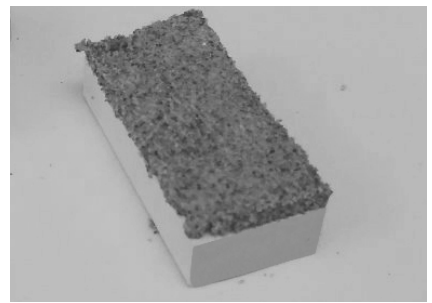


Fig. 5.27

Image of a brick covered with a shaped mortar joint after stripping from the jig.

Another device is built to ease the brick positioning: the experience gained during earlier tests highlighted the presence of issues in the final geometry of the arch, depending on the tilting of the bricks upon the centering. Better results are obtained by designing a tool (Fig. 5.28, 5.29) shaped to follow the curvature of the centering and to maintain a surface always orthogonal to the centering tangent: in this way the brick is always placed in the correct position. This simple tool is obtained by laser cut from 3 mm- thick Finnboard, with simple mortice-tenon joints glued together.

Centering

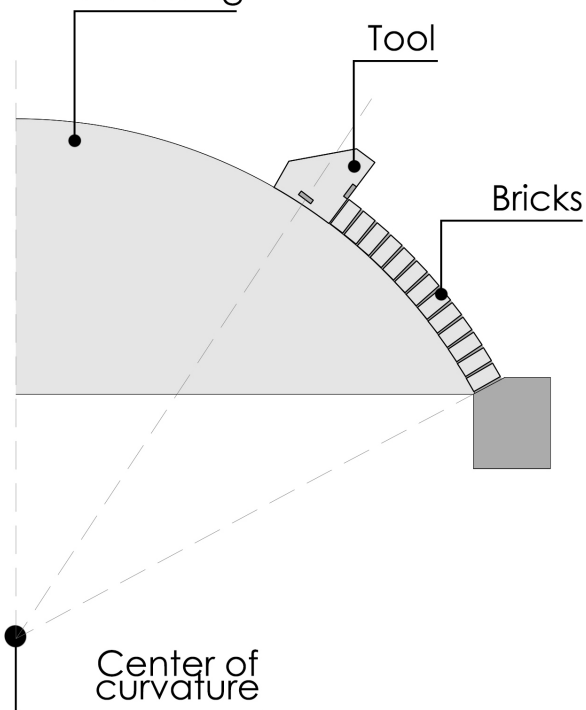


Fig. 5.28

Schematic description of the AR tool usage to keep the brick orthogonal to the centering.

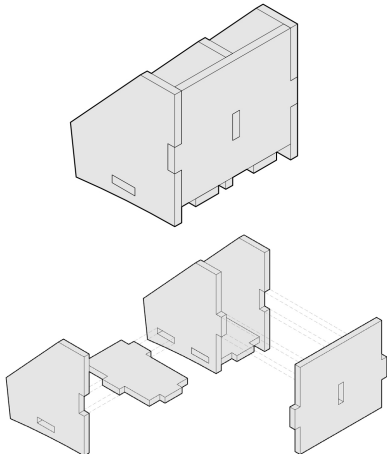


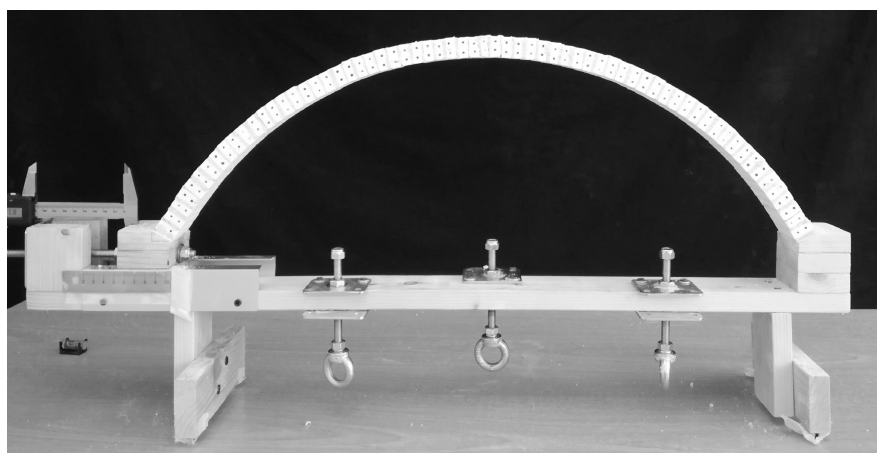
Fig. 5.29

Schematic description of AR tool design and assembling.

Fig. 5.30

Image of one AR model after the centering lowering.

The construction of the arch model starts from one of the abutments until 32 bricks are placed, before starting the construction from the opposite abutment. In every test, the key brick needs adjustment to fit the insertion between the two constructed portions. These adjustments, typically used in the masonry common practice, are performed giving the brick a slight wedge shape to ease the insertion. The whole construction of a single model takes about two hours. After 24 hours the centering is lowered and the opening test is performed on the structure. During the experimental campaign, a higher number of AR arch models (Fig. 5.30) were built to gain experience with bricklaying. The process involves the construction of nine different AR models, seven of which are tested.



5.3.1.2 Vertical arrangement

The construction of the arch models with vertical arrangement requires the modification of some bricks before the construction starts: the need to offset the head joint between adjacent courses means to start the construction from the abutment with the alternation of full-size and half-size bricks. These half bricks (20 x 20 x 10 mm) are obtained by manual sawing of the full-size ones. After several trials, a precise pattern of construction (Fig. 5.31, 5.32) is selected to ease the bricklaying: due to the absence of contrast surfaces for the bricks, the construction of single arches results difficult: so, each brick contrasts against the others with the interposition of the longitudinal mortar joint, allowing to exert a slight compression between each element.

The experience gained on the RA models leads to the construction of a new jig for the VA arches. This jig (Fig. 5.33) is shaped to allow the realization of both the radial and longitudinal joints at the same time on each brick. Each element,

Fig. 5.31

Images of the AV model construction.

once stripped from the jig, is covered with mortar which constitutes a portion of the total joints system, in both longitudinal and transversal directions (Fig. 5.34). Differently from the AR jig, this new one has a lateral slope to model the head joint on the bricks.

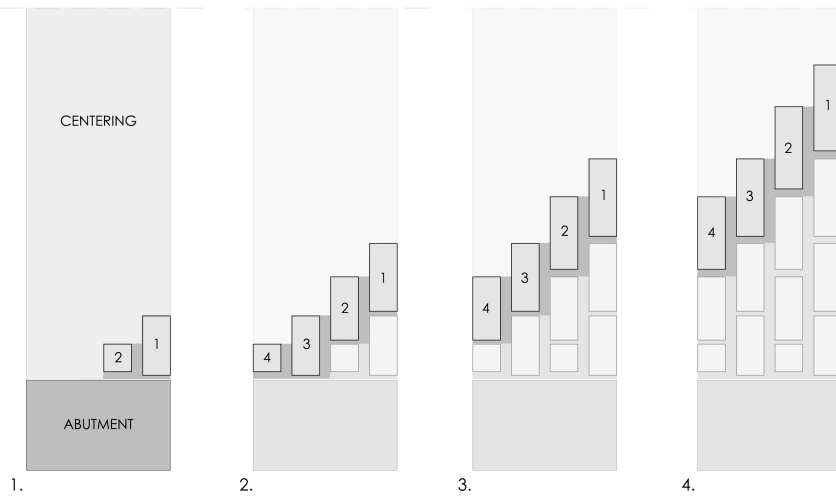


Fig. 5.32

Schematic description of the AV bricklaying pattern.

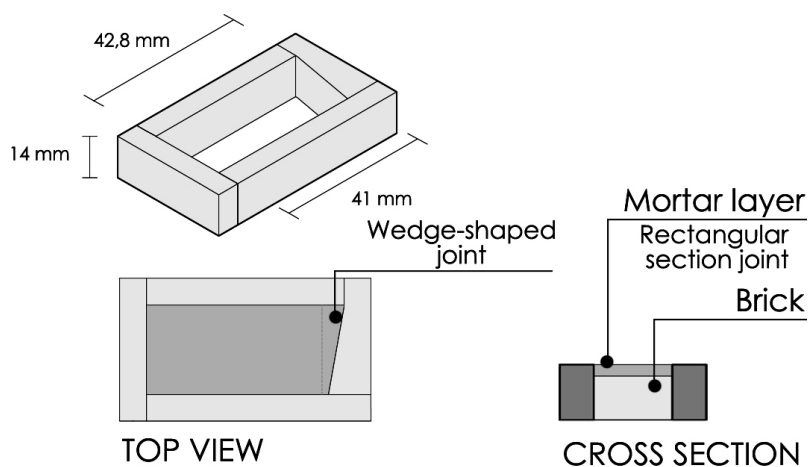


Fig. 5.33

AV jig: measures and description.

Also for the AV models, the key bricks need to be shortened to fit the constructed portions rising from the two abutments upon the centering. The closure of the arch, in virtue of the need to contrast the bricks towards one another, proceeds, on the two portions, from the first row by adding the bricks with the same pattern exposed before, in a symmetrical way (Fig. 5.43).



The whole construction of a single AV model takes about five hours, due to the tricky building methodology. As for the RV arches, after twenty-four hours the centering is lowered and the opening test is performed on the structure. At the end of the experimental campaign, a total of five AV models are constructed and four of them are tested.



Fig. 5.34

Image of the double layer of mortar upon a brick after the stripping from the AV jig.

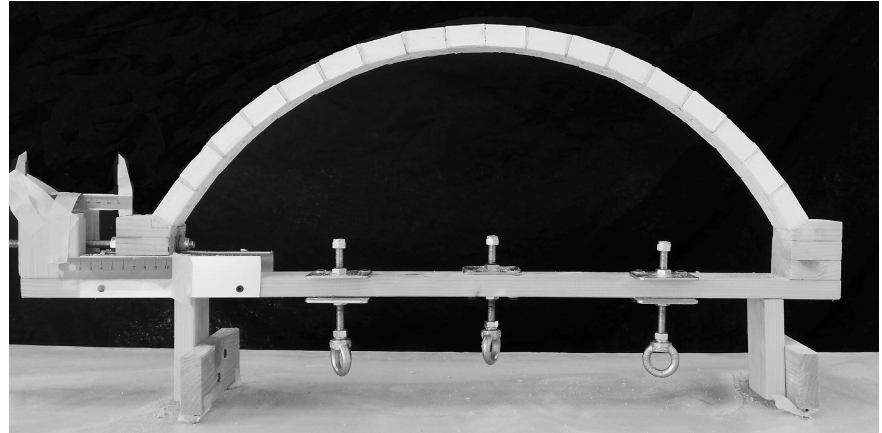
Fig. 5.35

Schematic description of the closure process of the arches in AV models.

During the proceeding of the AV tests, it was observed that the construction process heavily influenced the final behaviour of the structures under the imposed displacement: the first models, with low compression between the arches, lead to quite different failure mechanisms. A rudimental clamping system, with adhesive tape, is tested during the construction of the latter models to exert a little amount of pre-compression between the arches. As predicted, these models showed different behaviour than the previous ones. All the tests and the results are described in further detail in the next Chs.

Fig. 5.36

Image of one AV model after the centering lowering.



5.4 Vault Models

5.4.1 Models construction

5.4.1.1 Radial arrangement

The construction of the in-scale vault models with radial arrangement of the bricks (Fig. 5.37) follows the same procedure described for the radial arch models. The 1:5 in-scale nature of the model involves the realization of mortar joints with variable thickness between 0,8 mm and 1,75 mm: as a result of the experience gained during the first phase of the experimental campaign, two new wooden jigs (Fig. 5.38) are built with CNC laser cutting machine. The principle is to obtain two jigs (a major one for the normal bricks and a minor one for the half bricks, shaped to host a single brick and the precise mortar quantity desired for the realization of the wedge-shaped longitudinal joint and the rectangular cross-section transversal one. For this reason, the jigs are shaped to exceede the dimension of the bricks in two directions, in order to shape both the typologies of joints. During the construction of the models, an L-shaped aluminium profile is used to control the straightness of the brick rows (Fig. 5.39) to prevent the accumulation of errors due to different thickness in the longitudinal joints. The

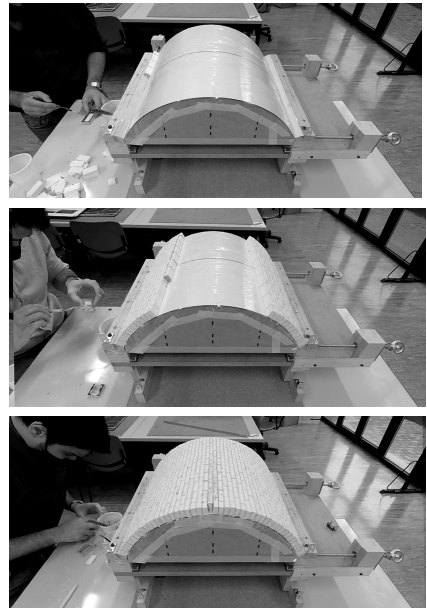
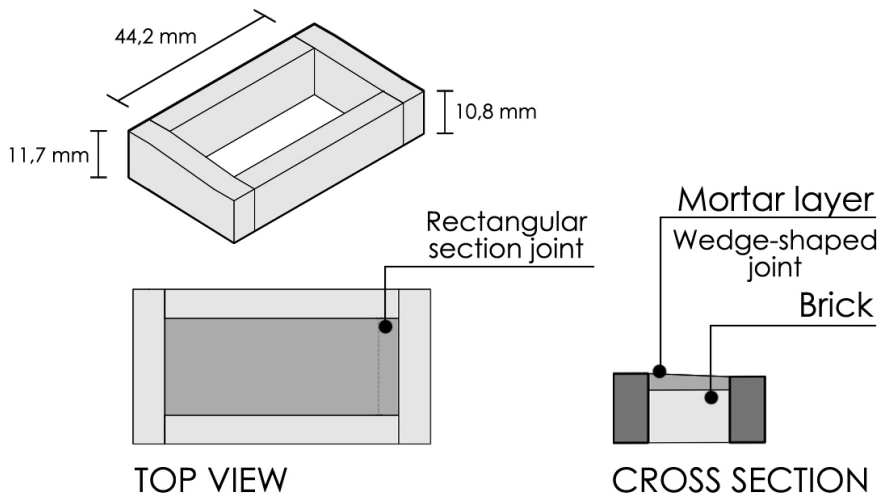


Fig. 5.37

Images of the VR model construction.



final configuration of the vaults with VR involves the presence of 450 cement-based bricks for each model. The model is composed of 45 rows of 10 bricks each. The head arches are realized by the alternance of full-size and half-size bricks, to offset the transversal joints. The construction proceeds by single rows on one abutment and continues symmetrically, for each row, to maintain an equilibrated load on the centering. The last two rows of bricks in the centre are laid together, with the mortar infill between them to work as key voussoirs for the two portions previously constructed starting from the abutments. The whole construction of a single VR model takes about twenty hours of work. After twenty-four hours the centering is lowered and the shear test is performed on the structure. Two VR models are constructed and tested during the campaign.

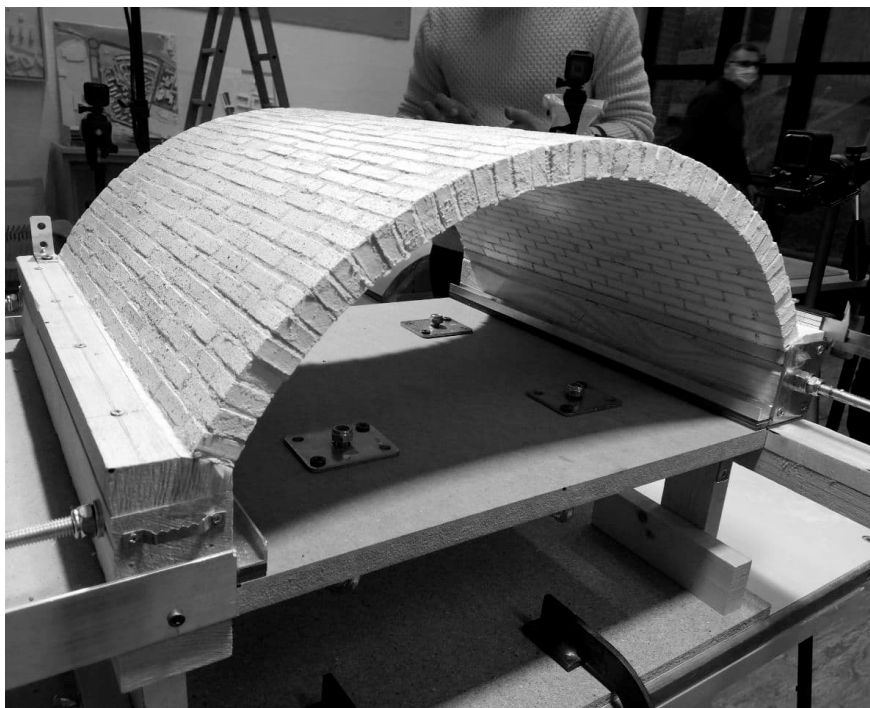


Fig. 5.39

Image of the straightness control of the brick rows during VR model construction.

Fig. 5.40

Image of one VR model after the centering lowering.

5.4.1.2 Vertical arrangement

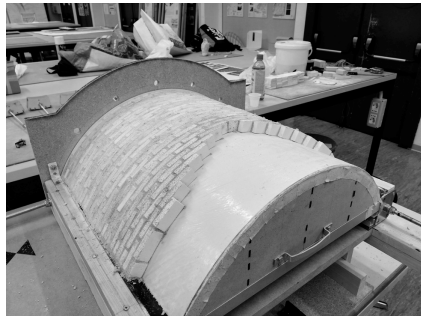


Fig. 5.41

Images of the VV model construction.

As for the AV models, there is the need to offset the joints from each row of bricks, meaning to start the construction from the abutment with the alternation of full-size and half-size bricks. The bricklaying pattern (Fig. 5.41) follows the one tested on the AV models: the only variation in the methodology regards the number of arches built simultaneously, with the construction of symmetric portions, made by a row of six or eight arches at time. Moreover, the presence of a contrast panel helps the positioning of each brick by easing the exerting of compression between each mortar layers. This feature is used also to maintain the elements on a vertical plane, ensuring the straightness of the arches. As reported in Section 5.2.1.2, a clamp system (Fig. 5.42) is used to allow exerting a slight pre-compression of the bricks. The closure of the arches proceeds by adding the bricks with the same pattern exposed before. The clamps are fixed to tight the arches after the construction procedure of a single portion and to prevent accidental falling of the head arches' bricks from the centering, while performing the surrounding laboratory activities before the performing of the shear test.

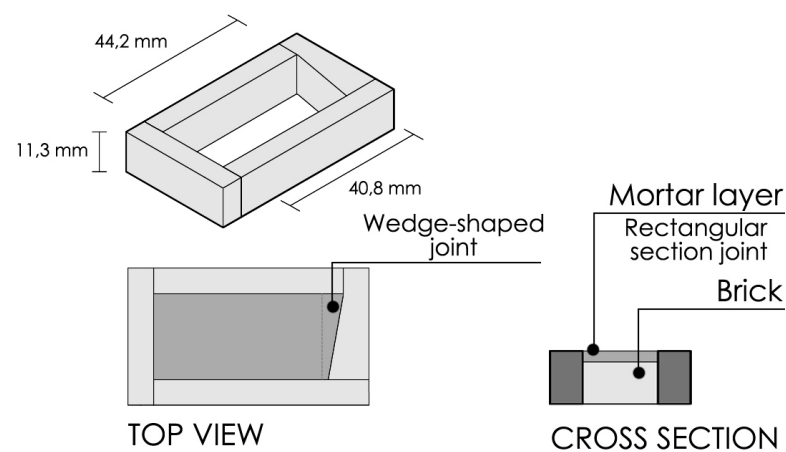
Two new jigs are built with the same principles and shape of the AV ones: these tools are shaped to allow the realization of both the radial and longitudinal joints at the same time on both full size (Fig. 5.43) and half size bricks. The VV models are composed of 450 cement-based bricks, organized in 35 arches: 18 of them are made by 12 bricks while the other 17 are composed by 13 bricks, which include two half-sized ones. These reduced bricks are laid as first on the abutment, in the respective arches, to offset the longitudinal joints. The total mass of the models completely is comparable with the VR one.

Fig. 5.42

Image of the clamp system in action during the VV model construction.

Fig. 5.43

VV major jig: measures and description.



The whole construction of a single VV model takes about thirty hours of works. As for the other models, after twenty-four hours the centering is lowered and the shear test is performed on the structure. During the campaign, two VV model are built and tested.

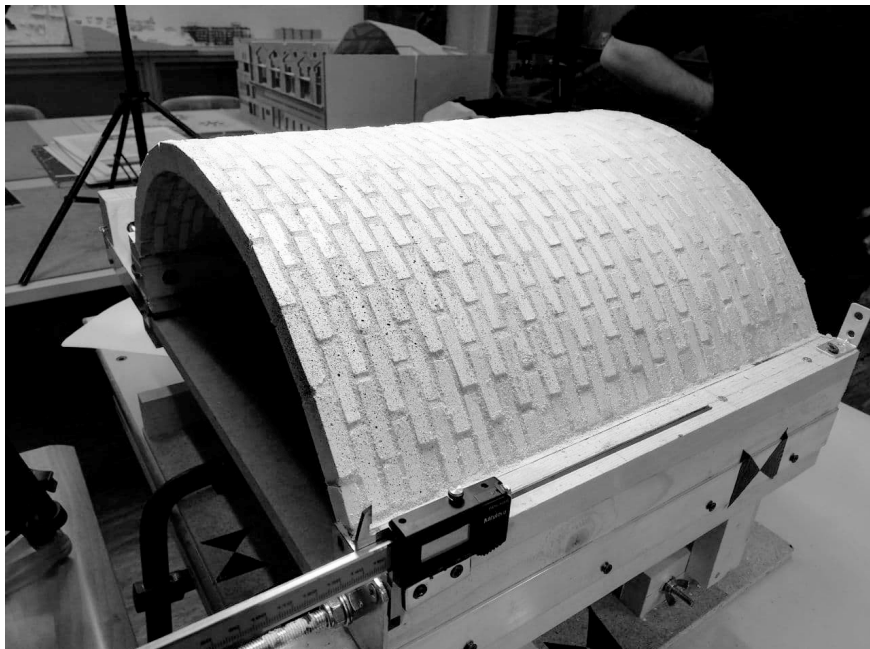


Fig. 5.44

Image of one VV model after the centering lowering.

6. Data Acquisition for in-scale model testing

6.1 Requirements

The acquisition of data concerning the tests on the in-scale models represented an issue of the work: the selected way is to find suitable and manageable solutions compatible with the experimental set-up realized and the aims of the experimental campaign.

During the tests, the direct observation of the phenomena needs to be implemented with methods capable of monitoring the situation, constantly or by steps, to have complete and clear management of the work. As explained, the research is based on a geometrical approach concerning masonry's arches and vaults subject to induced displacements and while on one hand this axial displacement is known and monitored with a digital caliper on the other hand local and global displacements and the crack pattern must be checked to understand the global behaviour of the structure before the failure. For these reasons, the process is managed to respond to a sequence of requirement:

- A constant monitoring to capture the failure mechanism.
- A constant monitoring to capture the local and global displacements.
- The acquisition of certain data related to particular events occurred during the test.
- The possibility of acquiring and managing the structures in a 3D environment to document the models was destroyed during the tests.
- Usage of suitable solutions to the model's sensitivity to avoid accidental failure of the structures.

Considering these requirements, the acquisition and postprocessing phases had been managed through a multidisciplinary approach with the integration of various methods:

- Simple image and video acquisitions or used to monitor the structure during the progress of the test, while the video acquisition is fundamental to capture the failure mechanisms, not even simple to catch live by the naked eye.
- Digital Image Correlation (DIC) was used to monitor the displacement of a portion of the structures derived from the axial displacement of the abutments.

- Close-range photogrammetry and structured light scanners are used, in combination with other Geomatics techniques, to obtain high-resolution 3D digital models of the structure in selected steps of the test, useful for metric documentation and to have replicas of the in-scale models, destroyed as a consequence of each failure test.

6.2 Geomatic techniques

The geomatic techniques involve various procedures in the 3D acquisition field: it is based on the mathematical representation of an object with three dimensions, through the use of structured data containing information about the object and interpreted by algorithms. These data, and the models in general, contain metric information, giving the possibility to know and interpret the geometric and spatial features of the object acquired in a digital ambient. The range of possibilities in the 3D acquisition field is very wide and well documented, with continuous developments in the devices and the integration between the various methodologies. A brief classification of the principal methodologies in moveable objects (magnitude $< 1 \text{ m}^3$) acquisition is reported in the following, with the focus on the selected techniques in virtue of the requirements established for the research aims and previously exposed. The first distinction between the methodologies suitable in the three-dimensional acquisition is represented by the contact with the interested object: the use of Coordinate Measurement Machine (CMM) is a structured practice in laboratory research e.g., in reverse engineering processes; this technique involves the use of a CMM machine with a probe connected to controlled axes able to calculate the coordinates of the points tested by the probe. As reported in the analyses of the requirements, the use of contact devices is not suitable with sensitive and deformed in-scale models, so the decision is to use only contact-less solutions. This is a vast category that includes many different approaches, with a division into the type of radiation used: we can divide it into passive and active techniques. The first ones involve the use of radiation already present in the environment where the object is located (e.g., light) and it includes image-based methodologies such as photogrammetry and stereoscopic. On the contrary, the active techniques involve the use of particular radiations wavelength (inside or not inside the visible spectrum) and their catch from a device sensor after the reflection on the concerned object. A further subdivision into the active sensor ca-

tegory can be performed into the range-based techniques based on the distance calculation methodology. For measuring short distances (<1 m) one of the most used approaches involves Triangulation: it is based on the evaluation of the distances and angles as elements of a triangle where a projector and a lens sensor are two of the vertexes, with a fixed distance, and the third vertex is the projection of the radiation on the object. This category contains laser scanners and structured light scanners. For medium distances (around 100 m), one of the most used technologies is based on the Phase Shift: though the superimposition of different electromagnetic waves, emitted and received, is possible to estimate distances with the Interferometry technique from the emitter device and the reflecting surface of an object. For longer distances (magnitude of more than 100 – 200 m) the measurement devices use the estimation of the Time of Flight of the radiation between the emitter and the receiver after the reflection on an object: this information is transformed into electric signals for the evaluation of the time needed for the return of the radiation, making possible to measure the distance, knowing the speed of light.

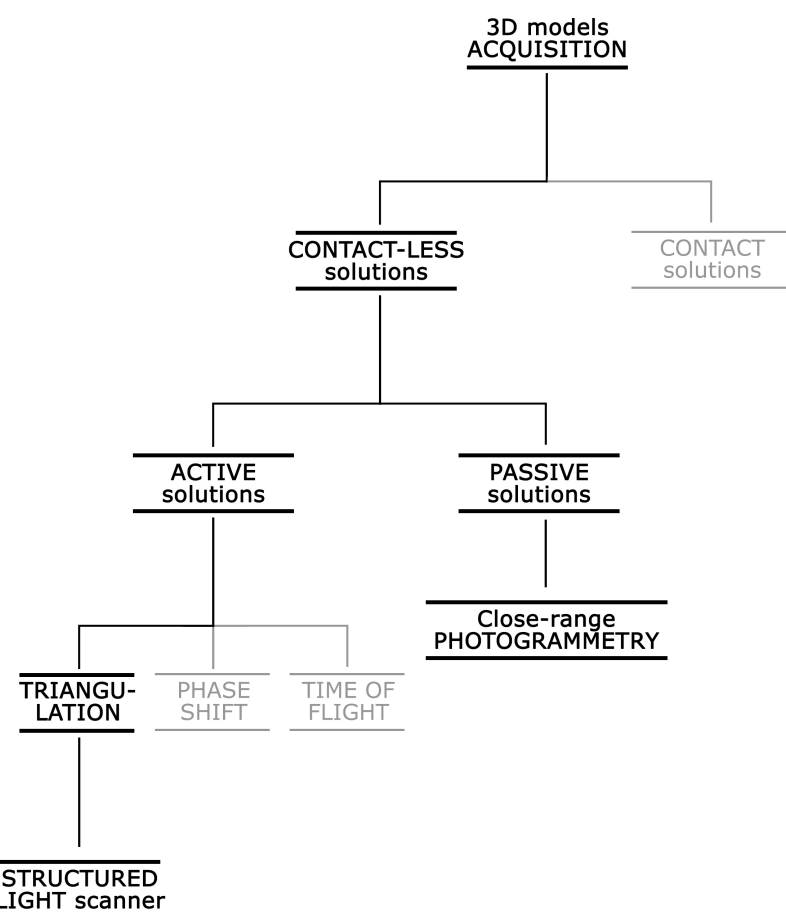


Fig. 6.1

Schematic classification of the 3D acquisition techniques.

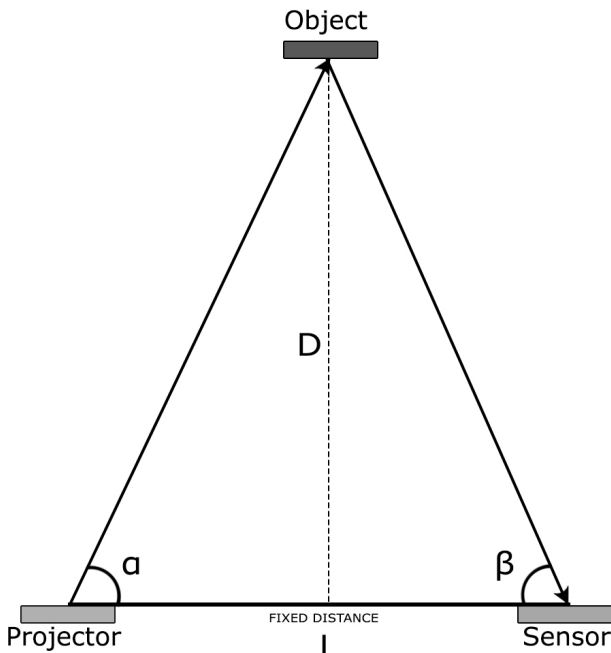
In the last years, geomatics' commitment in documenting movable heritage (Adami et al, 2015; Guidi et al, 2017), in museal or archaeological fields, has encountered the possibilities offered by the ongoing great technological development: this allows to obtain high-resolution 3D replicas of the concerned objects with relatively low efforts. In particular, image-based and range-based solutions, selected for the present work, offer the possibility to link to the metric information also to the radiometric component, allow to obtain detailed textures of the objects. With these premises, the geomatics approach, with close-range photogrammetry and the use of structured light scanners, responds to the fixed requirements of the work. These procedures and their integrated use are well documented in the literature and are continuously updated considering the already mentioned technological development (Adamopoulos et al., 2021). The use of these acquisition techniques permits to have a 3D reconstruction of particular steps of the tested models (failed at the end of the tests) with the imposed displacement, without any contact to the model.

6.1.1 Range-based acquisition: structured light scanner

As previously mentioned, the great development of the technology in the last decades has brought to new possibilities in the acquisition of data from objects: from the classical metrical survey, with its methodologies, the geomatic has developed new techniques of acquisition, complementary to the classical ones. In the classical survey (but also in the photogrammetry, as exposed in the following paragraph) particular points of the concerned objects represent the focus in the measures as guidelines to acquire the geometry (corners, intersections as natural points of the object but also markers placed by the operators). The development of range-based techniques, using active systems (e.g., the ones based on laser or structured light), allows acquiring the desired objects without the particular attention mentioned before: new technologies in the fields of photonics, computer vision, and electronics lead to the development of new devices and application in the survey, providing solutions that implement the traditional ones. The use of structure light scanners offers good solutions in the contactless acquisition of small objects ($magnitude < 1 m^3$). These systems use the principle of triangulation (Fig 6.2) in addition to a light projector and one or more cameras for the acquisitions.

Fig. 6.2

Principle of the triangulation method.



The principles are derived from the simpler laser light scanner: a source project a laser spot on the interested surface, while a sensor, through a lens, catch the image of the lighted spot, forming a triangle: the knowledge of its components like the fixed length L between the projector and the sensor, can integrate, through simple trigonometric calculations, the unknown distance D from the concerned point, estimating the angles α and β :

$$D = \frac{L \cdot \tan\alpha \cdot \tan\beta}{\tan\alpha + \tan\beta} \quad (1)$$

This method is defined as 1D because of the measurement interest only the axis coming out from the sensor. As a derivation from the exposed 1D system, a more complex solution, capable to acquire 2D (x,y,z coordinates) involve the use of a rotating reflection mirror for deviate in steps the laser light on a surface: the acquisition by the camera, as seen before, can reconstruct, by steps the coordinates of the points on a section of the concerned object, from planar surfaces to more complex ones. An improvement of this technique leads to obtain a 2.5D system (Guidi et al., 2010, a): with this name are intended the systems capable of manage only one point on the vertical axis of the sensor for each point on the horizontal surface of the sensor itself. It allows to map already the entire surface of an object, but it is not able to manage undercut portions. These systems can be divided into two typologies: moveable laser scanner (directly derived by

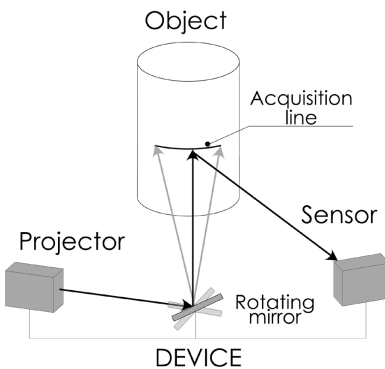


Fig. 6.3

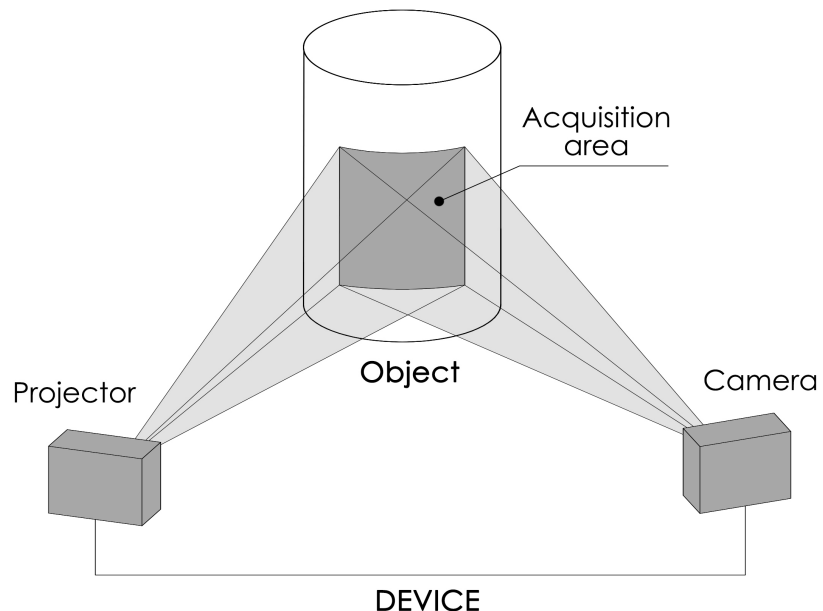
Schematic function of a 2D laser scanner device.

the scanner exposed previously) and structured light scanner (with common principles but different mechanisms). The first one involves a laser scanner sensor coupled with moveable components; the laser segment is projected, by steps, on a surface, rotating or translating on fixed axes. In this way it is possible to acquire a rectangular-shaped portion of the surfaces. This system requires complex and expensive mechanical parts for working properly due to the precise nature of the scanner's movement.

As mentioned, the structured light scanners use similar principles, allowing to acquire portions of surfaces by the projection of complex patterns (Fig. 6.4). Structured light scanner devices are typically composed of a pattern projector and a camera with converging orientation and can work both in visible or Near Infra-Red spectrums. Instead of using laser segments, moved to form a rectangular-shaped portion of the analysis, a bi-dimensional pattern of light is projected by a projector on the surface of the object, while a digital camera acquires the reflection: as for the laser scanner described before, the structured light scanners use the principle of triangulation in addition to the elaboration based on the pattern.

Fig. 6.4

Schematic function of a structured light scanner device.



The patterns can be composed of simple or complex geometric shapes, with the constant of knowing the undeformed state: once projected on a complex surface, this is deformed and elaborated by the algorithms to evaluate the coordinates of the point related to the pattern. This evaluation can be carried out by two principal methods:

- Gray code: this method uses a pattern composed of white and black stripes, and each transition between a white

te zone and black zone represents a profile, manageable as seen for the previously exposed scanners. Starting from a minimum number of stripes (one for each colour), the camera acquires a subsequent image with a new conformation of the pattern, with a larger number of stripes (until the maximum frequency required), representing a different level of the acquisition process. The increase of the black and white alternations, on a fixed-size portion of the object, consisting of the projection area, means a progressive increase in the acquisition of object profiles. Giving to each image a binary code corresponding to the black or white nature of each pixel, it is possible to relate all the levels of the acquisition, building a map of the surface's depth by the entities of the pixels.

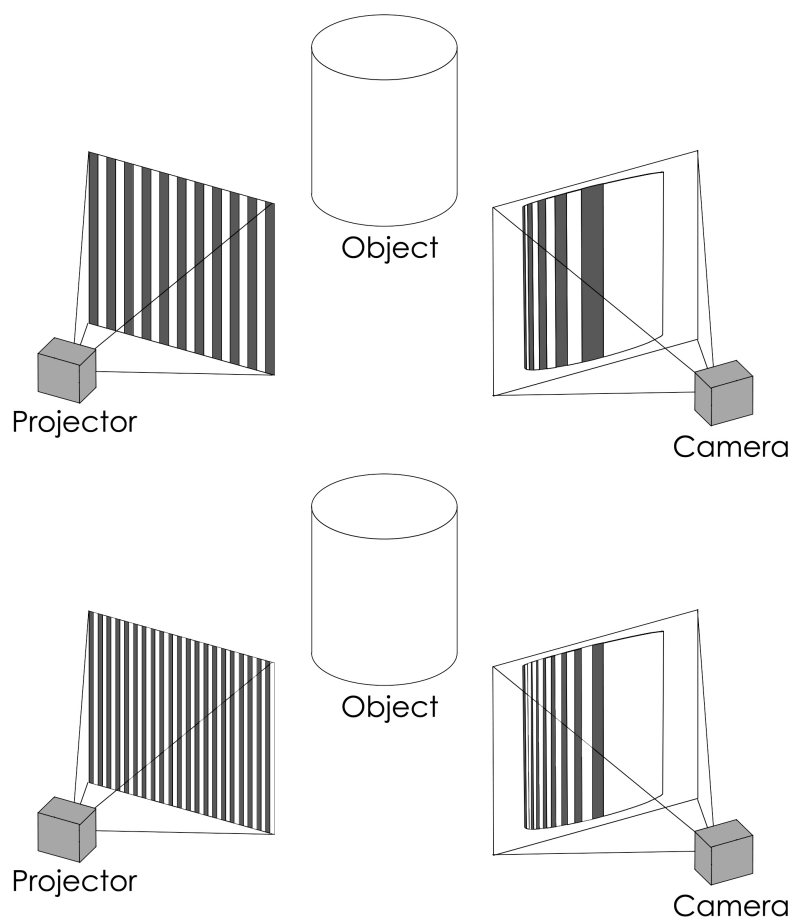


Fig. 6.5

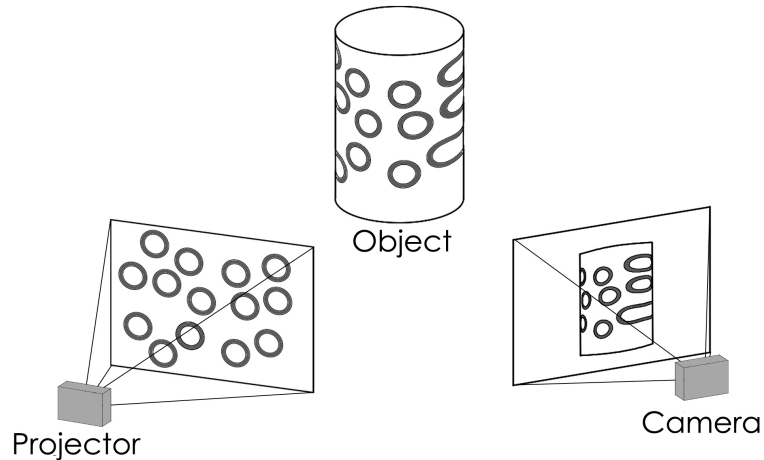
Schematic principles of structured light scanners with Gray code pattern.

- Moirè effect: this method is based on the difference between pattern overlaps (subtractive Moirè). Starting from a known pattern projected on a non-planar figure (alteration of the pattern), it is possible, by confronting the expected pattern with the altered one, to obtain the map of the surface variation. This is possible by creating interference figures made by the overlap of the two patterns

using a precise filter (as for beat phenomenon in the acoustic field) based on phase shifting. These filters work on the interference between two electromagnetic waves with slightly different frequencies. The Moirè effect works on the similarity between undeformed pattern and deformed ones after the projection on the object surface, allowing to use of a various number of different patterns arrangement (stripes, geometric shapes, random or organized dots).

Fig. 6.6

Schematic principles of structured light scanners with subtractive Moirè method.



Due to the projecting nature of the system, with variability in the patterns solutions, structured light scanners work well with a great number of surfaces, without the use of physical markers or manual measures. The biggest weakness of the method is in the acquisition of highly reflective surfaces: materials like metal, with a high reflection coefficient, can reflect the biggest part of the pattern projected, creating a blind spot in the acquisition. The point cloud generated with this method has an absolute scale in which each point has its coordinates in relation with the others, differently from other techniques, like photogrammetry (treated in the next paragraph), where the scale of the cloud is relative and depending on external measures. Nevertheless, once obtained the complete point cloud it is possible to reference it to an external coordinates system, using consolidated rototranslation methodologies.

In the last years, the use of structured light scanners has increased, with a great number of publications about the methodologies (Malik et al, 2018), the results obtainable with the new devices available on the market (Kersten et al, 2016; Kersten et al, 2018) and the comparison with consolidated techniques of survey (Patrucco et al, 2019). The development of new technologies, especially in the way of ease-to-use handheld scanners, offers new solutions for the acquisition of the moveable heritage or in the industry, especially in an integrated way with the consolidated techniques.

6.1.2 Image-based acquisition: close-range photogrammetry

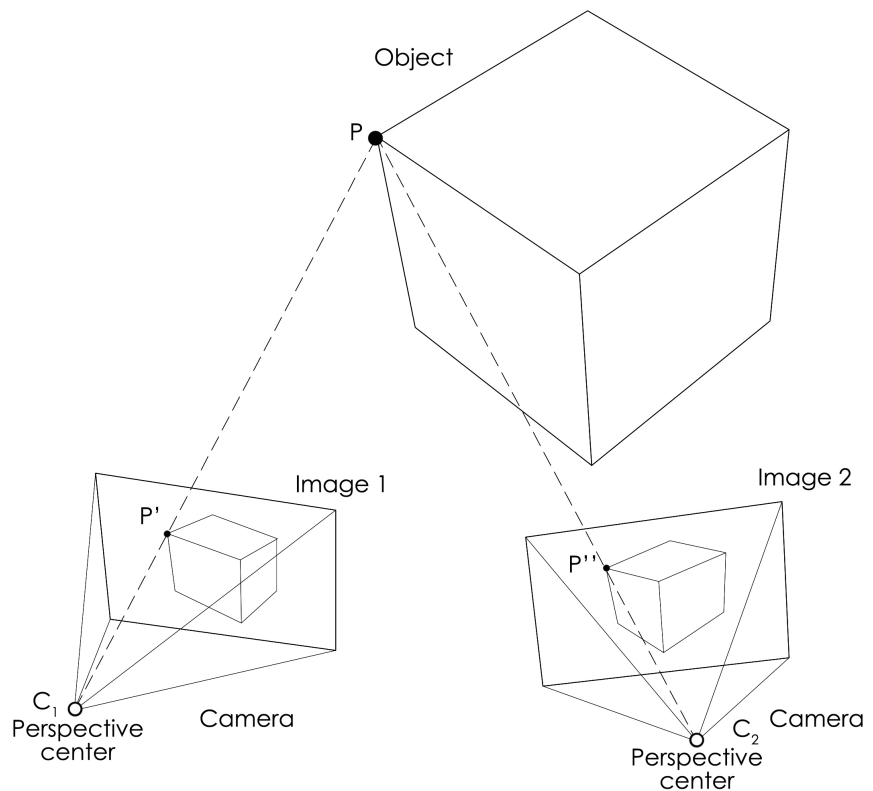
Photogrammetry is a survey method that allows the acquisition of objects of any shape and magnitude with a great number of acquired points: its applications go from cartography to little object reconstruction. It is commonly divided into two great categories, differenced by the acquisition approach: aerial photogrammetry, mostly used in cartography and architectural survey, and terrestrial photogrammetry, mostly used from architectural to moveable object scales. The term close-range photogrammetry indicates the situation in the photogrammetric techniques where the acquisitions of the images are taken from an inferior distance to 300 m and is common applied in architecture and engineering.

Photogrammetry uses one or more photographs of an object (measurable and photographable), from different positions, to derive its shape and location (Luhmann et al., 2013), through a three-dimensional reconstruction in digital or graphical form, based on inverse perspective and descriptive geometry (Guidi et al., 2010). The transition from a real 3D object to a 2D image involves a loss of information (hidden areas, a different magnitude of details, quality of the image, etc.), starting from a three coordinates system, needed to describe the position of a singular point in the reality, and working on a two coordinates system acquired by the sensor (camera). Is important to notice that at the base for this transition between the 3D entity (object) and 2D entity (image), a precise analytic-geometric relationship relates the points from the first system to the ones on the second system a one-to-one correspondence. In the digital photogrammetric procedure, not only spatial coordinate or geometric data are considered for the reconstruction of the objects, but also the radiometric component (colour), intended as the electromagnetic radiation of the light reflected by the object through a transmission media (usually air) and captured by the cameras. Starting from the acquisition, passing through the measurement of the images, the object can be reconstructed using mathematical transformations.

The technique is based on the central projection imaging (Fig 3.7): to determine the position and the shape of an object, a group of rays is projected from the photograph (Image 1, 2, ... x), starting from a perspective centre (C_1, C_2, \dots, C_x , with their distance from the image plane), passing from the image point (P', P'', \dots, P_x) and reaching the corresponding real object's point (P).

Fig. 6.7

Schematic principles of photogrammetric method.



The intersection of corresponding rays (at least two) for homologous points (visible, and then projectable, in the different images) allows the individuation of the position of the points in the space. The intersections between the homologous rays allow locating the object's point in a precise position on each ray, linking images from different perspectives. So, each image generates a bundle of rays capable of being linked with the bundles derived by other images, creating a network with high geometric strength, known as stereoscopic model. The obtained network can be oriented merging the image to reconstituting the object surface. The usage of reference points (from the direct survey of previous photogrammetric observation) links the reconstructed surfaces to the global object coordinate system. This is possible only if the perspective centres positions are known. These rays are related to the object space by knowing the geometry of the images and the position of the imaging systems (Fig. 6.7): internal orientation of the cameras, indicates the relation of the camera with the image, while external orientation indicates its relationship with the real space.

The internal orientation defines the geometry of the camera in relation to the single image; it has two main parameters for establishing the perspective centre position in the local image reference system:

- **η_{PP} , ξ_{PP} :** coordinates of the principal point PP in the came-

ra reference system.

- **c:** principal distance of the camera between the perspective and image centre.

Where the PP point is the orthogonal projection of the C point on the image plane. In theory, this point must coincide with the geometric centre of the photograph (intersection of the axes η and ξ) but in practice there is always a gap. The coordinate on the axes of the distance of PP to the centre is declared, along with the distance c, by the producers of the devices.

It is possible to estimate the coordinates (X, Y, Z) of a P' point of the image in a coordinate system related to the image plane with the formula:

$$\begin{aligned} X_{P'} &= \xi_{P'} - \xi_{PP}, \\ Y_{P'} &= \eta_{P'} - \eta_{PP}, \\ Z_{P'} &= c \end{aligned} \quad (2)$$

The ray from the perspective centre to the object, passing through an image, can be mathematically express with the co-linearity equation:

$$\frac{X_{P'} - X_C}{X_P - X_C} = \frac{Y_{P'} - Y_C}{Y_P - Y_C} = \frac{Z_{P'} - Z_C}{Z_P - Z_C} \quad (3)$$

Fig. 6.8

Main components of the photogrammetric process.

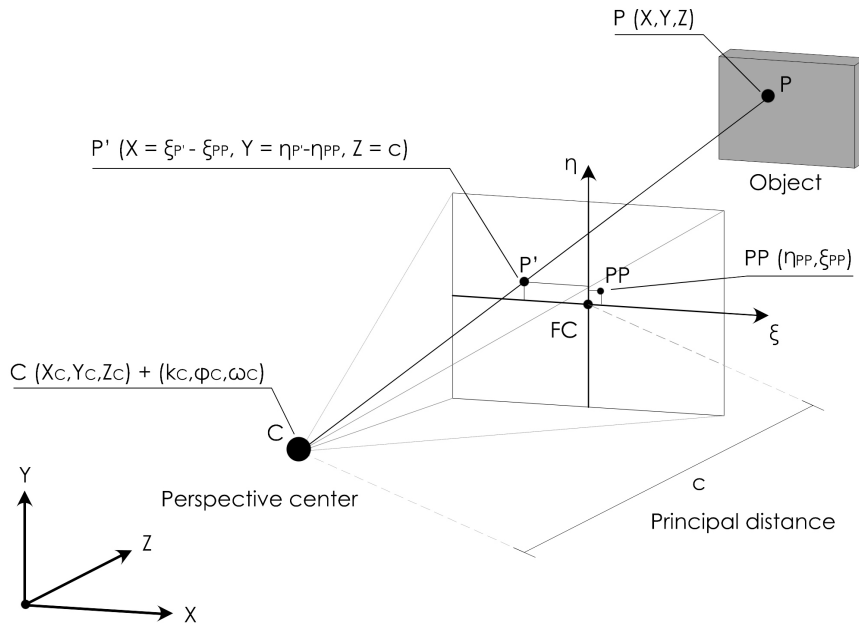




Fig. 6.9

External orientation of the camera.

This way for each image is possible to calculate the relation between the projecting rays of homologous points, by considering the coordinates of P (the point where the rays meet) as fixed. The external orientation (Fig. 6.9) defines the camera absolute position in a global reference system (typically the same system of the acquired object), with a total of six parameters (three translations on X, Y, Z and three rotations κ , ϕ , ω). Solving the external orientation of the system means fixing the stereoscopic model in an absolute position, not possible just by solving the internal one. For scale and rototranslate the obtained model, it is necessary to use at least three points measured on the object: two points allow to scale the stereoscopic measuring the difference between the segment joining the point on the object and the one on the model, while a third point allows to eliminate the problems linked to the rotation around these segments once the model and the object are overlapped in the same coordinate system. The general precision in the work highly depends on the acquisition phase: while in aerial photogrammetry the acquisition planning follows more severe rules, usually terrestrial close-range photogrammetry is organized by following more empirical rules. The distance between image shoots is assumed typically as a quarter of the distance from the object, estimating the image scale as 5 or 6 times higher than the representation scale desired. A fundamental datum to estimate the work precision is expressed by the Ground Sample Distance (GSD) that indicates the distance between the centre of two adjacent pixels, expressing the portion of the object captured by a single pixel in a single image.

The roots of photogrammetry can be related to the research about perspective conducted during Renaissance (Guidi et al., 2010, b), but its true birth is in the XIX century, along with the development of the photographic technique: the most influential experiences conducted in the field are related to the topographic purposes, with the usage of photographs to reconstruct parts of the cities, as for Laussedat in Paris in 1859. A remarkable development of the subject, in terms of methodology and technology, was recorded also during the two World Wars, with the usage of aerial analogic photogrammetry to map the combat fields. With the birth of the automatic calculator, from the '50, and the electronic calculator, in the '70, a great development in photogrammetry is obtained, due to the possibility of eliminating the camera distortion through computational processes: this allows the use of a normal camera instead of metric cameras used previously, and to consi-

derably shorten the time of elaboration. In addition, during the '90, the photogrammetry turns digital, with the development of high resolutions digital cameras and appropriate software, improving the process through automatic recognition of the object's features. One of the most recent steps involves the great diffusion of computer vision algorithms, based on the Structure from Motion (SfM) approach, which provides a great number of easy-to-use and low-cost software with a high grade of interoperability to other 3D CAD, BIM, and database managing systems.

The usage of the SfM algorithm in computer vision allows estimating the position of 3D points in a group of overlapping images, reconstructing the object (structure) and the position of the images acquisition (motion) also without knowing the precise orientation of them. This methodology work at its best with wide datasets, made of highly overlapping images taken from near positions one to another (Westoby et al, 2012). It uses the same principles previously exposed for the stereoscopic methodology, but with a higher number of images to match: the use of a highly redundant, iterative bundle adjustment procedure, on the base of a database created on the images dataset, allows to speed-up the orientation phases. This is possible by using the peripolar geometric rules (geometry on the base of the stereo imaging) putting in relation the perspective centre of the images and the points on the 3D object, in addition to the use of image matching algorithms, creating a sparse cloud of tie points: tie points represent features of the images invariant to changes of perspectives and illumination, giving the possibility to be matched trough a big part of the photoset. For these reasons, it is important to have good quality in the photo acquisition (higher resolutions correspond to a higher possibility of extracting tie points from matchable features) and a good quantity of photo overlapping. Tie points are estimated for all the different photographs.

The main algorithms used are:

- **Scale-invariant feature transform (SIFT)** (Lowe, 1999): it is based on the usage of a set of reference images, used to construct a database of keypoints. The features of the rest of the images are analysed through the estimation of Euclidean distance. These features are evaluated, and if less than three of them are matched to the object and its position, these features are taken into account by the proceeding of the process while outliers are discarded.

The probability of these feature distributions is calculated, along with the accuracy and the probability of false matches during the process.

- **Speeded up robust features (SURF):** it is based on the SIFT algorithm (Oyallon et al, 2015). It is considered a fast approximation of the SIFT method with the same robustness and invariance while being faster to compute.

The main aims of these algorithms are to filter the photo-set by selecting notable features of the object (corners, junctions, etc.) through the similarity transform parameters (location, scale, and orientation) and to evaluate the radiometric components in the pixels near to a precise point (correlation windows) recognizable in the images. The matching between these points leads to obtain a sparse dense cloud made by the homologous points. The use of SfM-based methodologies, in theory, allows avoiding the two principal scene preparation phases proper to the classical photogrammetry for the correlation of images: the knowing of the camera pose and the measurement of control points on the scene. This information is estimated directly by the algorithm, through the non-linear least-squares minimisation for refining iteratively the camera positions and the object coordinates. In the practice, the lack of information about external references corresponds, in an SfM-based sparse cloud, to the absence of precise scale and orientation of the model itself. So, the selection and the use of significant points on the scene, named Ground Control Points (GPs), is necessary for the scaling and the roto-translation of the model into the desired reference system. The design of a GPs network with a high redundancy of data is helpful to create a strong estimation system and to avoid issues depending on the accidental scarcity of acquisition coverage on object portions.

The acquisition and processing phases linked to the exposed range-based and image based techniques will be treated in detail in Ch. 7.

6.2 Digital Image Correlation

The Digital Image Correlation (DIC) is part of the image-based techniques, as described for the photogrammetry. In particular, it is finalized to the measurements of deformations starting from an image dataset and it found its bigger appliance in the field of experimental mechanics: in the last

years, its use increases especially in civil engineering, biomedical engineering, aerospace engineering, material science, and in industrial monitoring. Nowadays both 2D and 3D DIC are employed and in constant updating, both in scientific and engineering disciplines, in accordance with the technological development in the field of data acquisition and image sensing. The use of a continuum technique of acquisition provides good coverage in the evaluation of any changes in the structures, especially for unexpected ones.

The principle at the base of the DIC is the stereoscopic vision for the image reconstruction, already treated in the previous pages. The two cameras are calibrated to know the relation between raw and world space: once the two cameras' parameters are calibrated (definition of a stereoscopic model), the three-dimensional shape of the object is reconstructed from the data coming from the left and right camera by matching the pattern on the object. The reconstruction works in the same way, with the addition of the temporal component: after the lens distortion correction, the images are compared and matched on the basis of the acquisition time, subtracting the coordinates of a single point from the sequence of data concerning the same point. Basically, DIC involves the comparison between a pair of stereoscopic images, taken as reference, with other pairs of images of the deformed object (Pierré et al, 2017) (Fig. 6.9) Cross-correlation is used to estimate strain and deformation of the object tested by the evaluation of the greyscale variation in the subset's patterns between a reference image (typical the undeformed state) and the deformed state images (Niezrecki et al, 2018). In recent years, this technique is investigated, with a particular focus, in the application for real-time 3D acquisition in the fields of rotation and large displacements (Shao and He, 2021). With these premises, the DIC appears as a robust monitoring method in the field of small object deformations, and it is selected to be tested in the present research.

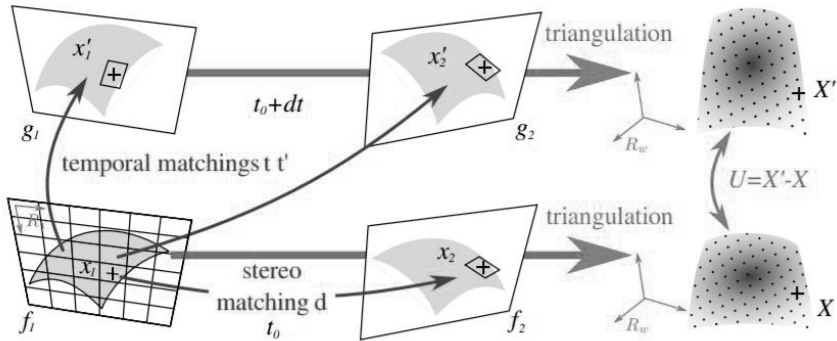


Fig. 6.9

Main steps of a 3D Displacement field measurement of a surface with classical Stereo-Digital Image Correlation

From: Pierré et al, 2017.

DIC works by tracking groups of pixels (usually facets with square base, with 10-50 pixels for each side), in the compared images, and measuring the surface displacement in building up 3D full field deformation vectors (Fig. 6.10) and strain maps. These groups of pixels must have unique features in terms of intensity level and contrast, to be recognised by the algorithm and matched in the time steps comparison. With these aims, in conditions of scarce light or with complex and not textured objects, a new custom texture is needed for the device to work properly. The most common way to characterize the surface to be analysed is to realize a black and white pattern (black dots on a white background or the reverse): in this way each image is considered as a matrix of integers with pixels in greyscale values, 0 for the white pixels and 100 for the black one (Niezrecki et al., 2018). In present days, a great number of

Fig. 6.10

Determination of the three-dimensional displacement vector.

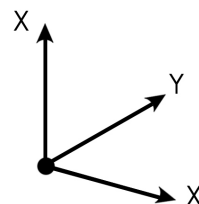
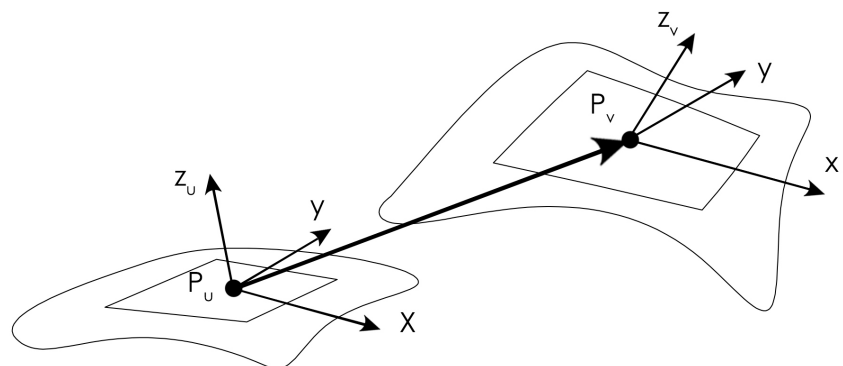
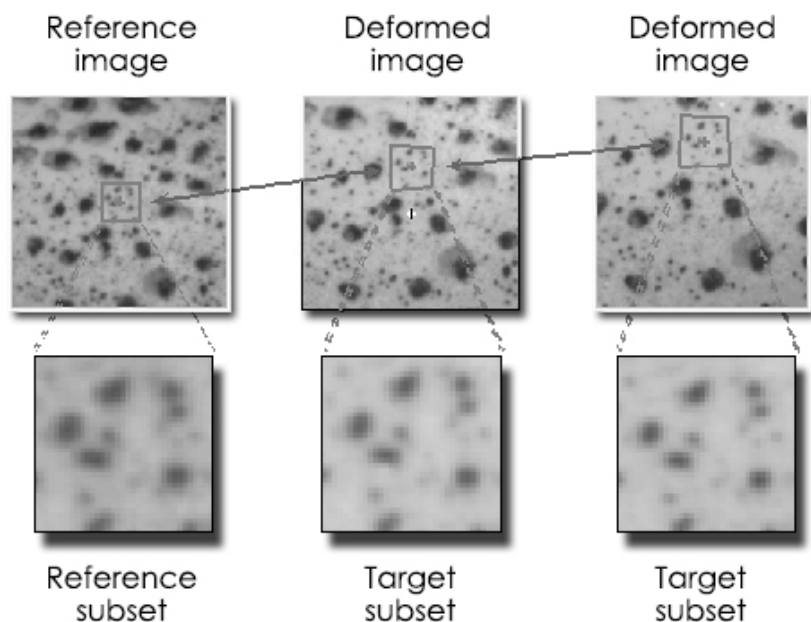


Fig. 6.11

Schematic principle of Digital Image Correlation.

From: Correlated Solutions Inc.w



software techniques are developed to improve the practical appliance of algorithms in DIC elaboration, in order to obtain sub-pixel resolutions (McCormic and Lord, 2010). As for the present work, the correlation algorithm adopted (integrated into the DIC System Q-400 system, Dantec Dynamics A/S, described in the following Ch.) is based on the tracking of grey value patterns in small local neighbourhoods.

The correlation algorithm:

$$\sum (G_t(x_t, y_t) - G(x, y))^2 \quad (4)$$

Where:

- **G(x,y)** is the grey value of a pixel pattern with the coordinate x and y inside of the subset or facet.
- **Gt (xt,yt)** = $g_0 + g_1 G(x_t, y_t)$;
- **x1** = $a_0 + a_1 x + a_2 y + a_3 xy$;
- **y1** = $a_4 + a_5 x + a_6 y + a_7 xy$;
- **g0, g1** are the illumination parameters;
- **a0, a1, ...a7** are the parameters of the similarity transformation.

Once the correlation algorithm minimizes the sum (4), by the variation of the illumination parameters (g_0, g_1) and the parameters of the similarity transformation ($a_0 \dots a_7$) accuracy for the matching of better than 0.01 pixel can be achieved. The correlation algorithm which is actually applied is a two-dimensional generalization of the case just described. It implies, in particular, a two-dimensional geometric transformation that is to rectify perspective distortion and relief displacement. In view of the small size of the image areas, it is sufficient to apply affine linear transformation (six a type parameters) (Ackermann, 1984). Once the 3D contour has been determined, the second step in digital 3D correlation is the measurement and the determination of the three-dimensional deformation of the object surface (deformed pattern). This process is carried out by correlation of the images, taken by both cameras with respect to their original reference images.

The acquisition phase linked to the DIC technique will be treated in detail in Ch. 7.

7. Experimental tests

7.1 Test description

7.1.1 Arch – Opening tests

The opening displacement is selected to test the arch models. This test involves the movement of one of the abutments apart from the other, which is fixed to the testing device (Fig 7.1). It simulates common phenomena of abutment settlements in historical buildings: these displacements can be generated by many factors such as soil movements or local abutment failures. Actually, arches and vaults are thrusting structures that commonly lead to spreads of their supports. This kind of test is one of the most adopted in masonry spatial structure modelling: as reported in Ch 3.3, a great number of contemporary research on the topic performs this kind of test on in-scale masonry models (Van Mele et al, 2012; Shapiro, 2012; Rossi et al, 2015).

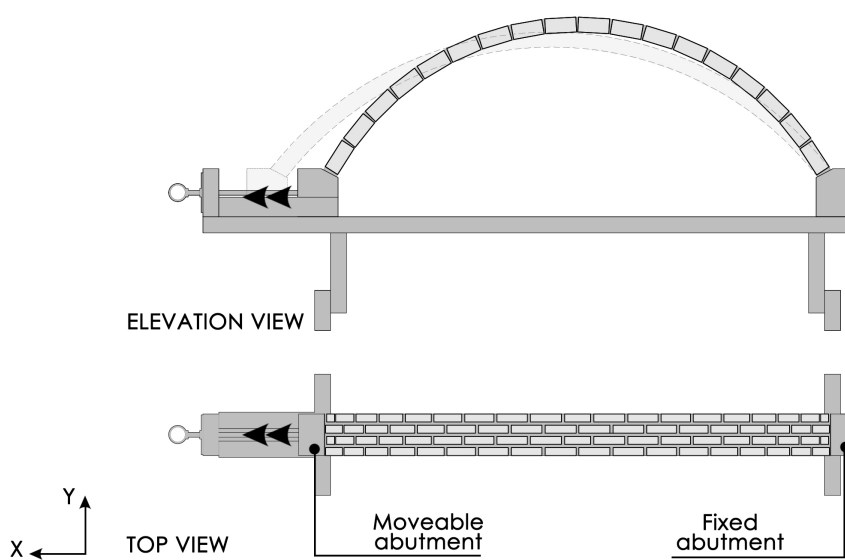


Fig. 7.1

Schematic description of the opening displacement imposed to the arch models.

In the first part of the experimental campaign, during the tests on the arch models, the imposed displacements are constantly monitored with a digital calliper, so the ultimate displacement (δu) is recorded for each test. The photographic acquisition provides images of the model during the deformation, helping to monitor the hinge opening during each step of imposed displacement. Moreover, the video acquisition allowed to capture the failure mechanisms of the models. In virtue of the bidimensional typology of the structures, all the data are extracted from the main vertical plane of the arches.

Tab. 7.1 reports a list of the tests performed on the arch models, together with the main information about each model: it shows the trials on the AR tests about the model features (different number of the blocks and material) and the different acquisition procedures (in the AV tests phase). All the other features concerning the methodology of the research All the features are settled to provide the best overlapping in the boundary condition of the different tests. As reported in the table, three of the tests have failed during the centering lowering because of the low stability of the timber material to the environmental conditions and errors of the research team during the procedures. All the remaining tests are performed by imposing the displacement (δx) to the abutment by twisting the activating rod at a low rate, to avoid failures by accidental movements of the set-up. The structural behaviour of the model is monitored in real-time by video acquisition. Images of the models are acquired by steps of 1 mm (Fig. 7.2), temporary stopping the displacement imposition. It is worth noticing the different behaviour of the AV_3 model, tested with opening displacement but not failed until the end of the experimental set-up range (further hypotheses and considerations about this phenomenon will be discussed in Ch. 8).

Tab. 7.1

List of the tests performed on the arch models. ¹¹

DATE	TEST	MATERIAL of blocks	NUMBER of blocks	ULTIMATE DISPLACEMENT [mm]	PHOTOGRAPHIC acquisitions	VIDEO acquisitions
25/05/2020	AR_1	Timber	69	10,56	ANE-LX1 HUAWEI camera Res. 4608x3456 [px]	Asus Zenfone Laser 2 camera Res. 1920x1080 [px]
10/06/2020	AR_2	Cement	62	13,2	ANE-LX1 HUAWEI camera Res. 4608x3456 [px]	Asus Zenfone Laser 2 camera Res. 1920x1080 [px]
14/06/2020	AR_3	Cement	65	13,95	ANE-LX1 HUAWEI camera Res. 4608x3456 [px]	Asus Zenfone Laser 2 camera Res. 1920x1080 [px]
20/06/2020	AR_4	Cement	65	16,14	ANE-LX1 HUAWEI camera Res. 4608x3456 [px]	Asus Zenfone Laser 2 camera Res. 1920x1080 [px]
03/07/2020	AR_5	Timber	65	-		
08/07/2020	AR_6	Timber	65	7,96	ANE-LX1 HUAWEI camera Res. 4608x3456 [px]	Asus Zenfone Laser 2 camera Res. 1920x1080 [px]
09/07/2020	AR_7	Timber	65	-		
16/07/2020	AR_8	Cement	65	13,91	ANE-LX1 HUAWEI camera Res. 4608x3456 [px]	Asus Zenfone Laser 2 camera Res. 1920x1080 [px]
17/07/2020	AR_9	Cement	65	13,15	ANE-LX1 HUAWEI camera Res. 4608x3456 [px]	Asus Zenfone Laser 2 camera Res. 1920x1080 [px]
25/09/2020	AV_1	Cement	74	10,62	ANE-LX1 HUAWEI camera Res. 4608x3456 [px]	Asus Zenfone Laser 2 camera Res. 1920x1080 [px]
27/09/2020	AV_2	Cement	74	16,70	ANE-LX1 HUAWEI camera Res. 4608x3456 [px]	Asus Zenfone Laser 2 camera Res. 1920x1080 [px]
12/10/2021	AV_3	Cement	74	-		
02/11/2020	AV_4	Cement	74	Structure not failed - end of the set-up range	Canon EOS 60D camera Res. 5184x3456 [px] DIC cameras	4 GoPro Hero 5 Session cameras Res 2704x1520 [px] 50 fps
05/11/2020	AV_5	Cement	74	29,32	Canon EOS 60D camera Res. 5184x3456 [px]	3 GoPro Hero 5 Session cameras Res 2704x1520 [px] 50 fps

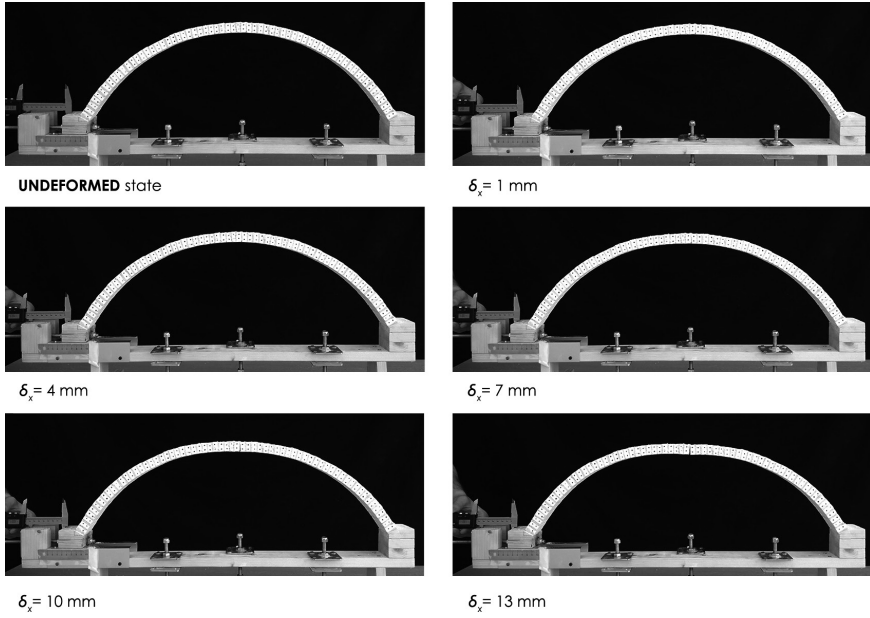


Fig. 7.2

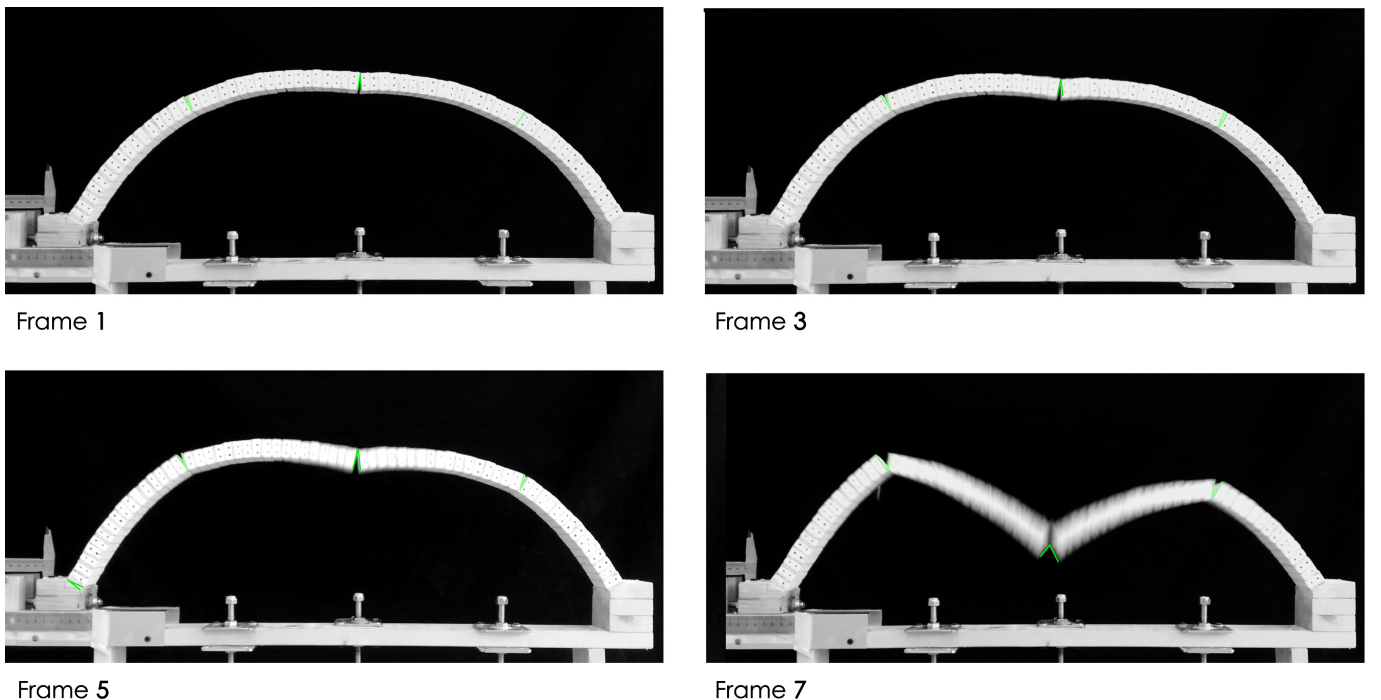
Image sequence of the arch model deforming during the opening test.

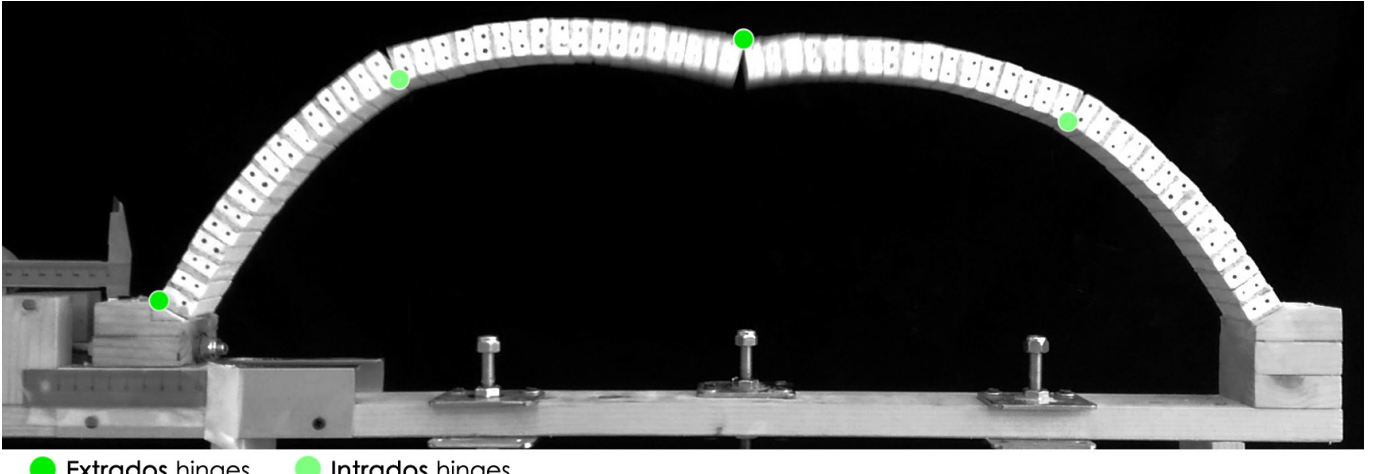
The failure mechanism is captured by slowing down the video acquisitions: several frames are isolated to have a more complete description of the hinge evolution during the test. As an example, Fig. 7.3, reports the collapse of the AR_9 model, where four frames are used to highlight the progressive opening of the hinges: in frame 1 and 3 the first three hinges are visible (green marks), while in frame 5 the fourth hinge that leads to the failure of the structure appears.

The failure mechanism is captured then in a single frame to highlight the position of the four hinges (Fig. 7.4) in the different tested models, making them comparable. In this representation the hinges are also classified by their position on the intrados or on the extrados of the arch.

Fig. 7.3

Sequence of frames extracted from the video of the arch model collapse.





● Extrados hinges ● Intrados hinges

Fig. 7.4

Description of the hinges position during the collapse of the AR_9 model.

7.1.2 Vault – Shear tests

The vault models are tested under in-plane shear displacement imposed to one of the abutments: this typology of tests is selected because of the scarce presence of data, in the scientific literature, about in-scale segmental barrel vault models, subjected to shear settlement. Similar tests are performed in Lagomarsino (2016), investigating the behaviour of an in-scale cross vault model, under simple and pure shear distortions. In the present work, the displacement setting is designed to simulate a simple shear mechanism (Fig. 7.5) obtained by sliding one abutment in the direction of the central axis of the vault: in this way, the two abutments remain always parallel (Fig. 7.6).

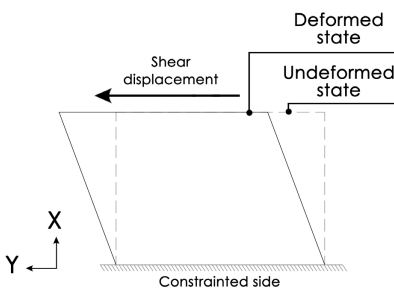


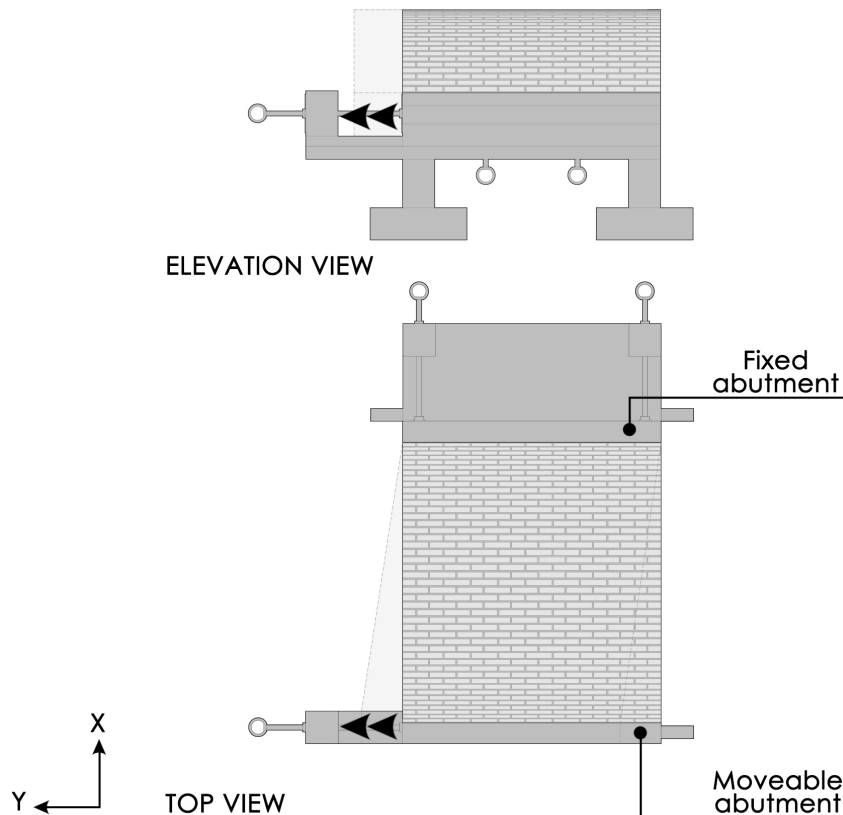
Fig. 7.5

Schematic description of the simple shear displacement.

The tests on the vault models are performed differently from the ones related to the arches. This difference is due to the more complex three-dimensional behaviour of the vaulted structures compared to the arched structures. In virtue of this complexity, the acquisition process is optimized with the use of new devices and techniques (deeply described in Ch. 5-6). The test is performed by manual activation of the displacement device and the imposed displacement is constantly monitored by a digital caliper. The test is stopped at fixed imposed displacements to allow the acquisition processes. Moreover, the test is also stopped when notable and visible phenomena occur to the model such as cracks, rotations, local failure, etc.

The need to describe these complex mechanisms leads to the realization of a schematic procedure to organize the description of the phenomena that occurred during the te-

Fig. 7.6

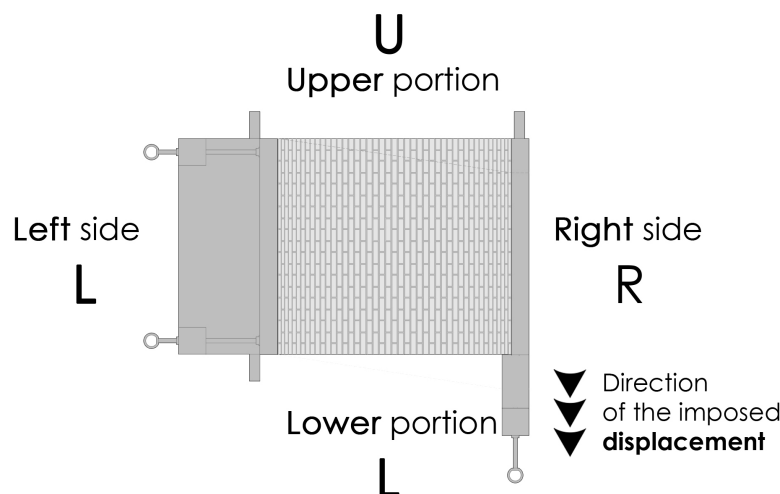


Schematic description of the simple shear displacement imposed to the vault models.

sts. This procedure involves, in the first phase, the collection of all the visible phenomena that take place, captured by the constant video monitoring or by the photographs of the specific events: these visible phenomena, like the position of cracks, hinges, or collapse, are referred to the scheme of the structure exposed in Fig. 7.7. The collection and organization of these phenomena are used as a base for the comparison of the digital acquisition products obtained from the models. This topic is discussed deeply in Ch. 5 6 and Ch. 6 8.

Fig. 7.7

Nomenclature of the vault models portion and subdivision legend.

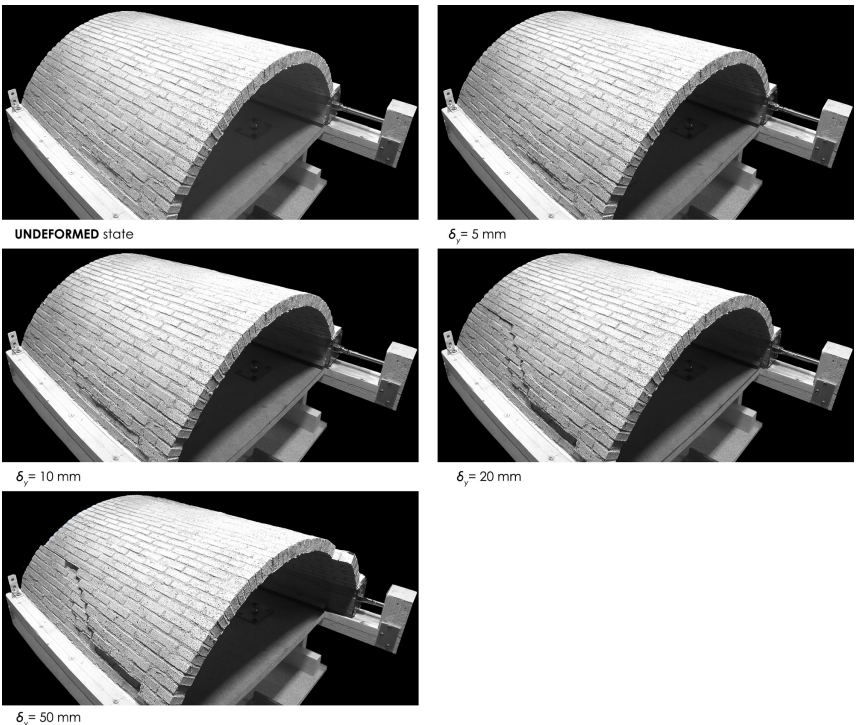


DATE	TEST	MATERIAL	NUMBER of blocks	ULTIMATE DISPLACEMENT [mm]	PHOTOGRAPHIC acquisitions	VIDEO acquisitions	GEOMATICS acquisition steps [mm]	DIC acquisition frequency [mm]
10/12/2020	VR_1	Cement	450	60,67	Canon EOS 60D camera Res. 5184x3456 [px] DIC cameras	4 GoPro Hero 5 Session cameras Res 2704x1520 [px] 50 fps	0 - 5 - 10 - 20 - 50	0,1
18/01/2021	VR_2	Cement	450	91,42	Canon EOS 60D camera Res. 5184x3456 [px] DIC cameras	3 GoPro Hero 5 Session cameras Res 2704x1520 [px] 50 fps	0 - 5 - 10 - 20 - 50	0,1
03/02/2021	VV_1	Cement	450	Structure not failed - end of the set-up range	Canon EOS 60D camera Res. 5184x3456 [px] DIC cameras Stonex F6 scanner	4 GoPro Hero 5 Session cameras Res 2704x1520 [px] 50 fps	0 - 6 - 15 - 25 - 46 - 50 - 85 - 130	1
03/02/2021	VV_2	Cement	450	93,77	Canon EOS 60D camera Res. 5184x3456 [px] DIC cameras Stonex F6 scanner	4 GoPro Hero 5 Session cameras Res 2704x1520 [px] 50 fps	0 - 6 - 15 - 25 - 46 - 75	1

Tab. 7.2

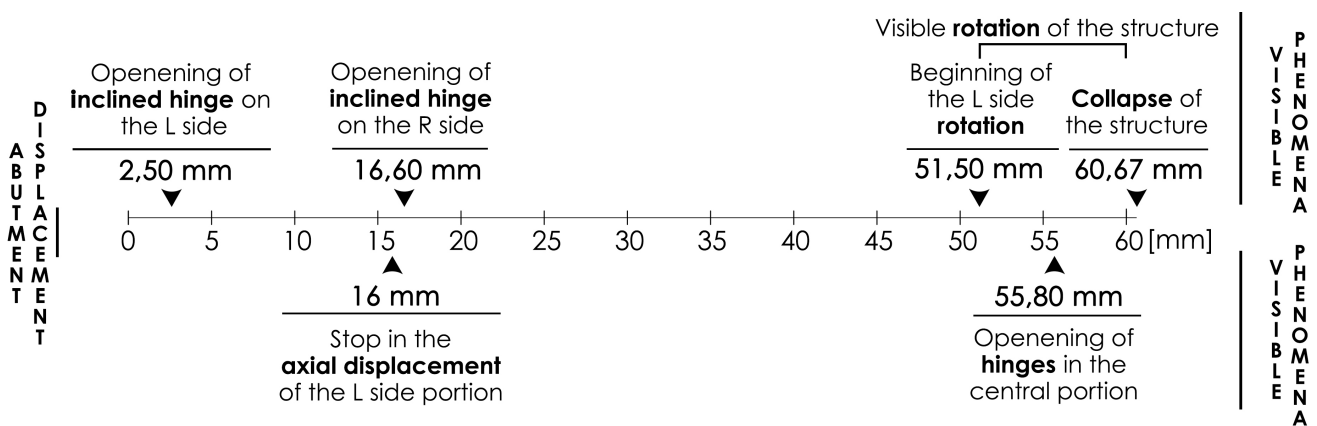
List of the tests performed on the vault models.

In Table 7.2 the tests performed on the vault models are listed, along with the main information about the composition, the ultimate displacement, and the acquisition techniques features.



As described for the arch tests, the imposed displacement is used as a basis to organize the proceeding of the work. The evolution of the model state, in terms of deformation, is constantly monitored and it is represented in Fig. 7.8 referred to the VR_1 model.

The tests on the different brick arrangements show the recurrence of specific phenomena. In order to map these phenomena and to compare the different tests, a schematic representation, like the one depicted in Fig. 7.9, is proposed. In the Figure the main phenomena collected by direct observation of the model behaviour and by comparing the simultaneous video and photo acquisition of the VR_1 model are highlighted along the “time line” of imposed displacements..



The collapse mechanism is captured in the video acquisition: the synchronization between the cameras allows to extract the correspondent frame from different perspectives (Fig. 7.10).

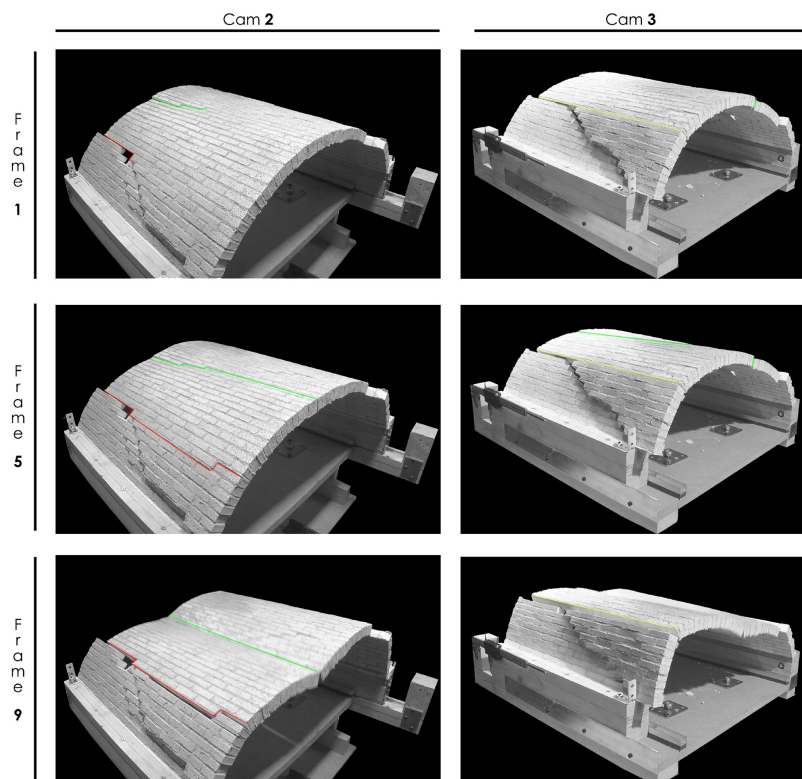


Fig. 7.9

Main phenomena occurred and registered during the AR_1 test.

Fig. 7.10

Image sequence of the VR model collapse during the shear test, acquired from different perspectives.

7.2 Acquisition and postprocessing

7.2 Image and video acquisition and processing

The photo and video acquisitions during the tests have been of fundamental importance in the documentation and understanding of the mechanisms developed by the structures. As for the research on the materials explained in Ch 3, also the research on the best solution for the acquisition has occupied a significant part of the work, starting from the first tests on the in-scale arch model with a radial arrangement of the bricks until the tests on the vault models.

In the first phase of the research the photographic acquisition is carried out with the use of an ANE-LX1 HUAWEI camera, integrated into a smartphone, with an image size of 4608x3456 px. This device, fixed on a photographic tripod, is used for taking pictures of the structure by steps of 1mm of imposed displacement. For the video acquisition the camera of an Asus Zenfone Laser 2 is used, with an image size of 1920x1080, which video output is cut to extract the frame of the failure of the structures. The use of these low cost easily available devices has helped, in the first phase of the experimental campaign, when it was not possible to access to laboratories, to have a chronology of the deformation from the beginning of the test to the failure. Recently, the use of these devices has been investigated also in the field of 3D digitization techniques for Heritage Objects, showing good results in the processing of datasets acquired with a smartphone (Adamopoulos et al., 2021).

While the tests proceeded, the acquisition process is modified reaching the final configuration used for the tests on the arch models with the vertical arrangement and on the vault models: the use of professional monitoring systems (such as DIC, photogrammetry and structured light scanners, exposed later in this Ch.) is introduced, while the video acquisition is improved with the usage of 4 GoPro Hero 5 Session cameras, used to film the whole tests from different perspectives (fig 7.11, 7.12). This is particularly useful in the arch models with radial arrangement, which have a significant out-of-plane behaviour. For this reason, as reported in the scheme in Fig. 7.12,b, one camera is positioned in front of the model, in a central position, while the other two cameras filmed the test with an angle from the centre. The last camera is positioned to film the failure from one side of the structure, to capture the opening of the hinges at haunches and between each row of bricks.

Fig. 7.11

GoPro Hero 5 Session, cameras used for video acquisitions.



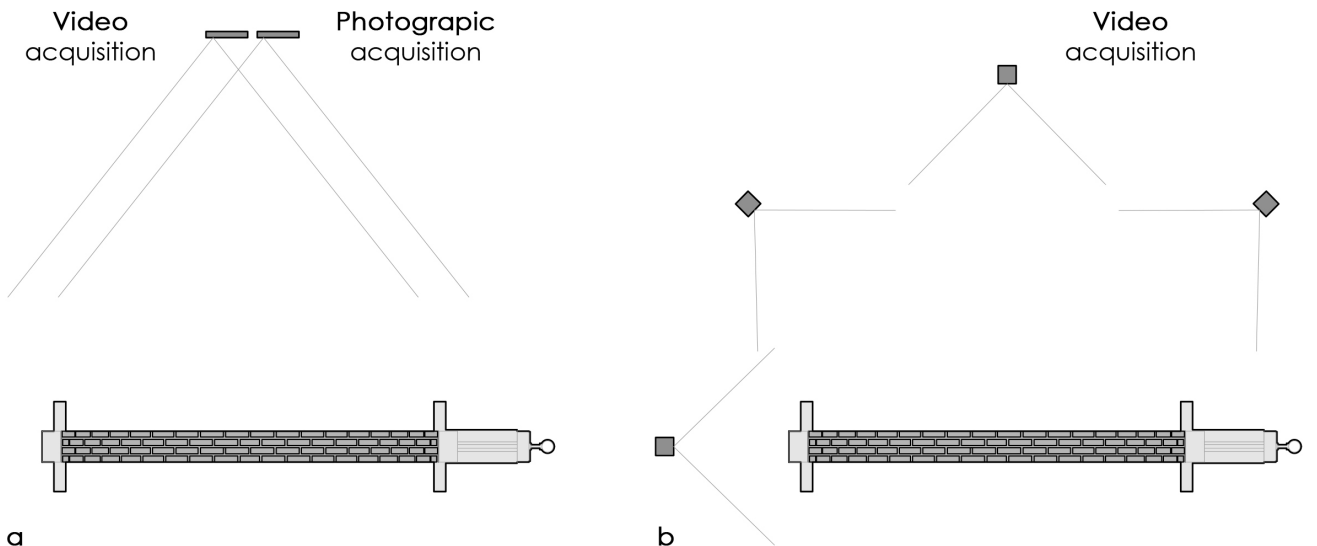


Fig. 7.12

Arch model tests – Image and video acquisitions scheme:

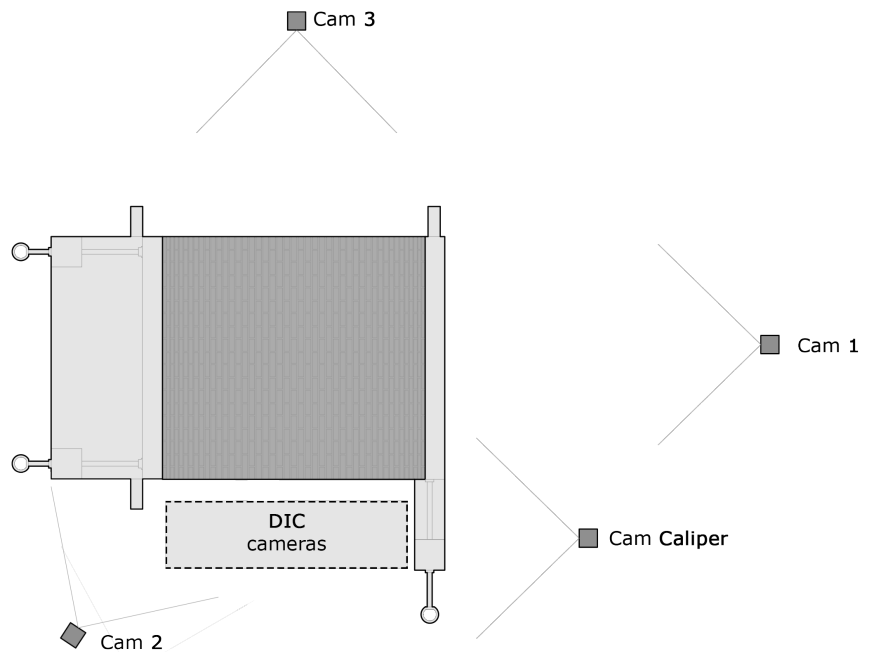
- a - Acquisition with smartphones:
- b - Acquisition with GoPro cameras.

The experience achieved during the arch's tests led to the selection of the camera positions in the vault's models tests. As shown in Fig. 7.13, due to the obstruction made by the DIC cameras, the position of each camera for the video acquisition is selected to take information on different parts of the model, in a compatible way with the other instrumentation: Cam 2 is used to film the behaviour of the vault's head, Cam 3 films from the left side the head and the haunches, while the Cam 1 is used to film the right side of the vault. Another camera (Cam Caliper) is used exclusively to film the calliper's display during the test, to correlate the images with the imposed displacement. The use of the app "Multi Camera Control for GoPro® Hero Cameras" allows synchronizing the four cameras, with a smartphone as a remote controller, making simpler the frame extraction at the same time steps from the videos. During all the tests the use of several smartphones and full frame digital cameras helps to take photographs of little portions of the model, collecting particular details of the masonry behaviour.

All the acquired material is analysed, helping to reconstruct the tests procedure and results: starting from the video acquisition it is possible to relate the visible phenomena that occurred to the models with the imposed displacement, visible on the calliper screen, and to relate these phenomena with the other detail photographs acquired. This type of control allows us to relate the macroscopic phenomena not acquired with range-based and image-based acquisition (treated in the next sections) with the models obtained from the processing of these geomatics' techniques. The results of these comparisons are reported in Ch. 8.

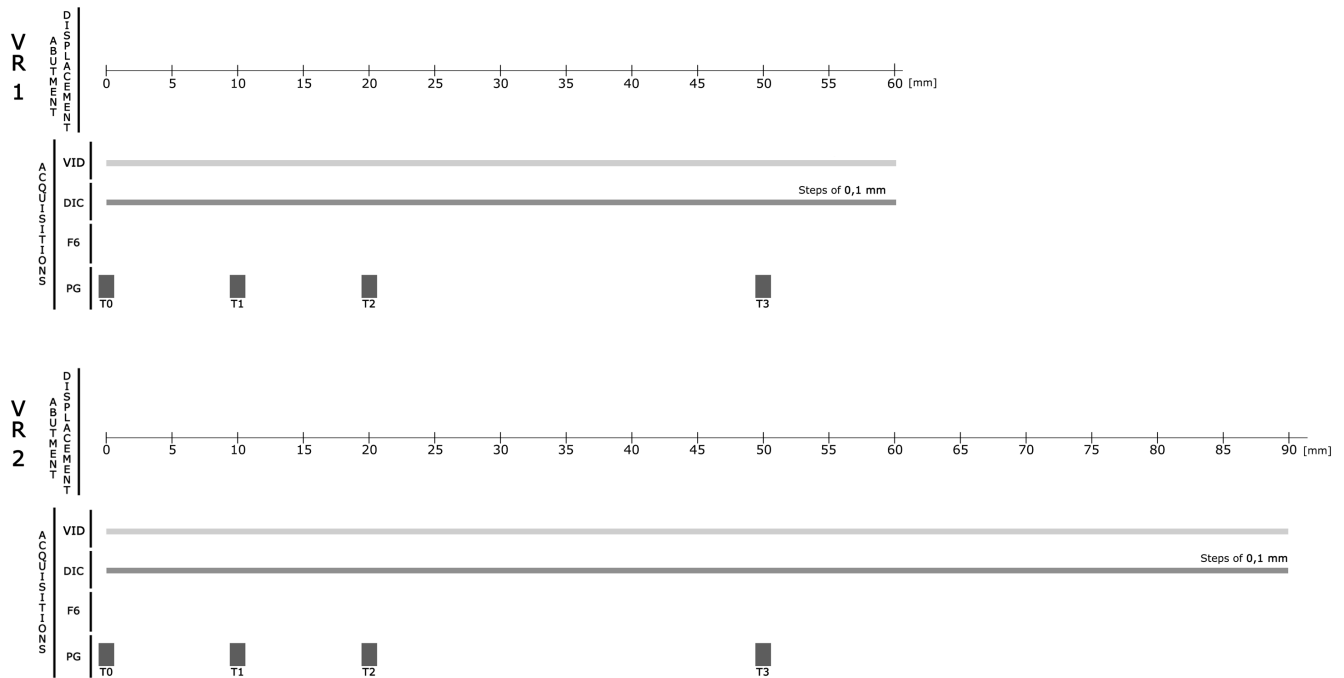
Fig. 7.13

Position of the fixed acquisition devices.



The use of video also provides interesting information about the behaviour of the models: using the open-source Meltytech Shotcut software the videos are examined in slow-motion and high-resolution frames are extracted to highlight interesting moments of the tests. These acquisitions are visible in Ch. 7, Ch.8, and Appendix in which the collapse mechanisms and the hinges evolution are reported. The video segmentation in single frames allows to reconstruct the entire development of the test .

VR TESTS



VV TESTS

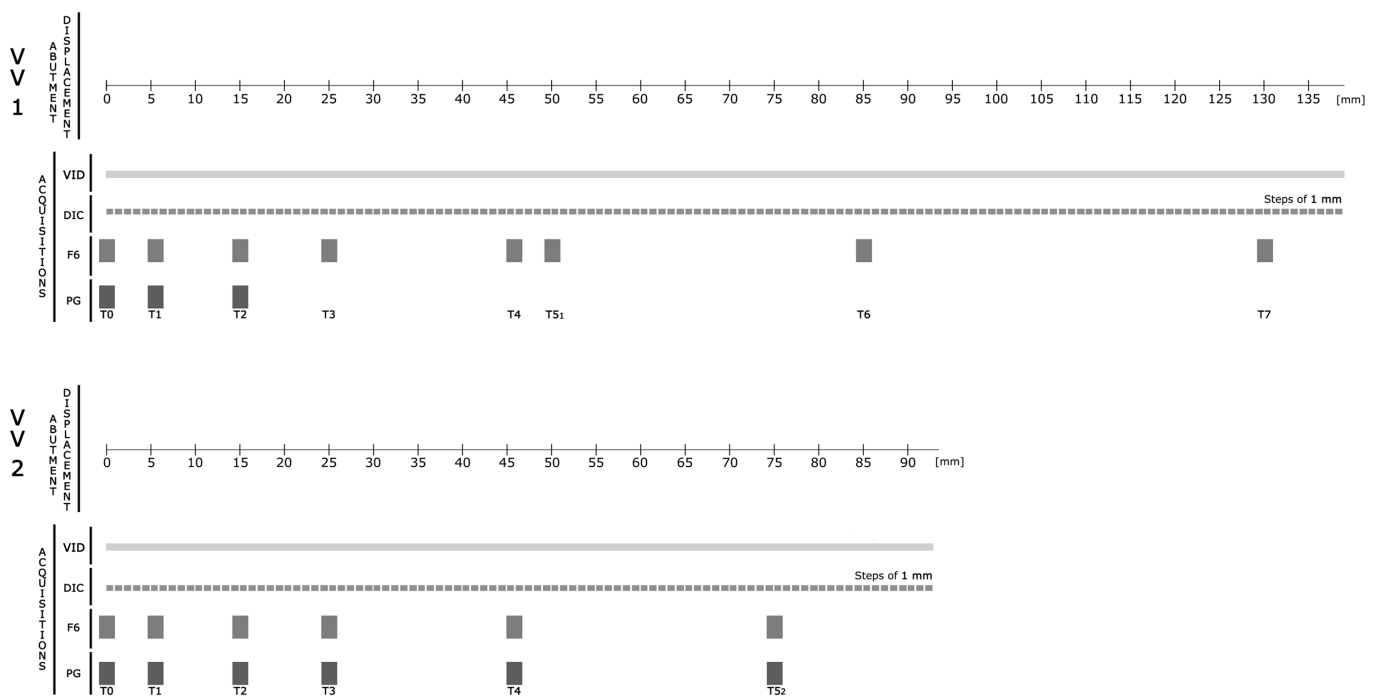


Fig. 7.14

Schemes of the acquisition program during the various tests

7.2.2 Geomatics' Techniques

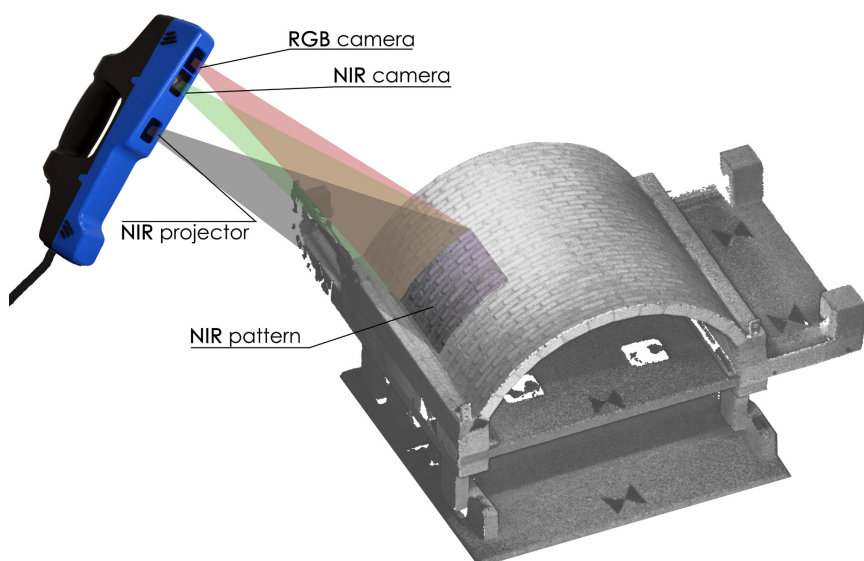
7.2.2.1 Range-based acquisition: Stonex F6 SR

7.2.2.1.1 Data acquisitions

The Stonex F6 SR structured light scanner (Fig. 7.15, 7.17) is used for the acquisitions of the in-scale model on two tests (VV_1, VV_2). It belongs to the Non-Contact Active Scanning category and works on the reflection of light for the measurement of objects. This hand-held scanner, as reported in the technical specification, is valid to survey small object, like the interested vault models. It has a certified accuracy of 90 µm acquiring 640,000 points per second, at a minimum distance of 250 mm (Tab. 7.3). The device is composed of a projector, using a Mantis Vision's proprietary pattern in near infra-red (NIR, wavelength from 780 nm to 2500 nm) light and two cameras: one with NIR and one with Red, Green and Blue (RGB). The cameras and projector direction converge, for using triangulation methodologies distance calculation. The device projects NIR light (invisible to the naked eye, wavelength – 850 nm) on the object, through a mask with a proprietary pattern, while the NIR camera (2D device) catch its reflection. The principle is close to the subtractive Moirè exposed in Ch. 6.1.1 (based on the deformation of a known pattern), using a particular triangulation algorithm able to calculate the third-dimension coordinate through the stereoscopic parallax effect. In this way the RAW data acquired are online registered together and processed by the Echo software's Decoder Algorithm, creating the depth maps. The NIR light projected is captivated, together with environment light, also by the RGB camera that acquires information about the radiometric components of the points.

Fig. 7.15

Schematic functioning of the Stonex F6 SR scanner.



The components from the two cameras are linked together by the online registration algorithm in the software, with the colour images meshed with the 3D models. The use of this software allows the registration of the coloured point cloud, by frames, in real-time, giving the possibility to evaluate the results during the process. One of the biggest issues, noticeable after the acquisition, is the excessive fragmentation of the point cloud: when the software detects a problem in the registration on the could portions, it automatically stops the acquisition of the current group, creating a new one. These issues are commonly solvable in post-processing, but it is important to be sure of the completeness of the material acquired for each step of displacement while working on an ongoing deformation test.

The acquisition is planned in respect of the boundary conditions of the laboratory's tests: the hand-held nature of the Stonex F6 gives the possibility to acquire the object surface by turning around the model, considering the impossibility of moving the model during the test. The presence of other fixed acquisition devices (DIC cameras and GoPro cameras) near the model, and the conformation of the experimental set-up, put limits on the accessibility of the object, giving the necessity of planning the acquisition in virtue of the possible results usages. For this reason, only the extrados and the upper head (see Ch.4, ...) of the vault models are chosen to be acquired, considering the single bricks as rigid bodies and their opposite faces as always parallel. These assumptions, according to the classical masonry theory, allow us to relate the detected extrados behaviour with the undetected intrados one. The acquisitions involve also fixed elements of the experimental set-up and the surrounding table; then the scene is prepared with the positioning of black tape markers: in the acquisition planning phase, it is decided to use the dataset from structured light scanning as reference for the data processing of the close-range photogrammetry and these markers are useful to relate the information from two methodologies.

Stonex F6 SR

Speed	640,000 [pts/s]
Range distance	250-500 [mm]
Accuracy	90 µm @ 250 mm
Resolution	0.4 mm @ 250 mm
RGB camera resolution	1.3 [MPx]
Video frame rate	8 [frame/s]



Fig. 7.17

Sonex F6 SR hand-held scanner plugged in a laptop.

Tab. 7.3

Stonex F6 SR main specifications.

The acquisitions with the F6 scanner are taken in different and selected moments of the test, along with the close-range photogrammetric procedures (Tab 7.4): the first one is done after the lowering of the centring, capturing the undeformed configuration of the model (reported as T0 in all the postprocessing phases and restitution). The enforcement of the abutment displacement stops at the reaching of these fixed values to allow the acquisition procedures: the other three acquisitions are taken respectively at 6 mm (T1), 15 mm (T2), 25 mm (T3) and 46 mm (T4) of imposed displacement. Some other spare acquisitions are taken in different moments of the two tests: for the VV_1 model other three steps have been acquired respectively at 0 mm, 85 mm, and 130 mm, while for the VV_2 model at 75 mm. In Tab. 7.4 are reported the acquisitions for each test.



Fig. 7.18

Stonex F6 acquisition process during the experimental test.

The workflow of acquisition followed the descriptions present in the literature (Patrucco et al, 2019). The scanner is connected by cable to a laptop, to improve the movability of the device around the model, and to connect it to Mantis Vision Echo software (version 2.0.0) for data management. The scanner is now used with slow and fluid movements, without interruptions, starting from a side of the experimental set-up and covering it all, from different perspectives, holding the device to a distance of about 1 m from the object (Fig. 7.18). The best results are obtained in the acquisition with no interruption or hesitations in the scanner passages. A single acquisition of the model with the Stonex F6 SR takes about two minutes. The use of the corresponding software gives real-time feedback of the ongoing data acquisition, and it allows to notice issues in the process: on some occasion during the experimental campaign the check of the data soon after the acquisition, with this device, helps the research team to notice problems in the acquired dataset, such as excessive segmentation of the point clouds and visible misalignment of the segments. The possibility of a real-time check of the data is a great deal for this kind of research: due to the destructive nature of the experimental tests carried on, it is important to be sure of the data quality before continuing the imposition of the displacement that leads to modifications in the involved structures. It is interesting to notice that the data from polished aluminium elements, like abutment rails, present some flaws in the acquisition by the scanner because of the high reflection of the NIR pattern on the surfaces. Nevertheless, this lack of information does not compromise the acquisition integrity, because of the marginality of the element involved.

Tab. 7.4

List of the structured light acquisition performed during VV tests.

DISPLACEMENT	TEST		NAME
	VV_1	VV_2	
0 mm	x	x	T0
6 mm	x	x	T1
15 mm	x	x	T2
26 mm	x	x	T3
46 mm	x	x	T4
50 mm	x		T51
75 mm		x	T52
85 mm	x		T6
130 mm	x		T7

At the end of the experimental campaign, a total of 16 data acquisitions performed with the Stonex F6 SR are processed: 12 of them contain data from a single step of the tests while the other 4 are the result of partial acquisitions of two different steps, depending on the issue detecting system of the software, previously mentioned.

7.2.2.1. 2 Data processing

The data acquired with the Stonex F6 scanner are directly imported in Mantis Vision Echo software (version 2.0.0) during the scans and are processed in the same ambient following the User Guide (Document Review 3.0.3).

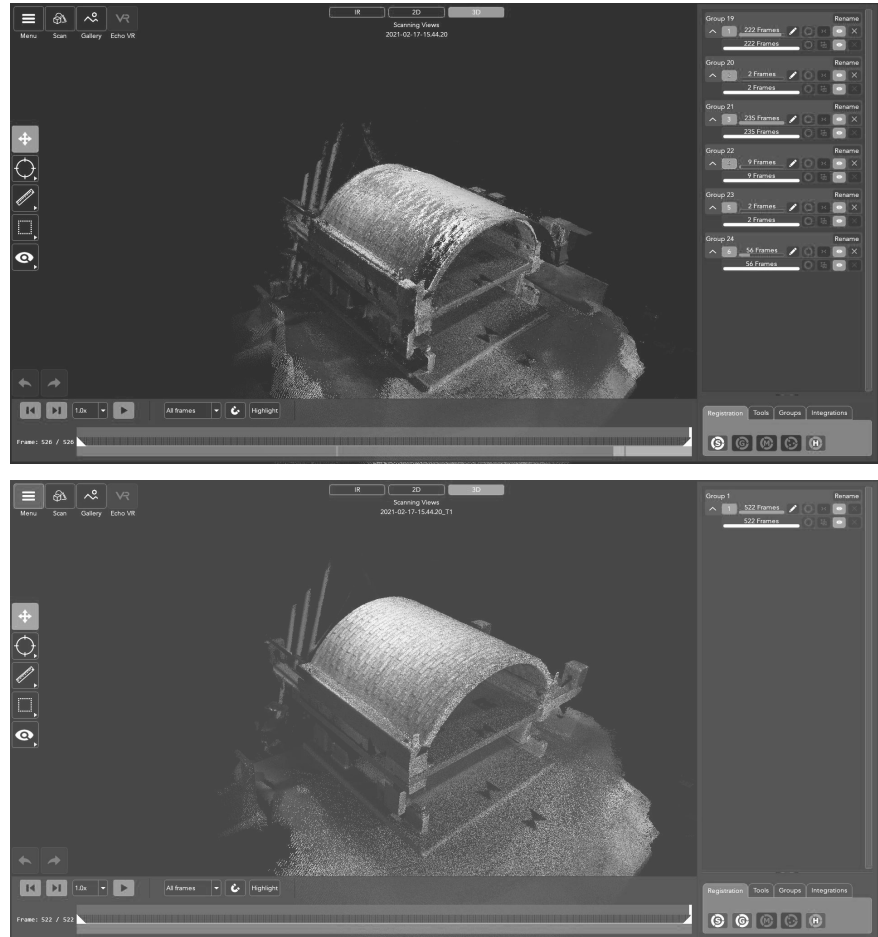
The first data processing is carried out in real-time and automatically by the software during the scans. All the image frame acquired from the NIR camera are converted into point-cloud frames and then registered together creating a three-dimensional model. This process, named Online Registration, is based on the redundancy of data extracted from overlapping geometries of the images. Each frame is matched (aligned and registered) with its direct neighbouring frame, coming from the acquisition stream process. The good overlapping between the frames, due to the dynamic acquisition process, provides enough data for merging together the point-cloud portions through the use of the Iterative Closest Points (IPC) algorithm: IPC algorithm is selected for the co-registration of the clouds due to its consolidated use in literature (Guidi et al, 2010, x). It works on the redundancy of data, involving the global shapes of the objects and the overlap between the portions of the segmented clouds. It works with the minimization of the distance error calculating the diffe-

rence between the overlapped scans and choosing the closest points evaluating the Root Mean Square (RMS): this value expresses the average error in the combining of the two datasets.

The Raws files obtained from the scans need a preliminary check before an ulterior registration. As reported, issues in the acquiring generate excessive segmentation in the point clouds due to the impossibility of the software to match the close frames: a manual check of the magnitudes of the segments can help to eliminate the groups with a low number of frames (e.g., in the same file can exist groups of 200 frame with groups of only one frame) (Fig. 7.19). This procedure helps to reduce problems linked to the registration, illustrated in the following. As a first step in the registration of the groups (segmented or merged) a High-Quality Registration (HQ) is performed: this is a general image quality registration improvement process that tries to merge all the segments. Differently from the Online registration performed during the acquisition, the HQ registration work on the totality of the frames and not frame-by-frame. In this way all the portions are matched and aligned together. The last build of Mantis Vision Echo software is implemented with photogrammetric features: is possible to use the texture acquired from the RGB camera to help the

Fig. 7.19

- | | |
|----------|---|
| Top - | Raw cloud with misaligned and segmented frames; |
| Bottom - | Processed cloud with registered and aligned frames. |



registration of the frames on the depth map acquired by the NIR camera. This feature is used in the HQ registration for the clouds of the VV_2 test, where the optimal light conditions helped the acquisition of the textures, demonstrating good results and fewer issues in frames aligning compared to the processing of the VV_1 test, conducted with worse light conditions. After all the frames are registered, a Global Registration (G) is performed. This algorithm tries to link every 3D frame, once coregistered together, in a single coordinates system estimated on the relative position of the frames. In this way is possible to rectify issues like cumulative errors in the registration. Once the frames of the cloud are registered, another manual check can help to optimize the work: some micro-misalignment of the groups (repetition or micro-tilting of the portions) can occur without the software noticing them. Using the Frame Bar allows investigating the acquisition process frame-by-frame (highlighting, by steps, the position of the currently visible frame), making it possible to individuate and discard the misaligned frames.

The obtained clouds, still noisy, can be filtered by the built-in denoise filters of Mantis Vision Echo: the Statistical Outliers Removal (SOR) cleaning algorithm and the Moving Least Squares (MLS) smoothing algorithm. Both are typically used in point cloud management and are well documented in the scientific literature. The SOR filter can reduce the errors, typical in laser scanning, due to the presence of sparse points far from the major cloud. It is based on the computation of the statistical distribution of points in a neighbourhood, calculating mean distances. The software, after the input of the filter intensity (Fig 7.20), trims away from the dataset the point outside the Gaussian global distances mean and standard deviation. The Mantis Vision Echo's interface allows the selection between standard intensities of the filters and after empirical trials, it was used a +1 level of SOR cleaning algorithm. The MLS provide a solution to denoise the points not so far from the actual model. It estimates a continuous function from a set of point samples through weighted least squares measure of the area. This allows obtaining a smooth surface from a noisy portion of the point cloud. As for the SOR filter, also for the MLS, the level of filtering was found out of empirical trials, selecting a +2 level (Fig. 7.20).

A total of 12 point clouds are obtained from a single step of the tests while the other 4 are the result of partial acquisitions of two different steps. These partial point clouds are exported

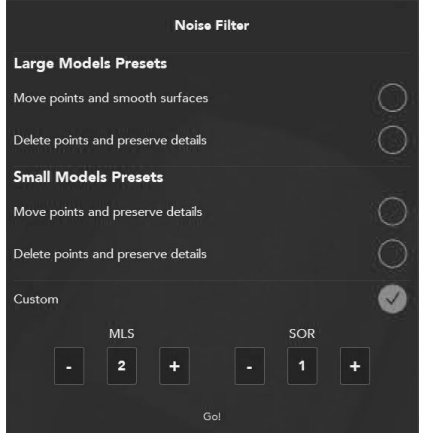


Fig. 7.20

Mantis Vision Echo Filtering options. Settings used in the cloud processing.

for being merged with a consolidated workflow, exposed in the next section.

7.2.2.1.3 Coordinate system setting

Once obtained, the filtered dense clouds (Fig. 5.9) are exported to other software for managing the information.

The 4 segmented point clouds, coming from partial acquisition steps, are merged by importing the concerned portions in Cloud Compare software, pre-aligning them manually and then performing an ICP registration. ICP is a semi-automatic algorithm because the processing needs a pre-alignment phase, depending on the operator's work and it is used as a base for most of the co-registration operations during the present work. In this way other two point clouds corresponding to single steps of the tests are obtained, for a total of 14 three-dimensional models.

Once obtained all coherent point clouds of the various steps of the displacement, the first task, necessary to compare them, is to co-register all the models in a unique reference system. The VV_1_T0 model is selected as the base for the registration of the other steps: this cloud is selected because representing the undeformed in-scale model, giving the possibility to manage all the measures regarding the experimental set-up, collectable also after the tests, in case of accidental errors during the tests. The VV_1_T0 cloud is imported in 3Dre-shaper software where is possible to extract an approximating vertical plane laying on the bottom head (Fig. 7.21) of the vault model and a second horizontal plane out of the base panel of the experimental set-up (Fig. 7.21). These planes are used to create an arbitrary reference system orthogonal to the principal axes of the model: the imposed displacement of the abutment lay on the Y-axis, derived by the base panel,

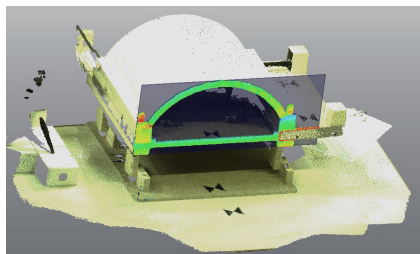
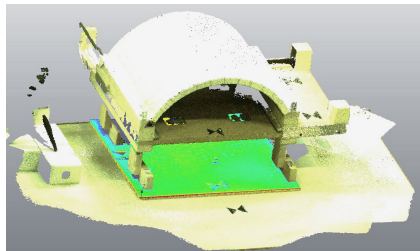


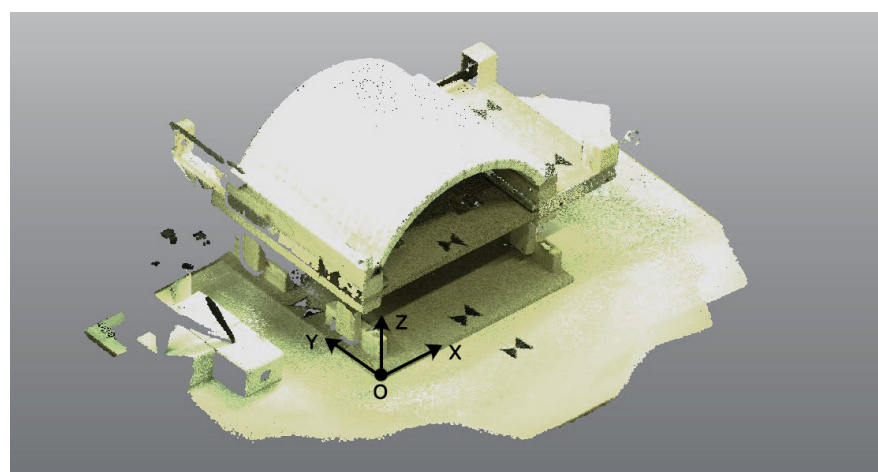
Fig. 7.21

Planes used for the local coordinate system.

- Top - Horizontal plane from the vtbase panel;
- Bottom - Vertical plane from head arch's plane.

Fig. 7.22

Origin and directions of the arbitrary coordinate systems



while the X-axis lay on the approximated plane of the vault's head. The obtained Z-axis is oriented with the positive values following the rise of the vault. The origin of the system is settled in the corner of the base plane (Fig. 5.13); this allows to have only positive values in the coordinates on the vault clouds (working with only positive coordinates is useful for the managing of the data in the software).

Because of the great differences between the obtained clouds, depending on the vault deformation and on the different acquisition of the marginal portions of the scene, this preliminary phase of the pre-alignment before the use of the ICP algorithm is articulated in 3 different steps:

- Pre-alignment: through the extraction of a plane from the base panel (described previously) is possible to pre-align the clouds before the use of the ICP. A provisory plane is extracted from every model and it is used for aligning the various point cloud through the orientation of the main axes (X, Y).
- Segmentation: the fixed part of the experimental set-up is segmented from the moveable part (Fig. 7.23) allowing to obtain similar portions among the various steps of registration. The vault and abutment portion are separated from the main device. Once the clouds are pre-aligned, they are cleaned from the undesired portions of the scene, not needed for the work.
- Adding reference points: due to the impossibility of using the ICP algorithm with the pre-mentioned moveable portions because of the will of not altering the segment containing the vault, five reference points are added around the clouds, in random coordinates, without contacting them. The use of these point allows to re-locate the move-

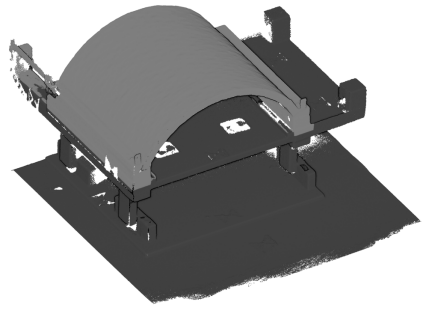


Fig. 7.23

Initial segmentation of the clouds.

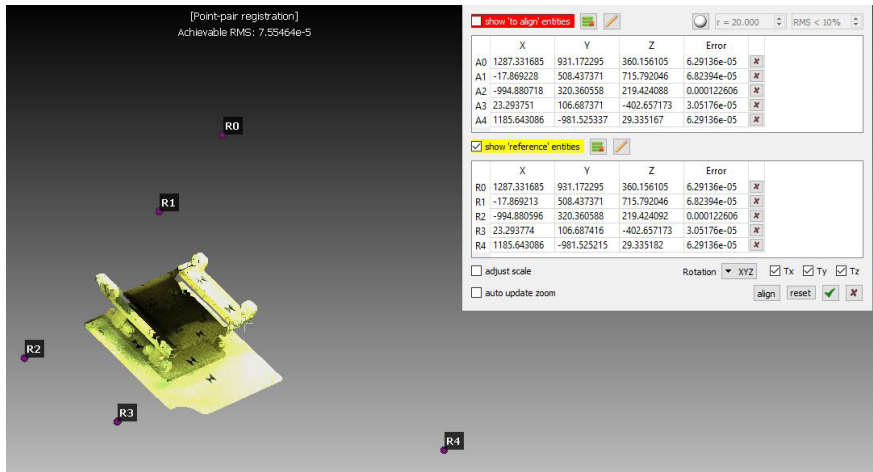


Fig. 7.24

Using of fixed point for clouds co-registration.

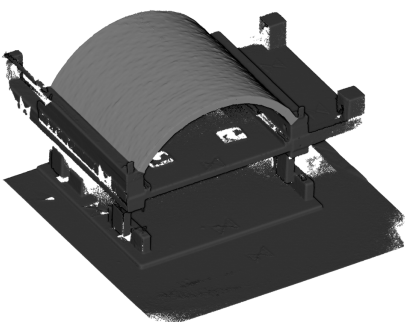


Fig. 7.25

Final segmentation of the clouds.

able portion on the corresponding fixed portion (Fig. 7.15) after the co-registration of the latter.

Once obtained the segmented clouds of the fixed portions, they are exported in Cloud Compare software because it offers the possibility to set a percentage of overlap during the ICP fine registration: the possibility of not requiring a complete overlapping of the clouds is important to reduce the errors depending on the little differences between the clouds (fallen bricks on the panel during the tests, little issues in the acquisition of the zone covered by the vaults, etc.). Several empirical trials on the overlapping percentage are made to obtain a good result, fixing it finally to 80%. The co-registration obtained has the final RMS with variations between 1,5 mm and 2 mm, considered acceptable for the percentage of overlap and the purposes of the work. Now, after the co-registration the fixed parts, the moveable ones (composed by the vault and abutment portions) are matched with the corresponding bases using alignment by the previously mentioned points. The dense clouds are now segmented one more time, separating the abutments from the vault, and merging them with the fixed parts, obtaining two resultant clouds (Fig. 7.25): the experimental set-up, maintained for hypothetical further checking of the models, and the stand-alone vault, now comparable for the structural analysis work.



Fig. 7.26

Images of the photogrammetric acquisition process during the experimental tests.

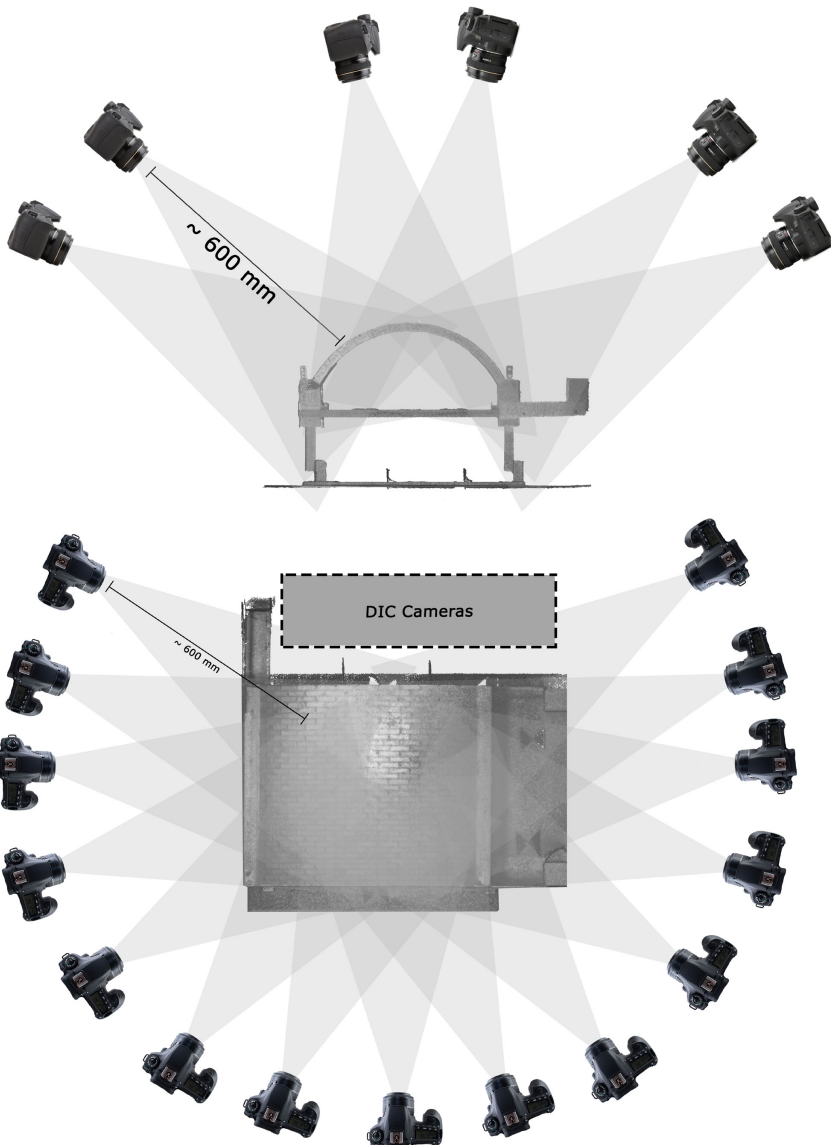
7.2.2.2 Image-based acquisition: close-range photogrammetry

7.2.2.2.1 Data acquisitions

The close-range photogrammetry is used for the tests on the vault models (VR_1, VR_2, VV_1, VV_2). As it will be exposed in the following paragraphs, the photogrammetry processes used can be divided into two different workflows with slight differences: the first two tests (VR_1 and VR_2) were planned with the use of only the close-range photogrammetry, while for the remaining tests it is integrated with the usage of the structured-light scanner. This improvement in the acquisition process, with many others, corresponds with the joining of the Geomatics for Cultural Heritage Lab (G4CH) researchers into the research team.

The photogrammetric acquisition of the models had to deal with the same issues exposed for the range-based acquisition: the impossibility of moving the experimental set-up du-

ring the tests and the presence of fixed devices, such as DIC cameras and GoPro cameras. For speeding up the acquisition the image takes are planned without the use of a photographic tripod, with the operator turning around the set-up. The acquisitions are taken from a distance of about 600 mm from the models with multiple rows of convergent and nadir images (Fig. 7.27) to collect a good overlapping of the photographs. With these parameters of acquisition is possible to estimate the Ground Sample Distance (GSD) of the images as 0,01 cm/px (Tab. 7.5).



Camera	Canon EOS 60D
Sensor	CMOS APS-C - 18 [Mpx]
Image size	3456 x 5184 [px]
Focal lenght	24 [mm]
Sensor size	25,1 x 16,7 [mm]
Distance of acquisition	mean 600 [mm]
GSD	0,01 [cm/px]

Fig. 7.27

Schemes of the acquisition process, with rows of convergent and nadir images.

Tab. 7.5

Ground Sample Distance parameters.

As for the range-based acquisition, the use of photogrammetry is focused on the extrados and the head of the vault models. The acquisitions are taken in different moments of the test (Tab. 7.6): a first one is done after the lowering of the centring, with an undeformed configuration of the model, the other three acquisitions are taken respectively at 10 mm, 20 mm and 50 mm of imposed displacement. The tests are stopped at the reach of these fixed values to allow the acquisition procedures.

Tab. 7.6

List of photogrammetric acquisitions performed during VV and VR tests.

DISPLACEMENT	TEST		NAME
	VR_1	VV_2	
0 mm	x	x	T0
10 mm	x	x	T1
20 mm	x	x	T2
50 mm	x	x	T3

DISPLACEMENT	TEST		NAME
	VV_1	VV_2	
0 mm	x	x	T0
6 mm	x	x	T1
15 mm	x	x	T2
26 mm		x	T3
46 mm		x	T4
50 mm		x	T51
75 mm			T52
85 mm			T6
130 mm			T7

For all the acquisition is used the Canon EOS 60D camera (Fig. 7.28, a), equipped with two different macro lenses. In Tab 7.7 are reported the main characteristics of the devices.

Tab. 7.7

Main specification of the Canon EOS 60D and the lens used in the acquisitions.

Canon EOS 60 D

Sensor	CMOS APS-C 18 [Mpx]
Sensor size	25,1×16,7 [mm]
Image size	3456 x 5184 [px]
Lens	I. Canon ef 24-105mm f/4l is ii usm II. Canon ef 24-105mm f/4l is ii usm with focal lenght block
Focal length	I. Variable II. 24 [mm] Fixed

The image acquisitions of the VR models are carried out with a Canon ef 24-105mm f/4l is ii usm macro zoom lens (Fig. 7.28, b) mounted on the camera, illuminating the scene with two fixed, high intensity, LED lights and the LED light integrated into the DIC cameras set-up. The images are acquired in circular paths around the model, with two different inclinations,

capturing sequential portions of the object. In addition, four photographs of the top part of the model are taken. With this set-up are acquired 467 images, subdivided into 8 steps, four for each test VR_1 and VR_2. The acquisitions for the VV models are improved with the use of portable LED light, moving around the model with the camera (Fig. 7.26), heavily reducing shadows and blur effects compared with the images of VR tests. The Canon EOS 60D camera is equipped with a Canon EF 24-105mm f/4L IS II USM (Fig. 7.27,c) with a focal length lock. The use of a macro lens with a fixed focal length for the image acquisition results to be more efficient in the processing of the data compared to the use of a zoom lens as will be exposed in the following paragraph. The images are acquired in circular paths around the model, with three different inclinations, capturing sequential portions of the object with a wider perspective on the object than the previous test. With this set-up the images are acquired, subdivided into 9 steps, three for the VV_1 test and five for the VR_2 test. The scene is prepared before the starting of the test applying eight markers made of black tape. These markers help to extract control points from the clouds acquired with the range-based method, selected as ground truth, as exposed before in this Ch.

7.2.2.2 Data processing

The data processing of the close-range photogrammetry images is carried out with the SfM-based Agisoft Metashape software, to obtain dense clouds comparable with the structured-light ones. All the acquired images are imported in the software and, through the Camera calibration tools, is possible to check their data: this way it is possible to control the focal length of each image, discarding the minority of photographs with different focal length from the dataset, because of the difficulty for the software to correctly calibrate the images with this different feature. As exposed before, this variation is solvable with the use of a fixed focal length lens instead of a zoom lens. All the images uploaded in the software are manually masked (Fig. 7.29) to reduce the noise of the background: those masks reduce the portion analysed by the algorithm to only the experimental set-up and the vault model; the presence of the fixed parts of the set-up allows to reference the object and later to control alignment and registration with other clouds. After the masking, all the photos are aligned, generating the sparse clouds of tie points (Fig.



Fig. 7.28

Equip used for photographic acquisitions:

- a. Canon EOS 60D camera
- b. Canon ef 24-105mm f/4l is ii usm
- c. Canon ef 24-105mm f/4l is

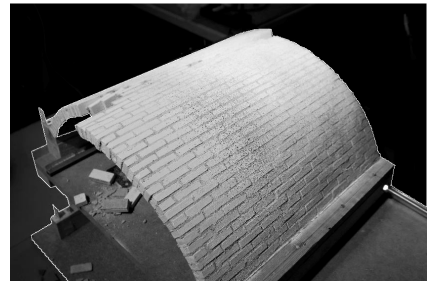


Fig. 7.29

Masking of the acquired images

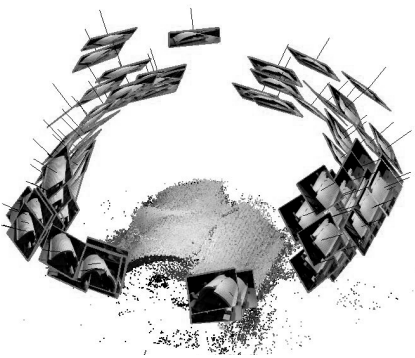


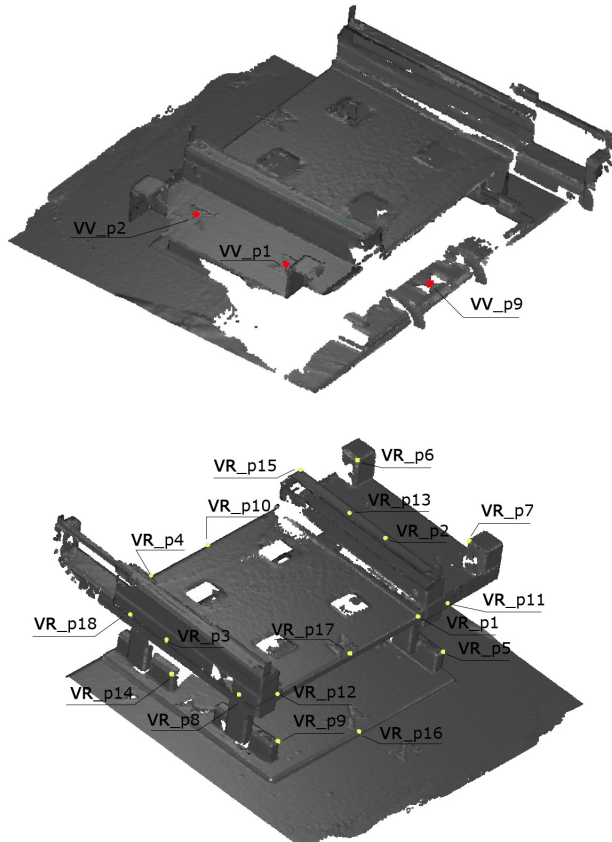
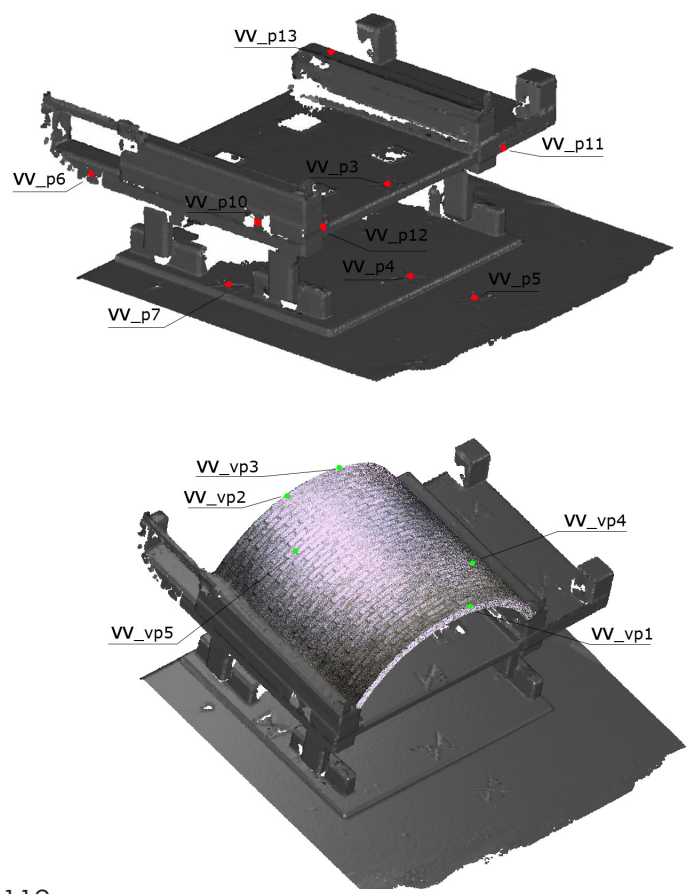
Fig. 7.30

Sparse cloud of tie points with cameras' position reconstruction.

7.30). The VV_2_T0 cloud, from structured-light scanner acquisition, are used to extract reference points to use for the scaling and aligning of the photogrammetry models: a mix of marked point (black tape markers) and natural points (recognizable features like edges, screw, etc.), from the set-up (Fig. 7.31), are used for the VV models while for the VR models only natural points, extracted from the set-up, have been used. All the models used a minimum of 12 Ground control points (GCPs) and 4 Control points (CPs) selected by the operator, depending on the number of projections of the points in the image dataset.

The software uses GCPs with the double aim of refining the calculation of the internal camera orientation and perform the rototranslation of the model into the coordinate system imported from the structured light acquisition. The use of CPs allows estimating the accuracy of the camera alignment through the evaluation of the RMS error as the difference between the coordinates of the markers and their position on the images calculated over all photos where markers are visible.

In all the cloud processed the magnitude of the estimated error is around 1 mm for the CPs and submillimetre for the GCPs. Once obtained these values, considered acceptable,



the models are processed to generate high quality dense coloured point clouds. The dense clouds obtained (Fig. 7.32) this way, are already registered with the structured-light ones processed previously, due to the use of the same arbitrary local coordinate system settled during the co-registration of the VV tests clouds (Fig 7.22) This allows to compare every single cloud with other clouds from every step of the acquisition of every test and to double-check the model, comparing the clouds of the same steps obtained with the two technologies, revealing submillimetre difference.

The dense clouds are now imported in Cloud Compare where they are segmented, separating the vault from the set-up; the obtained models of the structures are also filtered with the SOR algorithm to be denoised. After these steps, the clouds are all similar and it is possible to compare them. For this works, Cloud to Cloud (C2C) comparison and the Multiscale Model to Model cloud comparison (M3C2) algorithms (Fig. 7.34) are used, both documented in the literature for the deformation analyses (Wunderlich et al, 2016; Holst et al, 2017). These algorithms work with the subdivision of the three-dimensional clouds in octrees (tree data structures) used to compute the distance vectors between the reference and the compared objects. The three-dimensional point cloud obtained,

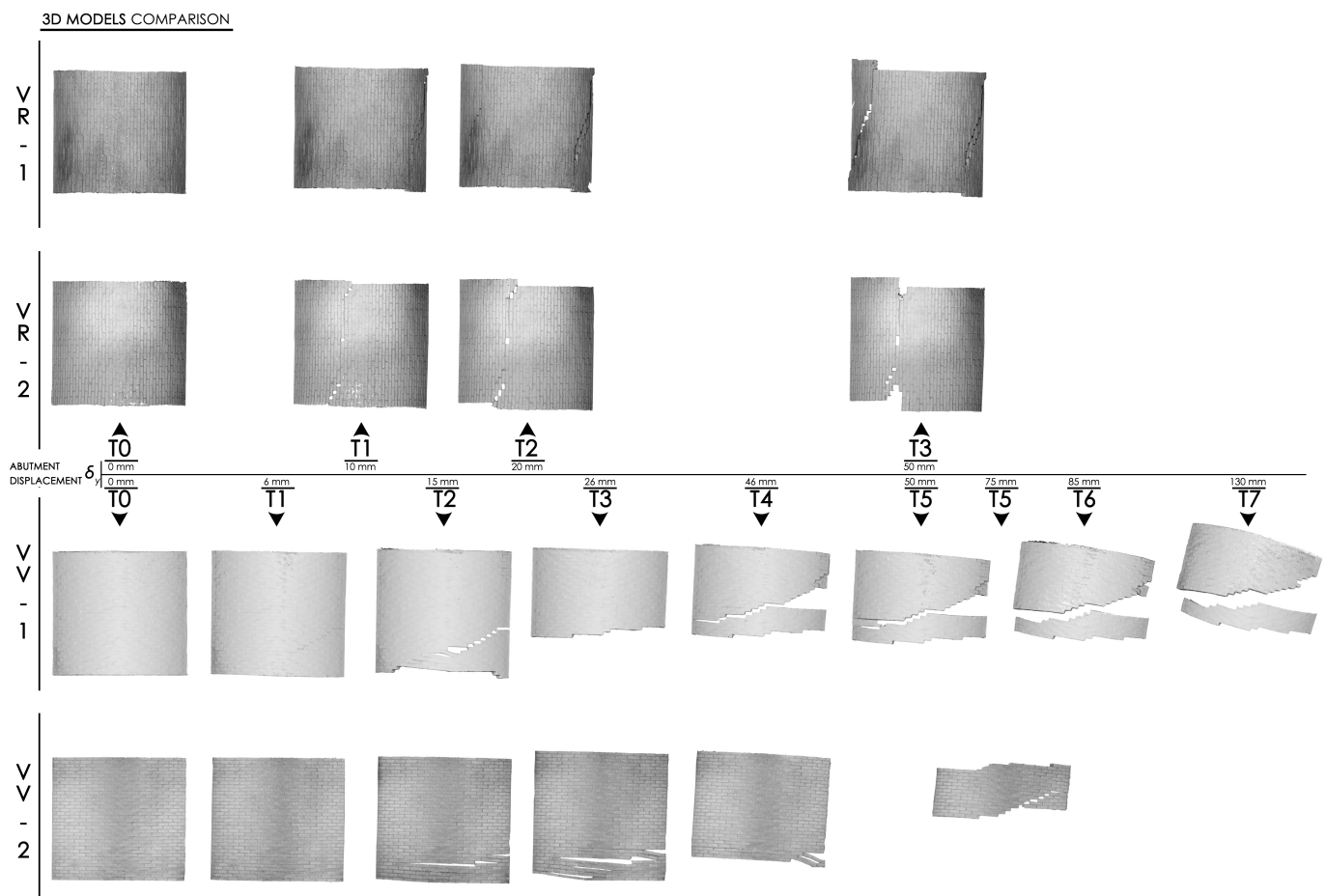


Fig. 7.32

Photogrammetric dense cloud of VR_2_T3.

Fig.7.33

List of all the clouds obtained with both acquisition methods.



allows the extraction of orthophotos from the main planes of the in-scale models: because of the limits in the acquisition possibilities, previously exposed, these metric representations are extracted only from top and frontal views of the models, representing respectively the extrados and the head arch of the vault. The orthophotos obtained are now manageable in Computer-Aided Design (CAD) ambient to evaluate geometrical and metrical information such as the crack pattern and the magnitude of the structure's rotations. The interpretation of the information provided by the three-dimensional acquisition products, along with other methodologies evidence is exposed in Ch. 6.

Fig. 7.34

Example of C2C comparison between different clouds of the same test.

Reference: VV_2_T0,

Compared: VV_2_T2



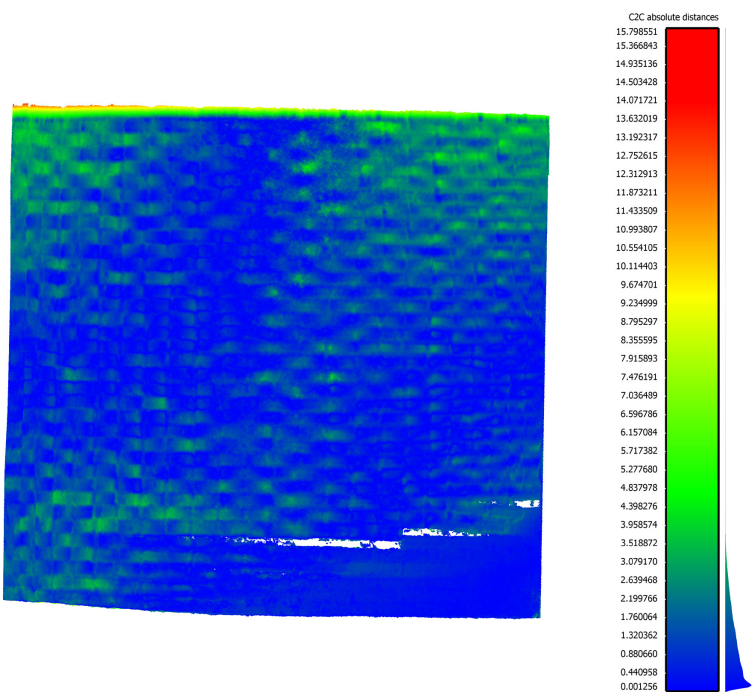
Fig. 7.35

Preparation of the models to the DIC procedure.



Fig. 7.36

Random black dotted pattern.



7.2.3 Digital Image Correlation

7.2.3.1 Data acquisitions

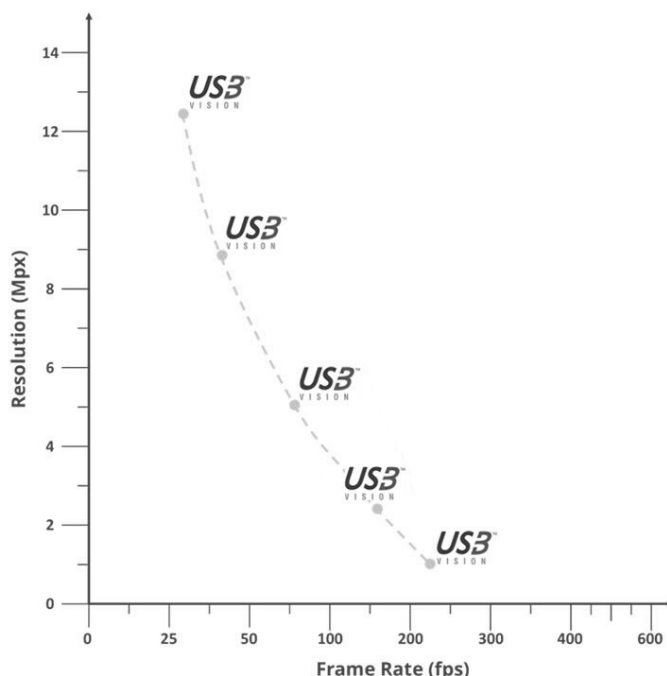
A first use of the Digital Image Correlation monitoring is performed on the AV_4 model, during the test, to develop a suitable methodology in data acquisition for in-scale masonry models. After this first experience, the DIC is performed on the four tests involving the vault in-scale models (VR_1, VR_2, VV_1, and VV_2).

The cement-based bricks used in the in-scale vault model construction present a surface that appears too smooth and uniform to be acquired by the DIC system: as reported in Ch. 6, the process needs a group of pixels with recognizable and unique features to evaluate the deformation in each time step. With this aim, the model is first covered by a thin layer of acrylic paint (Fig. 7.35), which also covers the irregular join-

ts, and later by spraying of black acrylic paint reproducing a cloud of points with the target function in the DIC subset evaluation. The final result is an irregular and dense pattern of black dots (Fig. 7.36).

The device used in the procedure is the DIC System Q-400 from Dantec Dynamics A/S, equipped with two convergent t (Fig. 7.37). The tool is composed of an adjustable tripod and a spacer bar to hold the cameras in position. Following the empirical rule suggested by the developer, the distance from the camera to the object is assumed as equal to the distance between the cameras. For this reason, the DIC device is placed in the proximity of the vault models, near to the lower portion (Fig. 7. 15), on elevated support, to reach the best possible field of view. Due to this limit in term of distance, only a section of the model is acquired (7.35), approximately corresponding to the key voussoirs zone of the L portion (Fig. 7.7). A cold LED light panel is added to the device to improve the light condition of the test.

Camera	Dantec USB 3 x 2
Resolution	from 1,5 to 12 [Mpx]
Frame rate	from 30 to 220 [Hz]
Configuration	from 2 to 16 cameras



The intrinsic (focal length, principal point, distortion parameter) and extrinsic parameters (translation vector and rotation matrix) of the system are directly estimated and fixed during the calibration through the connected software. This



Fig. 7.36

DIC system set-up configuration.

Tab 7.7

Dantec Dynamics USB 3 vision camera main specification.

Fig. 7.37

Dantec Dynamics USB 3 vision cameras resolution and the frame rate ratio.

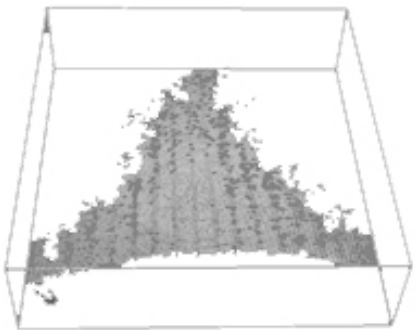


Fig. 7.38

Resolution/Frame rate ratio of the Dantec Dynamics USB 3 vision camera.

procedure takes several minutes before the test starts, to obtain the best fitting in the evaluation. It is performed by capturing a target, made of custom patterns and QR codes, in different positions to estimate the required parameters.

The acquisition steps are fixed before the test starts: during AR tests, images are acquired by steps of 0,1 mm of imposed displacement. This discretization leads to a great amount of data, involving difficulties in the postprocessing. For this reason, during VV test, the acquisition ratio is reduced to steps of 1 mm of imposed displacement.

8. Results

This chapter offers an overview of the results of the tests performed on the structural models and the consequent data processing on the acquired information. A critical interpretation of the tests, the models, the methodologies and the results are presented in order to evaluate the strategies and the tools used during the research.

8.1 Arch models

The methodologies of data acquisition and monitoring involving the opening tests on the arch model are exposed in the previous chapter: in light of these data, it is possible to describe the bi-dimensional behaviour of the. The models tested and discussed in this chapter are reported in Tab. 7.1: for the arch model with the radial arrangement, the considered tests are the AR_3, AR_4, AR_8, and AR_9, while for the vertical arrangement are taken into account the models AV_1, AV_2 and AV_5.

The opening displacement imposed during the tests leads to the failure of the arch models, with the formation of cracks along the joints, assumable as hinges: as previously described, the arch deformation during the test allows the shape accommodation through a maximum of three hinges, while the structure remains stable. The theoretical failure mechanism must appear with the formation of the other two hinges simultaneously, for a total of five, to transform the stable structure into a symmetric mechanism. Despite this theoretical assumption, in reality little asymmetry in the arch construction can lead to imperfect asymmetrical mechanisms, triggered by the opening of just a fourth hinge (Heyman, 1995; Ferrero, 2021). Therefore the obtained four-hinges mechanisms are considered acceptable, as the reflection of the real behaviour of the arches.

The collapse mechanism is recorded, along with the hinges position and the ultimate displacement. The results are compared by putting together the position of the hinges on the ideal undeformed state of the structure (Fig. 8.1).

The ultimate displacements recorded in the AR models are in a close range, while more variations are recorded in the AV models. The hinge positions, and the related collapse mechanisms, show the same tendencies. It is worth noticing that, despite the different discretization of the arch geometry

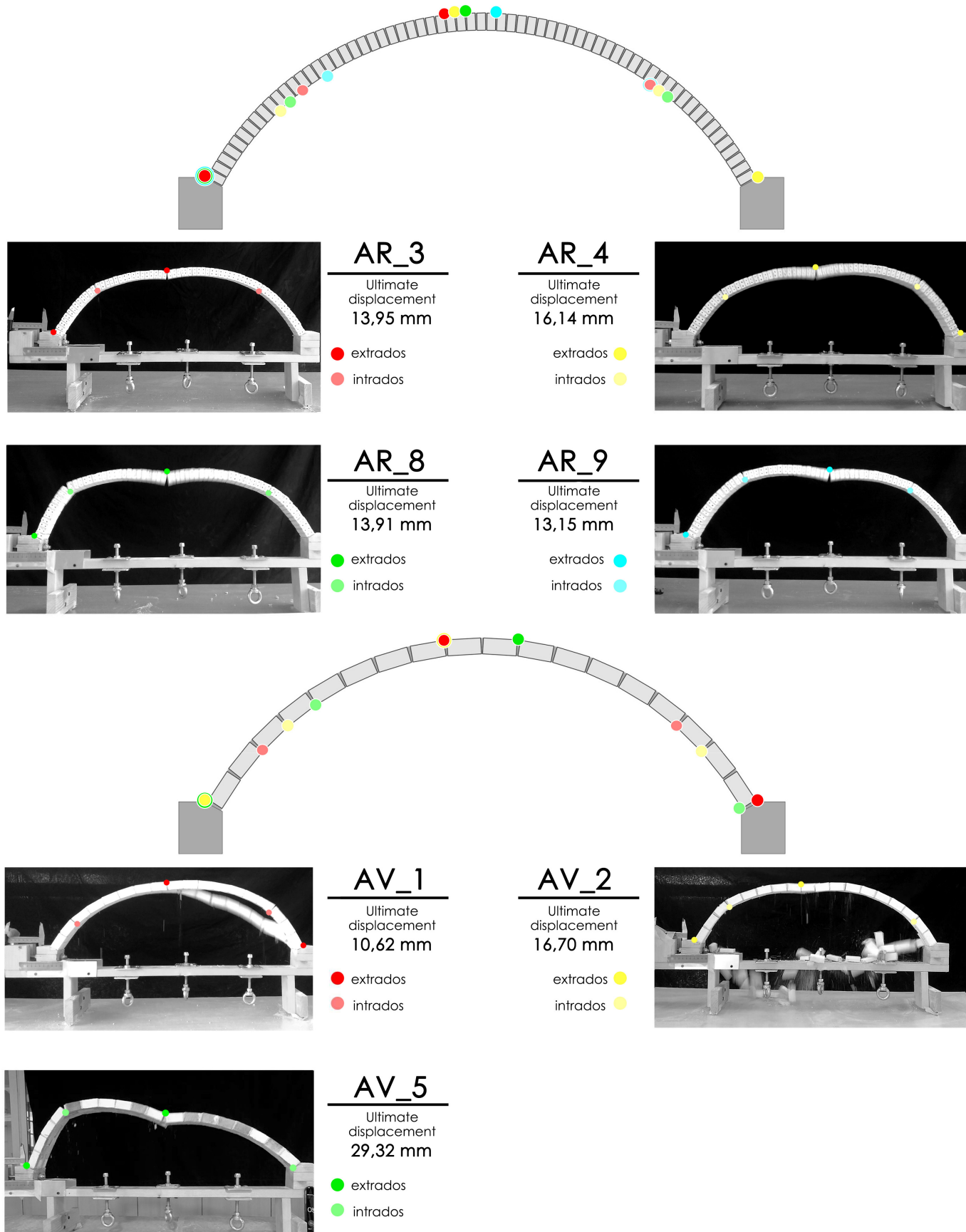


Fig. 8.1

Hinges position and ultimate displacements recorded during the arch model tests.

deriving from the two different brick arrangements, the hinges positions in both typologies vary within a close range of angles (Fig. 8.2).

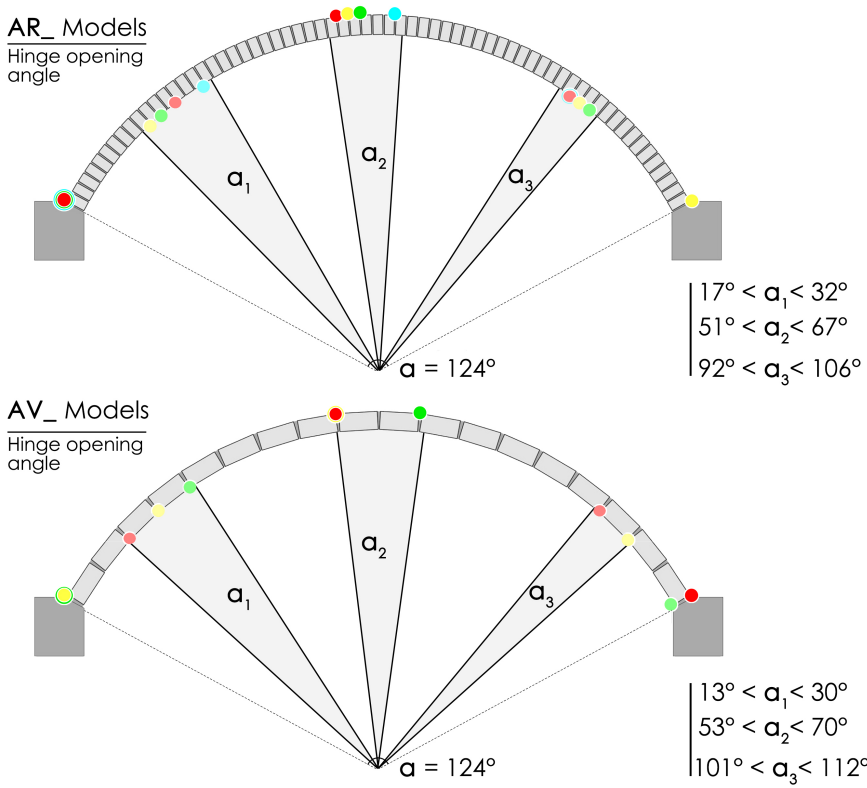


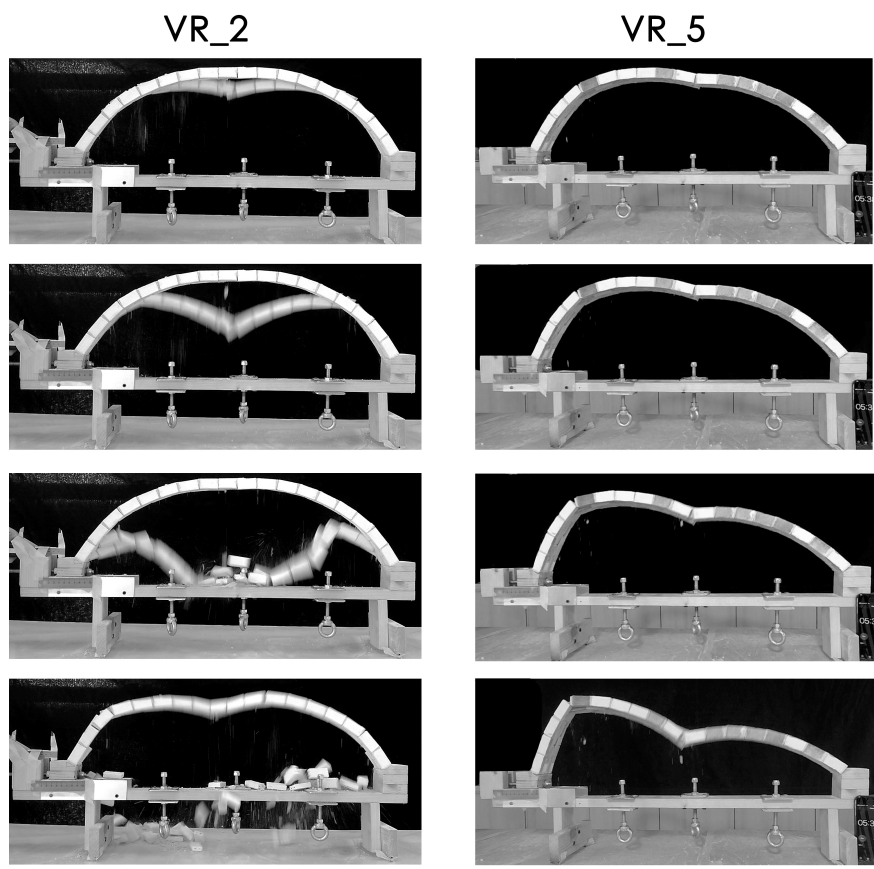
Fig. 8.2

Range of angles in which are concentrated the hinges in both the model tested.

The good overlapping in the AR models' results can be attributed to the high accuracy in the reproduction of the model along with the several trials. On the other hand, the different behaviours recorded in the AV models appear quite different in terms of ultimate displacement and hinge opening. This variation can most likely be linked to the construction procedure of the model: after the first trials with the vertical arrangement (AV_1 and AV_2), it was noticed the separation of the arches at an early stage of imposed displacement, leading to differential collapse mechanisms between the arches (Fig. 8.3), whose out-of-plane collapse probably compromised the global stability of the structure. This kind of failure is very difficult to elaborate because of the formation of different hinges in the head arch both during the displacement and the local collapses in the various arches. To avoid this problem, the construction process of the successive models is modified by imposing a small amount of pre-compression between the longitudinal mortar joints that bond the different arches together. As a result, the ultimate displacement has meaningfully increased in the two models tested after this variation (AV_4, not failed until reaching the end of the displacement range, and AV_5). The collapse mechanism also shows a variation after the change in the construction techniques, with the absence of differential failures of the successive arches and the formation of hinges at both the abutments (Fig. 8.3).

Fig. 8.3

Different modalities of collapse between the arches in presence of pre.compression in the joints.



It is worth noticing that all the recorded collapse mechanisms present an alternation in the hinge location between the intrados (I) and extrados (E) interfaces, in accordance with the other experimental and analytical investigations on this topic (Ferrero et al., 2021). In particular, the tests on AR_3, AR_8, AR_9, AV_2, and AV_5 models present a E-I-E-I hinge pattern, starting from the moving abutment, while the AR_4 and AV_1 models present I-E-I-E patterns.

8.2 Vault models

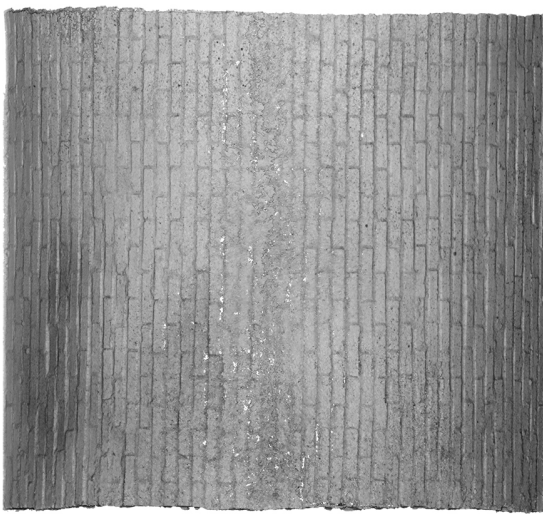
Chapter 7 has introduced the need for more complex monitoring and description in the evaluation of the three-dimensional structural behaviour of a spatial structure compared to the simpler procedure suitable to evaluate the bi-dimensional behaviour of an arch inside his plane. For this reason, the following section is organized on the basis of a schematic recollection of the experimental results on vault models and their post-processing through dense point cloud acquisition and DIC monitoring. The work has to be intended as an organic and planned procedure (exposed in the previous chapter), while in following are only the most notable results and remarks are reported. The complete list of the results is available in the Appendix, at the end of the present Thesis.

8.2.1 Crack patterns, rotations and collapse mechanisms

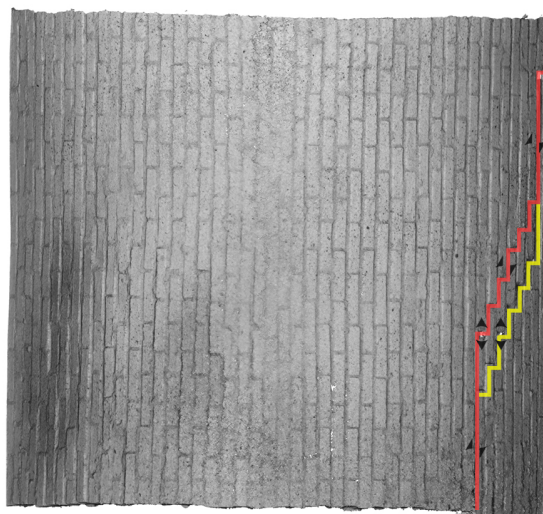
The crack patterns (Fig. 8.4, 8.5, 8.6, 8.7) patterns obtained during the various tests on the vault models are recollected by the integration of the visible phenomena observed during the tests development, by the comparison between the synchronized video acquisitions from different perspectives, and by the evaluation made on the basis of the three-dimensional data managing through the dense point-clouds. To ease visualization of the cracking evolution, the crack pattern is depicted on the orthophotos of the vault models extrados. At each step acquired in the point clouds, each crack is highlighted by a single colour, to represent its evolution during the test. The legend reported beneath the image of the undeformed state (T0) reports the symbols used to highlight the opening or sliding nature of the crack in a particular position of the brickwork, and to evidence lowering phenomena, not clearly detectable in a top vision of the extrados. The collapsed portions, subject to local failure, are reported in the various steps of acquisition (T1, T2, etc..) through a lighter colour to highlight the missing portions of the models between the fixed steps of displacement, and therefore must be not intended as the actual positions of the collapsed bricks. The legends beneath the images of the deformed states report the hinges typologies and their development during the test.

CRACK PATTERN - VR_1

T0
 $\frac{\delta_y}{\delta_y}$
 0 mm



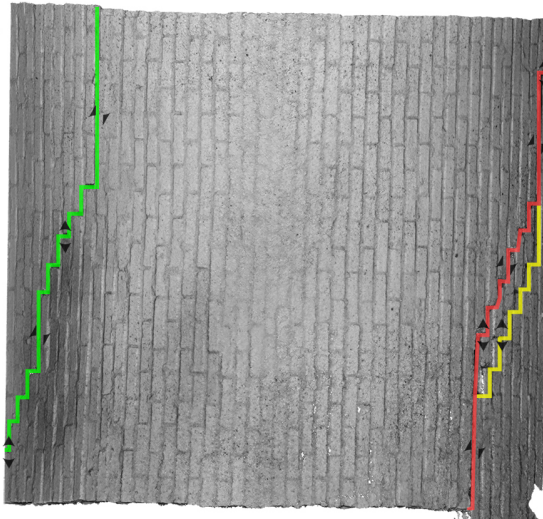
T1
 $\frac{\delta_y}{\delta_y}$
 10 mm



▲ Sliding
 ▲ Opening

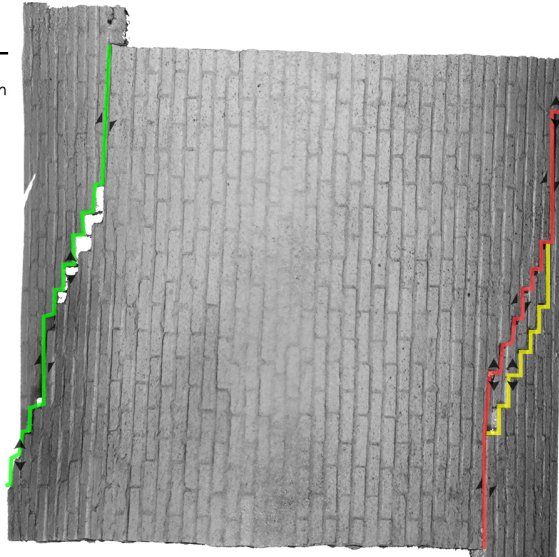
— Inclined longitudinal hinge started from 2,50 mm of displacement
 — Minor longitudinal hinge started from 2,50 mm of displacement

T2
 $\frac{\delta_y}{\delta_y}$
 20 mm



— Inclined longitudinal hinge started from 2,50 mm of displacement
 — Minor longitudinal hinge started from 2,50 mm of displacement
 — Inlined longitudinal hinge started from 16,60 mm of displacement

T3
 $\frac{\delta_y}{\delta_y}$
 50 mm



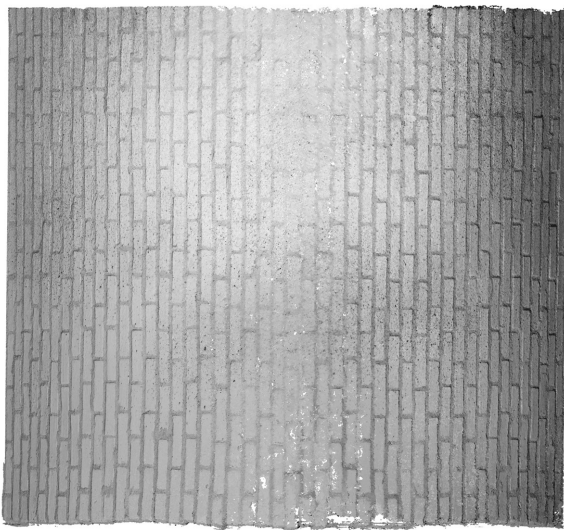
— Inclined longitudinal hinge started from 2,50 mm of displacement
 — Minor longitudinal hinge started from 2,50 mm of displacement
 — Inlined longitudinal hinge started from 16,60 mm of displacement

Fig. 8.4

VR_1 model: crack pattern.

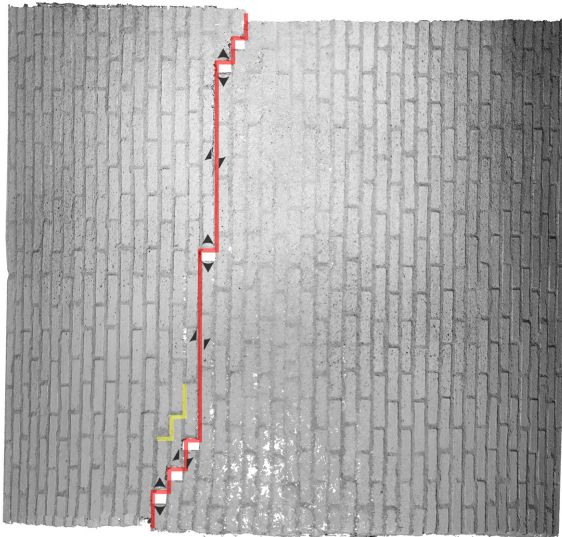
CRACK PATTERN - VR_2

T0
 $\frac{\delta_y}{\delta_y}$
 0 mm



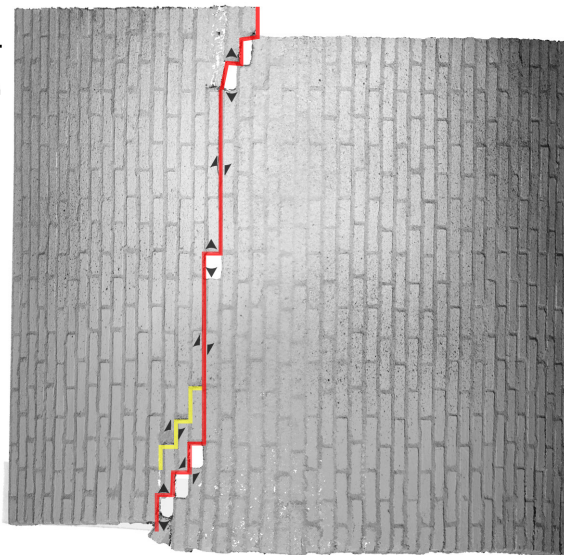
- ↗ Sliding
- △ Opening
- ▼ Lowering

T1
 $\frac{\delta_y}{\delta_y}$
 10 mm



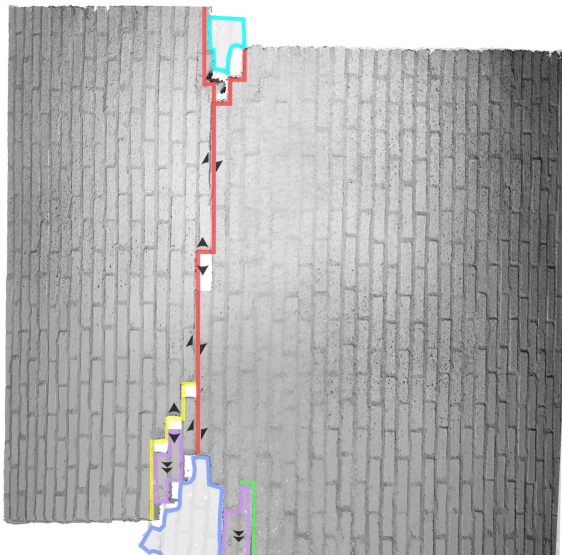
- Inclined longitudinal hinge started from 1,40 mm of displacement
- Minor longitudinal hinge started from 6,10 mm of displacement

T2
 $\frac{\delta_y}{\delta_y}$
 20 mm



- Inclined longitudinal hinge started from 1,40 mm of displacement
- Minor longitudinal hinge started from 6,10 mm of displacement

T3
 $\frac{\delta_y}{\delta_y}$
 50 mm



- Inclined longitudinal hinge started from 1,40 mm of displacement
- Minor longitudinal hinge started from 6,10 mm of displacement
- Minor longitudinal hinge started from 22,30 mm of displacement
- Collapsed portions after 20,13 mm of displacement
- Collapsed portion after 21, 56 mm of displacement
- Lowered portions after 22, 30 mm of displacement

Fig. 8.5

VR_2 model: crack pattern.

CRACK PATTERN - VV_1

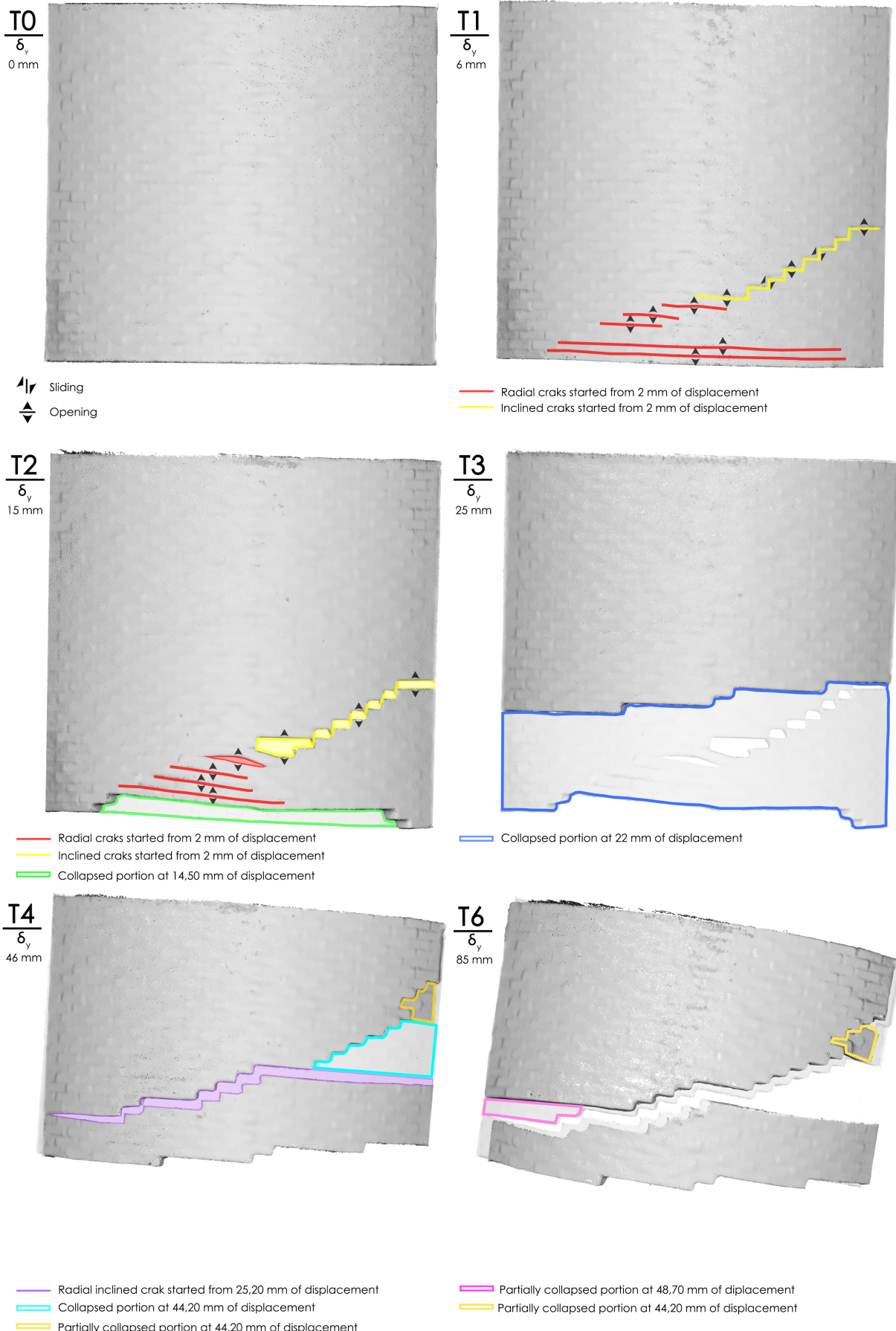


Fig. 8.6

VV_1 model: crack pattern.

CRACK PATTERN - VV_2

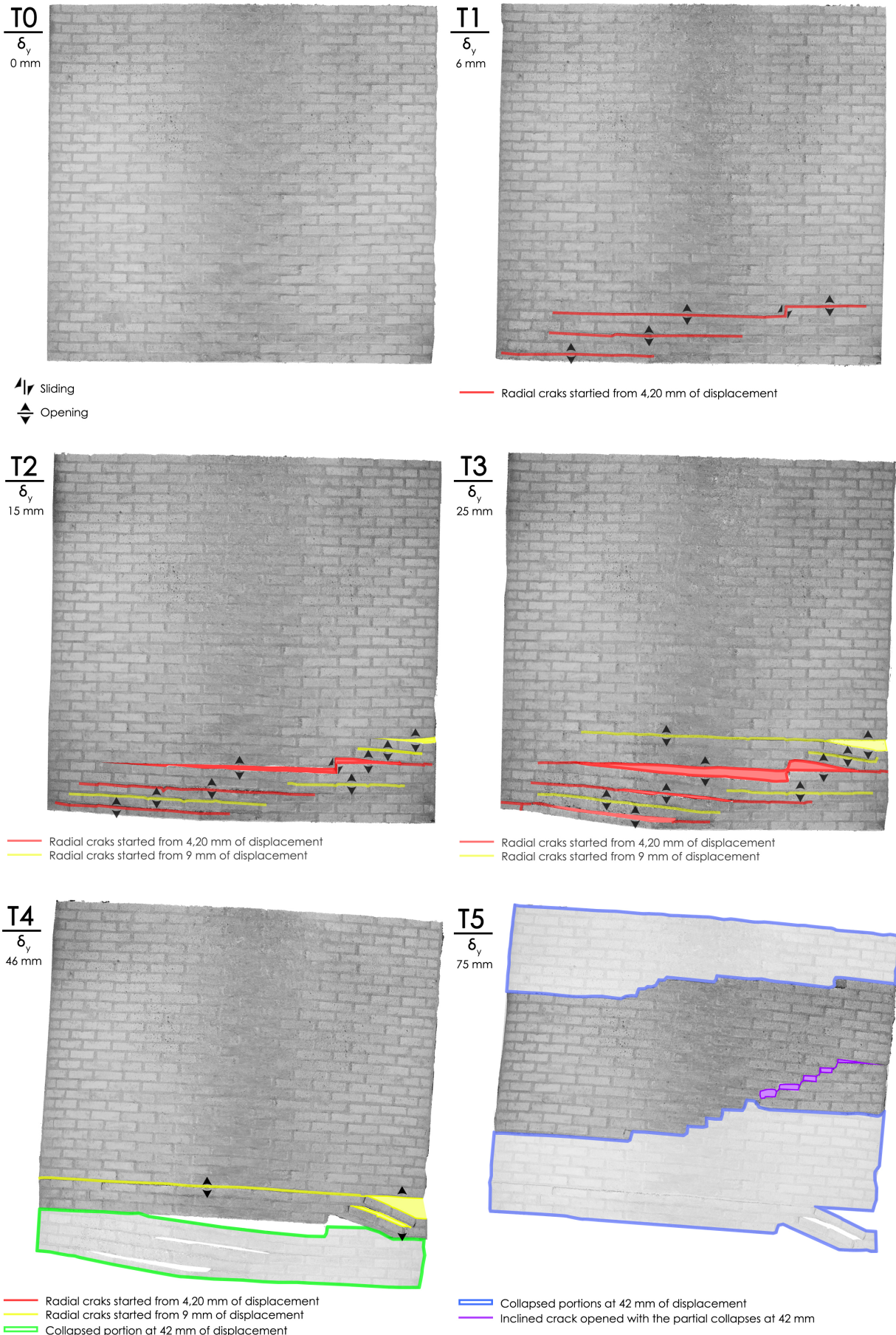


Fig. 8.7

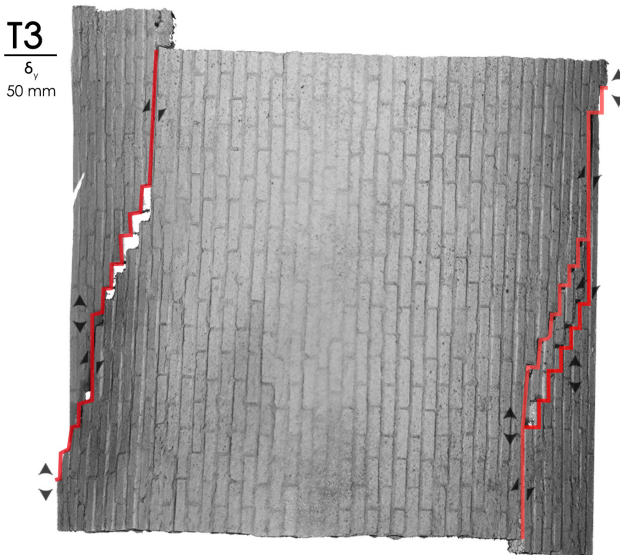
VV_2 model: crack pattern.

The critical analyses of the crack patterns experienced in the models reveal slight differences between the models with the same brick arrangements and substantial differences between the two bricks patterns. It is worth noticing that in the VR_1 and VR_2 models most of the cracks are represented by fractures occurring along the longitudinal joints, with an excursion more or less coinciding with the whole depth of the vault model. These major cracks appear to be quite straight along a single longitudinal joint or inclined involving multiple rows of bricks. The difference about the major crack position is reasonably assumed to depend on construction issues: the major crack experienced in the VR_2 model (in the key voussoir proximity) appears at the very beginning of the displacement imposition, starting from a compromised head joint. The progress of the VR tests shows also differences in the global behaviour of the two models (see the Appendix for further details on the main phenomena recorded during the tests): in the VR_1 vault the two major cracks lead to the separation of the central portion, that starts rotating upon the sliding haunches; in the VR_2 model, the major crack along the top of the vaults extrados leads to a major sliding between the two portions, which cause small local failures near the heads and the rigid rotation of the two haunches upon the abutment, while the contact surface between them is reducing. On the other hand, the VV models show a different behaviour in terms of crack pattern: in both models, the major cracks occur in the radial joints, leading to the formation of separate portions of the structure. These portions behave differently in relation to the imposed displacement, involving the opening of wide cracks (as in VR_2) or the total separation of a series of arches (as experienced in VR_1). Both phenomena have led to the local collapse of the involved portions. Also in VV models, the major cracks can assume either straight or inclined directions, reasonably depending on construction issues.

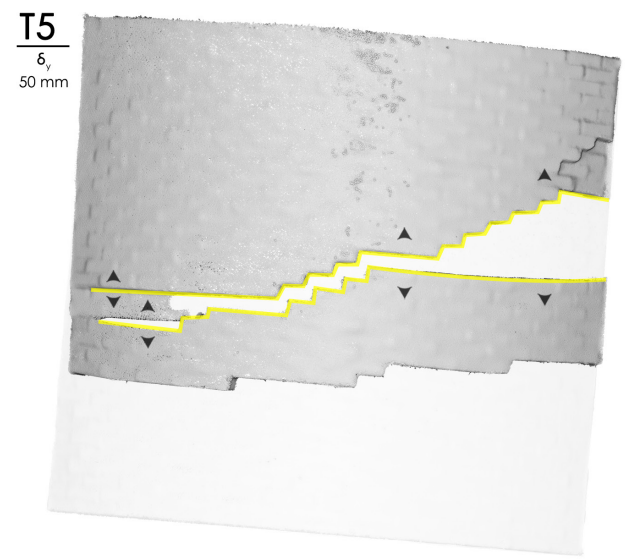
The results of this brief analysis evidence the presence of two characteristic crack typologies into the structural behaviour of barrel vaults under shear displacement of the abutment, which depends on the brick arrangement. These two typologies are reported in Fig. 8.8, where the opening or sliding nature of the fractures is highlighted.

CHARACTERISTIC Crack pattern

Radial Arrangement - VR_1



Vertical Arrangement - VV_1



The clouds compared in Fig. 8.8 are referred to the same step of imposed displacement ($= 50 \text{ mm}$) for the two brick patterns, and further evidence the two completely different behaviour discussed before. In particular, the following characteristic crack typologies are detected:

- **longitudinal cracks** (Fig. 8.9): experienced in the models with the radial arrangement of the bricks. This kind of crack runs along the longitudinal joints, creating sliding surfaces between the separated portions. This crack typology is clearly recognizable by its direction that goes along the depth of the vault, both in straight and inclined configurations.
- **radial cracks** (Fig. 8.10): noticed in the models with the vertical arrangement of the bricks. This kind of crack develops along the radial joints of the vault, creating wide fissures and separation between the arches, that can lead to local collapses of various entities. They are recognizable by the direction of the hinges, running across the vault. Both straight and inclined radial cracks are experienced in the presents work. The difference between the two typologies of inclined hinges is recognizable by the profile of the cracks. In both model typologies, the inclined cracks noticed follows the brick pattern, with major portions along the longitudinal (in VR) and transversal (in VV) joints, and minor racks excursion in the transversal (in VR) and longitudinal (in VV) ones.

Fig. 8.8

Characteristic crack typologies into the structural behaviour of the barrel vaults

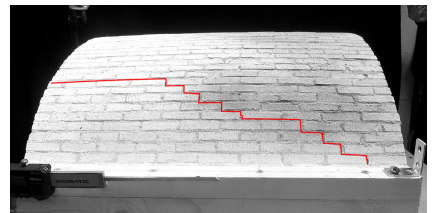


Fig. 8.9

Longitudinal inclined crack.

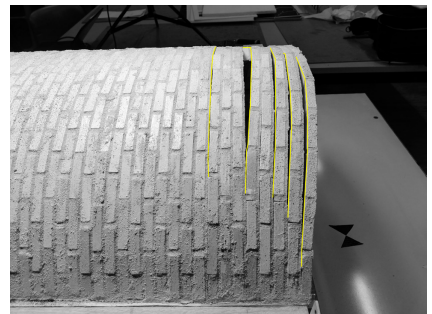
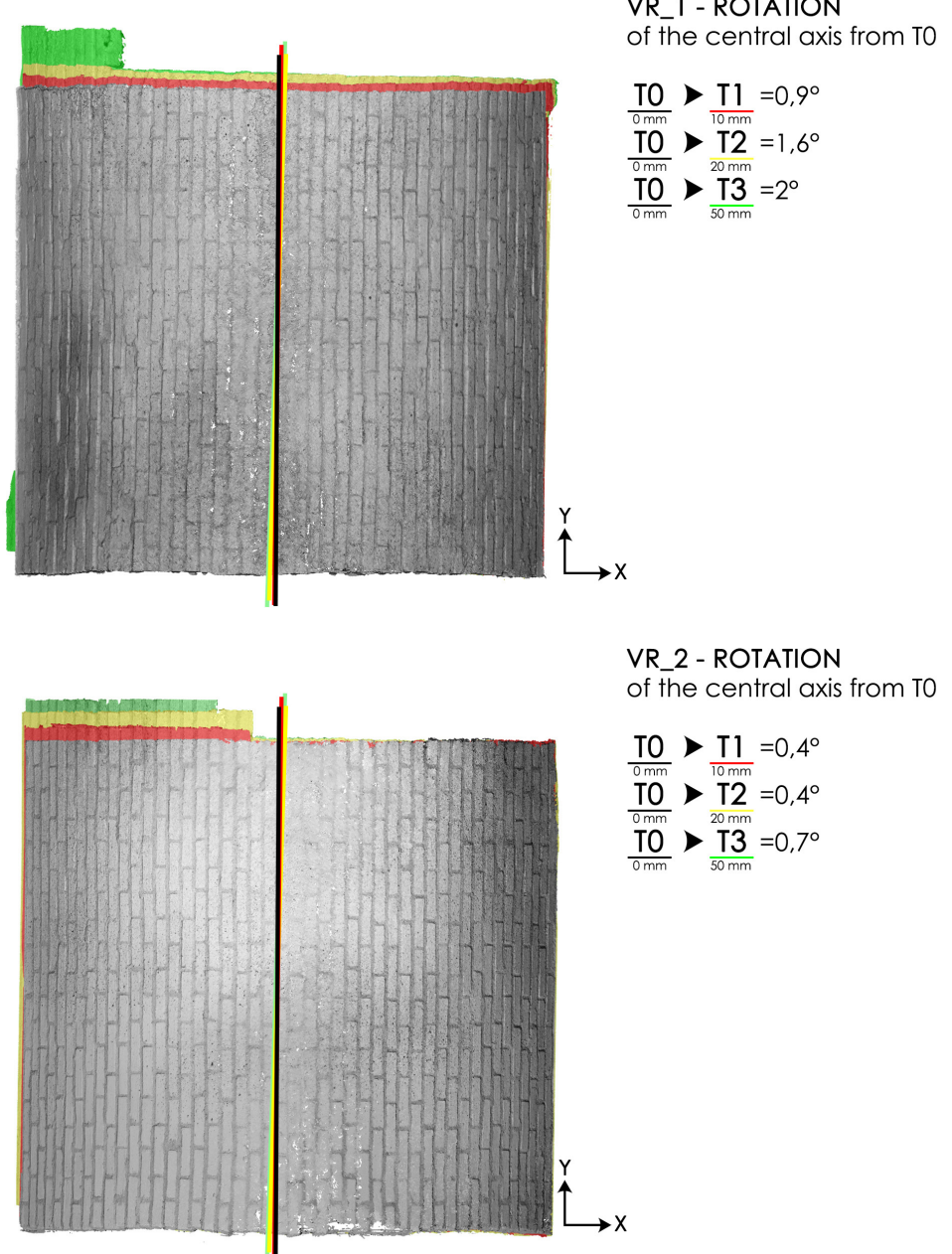


Fig. 8.10

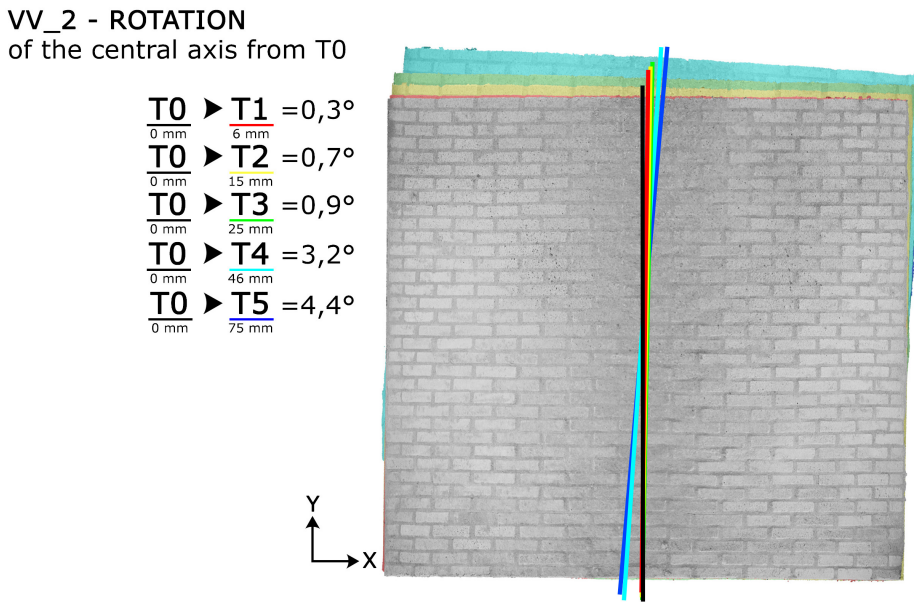
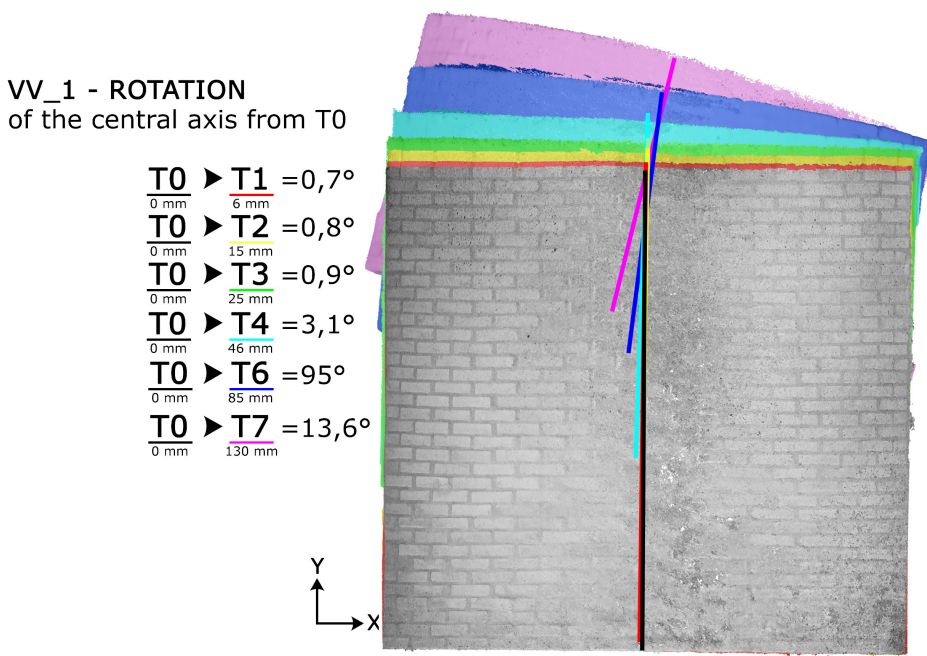
Radial cracks.

Fig. 8.11

VR_1 and VR_2 models: rotation of the main axis



During the tests it was observed that, besides the visible cracks and collapses occurring to the vault models, these are rotating on the x-y plane. During the postprocessing phase, these rotations are evaluated (Fig. 8.11, 8.12) through the geometric measurement of the angle between the main axis of the vaults (virtually passing in the middle of the joint bonding the key bricks rows) in the undeformed state and the same axis reported on the deformed states. From this comparison, it appears that the vault models with the radial arrangement of the bricks have smaller rotations, focused in specific areas (the central portion in VR_1, visible in the crack pattern representation, and along the haunches in the VR_2), due to the sliding surfaces between brick rows after cracking. On the



other hand, the VV models a rigid rotation mechanism involves the entire structure and influences, in the VV_2 model, the progress of the test.

The described rotations occurring on both vault typologies can be ascribed to the fact that the abutments are not able to prevent the sliding between the vault and the supports and to lack of boundary structures to contain the head of the vault models. This is a shortcoming of the built experimental set-up, which should be improved for future experimental tests, since it causes a non-realistic behaviour of the structure, with the adding of shear transmitting devices to help the transmission of the imposed displacement directly to the brick rows and reduce the sliding

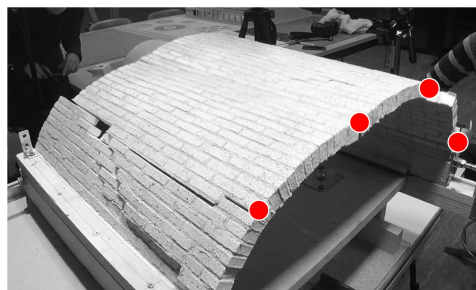
Fig. 8.12

VV_1 and VV_2 models: rotation of the main axis

The high-speed and high-resolution cameras provide images of the collapse mechanisms of the tested models. In Fig. 8.x a selection of images of the failure, from the most representative perspective, is reported. As stated in the introduction, differently from the arches, the vaults involve complex three-dimensional failure mechanisms. The tested specimen on vault models demonstrates such different behaviour also in the failure modes between the ones with the two different brick arrangement. The VR models reach the collapse at quite different ultimate displacements (60,67 mm in VR_1 and 91,42 mm in VR_2) and both shown a four hinges mechanism, not so far from the ones occurred in the arch models (Fig. 8.1), despite the visible rotation of the two main portions visible in VR_2. These hinges run across the whole depth of the model, corresponding to as many longitudinal joints, with two of them placed at the abutment interface and one in the proximity of the key bricks. On the contrary, the VV models show a different behaviour, characterized by an apparent higher global stiffness that leads to the rigid rotation of the separated portions after the local collapse of some arches and by the difficulty to perform the manual activation of the displacement mechanism. It is worth noticing that the VV_1 model reaches the end of displacement range (fixed at 150 mm) without a global failure, but with a great rotation on the abutments (visible in Fig. 8.13). The VV_2 reaches the global collapse at 93,77 mm of imposed displacement, triggered by a three-hinges mechanism, developed among the arches still in compression, with the slipping of the structure from one of the abutments.

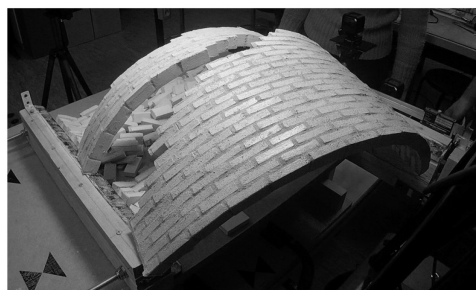
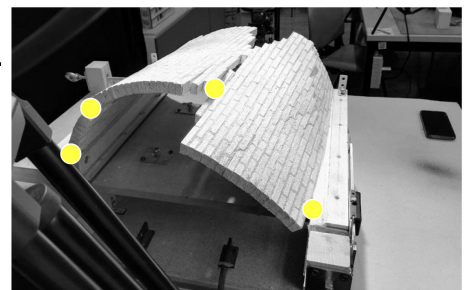
Fig. 8.13

Images of the vault models failure with hinge positions and ultimate displacements.



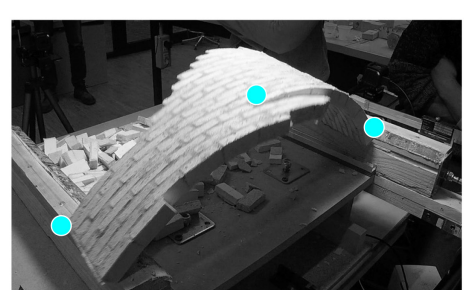
VR_1
Ultimate displacement
60,67 mm

VR_2
Ultimate displacement
91,42 mm



VV_1
No global FAILURE

VV_2
Ultimate displacement
93,77 mm



8.2.2 Point cloud comparison

In the last decade, the use of point cloud in the deformation analyses has largely increased in the engineering field (Neuer et al, 2016): most of the employments involve geometry-based or surface-based model types in the comparison of different time steps of a structure. This method is currently applied in bridges, dams, towers, and tunnel monitoring in the civil engineering field. Despite such remarkable progress, this is still an open field of research due to the high number of variables involved in the deformation analyses. The nature of the deformation and the nature of the acquired objects need specific investigation in relation to other features such as the direction of the deformation and its magnitude. Misinterpretation of these aspects in performing structural analyses through point cloud comparison can lead to misleading information (Holst et al., 2017). However, as mentioned, the use of point clouds comparison in the deformation analyses of superstructures is quite a common and robust process in the contemporary professional practice and research, while their use in the field of experimental in-scale modelling still needs deep investigation in order to assess robust and functional procedures.

The research of Holst et al. (2017) indicates the importance of the knowledge about the ongoing deformation phenomena while evaluating an object through point clouds comparison: in-plane and rigid movement (Fig 8.x, b) with little magnitudes are hardly detected by the computing software because of the overlapping between portions with the same features. On the contrary, out-of-plane and shape deformation movement result more clearly visible during the comparisons, in virtue of the scarce overlapping between the point cloud portion characterised by similar feature (Fig 8.x, a).

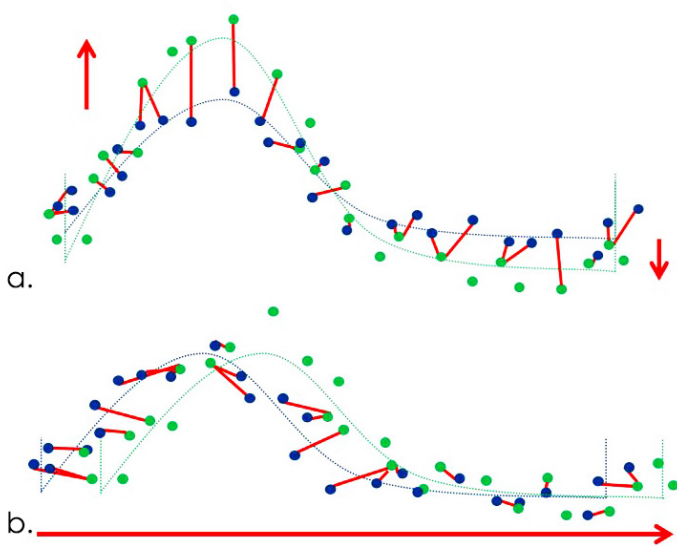


Fig. 8.14

Types of deformation:

- a. out-of-plane shape deformation;
- b. in-plane rigid movement.

From: Holst et al, 2017.

With the abovementioned theoretical premises, the methodology of cloud comparison appears to be suitable in the deformation analyses of the models in the present work: despite the in-plane nature of the imposed displacement and the regular shape of the vault models, it allows recording the local and global changes in the geometry of the object, due to rotations, local failure, ongoing cracks, etc. In the present work, the testing methodology offers the advantage of knowing for each time step acquired the magnitude of the imposed displacement. This knowledge in the phenomena makes it possible to reasonably evaluate the response of the computed distance between the point clouds.

The distance evaluation is performed using CloudCompare software, through the Cloud to cloud distance (C2C).

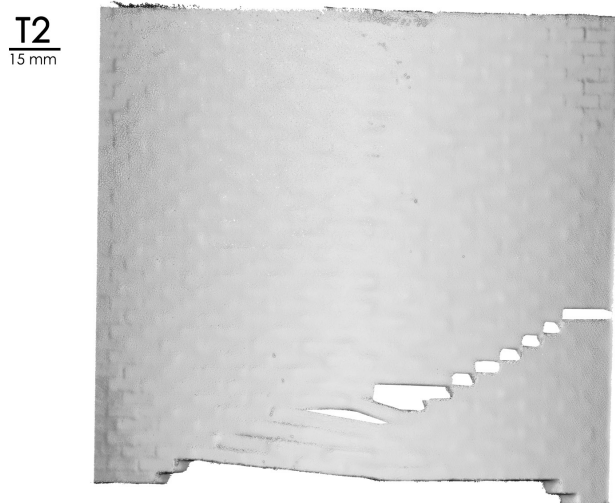
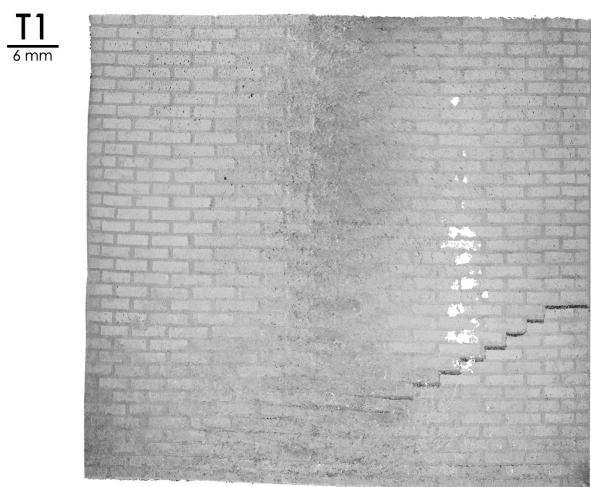
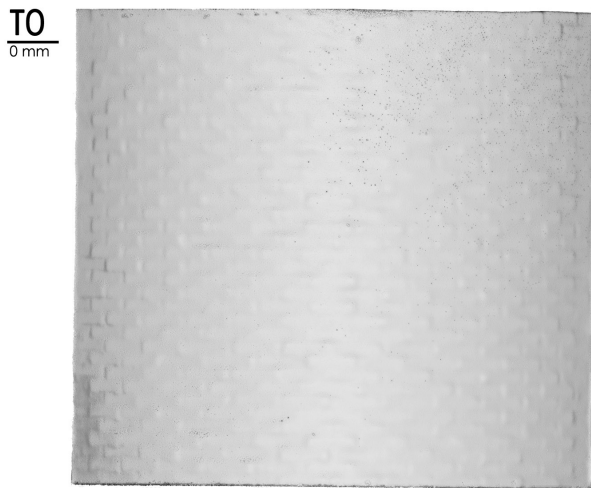
8.2.2.1 Absolute displacements

8.2.2.1 Absolute displacements

The dense point clouds obtained for each step of displacement in each model (described in the previous chapter) are compared to obtain an evaluation of the global deformation of the structure during the tests: the undeformed state of the vault (T0) is set as reference and the distance is computed in relation of the other acquired steps (T1, T2, etc.) by plotting the results upon the compared cloud (e.g. the plot contour of the distance evaluation between T0 as a reference and T2 as the compared element, are plotted upon the T2 surface) (Fig. 8.15). The display ranges and the parameters of the absolute distance contour plot are set to highlight the different portions of the point clouds as follows: in the image it is possible to appreciate the maximum distance plotted in the proximity of the vault model head arches (in red), while the green zones of the graphs indicate the portion of the vaults where a deformation is recognized, depending on both cracks and the consequent lack of surface data or in actual deformations of the extrados. The blue zones represent the portion of the clouds where the deformations are not detected, accountable to an actual lacking of deformation or to the presence of rigid translation along the Y-axis.

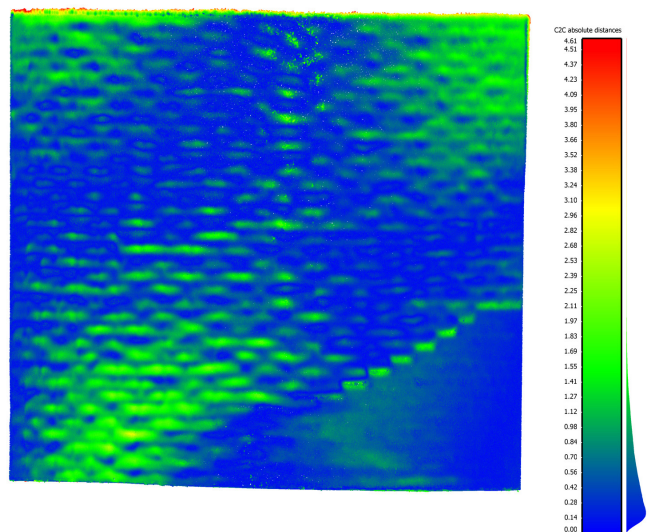
This kind of comparison highlights the changes in the shape experienced along the boundaries of the models, where the lack in the cloud surfaces overlapping shows the magnitude of the global displacement, according to Holst (2017). It wor-

Dense Point Clouds



Cloud to Cloud (C2C) distance

T0 ► **T1**
0 mm ► 6 mm



T0 ► **T2**
0 mm ► 15 mm

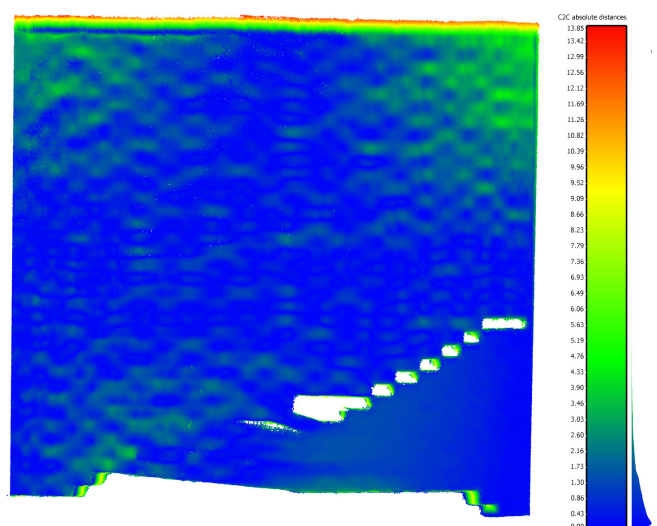


Fig. 8.15

VV_2 model: C2C distance, global absolute displacement.

th noticing that a good agreement is achieved between the known imposed displacements and the computed distance values, with slight differences reasonably accountable to the overall error of the three-dimensional models (submillimetre magnitude) and the effective quantity of displacement transmitted between the abutment and the masonry structure.

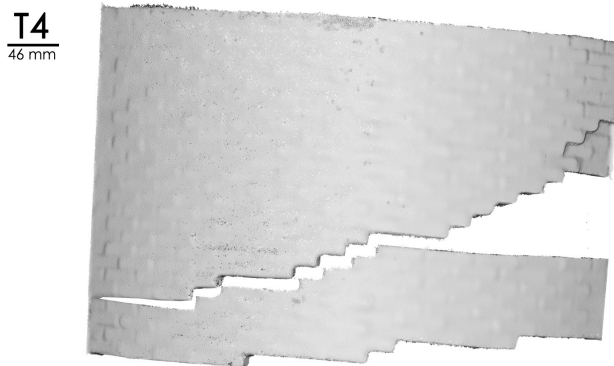
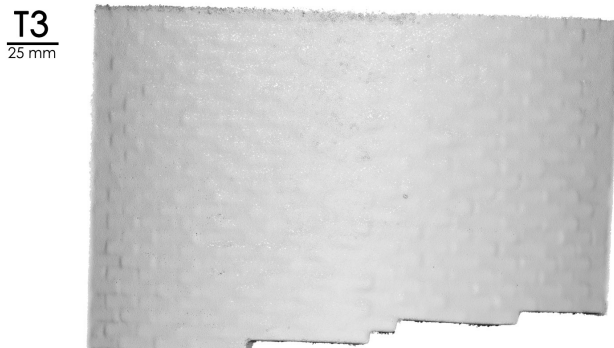
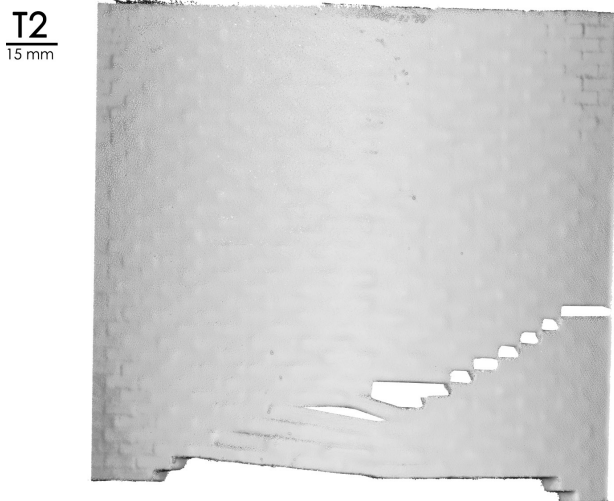
All the distance computations performed with this methodology, on the various models, are reported in the Appendix.

8.2.2.2 Relative displacements

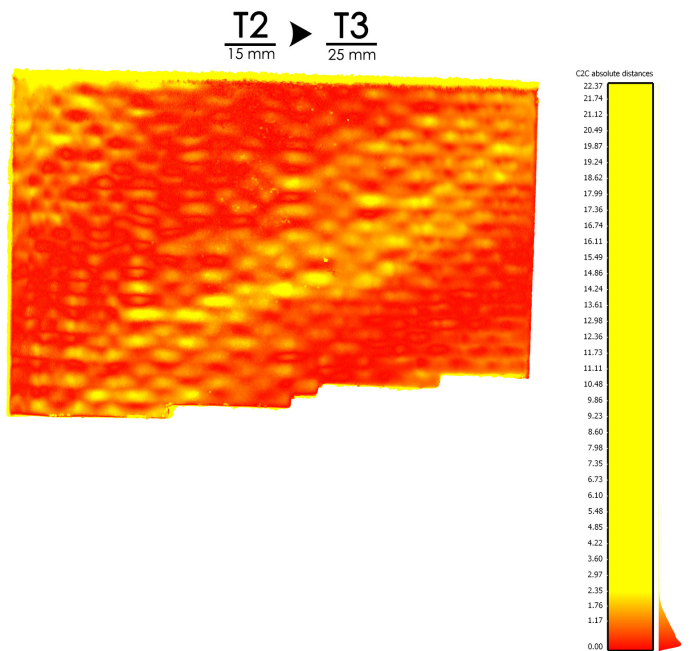
After the computing of the absolute distances between the dense clouds of the various time steps of a single model, another deformation analysis is performed to evaluate the ongoing deformation of the vaults: in this second analysis the reference cloud is selected each time to obtain the computing of the distance from its direct successive time steps: e.g. in a first analysis, T0 is used as a reference and T1 as compared and the results are plotted upon the T1 model (in a similar way than the absolute distance analysis), then the reference model is shifted to T1 and it is compared to its direct successive step of acquisition, T2, and the distances are plotted upon the T2 surface. This iterative process shows good results in the highlighting of the deformations between the models. In Fig. 8.16 it is possible to see the relative cloud distance computed between the T2 and the T3 steps of the VV_1 model test. The display ranges and the parameters of the relative distance contour plot are set to highlight the different portions of the point clouds as follows: the red/yellow colour scale is stressed by strongly reducing the display range in order to highlight the portions of the model surface where a deformation, even small, is detected. The red area displays the zones where the deformation is not present or detected while the yellow zones highlight the portion in which the surface is changed between the two consecutive acquisitions. As reported for the previous analysis method, the relative distance computing shows good results in the global shape changes, in accordance with the literature, and it evidences the distances at the edges of the vaults models. Good results are obtained also in showing the surface deformation in specific portions of the vaults.

It is worth noticing that the distance analysis illustrated in Fig. 8.16 represents one of the best results obtained in the data processing phase of the present research. In fact, the distance computing between the T2 and T3 steps of the VV_1

Dense Point Clouds



Cloud to Cloud (C2C)
distance



model clearly shows a deformation in the central portion not visible by the naked eye in the T2 cloud. The profile of this deformation coincides well with the actual radial inclined crack that occurred to the model at 25,20 mm of imposed displacement and captured in the T4 dense cloud. The prediction of this crack appears as a good result in the use of the cloud distances: the deep knowledge on the ongoing phenomena deriving by imposing displacement in laboratory tests together with the presence of complete data about the different deformed states of the structures lead to a good awareness in the evaluation of the results. It is to remark that inside the small

Fig. 8.16

VV_2 model: C2C distance, global absolute displacement.

number of considered specimen only this relative distance comparison has shown this kind of results in cracks prediction. The other comparisons show local deformation without straight relation to the visible cracking phenomena that occurred to the model. As a matter of fact, this kind of evaluation is strongly influenced by the time steps acquisition magnitude: the more the acquisitions are performed close to each other, the more the comparisons between the successive deformed state can reveal interesting information about the deformation analysis.

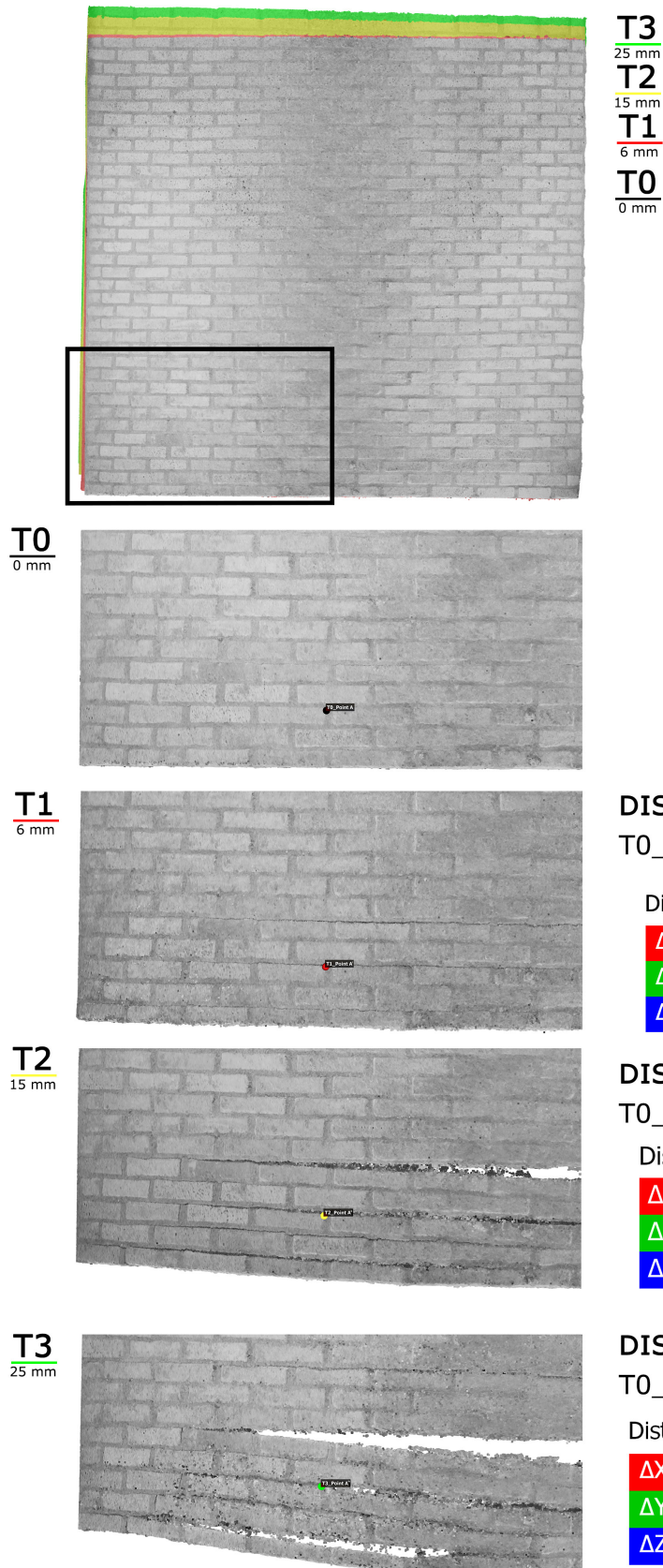
In virtue of the reduced magnitude of the specimen treated, the use of global relative displacement evaluation with direct dense point cloud comparison in deformation analysis needs to be more investigated in the development of automated solutions. Despite the large use of three-dimensional acquisition techniques in building health monitoring, it is proven that a simple representation, even high-quality texturized, is not always enough to detect the issues of the construction, especially in the subsurface field (Sabato et al., 2020). Very recently, the use of conventional methods in damage assessment, expensive and time-consuming, starts to be reduced in favour of Non-Destructive Evaluation (NDE) such as infrared thermography, acoustic emissions, and computer-vision-based crack analysis. The use of these techniques can provide robust methodologies in structural health monitoring with less economical and time expense and without service interruption for in-use construction. In particular, the last commitments in this field involve the introduction of algorithms based on computer vision and machine learning in automated damage detection (Montaggioli et al, 2021), applied on great infrastructures, and the use of thermographic images in the creation of Sfm models to evaluate the damages (Sabato et al., 2020) in an automated way. In light of these examples reported, along with other methodologies, the research in this field needs to be investigated deeply, representing an interesting and open topic.

All the distance computation performed with this methodology, on the various models, are reported in the Appendix.

8.2.2.3 Sample points distance

Along with the use of the C2C distance algorithm, the possibility of manually tracking a singular point on the structure is investigated, in order to assess the reliability of the process

POINT DISPLACEMENT - VV_2



DISTANCE

T0_Point A to T1_Point A'

Distance: 2.54.

ΔX	-0.67	ΔXY	2.46
ΔY	2.37	ΔXZ	0.92
ΔZ	-0.62	ΔZY	2.45

DISTANCE

T0_Point A to T2_Point A''

Distance: 6.26

ΔX	-0.96	ΔXY	6.25
ΔY	6.17	ΔXZ	1.00
ΔZ	-0.28	ΔZY	6.18

DISTANCE

T0_Point A to T2_Point A'''

Distance: 15.41

ΔX	-2.82	ΔXY	15.41
ΔY	15.15	ΔXZ	2.82
ΔZ	-0.17	ΔZY	15.15

Fig. 8.17

VV_2 model: evaluation of the displacement vector of a sample point.

and the possibility to match the results with the DIC monitoring measures. The aim is to evaluate the consistency of the results in the measure of the vector of displacement between the same point in the two deformed states. For the procedure a point on the VV_2 model is selected to be monitored: this specific model is selected in virtue of the high quality of the textured extrados surface, helpful to individuate the point on the various dense cloud. The selected point, (point A) is located on the geometric edge of a brick placed on one of the radial cracks developed during the tests: this is intended so as to evaluate the development of ongoing cracks. The dense point clouds are managed in CloudCompare software where the points are picked manually, and their distance is calculated in an iterative way. Point A_T0 is fixed as a reference, on the undeformed state of the model. The modules of the obtained displacement vectors are 2,54 mm in T1, 6,26 mm in T2, and 15,41 mm in T3. These vectors are evaluable through their ΔY component because the imposed displacement in that direction is known. Considering the global errors of the clouds (around 1 mm), the uncertainty linked to the operator selection of the point, and the magnitude of the object, the obtained measures seem reasonable according to the global displacement of the model.

In the next section, a similar evaluation is produced for the AR_1 model in order to compare the results with the DIC elaboration of the same test.

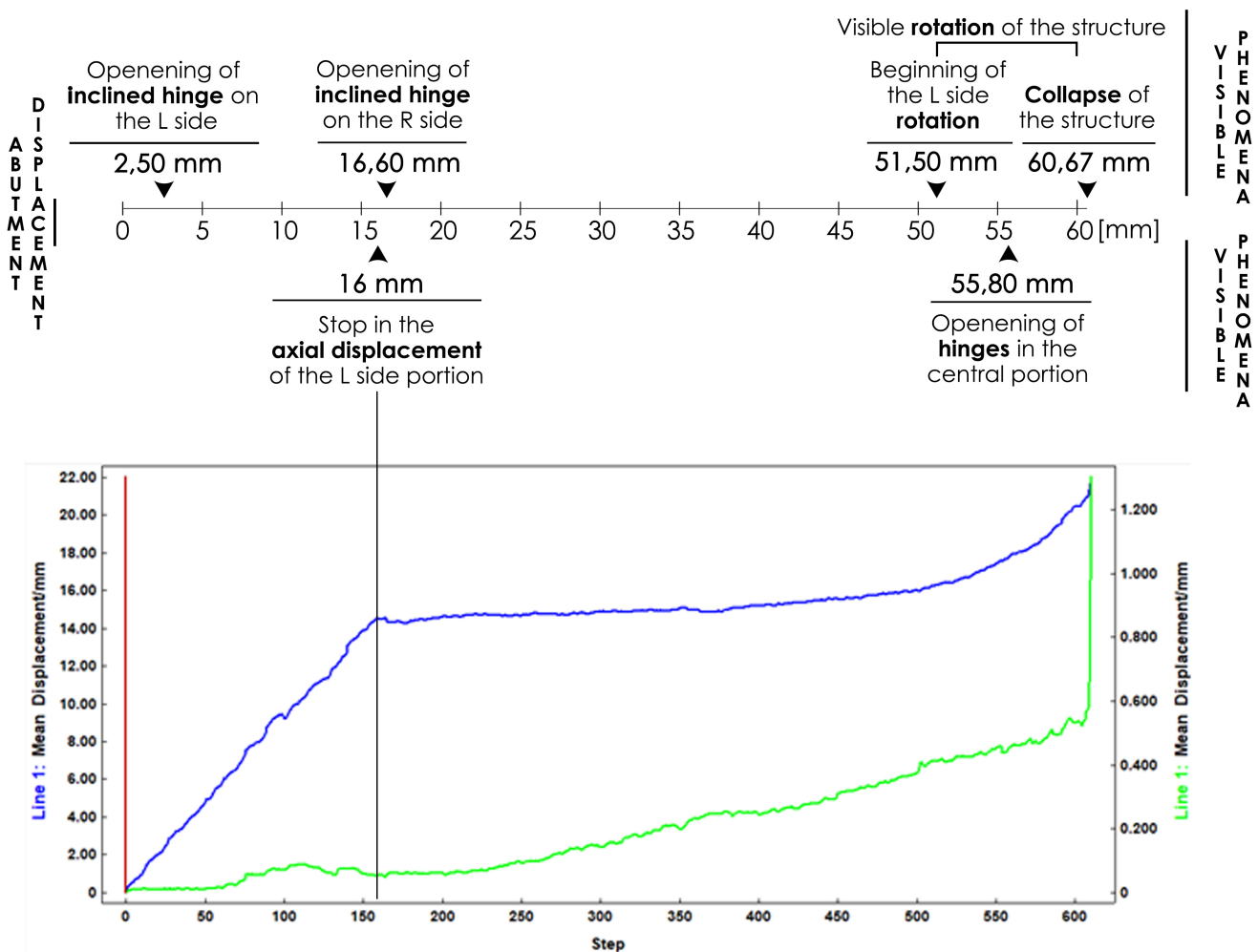
8.2.3 DIC monitoring

In the present section the Digital Image Correlation (DIC) analyses for the VR_1 model are reported. The DIC analysis performed in this work estimates the masonry specimen response during the simple shear test. In particular, the model deformations are individuated by the DIC device with a series of frames that involve the tracing of every texture of the specimens.

As reported in the previous chapter, due to the dimension of the models and of the DIC support, the field of view of the stereographic acquisitions is limited to a triangular-shaped portion in the proximity of the lower head arch (Fig. 8.18). During the test execution, a total of 610 steps of acquisition are performed, one each 0,1 mm of imposed displacement. Each acquisition involves a picture captured from both the calibrated cameras.

Fig. 8.18

DIC: facquisition area.



The mean displacements regard the minimum and the maximum displacement noticed in the specimen. These two data are evaluated and plotted on a temporal scale (Fig. 8.19). The obtained curves are compared to the temporal disposition of the macroscopic visible phenomena, reconstructed by the direct observation, the video acquisition and the three-dimensional data managing of the range-based and image-based acquisition techniques. This comparison shows how the maximum displacement curve has a sudden variation in correspondence of the reduction in the axial displacement (Y) of the central portion of the vault and the development of the inclined longitudinal crack that separates the right haunch portion. This behaviour is totally in agreement with the boundaries on the tests: the DIC acquired portion is quite coincident with the central portion of the vault, which stopped the main Y displacement and began to rotate (as reported in the previous sections). The flat portion of the maximum displacements' graph (Fig. 8.19, blue curve) shows this stop in the Y translation, with very little variations, until the reaching of the collapse (at step 610).

Fig. 8.19

Relation between the visible phenomena occurred to the model and the mean maximum and minimum displacements.

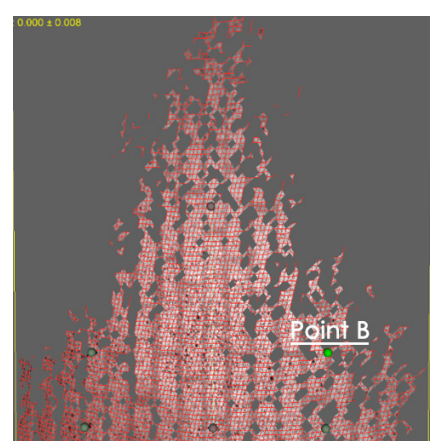


Fig. 8.20

Position of Point B in the monitored portion.

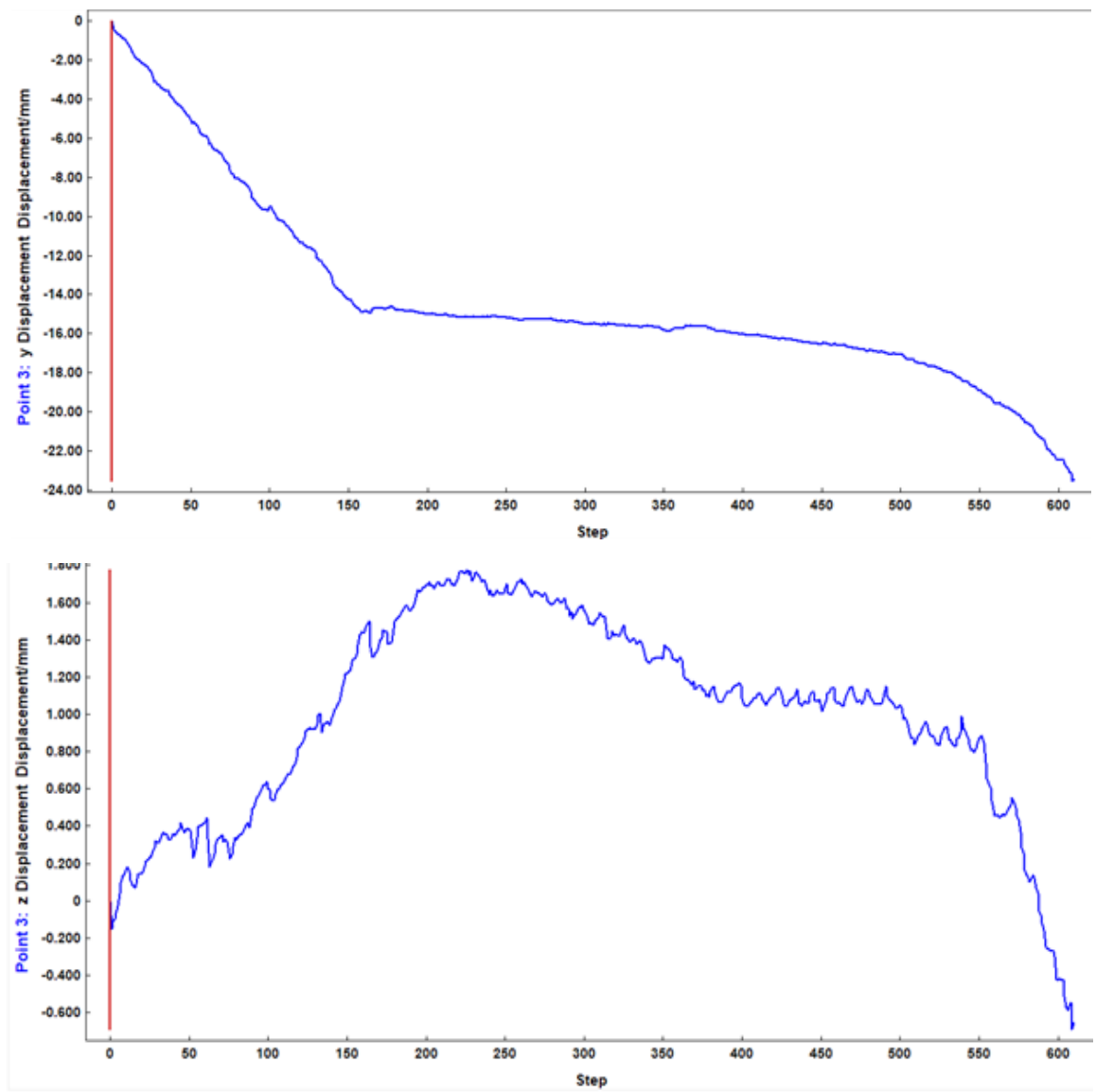


Fig. 8.21

Point B: Y displacement.

Another evaluation is conducted on the displacement of a single point located on the extrados. Point B (Fig. 8.20) is selected by the operator on a geometrical edge of a head arch's brick and its displacement on the Y-axis (Fig. 8.21) and Z-axis (Fig. 8.22) are plotted.

Fig. 8.22

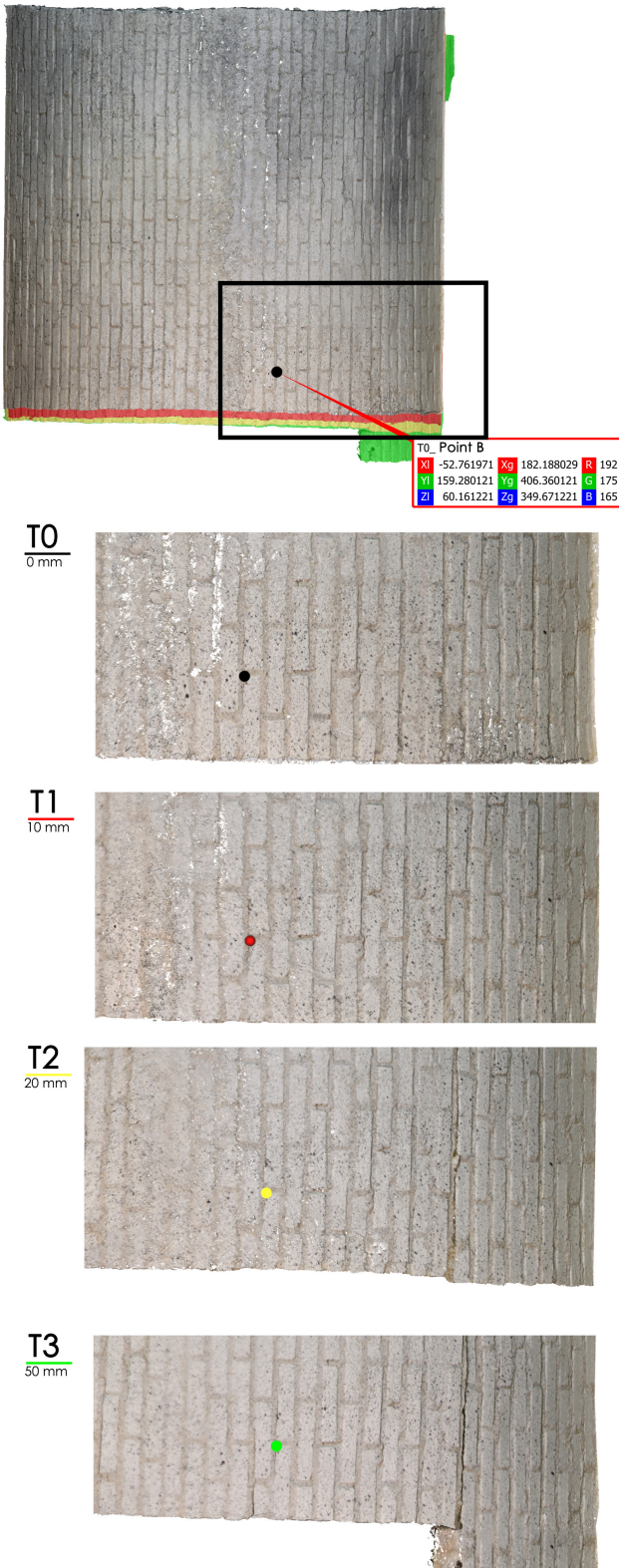
Point B: Z displacement.

Fig. 8.x reflect the same situation evaluated in the mean displacement contour: the location of Point B is in the central portion that drastically reduces the Y displacement after 16,60 mm of imposed shear displacement. The Z-axis displacement reported in Fig. 8.22 appear to be more variable during all the tests, with a sudden drop near the collapse of the structure.

As reported in the previous section, an evaluation of the displacement vectors is performed for the same point location on the dense clouds of the VR_1 model, representing respectively: T0 ($\delta y = 0$ mm), T1 ($\delta y = 10$ mm), T2 ($\delta y = 20$ mm), and T3 ($\delta y = 50$ mm). The clouds correspond to the step 0, 100, 200, and 500 of the DIC acquisition process. In Fig. 8.23 the performed analysis is reported, with the same procedure exposed

before, and the ΔY and ΔZ components are highlighted in order to be compared with the DIC results.

POINT DISPLACEMENT - VV_2



DISTANCE

T0_Point B to T1_Point B'

Distance: 8.25

ΔX	0.55	ΔXY	8.21
ΔY	8.19	ΔXZ	0.96
ΔZ	-0.79	ΔZY	8.23

DISTANCE

T0_Point B to T2_Point B''

Distance: 13.93

ΔX	2.65	ΔXY	13.75
ΔY	13.49	ΔXZ	3.45
ΔZ	-2.21	ΔZY	13.67

DISTANCE

T0_Point B to T3_Point B'''

Distance: 16.34

ΔX	2.04	ΔXY	16.03
ΔY	15.90	ΔXZ	3.77
ΔZ	-3.17	ΔZY	16.22

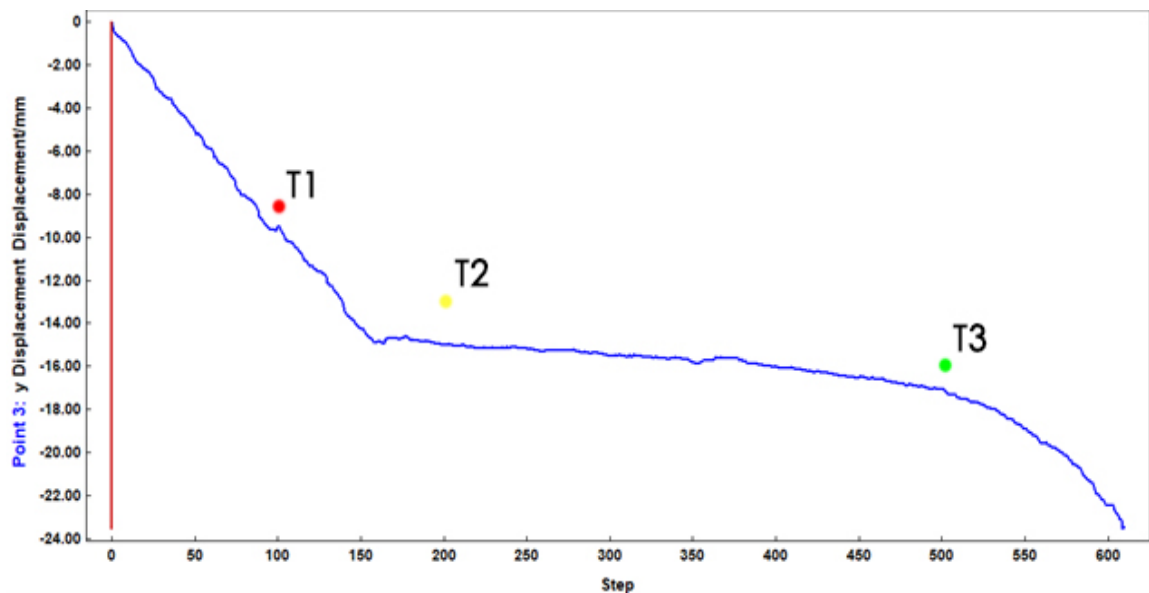
Fig. 8.23

Y components of the displacement vectors of point B translation plotted on the Y displacement DIC graph.

Fig. 8.24

VR_1 model: evaluation of the displacement vector of point B.

The results obtained with the sample point distance for the ΔZ components of the displacement vectors appear to be very far from the ones obtained with the DIC, while the ΔY component seems to fit in a better way. In Fig. 8.24, the ΔY data are plotted upon the DIC Y displacement curve, showing quite a systematically shift of the two data sets, with a magnitude of about 1 mm. These shifts appear to be acceptable in virtue of the three-dimensional models' error and the manual practice of the point selection in both cloud comparison and DIC.



In conclusion, the results obtained in the deformation analysis through the point cloud comparison appear reliable: the use of close-range photogrammetry and structured light scanner shown good results in the acquisition process for in-scale masonry structures. The comparison of the data obtained, also through the use of open-source software, demonstrates a good overlap with the DIC analyses, performed with structural aims designed tools. Nevertheless, the possibilities of the point cloud distance computation must be investigated deeply, in order to assess a robust procedure in the automatic deformation detection.

9. Conclusions

The present thesis dealt with the use of physical modelling in the structural analyses of masonry arches and vaults, which is investigated through an experimental campaign on in-scale models of arches and barrel vaults. This last chapter summarises the main findings of the work along with some remarks about their possible implications in terms of scientific contribution.

The main objectives of the work are exposed in Chapter 1, while a brief excursus about the arch and vault evolution through the history is reported in Chapter 2. The evolution in the design principles is also defined, along with the main construction techniques involving bricks and mortar joints. A critic literature review revealed the scarce presence of information and research about the brick arrangement contribution in the structural behaviour of arched and vaulted structure.

Chapter 3 reports a series of example of the physical modelling in architecture through the centuries, with a focus on their uses in the structural analysis and design. A review of the scientific literature about the topic is performed, leading to a wide overview about the state of the art in the experimental tests on masonry arched and vault structures. This review highlighted the scarce availability of scientific investigation on the brick pattern theme, both from the numerical and experimental point of view. Moreover, despite the increasing interest of the scientific community about the topic of experimental testing on masonry structures under support displacements, the behaviour of barrel vault under shear settlement of the abutments has been so far disregarded. These factors contributed to define the main focus of the experimental campaign, conceived to investigate the behaviour of in-scale barrel vault models with different brick arrangements under simple shear displacements. Two of the most used arrangements, radial and vertical, are identified and selected to be tested.

The design phase of the models is explained in Chapter 4, where the historical and scientific sources adopted to select the case studies of the in-scale models, both in terms of global geometry and brick arrangement, are reported.

Chapter 5 exposes the procedure adopted for the construction of the models. During the first phase of the experimental campaign, different materials are tested to simulate the masonry behaviour: two lime mortar mixes present in the

literature are tested without showing substantial differences in terms of structural behaviour. The mix reported by D'Altri et al. (2019) is selected due to the ease in the construction process. Wooden-based and cement-based bricks are tested, and the latter are selected because of their more performant behaviour in terms of stability to the environmental conditions and reusability. Various methodologies in the bricks fabrication are tested, individuating a procedure, with a silicone rubber mould, to produce a great number of unities with good results in terms of global shape. A new experimental set-up is designed and constructed in the ModLab Arch of the Politecnico di Torino with the usage of CNC machine to achieve the best performances in terms of geometry. The experimental set-up is designed with modular elements to allows the testing of different structures, in future works, by only changing specific elements.

Chapter 6 is devoted to the adopted techniques of data acquisition and processing in the testing of in-scale models. The selected techniques are the close-range photogrammetry and the structured light scanning to acquire three-dimensional point clouds of the models during specific steps of imposed displacement. The Digital Image Correlation is selected as methodology to perform a continuous monitoring of a portion of the structures. High-frames and high-resolution cameras are adopted to capture the collapse mechanisms of the vault models from different perspectives.

The experimental campaign is exposed in detail in Chapter 7, while the results are detailed in Chapter 8. The first phase of the campaign involves the evaluation of the structural behaviour of the in-scale arch model with both radial and vertical arrangement of the bricks under opening displacement. A total of 14 models are tested and 7 of them are selected to be compared. The opening tests in the arch models with the radial arrangements of the bricks show results in terms of ultimate displacement and failure mechanisms. On the contrary, the first tests on the model with the vertical arrangement highlighted the need to exert a small amount of pre-compression between the bricks is introduced during the construction process to avoid detachment between successive courses. In general, these preliminary tests evidenced the great influence of the construction procedures and techniques in the final behaviour of the structures, experienced during the tests. The hinge patterns obtained for both the model typologies are in accordance with the literature evidence. During the second

phase of the experimental campaign, four in-scale vault models are tested under simple shear displacement, two for each brick arrangement. The tests are performed according to the planned acquisition strategies, involving the use of fixed cameras, DIC cameras, high resolution camera for photo acquisition, and a hand-held structured light scanner. The photogrammetric and structured light-based data are processed with an integrate process. This process involves the use of the range-based data to obtain dense point clouds used to set an arbitrary coordinate system on which the photogrammetric process can be referenced. The obtained clouds are co-registered together by separating the fixed set-up portion, on which are performed the best fit registration, from the vault portions. This separation prevents issues in the co-registration of the various steps and prevent accidental modification of the clouds. Once the data are processed and the dense point clouds are obtained for every step of displacement acquired, these are compared to the data provided by the direct phenomena observation and by the video monitoring: as a result, the crack patterns are plotted upon the orthophotos extracted from the dense clouds, and rigid rotations of the structures are evaluated. The analysis of recorded data highlights two different characteristic crack patterns for the two tested brick arrangements: longitudinal cracks, noticed on the in-scale models with radial arrangement, which goes along the longitudinal bed joints, and the radial cracks, noticed in the models with vertical arrangements, which goes along the radial joints between the arches that compose the vaults. Both can have a straight direction, by the laying in single longitudinal or radial joints, or an inclined direction, involving several adjacent joints. Moreover, the four models show different behaviour both in terms of ultimate displacement and collapse mechanisms. The structures show different responses to the imposed displacement depending on the crack developing, with visible rigid rotations of the models on their abutments. In the models with radial arrangement the failure is triggered by the development of a four-hinges mechanism. In the models with vertical arrangement, local collapses are triggered by the sliding of the vault apart from the abutments. This represents one of the main limits of the work: the absence of shear transmitting devices allows the sliding between the longitudinal joint, especially at the interfaces between the model and the abutments.

Cloud to cloud distance algorithm is used to evaluate the deformation of the models in the acquired steps of displace-

ment. Two typologies of analyses are performed. The global absolute analysis is obtained by fixing the undeformed state of a model as reference and iteratively comparing it with the various correspondent deformed states. The results are able to show changes in the global shape, especially along the edges of the clouds, and a good precision in the numerical evaluation of the distances is achieved, in virtue of the awareness concerning the imposed displacement. A second deformation analysis is performed by the iterative step-by-step comparisons of all the deformed state recorded in a single test. The stressing of the colour plot contour highlights the deformed portion rather than the zones with no changes. This analysis allows to clearly detect the shape and position of a crack not yet totally formed and invisible to the naked eye. This result represents one of the most significant contributions of the present work in the field of data acquisition and processing for in-scale model testing. Along with the use of algorithms in distance evaluation, some trials are performed about sample point distance evaluation. The obtained data are also compared with the displacement evaluation performed with the Digital Image Correlation methodology in a single model test. The results show sufficiently good agreement in the evaluation of the main axial displacements. Nevertheless, in virtue of the small specimen considered in terms of experimental tests and data acquisition, more investigations need to be performed in order to assess a robust correspondence between the different methodologies.

The main contributions of the work can be summarised as:

- The suggestion of different procedures in the organization of an experimental campaign involving the in -scale physical modelling of masonry structures.
- The evaluation of different solutions, both original and present in literature, about the construction of the in-scale masonry models.
- The design and construction of a modular experimental set-up to test different in-scale masonry vault models.
- The investigation about the different behaviour of masonry arches with the same global geometry and under the same imposed displacement in relation to the construction process. In particular, it worth noticing the substantial changes in terms of ultimate displacements and behaviour during the collapse obtained during the tests of arches with verti-

cal brick arrangement when a small amount of pre-compression between adjacent brick courses is exerted.

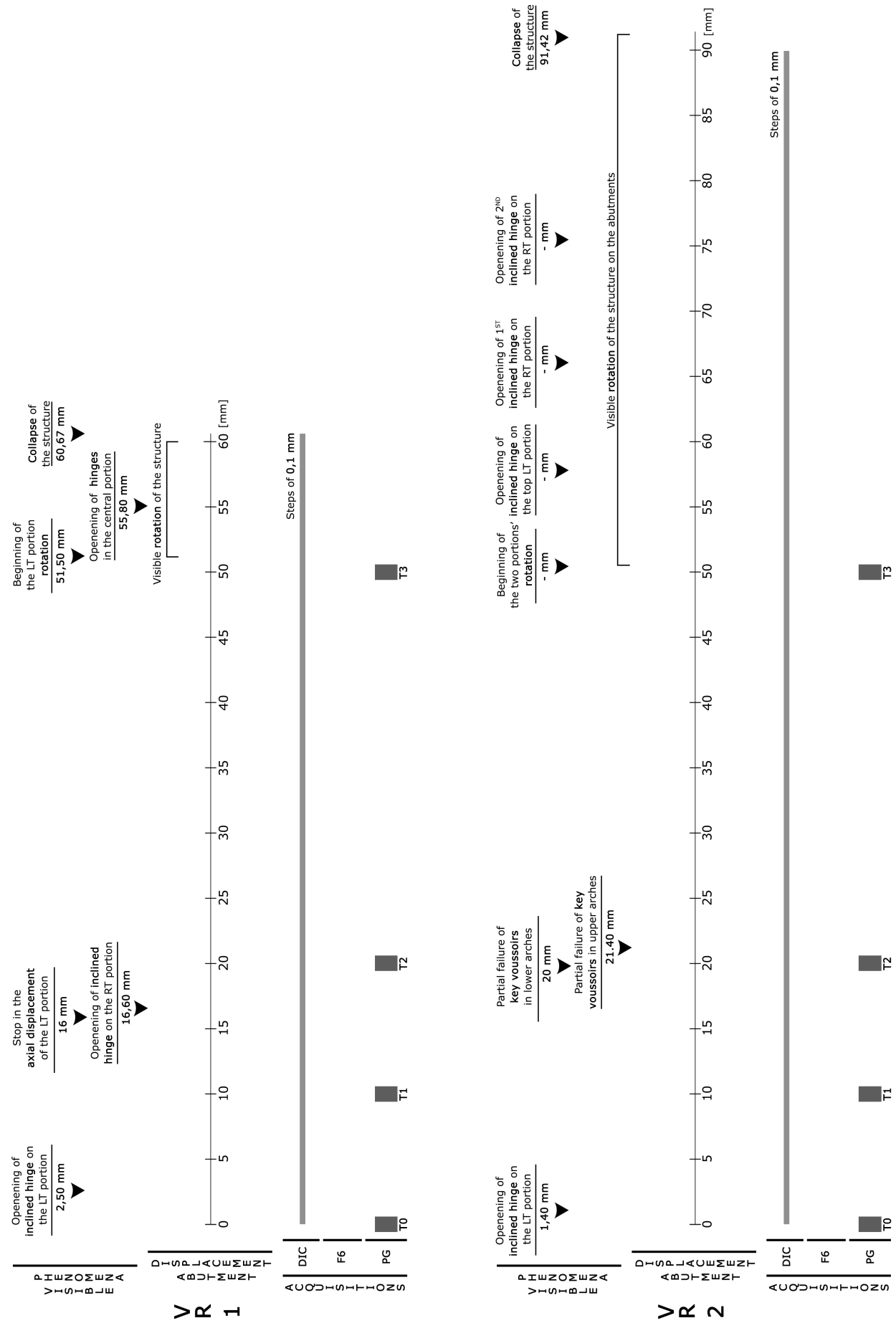
- The assessment of two different typology of characteristic cracks in barrel vault, with radial and vertical arrangements, under shear settlement. The definition of these two crack phenomena can help practitioners and scholars in the evaluation of masonry vault behaviour, both in terms of understanding the ongoing shear displacement of the abutment or by monitoring the direction and the shape of the cracks when the bricks arrangement of the structure is not visible.
- The proposal of a methodology in the data acquisition for in-scale modelling that involves various techniques present in the scientific literature, with a specific workflow tested to overcome the issues of the present work.
- The suggestion of a methodology in the deformation analyses through iterative cloud distances computations, to be deeply investigated. It is worth noticing the result obtained in the VV_1 global relative displacement analysis, in which the ongoing invisible fracture is predicted by the distance computation between two deformed states of the vault model.
- The suggestion of an interaction between the consolidated techniques of the close-range photogrammetry and the structured light scanning, in the field of the little objects, with the DIC methodology, less used, but in constant growing in the engineering field.
- The production of experimental data about arches with different patterns under opening displacement and barrel vault with different arrangements under shear displacement, both scarce in the present literature. The data could be used to validate numerical tools used in the analysis of masonry structures.

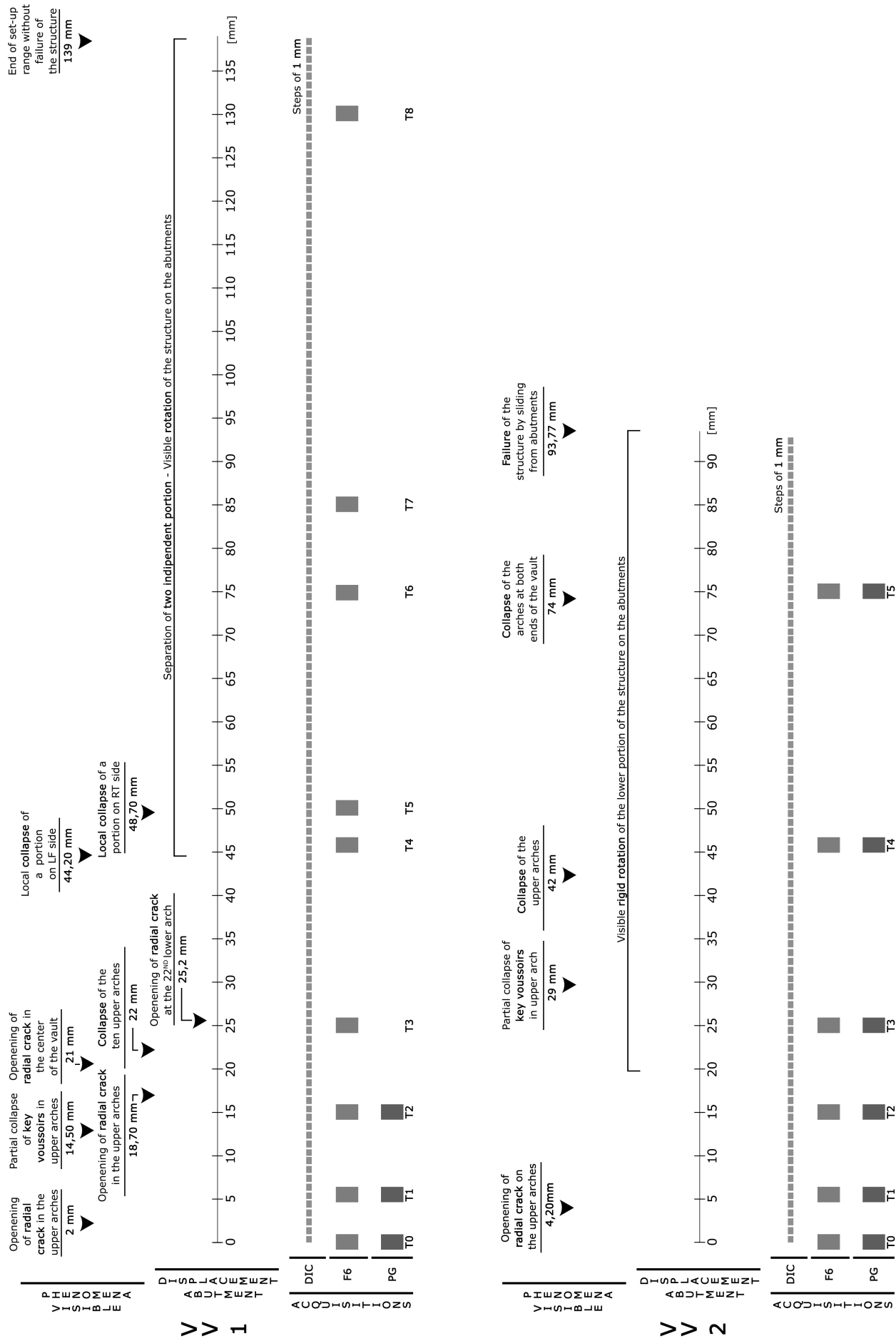
Future work could include:

- The use of the tested case studies as benchmarks to validate numerical models.
- New experimental campaigns on barrel vault models, to evaluate the influence of the bricks pattern on the global behaviour of the structure under opening displacement.

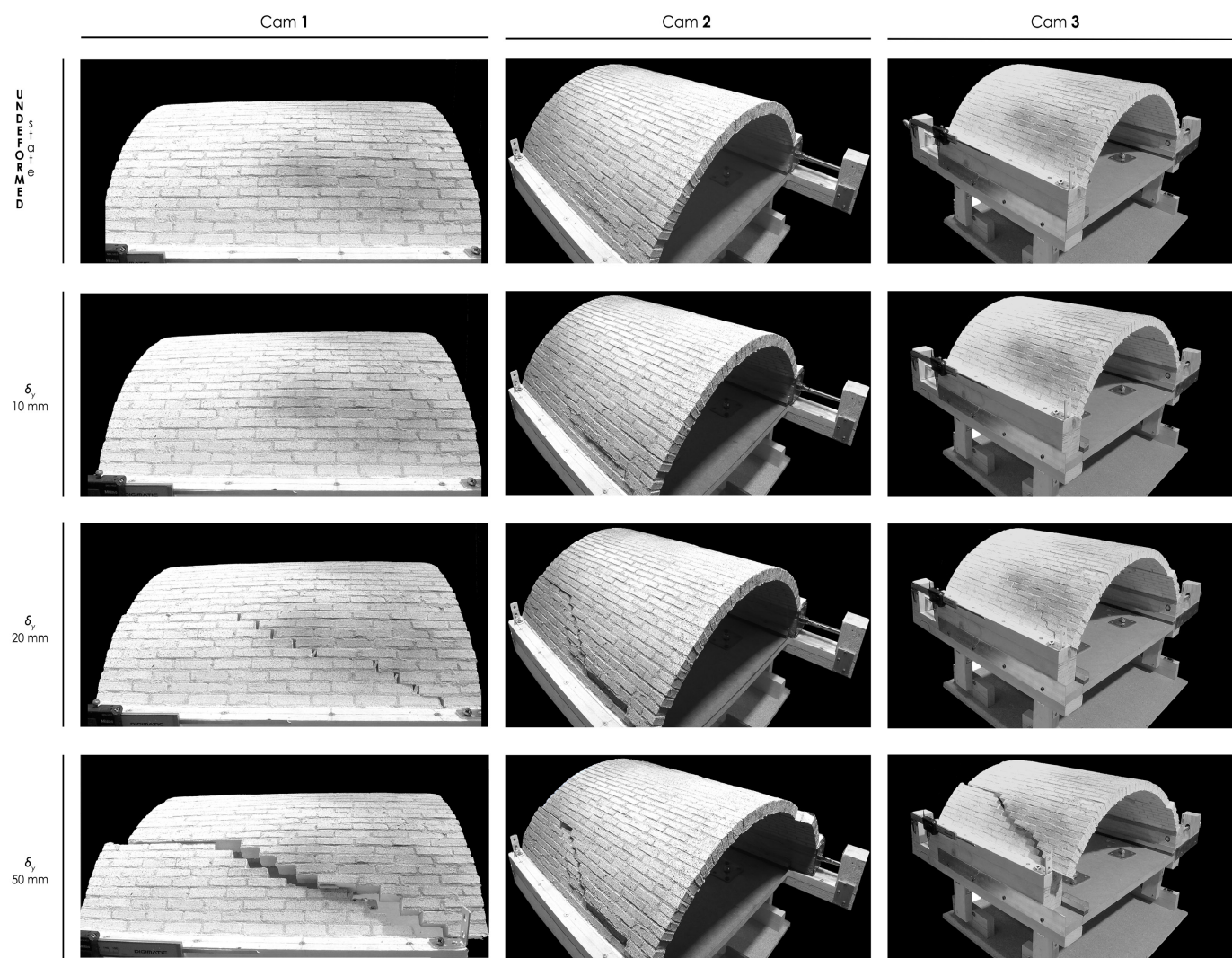
- New experimental campaigns on vaults with different typologies (e.g. cross, pavilion, etc.) to evaluate the influence of the bricks pattern on the global behaviour of the structure under opening or shear settlements.
- The evaluation of the role of mortar joints in the structural behaviour of arched and vaulted structures by the comparison of experimental and numerical results.
- The application of the cloud distance computation between different deformed state of real structures, e.g., periodically acquiring point clouds of structural elements in historical masonry building.
- The deeper investigation about the iterative and comparative uses of the new acquisition techniques in the field of in-scale model testing, in virtue if the growing interest about the topic in the scientific community.

10. Appendix

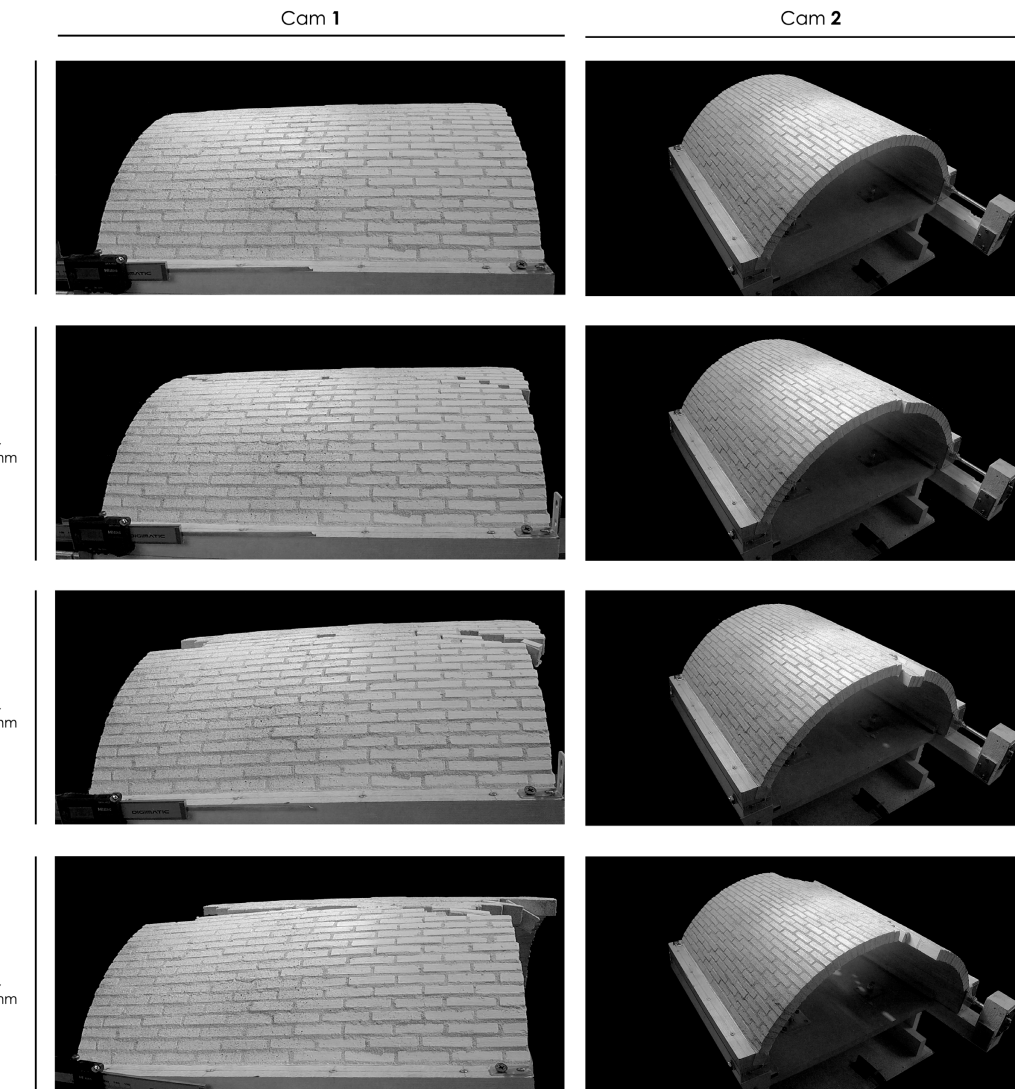


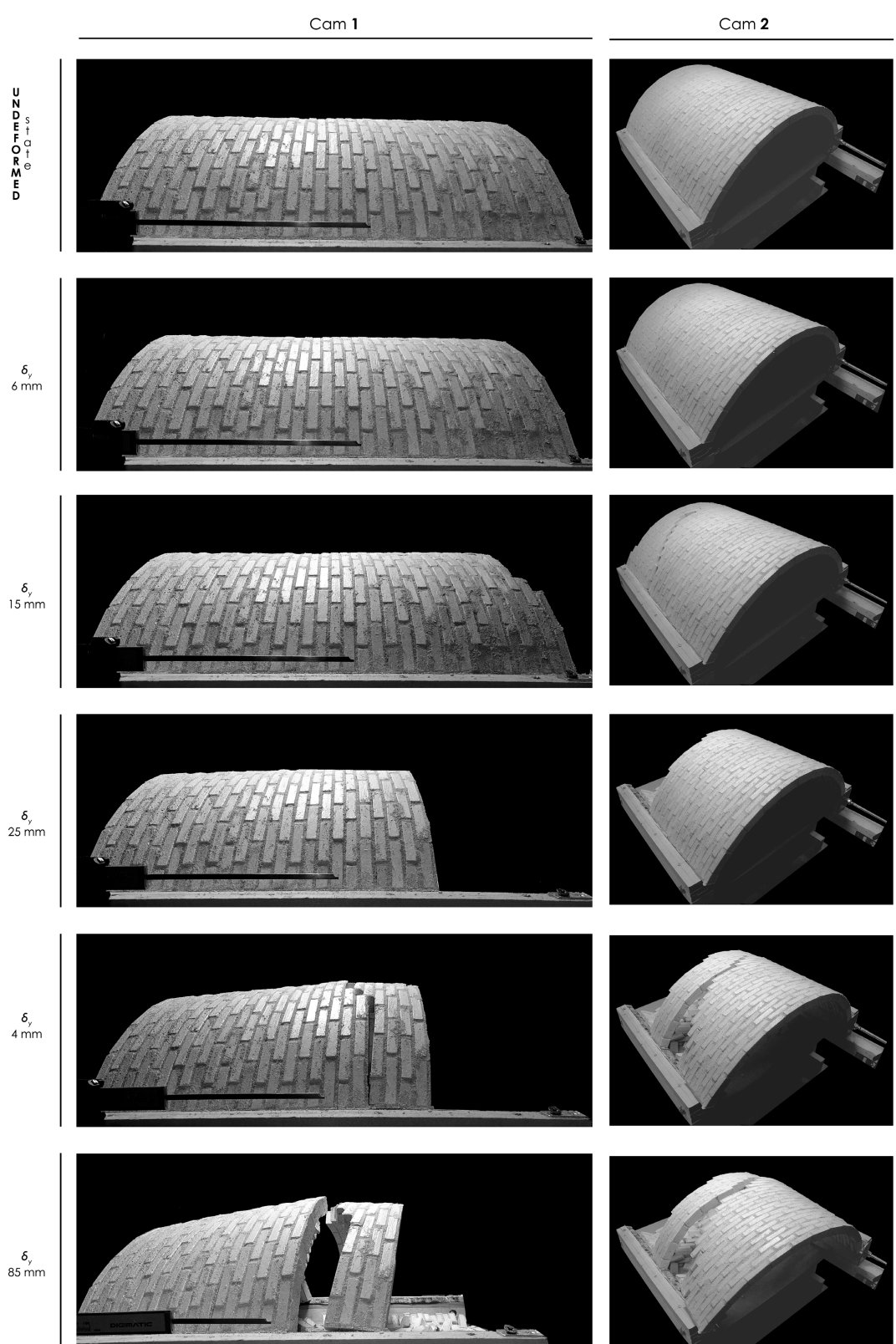


VR_1



VR_2



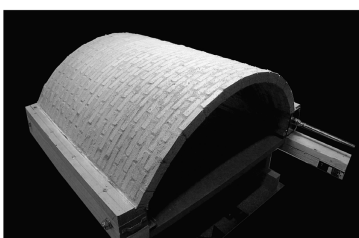
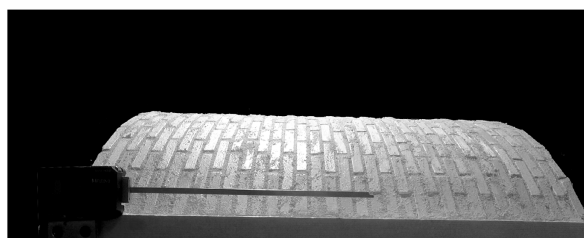


VV_2

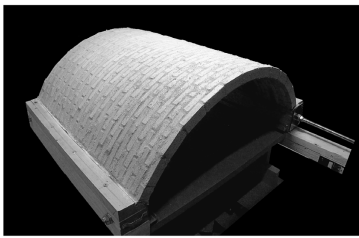
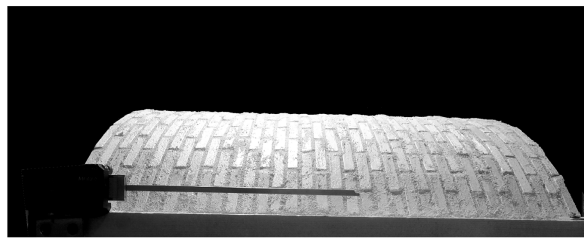
Cam 1

Cam 2

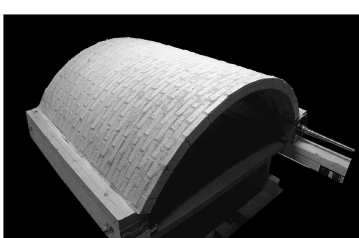
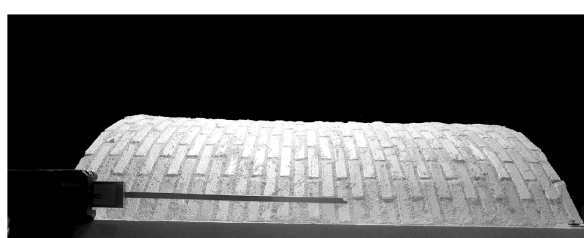
UNDEFORMED



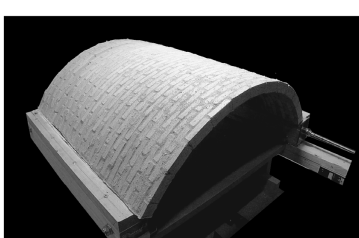
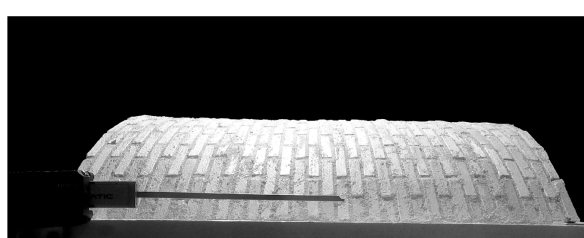
δ_y
6 mm



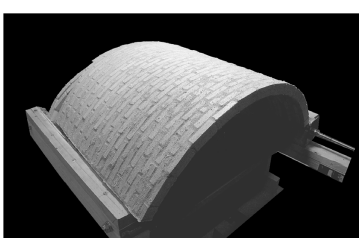
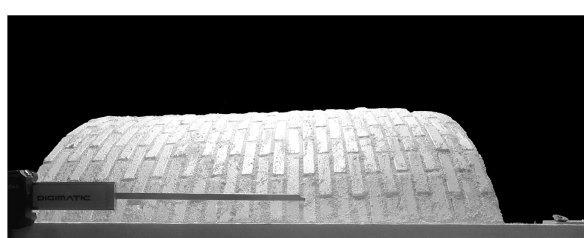
δ_y
15 mm



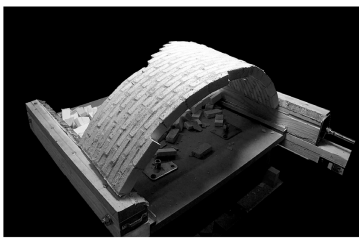
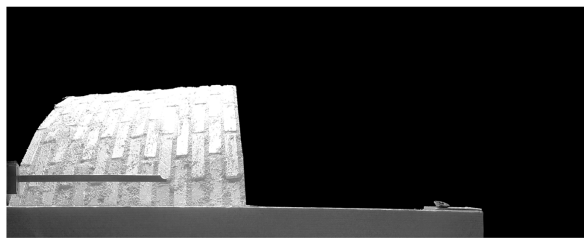
δ_y
25 mm



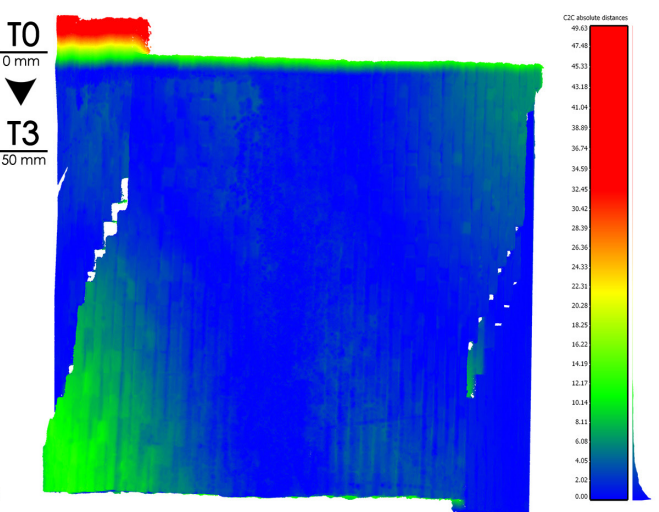
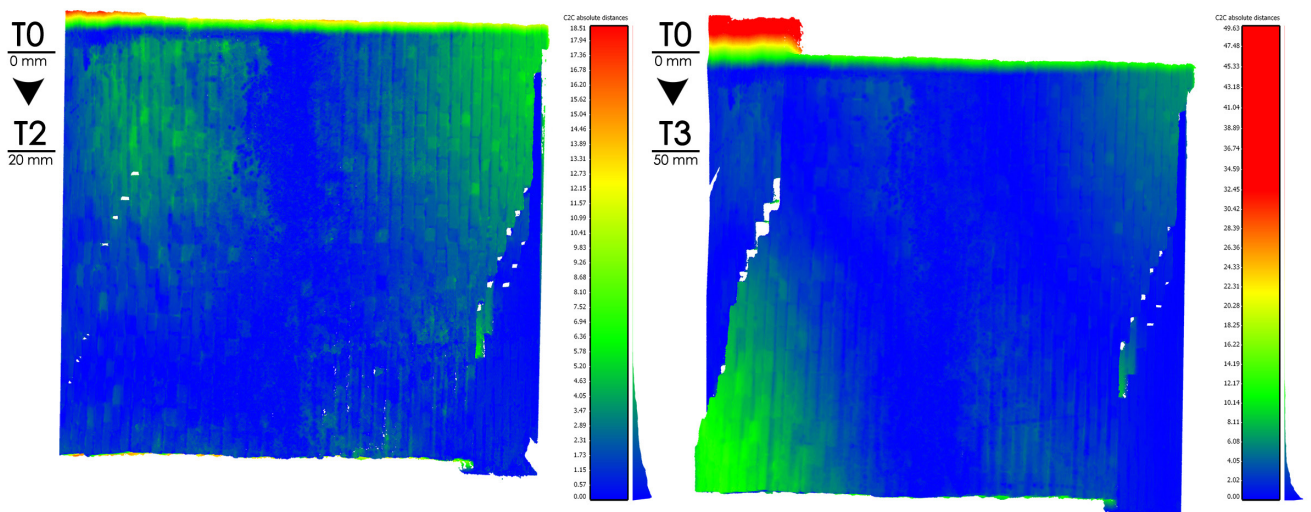
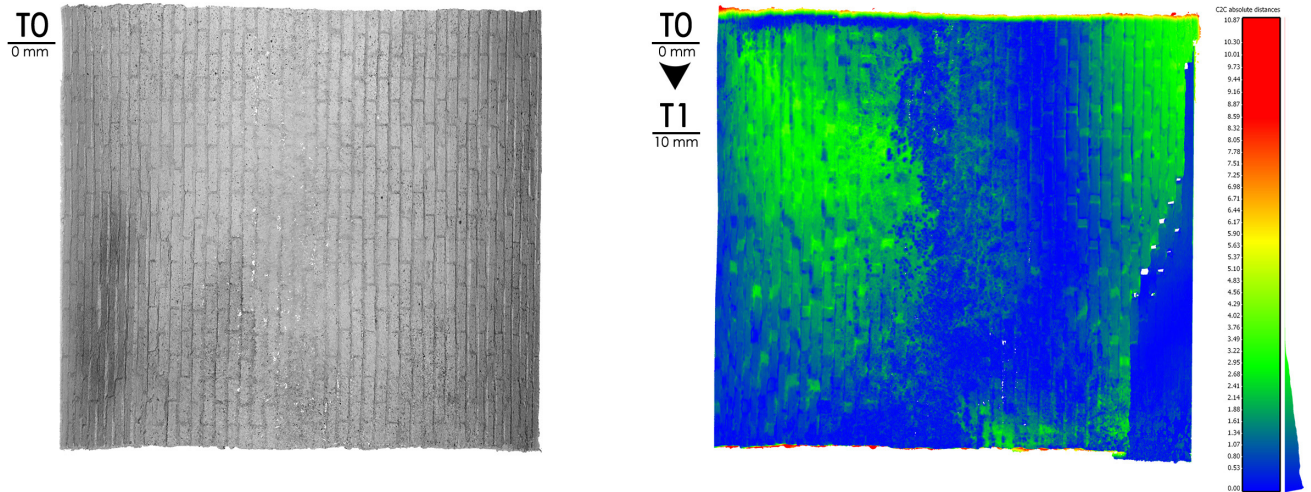
δ_y
4 mm



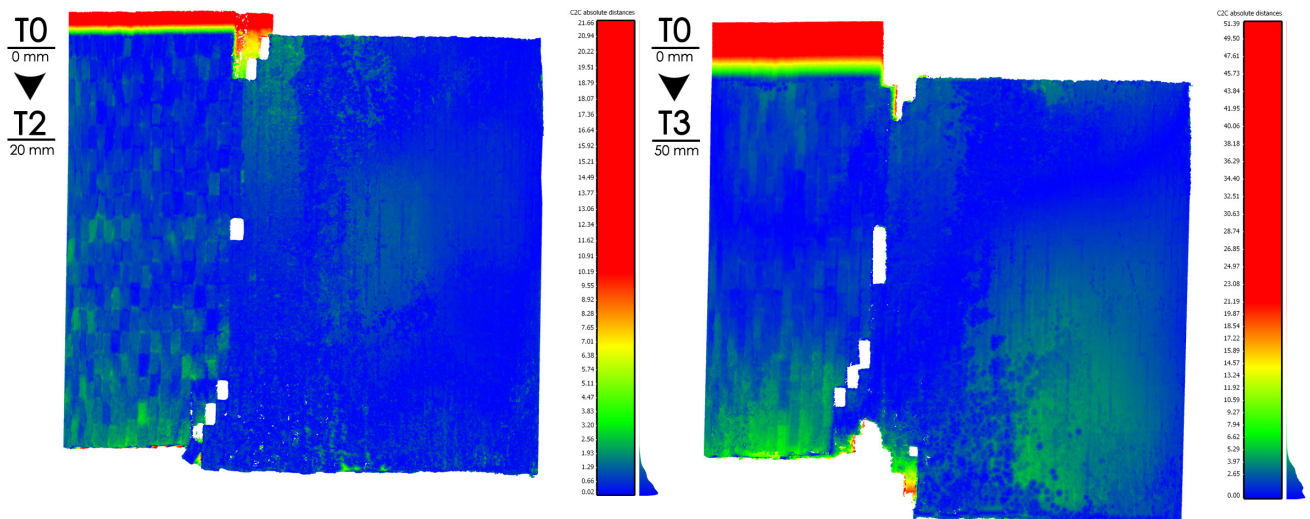
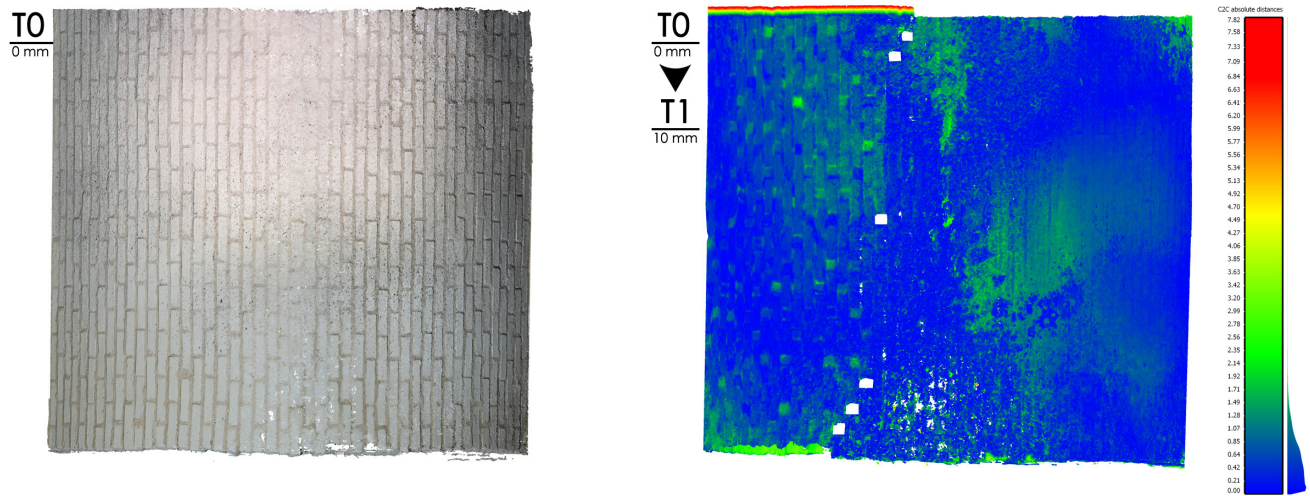
δ_y
75 mm



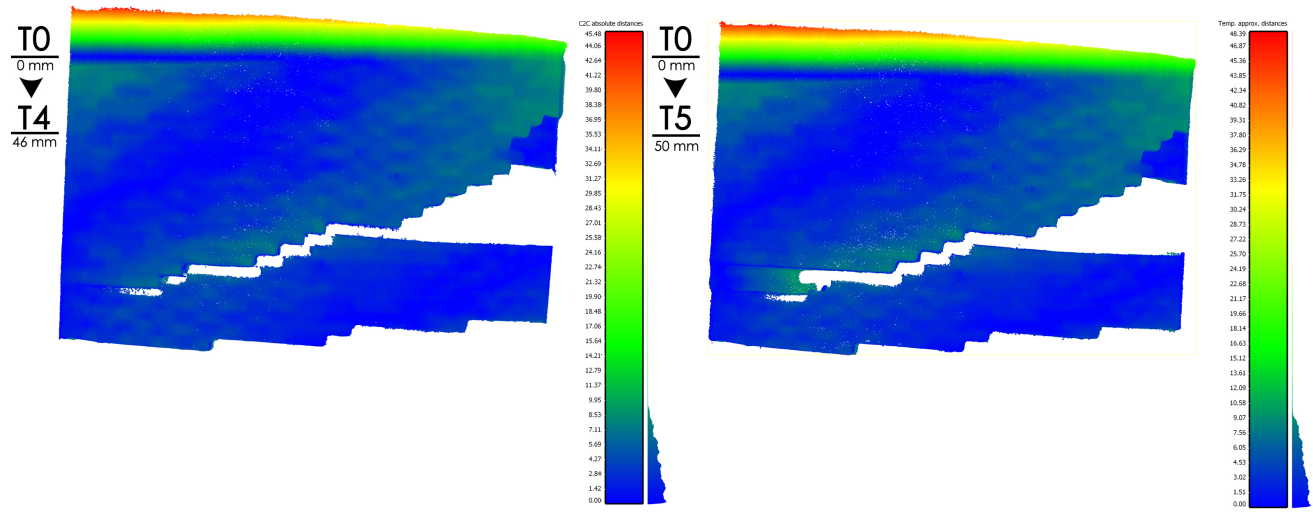
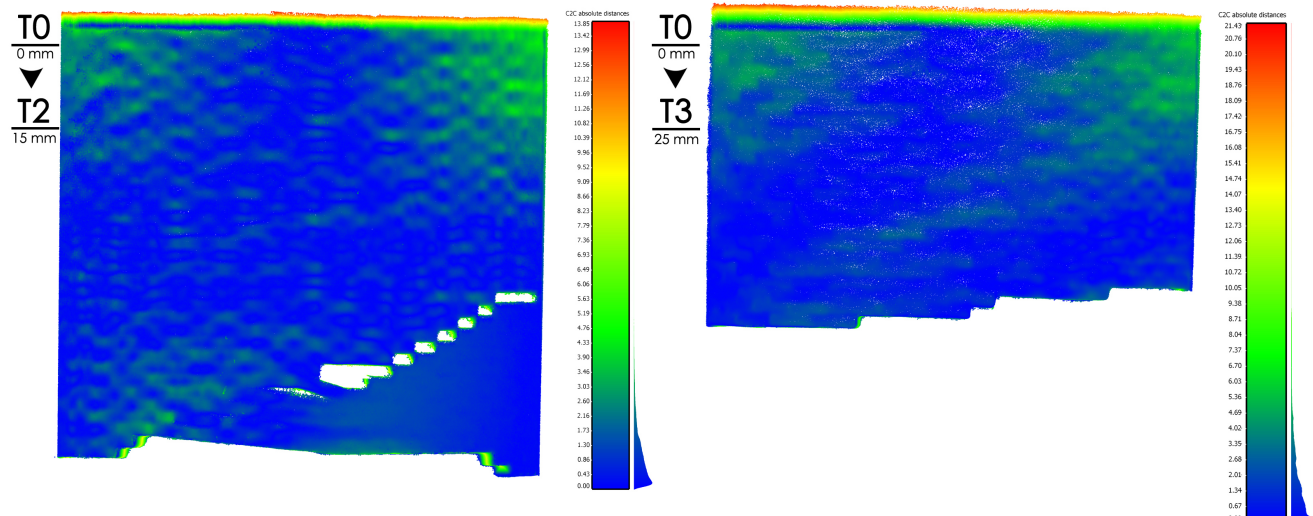
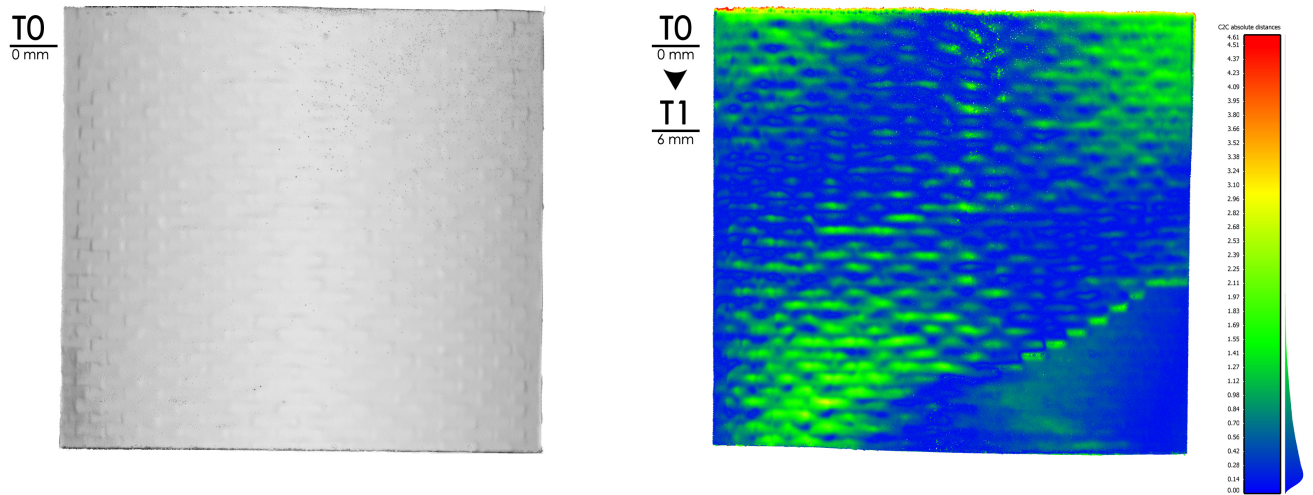
GLOBAL ABSOLUTE DISPLACEMENT - VR_1



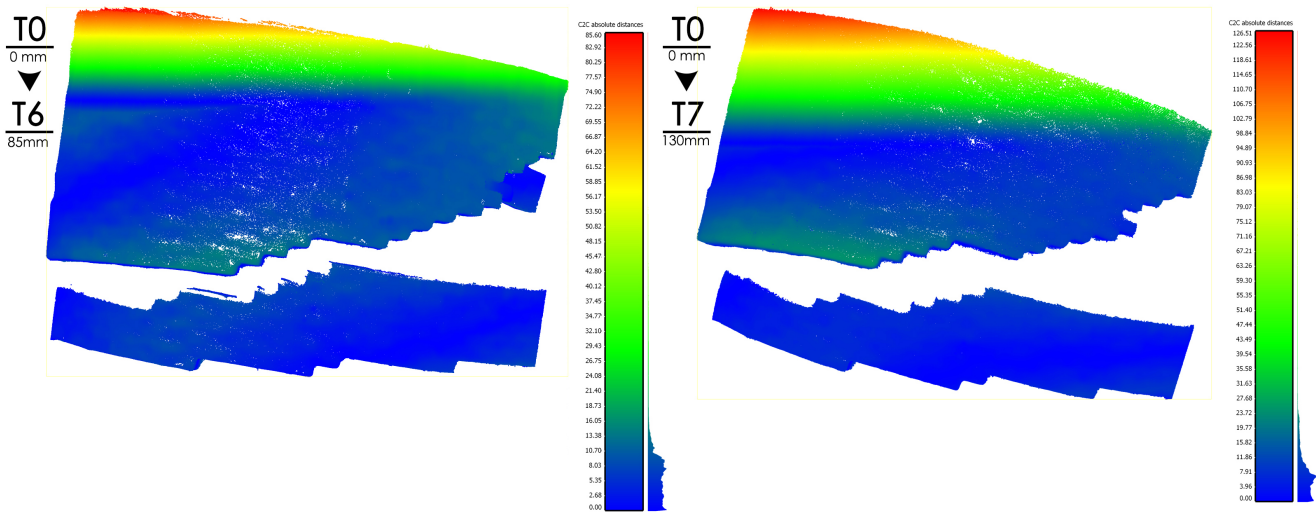
GLOBAL ABSOLUTE DISPLACEMENT - VR_2



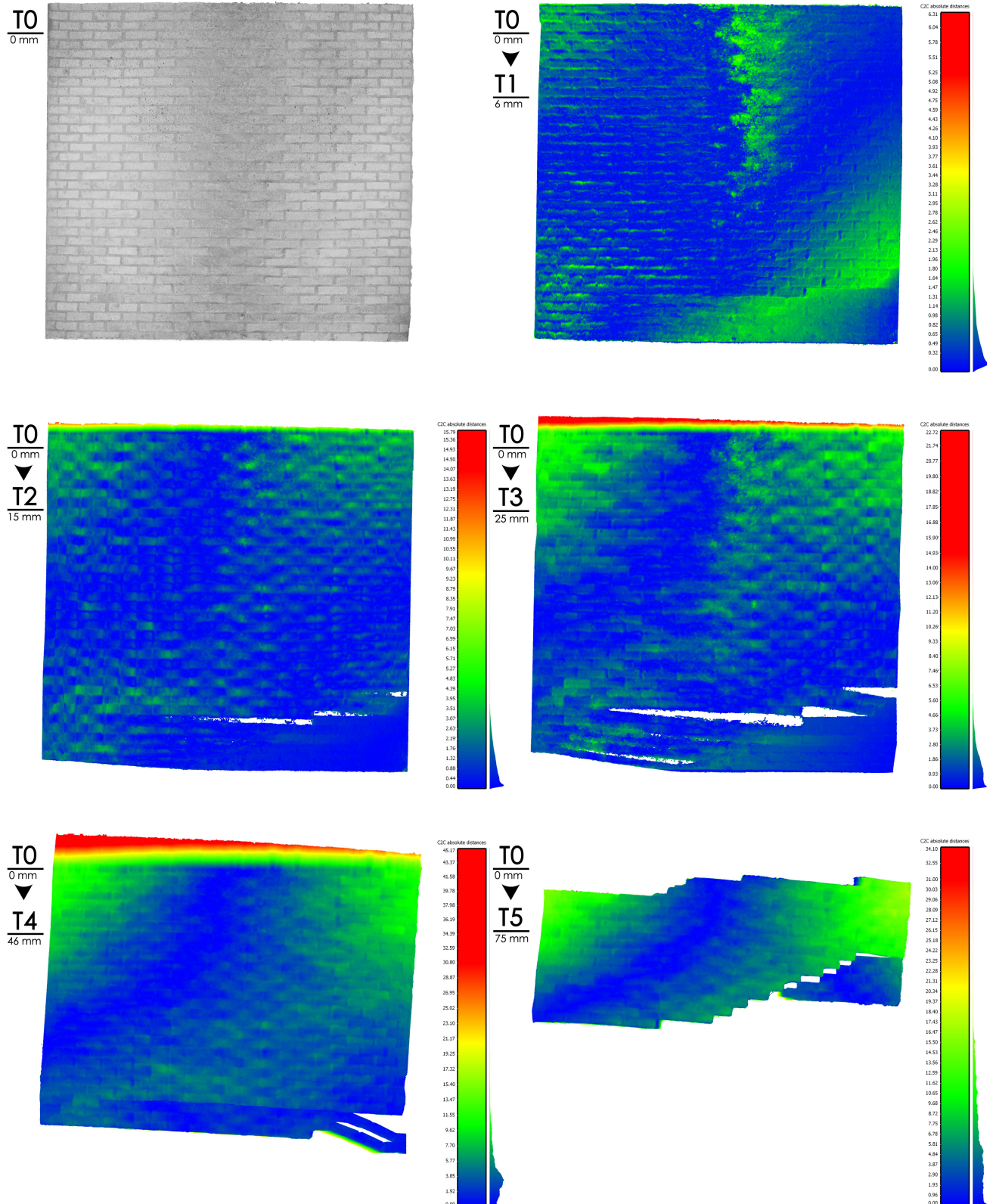
GLOBAL ABSOLUTE DISPLACEMENT - VV_1



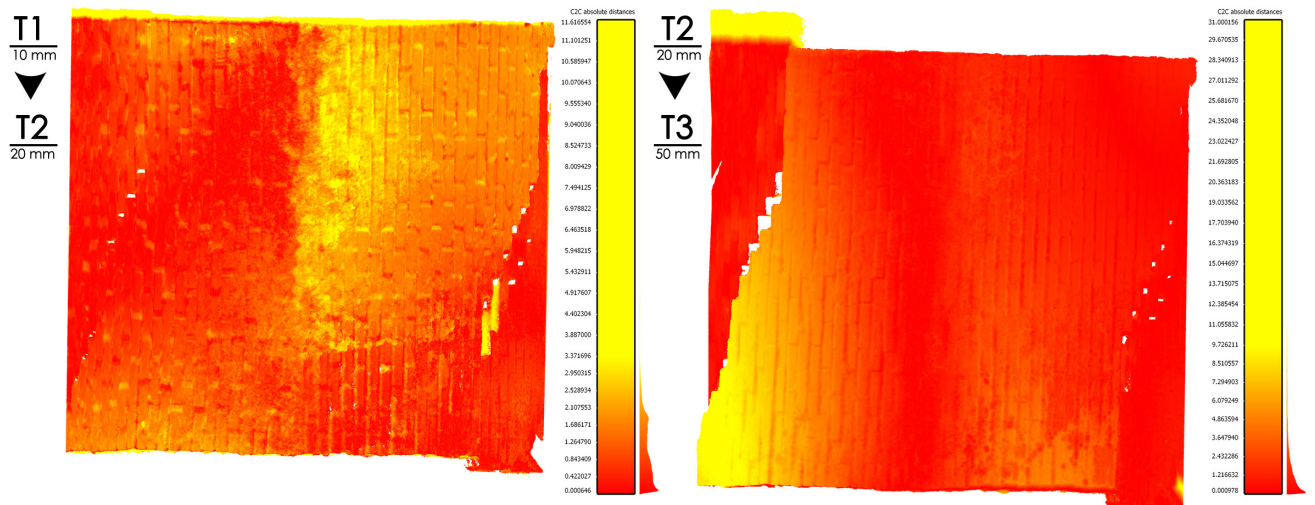
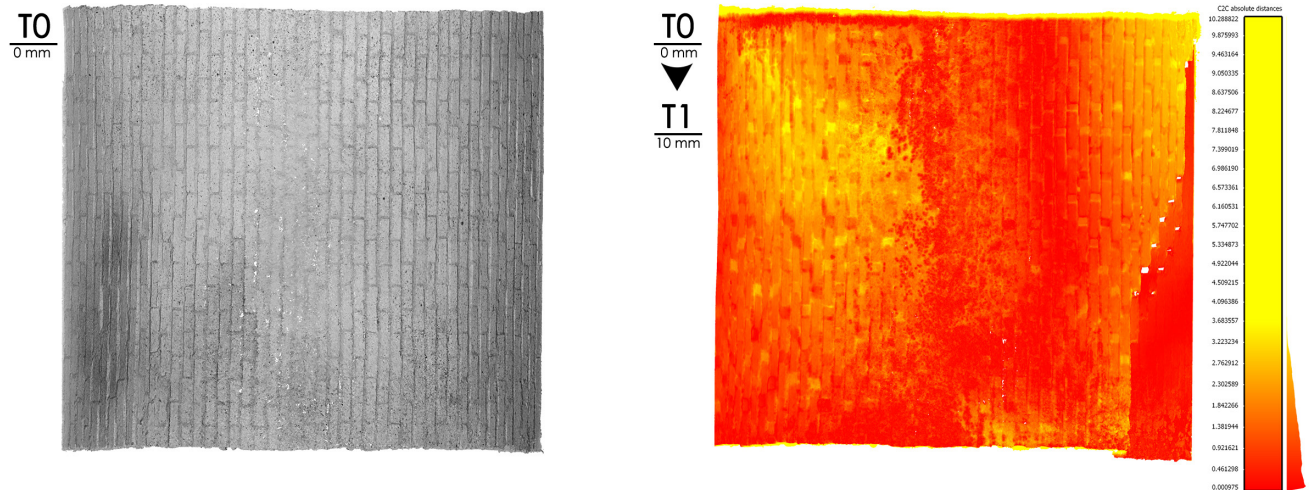
GLOBAL ABSOLUTE DISPLACEMENT - VV_1



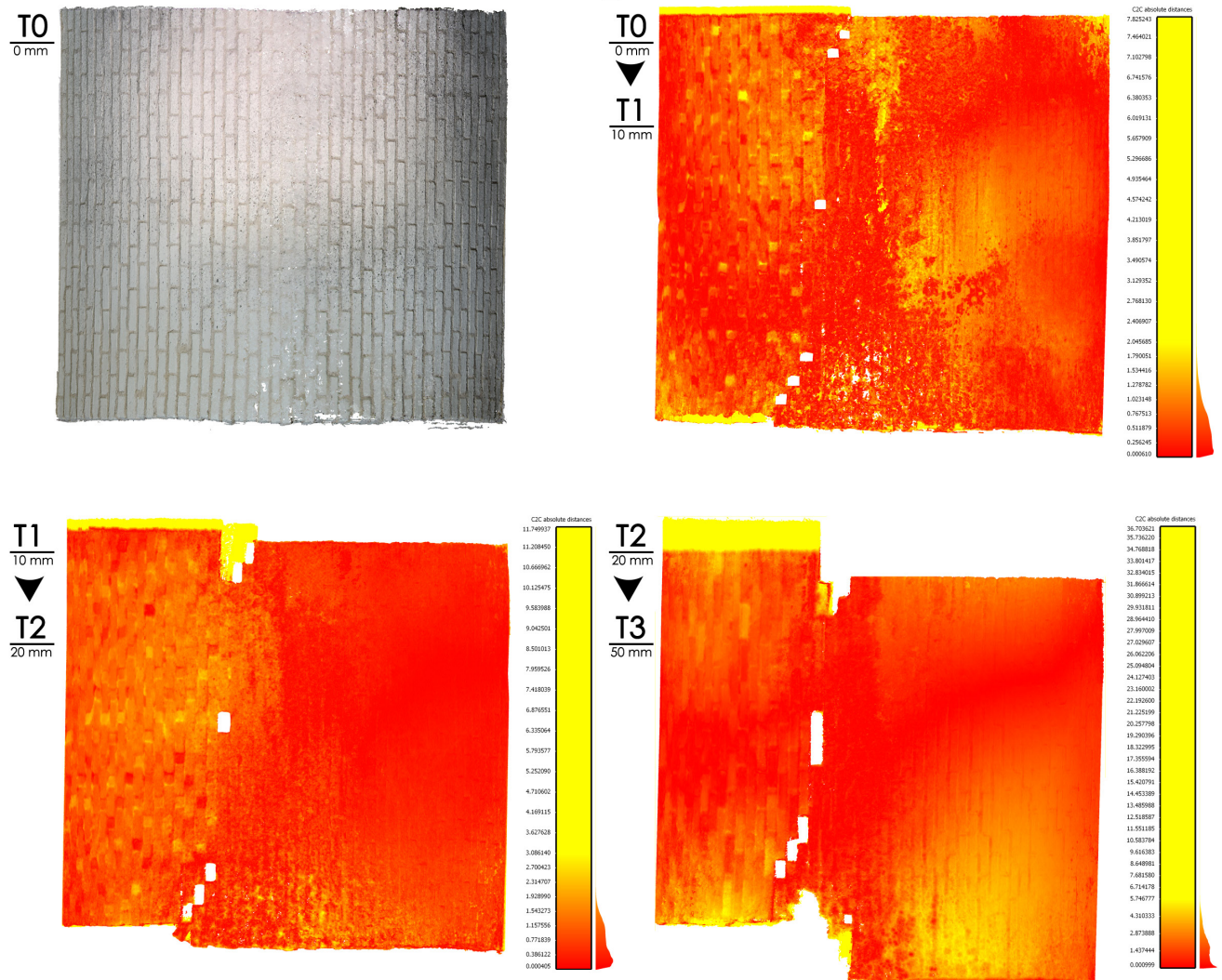
GLOBAL ABSOLUTE DISPLACEMENT - VV_2



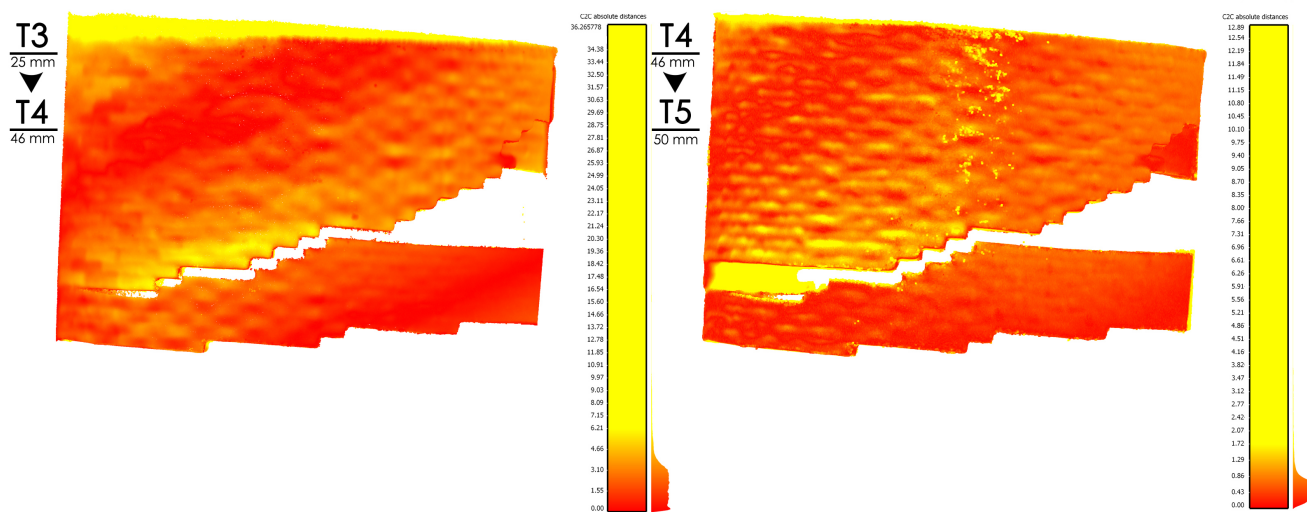
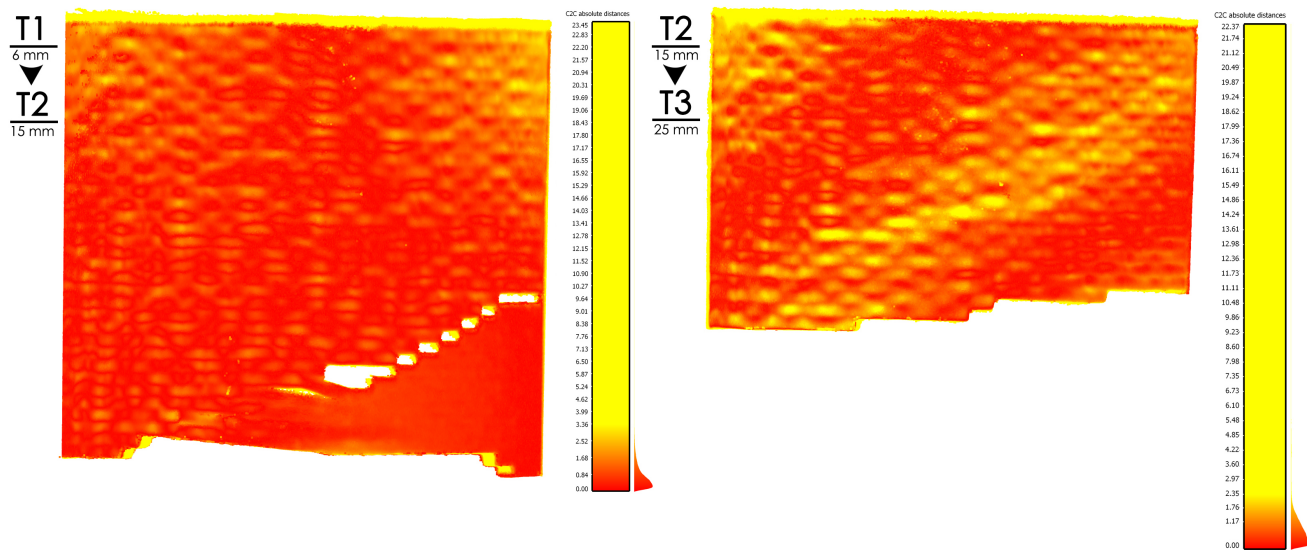
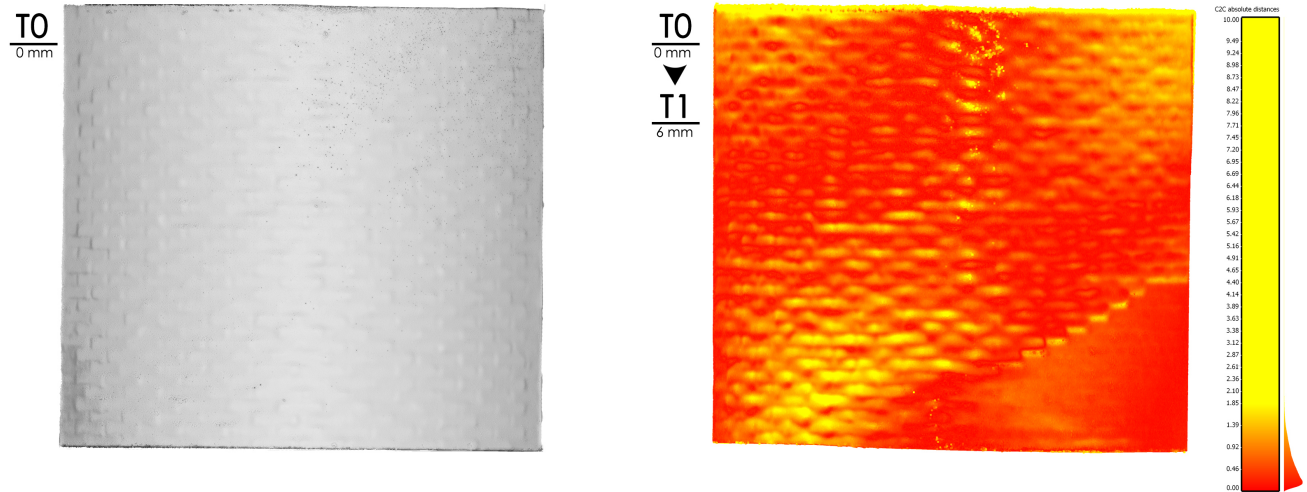
GLOBAL RELATIVE DISPLACEMENT - VR_2



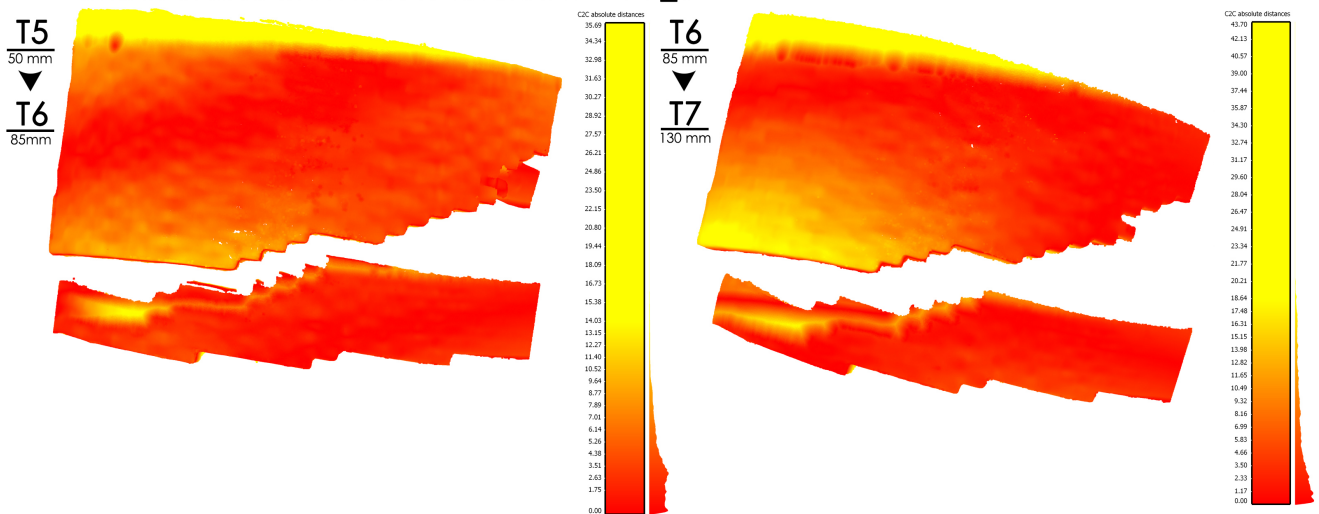
GLOBAL RELATIVE DISPLACEMENT - VR_2



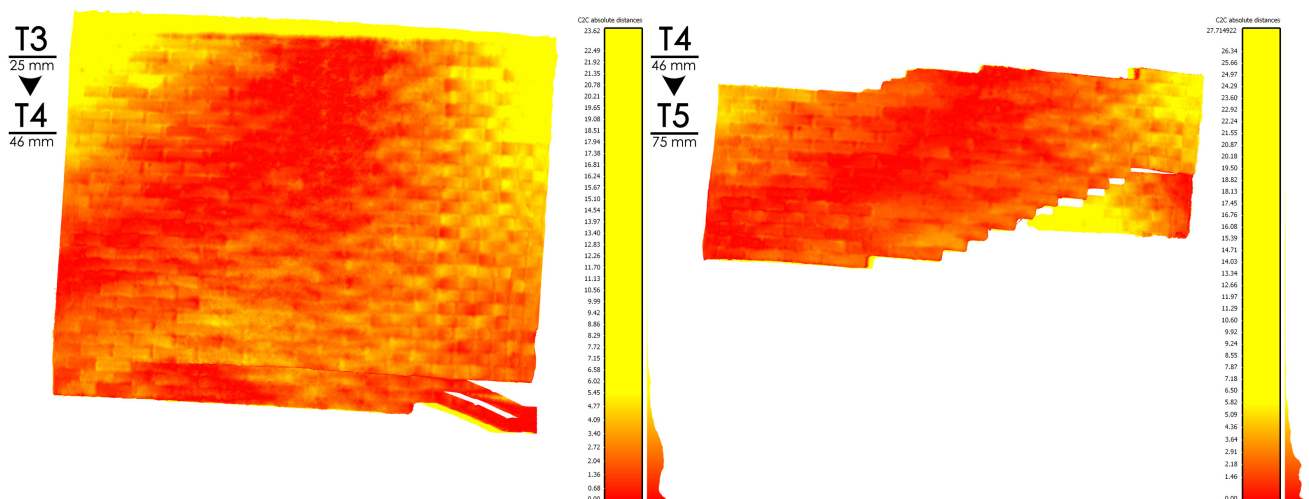
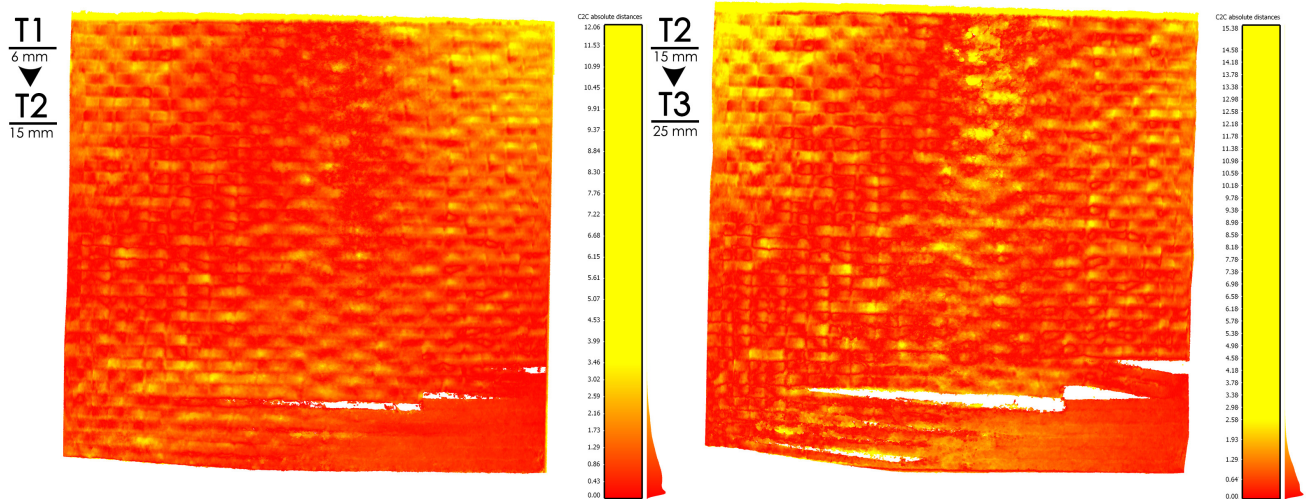
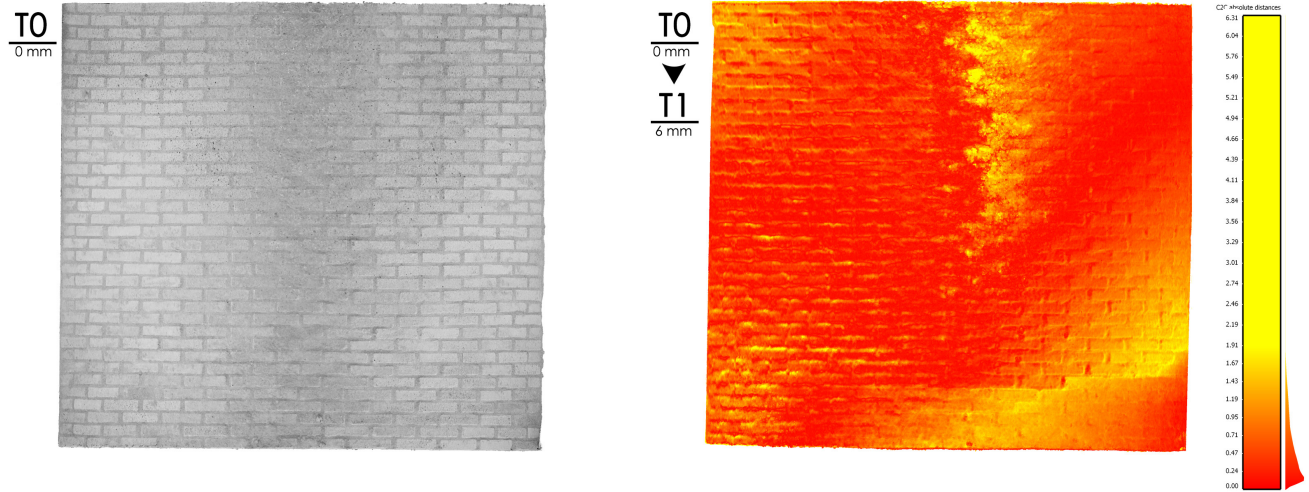
GLOBAL RELATIVE DISPLACEMENT - VV_1



GLOBAL RELATIVE DISPLACEMENT - VV_1



GLOBAL RELATIVE DISPLACEMENT - VV_2



11. Bibliography

ACKERMANN F., Digital Image Correlation: Performance and Potential Application in Photogrammetry. Photogrammetric Record, 11(64), 429-439, 1984.

ADAMOPOULOS E., RINAUDO F., ARDISSONO L., Comparison of 3D Digitization Techniques for Heritage Objects. ISPRS Int. J. Geo-Inf. 2021.

ALBERTI L.B., De re aedificatoria, Libro II, 1966,

ALFORNO M., MONACO A., VENUTI F., CALDERINI C., Validation of Simplified Micro-models for the Static Analysis of Masonry Arches and Vaults, in International Journal of Architectural Heritage, 2020.

BOYD T. D., The Arch And The Vault In Greek Architecture, in American Journal of Archeology, 1978, pp. 83-100.

BRUMANA R., CONDOLEO P., GRIMOLDI C A., LANDI A. G., Shape And Construction Of Brick Vaults. Criteria, Methods And Tools For A Possible Catalogue, in The International Archives of the Photogrammetry, Remote vSensing and Spatial Information Sciences, 2017.

BURNS H., Leon Battista Alberti in FIORE F.P., a cura di, "Storia dell'architettura italiana - Il Quattrocento", Electa, Milano, 1998, pag.150

C. PERRAULT, Mémoires de ma vie, a cura di F. BONNEFON, Paris, 1909

CABANILLAS CUESTA A., Convention Hall. Chicago 1953. Contexto e implantación urbana. Mies van der Rohe, master thesis, Escuela Técnica Superior de Arquitectura, a.a. 2018-2019, tutor L. Lizondo Sevilla, corelatore J. Santatecla Fayos, 2018.

CANGI G., Manuale del recupero strutturale e antisismico. Ed. DEI , 2012.

CARFAGNINI C., BARACCANI S., SILVESTRI S., THEODOSSOPOULOS D., The effects of in-plane shear displacements at the springings of Gothic cross vaults, in Construction and Building Materials, 2018.

CHOISY A., L'art de batir chez les byzantins. [Anastatic reprint]
Ed. Arnaldo Forni, 1883

COMO M. T., L'Architettura delle tholoi micenee. Aspetti costruttivi e statici, University Suor Orsola Benincasa, Napoli, 2007.

CURCIO G., La professione dell'architetto: disegni, cantieri, manuali, in **G. CURCIO-E. KIEVEN** (edited by), Storia dell'architettura italiana. Il Settecento, Milano 2000, I.

DELL'ENDICE A., IANNUZZO A., DEJONG M. J., VAN MELE T., BLOCK P., Modelling imperfections in unreinforced masonry structures: Discreteelement simulations and scale model experiments of a pavilion vault, in Engineering structures, 2020.

DI MARCO F., Carlo Camporese "Capo Mastro Falegname"
Nella Roma della prima metà del Settecento, in in "Bollettino dei Musei Comunali di Roma", XXXI (2017), pp. 35-48,

DÍAZ J.G., GONZÁLES G.L.G., GONZÁLEZ J.A.O., FREIRE J.L.F., Analysis of Mixed-mode Fatigue Crack Growth Using DIC Displacement Fields, in 24th ABCM International Congress of Mechanical Engineering, December 3-8, 2017, Curitiba, PR, Brazil, 2017.

FERRERO C., CALDERINI C., PORTIOLI F., ROCA P., Collapse Mechanisms Of Masonry Arches On Moving Supports, in Minisymposium @ 14th WCCM & Eccomas Congress 2020 |

MS 166: Modelling of historical masonry structures under extreme events: earthquakes, impacts and soil movements, 2021.

FERRERO C., CALDERINI C., PORTIOLI F., ROCA P., Large displacement analysis of dry-joint masonry arches subject to inclined support movements, in Engineering Structures, 2021

FILARETE, Trattato di architettura, Libro II, 1972

GABETTI R., LUPANO M. (a cura di), Alessandro Antonelli, CLUP, Milano, 1989.

GALASSI S., MISSERI G., ROVERO L., TEMPESTA G., Analysis of Masonry Pointed Arches on Moving Supports: A Numeric Predictive Model and Experimental Evaluations in Proceedings of XXIV AIMETA Conference 2019, 2020 pp.2048-2068.

GERMANASCA M. A., Elementi di Geomatica, Associazione italiana di Telerilevamento (AIT), 2004, Milano.

GUARINI G., Euclides ad auctus et methodicus, matematica que universalis, Torino, 1671

GUIDI G., BERALDIN J., CIOFI S., ATZENI C., Fusion of Range Camera and Photogrammetry: A Systematic Procedure for Improving 3-D Models Metric Accuracy, in IEEE Transactions On Systems, Man, And Cybernetics—Part B: Cybernetics, Vol. 33, No. 4, August 2003.

GUIDI G., RUSSO M., BERALDIN J., Acquisizione 3D e Modellazione Poligonale, McGraw-Hill, Milano, 2010.

HEYMAN J., The Stone Skeleton, in International Journal of Solids and Structures 2, 1966, pp. 249-279

HEYMAN J., The Stone Skeleton, Cambridge University Press, Cambridge, 1997

HEYMAN J., The Stone Skeleton, Structural Engineering of ma-

sonry architecture, Cambridge University Press, Cambridge, 1995.

HOLS, C., SCHMITZ B., KUHLMANN H., Investigating the applicability of standard software packages for laser scanner based deformation analyses, in FIG Working Week 2017, 2017.

HOLST C., KLINGBEIL L., ESSER F., KUHLMANN H., Using point cloud comparisons for revealing deformations of natural and artificial objects, in INGEO 2017 – 7th International Conference on Engineering Surveying At: Lisbon, Portugal, 2017.

I. LIDDELL, Frei Otto and the development of gridshells, in Case Studies in Structural Engineering, 2015

LUHMANN T., ROBSON S., KYLE S., BOEHM J., Close-Range Photogrammetry and 3D Imaging, De Gruyter, Berlin/Boston, 2013.

MCCORMICK N., LORD J., Digital Image Correlation, in Materials Today, 2010.

MONTAGGIOLI G., PULITI M., SABATO A., Automated damage detection of bridge's sub-surface defects from infrared images using machine learning, in Health Monitoring of Structural and Biological Systems XV, 2021.

NAPOLI P., A Structural Description of the Chapel of the Holy Shroud in Torino, IN Nexus Network Journal, 2009.

NEUNER H., HOLST C., KUHLMANN H., Overview on current modelling strategies of point clouds for deformation analysis, in Allgem. Verm. Nachr., 11/2016, 2016.

NICOLETTI M., Sergio Musmeci. Organicità di forme e forze nello spazio, Torino, 1999.

NIEZRECKIA C., BAQRSAD J., SABATO A., Digital Image Correlation Techniques for Non-Destructive Evaluation and Structural Health Monitoring, in Handbook of Advanced Non-Destructive Evaluation, IDA N., MEYENDORF N. (edited by), Springer, Cham, 2018, pp.1-46.

NOVA A., Il ballatoio di Santa Maria del Fiore a Firenze in H.A. MILLON, Rinascimento da Brunelleschi a Michelangelo, La rappresentazione dell'architettura, Bompiani, Milano, 1994

OCHSENDORF J., The masonry arch on spreading supports, in Structural Engineer, 2006

OTTO F., Thinking by Modeling, edited by Georg Vrachliotis, Leipzig, 2017.

PATRUCCO G., RINAUDO F., SPREAFICO A., A New Handheld Scanner For 3d Survey Of Small Artifacts: The Stonex F6, in The International Archives of the Photogrammetry, Remote Sensing and Spatial Information Sciences, Volume XLII-2/W15, 2019 27th CIPA International Symposium "Documenting the past for a better future", Ávila, Spain, 2019.

PATRUCCO G., Tecniche innovative UAV e LIDAR per l'analisi stratigrafica delle murature: il chiostro dell'abbazia di Novalesa, Torino, 2016.

PICCOLI E., Volte composte nell'architettura piemontese del Settecento : le volte planteriane, in Palladio , pp. 87-100, 1999

PIERRE' J.-E., PASSIEUX J.C., PERIE' J.-N., Finite Element Stereo Digital Image Correlation: Framework and Mechanical Regularization, in Experimental Mechanics, 2017.

POLIDORO M., Segreti e tesori del Vaticano, Edizioni Piemme, Milano, 2017

POLITECNICO DI TORINO. MUSEO DELLE ATTREZZATURE PER LA

DIDATTICA E LA RICERCA, Capolavori di minuteria al servizio della scienza delle costruzioni: la collezione ottocentesca di modelli di costruzioni della R. Scuola di Applicazione per ingegneri in Torino: Torino, 22 novembre-16 dicembre 1989, Celid, Torino, 1989

REDA TAHA M. M., Design of Masonry Arches, in ENCI 595.05-Masonry Arches, 2005.

RICCI M., Il fiore di Santa Maria del Fiore: (ipotesi sulla regola di costruzione della cupola), Alinea, Firenze, 1983

ROMANO A., OCHSENDORF J., The Mechanics of Gothic Masonry Arches, in International Journal of Architectural Heritage, 2010.

ROSSI M., CALDERINI C., LAGOMARSINO S., Experimental testing of the seismic in-plane displacement capacity of masonry cross vaults through a scale model, Settembre 2015

ROSSI M., CALVO BARENTIN C., VAN MELE T., BLOCK P., Experimental study on the behaviour of masonry pavilion vaults on spreading supports, in Structures, 2017.

SABATO A., PULITI M., NIEZRECKIA C., Combined Infrared Imaging and Structure from Motion Approach for Building Thermal Energy Efficiency and Damage Assessment, in Conference: Health Monitoring of Structural and Biological Systems IX, 2020.

SAKAROVITCH J., Stereotomy, a multifaced technique, in Proceedings of the First International Congress on Construction History, Madrid, 2003,

SARDO N., La figurazione plastica dell'architettura: modelli e rappresentazione, Kappa, Roma, 2004

SEBASTIANELLI M., MUSCARELLI C., Modelli architettonici: sviluppo e tecniche di costruzione, in OADI : Rivista dell'Os-

servatorio per le Arti Decorative in Italia, June 2016

SHAO X.X., HE X.Y., Real-time 3D Digital Image Correlation for Large Deformation and Rotation Measurements Based on a Deformation Transfer Scheme, in Experimental Mechanics, 2021.

SHAPIRO E.E., Collapse Mechanisms of Small-Scale Unreinforced Masonry Vaults, Giugno 2012

SPALLONE R., Rappresentazione e progetto. La formalizzazione delle convenzioni del disegno architettonico, Edizioni dell'orso, Alessandria, 2012

STANGA C., HASNÍKOVÁ H., BRUMANA R., GRIMOLDI A., BANFI F., Geometric Primitives Assessing Italian-Czech Vault Construction Techniques In Baroque Period, in The International Archives of the Photogrammetry, Remote Sensing and Spatial Information Sciences, 2019.

TOSCO C., L'architettura medievale in Italia (600-1200), Il Mulino, Bologna, 2016

VAN MELE T., MCINERNEY J., DEJONG M.J., BLOCK P., Physical and computational discrete modeling of masonry vault collapse, Gennaio 2012

VASARI G., Le vite de' più eccellenti pittori, scultori, e architetti, Einaudi, Torino, 1986

VERSTRYNGE E., SCHUEREMANS L., SMARS P., VAN GEMERT D., Design and testing of masonry arches: a project of bachelor students in civil engineering, in ARCH'07 – 5th International Conference on Arch Bridges, 2007.

VRONTISSI M., The physical model in the structural studies of Robert Le Ricolais: "apparatus" or "hierogram", in Structures and Architecture, 2016

WUNDERLICH T., NIEMEIER W., WUJANZ D., HOLST C., F. NEITZEL,

KUHLMANN H., Areal deformation analysis from TLS point clouds – the challenge. Allgem. Verm. Nachr., 2016, Wichmann Verlag, Berli,, 2016.